

# 学位論文

**A chronological study of differentiated meteorites:  
elucidation of crustal evolution  
and accretion history of protoplanets**

(分化隕石の年代記録を用いた原始惑星の  
地殻進化・天体衝突史の解明)

平成 29 年 12 月博士 (理学) 申請

東京大学大学院理学系研究科

地球惑星科学専攻

小池みずほ



# Abstract

Elucidation of the planetary formation process is a long-standing issue in planetary science. Scarcity of the surviving small bodies (planetesimals ~ protoplanets) makes it difficult to reveal the early history. Rocky small bodies with sizes up to 100s–1000 km are considered to have been common in the early solar system. However, most of them were lost to date. Meteorites from the ancient differentiated bodies, (i.e. differentiated meteorites), are valuable recorders of past evolutionary processes of the protoplanets, including igneous crystallization of the primary crusts, thermal metamorphism, hydrous alteration, and/or impact brecciation. This study aims to reveal the planetary evolution histories from the meteoritical records. Especially, I focus on Vesta and Vesta-like protoplanets

In the present study, I investigate the meteoritical samples from asteroid 4–Vesta (eucrites; Chapter 2), and those from Vesta-like unknown body (mesosiderites; Chapter 3). Co-authors and I previously established *in-situ* U-Pb dating protocols of extraterrestrial phosphates using NanoSIMS 50 (Koike et al., 2014; 2016). In the present work, I have also established *in-situ* Hf-W dating protocols of meteoritical zircon (reported in Koike et al., 2017; Chapter 3). Taking advantages of the *in-situ* techniques, I have analyzed the U-Pb and Hf-W records of these samples, which indicate the ancient histories of their parent protoplanets.

In Chapter 2, I investigate the crustal metamorphic history of asteroid 4-Vesta. Vesta, a large (R~280km) rocky body in the main asteroid belt, is the only surviving differentiated protoplanet currently known. Their crustal samples are known to be available as the common meteoritical groups (howardites-eucrites-diogenites; HEDs). Eucrites, the largest group in HEDs, are basaltic composition rocks, which represent Vesta's crusts. A number of previous studies investigated their mineralogy, geochemistry, and chronology, and proposed their complicated histories. *In-situ* U-Pb dating were previously conducted on zircons in several eucrites, which indicate high-temperature ( $\geq 900$  °C) thermal process at 4554 Ma. The U-Pb systems in Ca-phosphates (apatite [ $\text{Ca}_5(\text{PO}_4)_3(\text{F},\text{Cl},\text{OH})$ ]) provide moderately robust thermo-chronometer, which records thermal events at typical temperature ranges of ~450–600°C<sup>[7]</sup>. In order to understand the complicated history of Vesta's crusts, it is important to investigate various chronological records with *in-situ* techniques, and compare them to each other. The goal of this study in Chapter 2 is to reveal the crustal metamorphic history of Vesta at moderate temperatures (ca. 600°C), by *in-situ* U-Pb dating of phosphates in basaltic eucrites.

I have analyzed four basaltic eucrites (Juvinas, Camel Donga, Stannern, Agoult) and

an anomalous basaltic achondrite (Ibitira). Three of the five (Juvinas, Camel Donga, Stannern) are severely brecciated by impacts, whereas the others (Agoult, Ibitira) are unbrecciated. From apatite in Agoult, a precise  $^{207}\text{Pb}$ - $^{206}\text{Pb}$  age of  $4522 \pm 11$  Ma is determined. Similar  $^{207}\text{Pb}$ - $^{206}\text{Pb}$  age at ca. 4530 Ma is also obtained from apatite in Juvinas. This ca. 4530 Ma period is significantly younger than the igneous age of  $\geq 4560$  Ma. It is inferred that Vesta's crust experienced either the slow cooling from earlier thermal events, or additional moderate reheating (ca.  $600^\circ\text{C}$ ) at 4530 Ma. In contrast, merrillite in the same Juvinas samples has a significantly younger  $^{207}\text{Pb}$ - $^{206}\text{Pb}$  age of ca. 4200 Ma, suggesting its U-Pb system was completely reset at the later impact reheating with partial remelting. This study is the first report that has identified the local disturbances of the U-Pb systems in phosphates from the single sample, owing to the *in-situ* methods. The  $^{207}\text{Pb}$ - $^{206}\text{Pb}$  age of another brecciated eucrite, Stannern, is also as young as 4130 Ma. The other breccia, Camel Donga, has the disturbed U-Pb system around  $\sim 4500$ – $4400$  Ma. Partially remelted textures in these brecciated samples, especially in Juvinas, suggest that reheating temperatures at the 4200 Ma event(s) may have locally exceeded the melting points of basalts ( $\sim 1060^\circ\text{C}$ ). Consequently, it is inferred that Vesta suffered the intense impacts with brecciation and partial remelting during ca. 4200 Ma.

In Chapter 3, I investigate the impact and reheating history of the mesosiderites parent body (MPB). Mesosiderites are unique mixtures of brecciated silicates ( $\sim 50\text{wt}\%$ ) and Fe-Ni metals ( $\sim 50\text{wt}\%$ ). The silicate parts are similar to eucrites in their mineralogy, geochemistry and isotopic compositions e.g. [8][9], suggesting similar parent bodies for the two. Nasa's Dawn mission did not identify mesosiderite-like regolith on the surface of Vesta. Hence, MPB is likely to be the past Vesta-like protoplanet (not exactly Vesta itself), which may not exist today. Although formation process of mesosiderites is still enigmatic, their silicates-metal mixing should have occurred during impact(s) and subsequent reheating(s). Records in mesosiderites are valuable hint for the collisional destruction and/or accretion processes of protoplanets in the early solar system. However, little is uncovered for these meteorites. The goal of this study in Chapter 3 is to reveal the MPB evolutionary history, from chronological constraints of the high-temperature events recorded in the mesosiderite zircons.

I have conducted *in-situ* U-Pb and Hf-W dating on a single zircon grain in Asuka 882023 (A88) mesosiderite, using NanoSIMS 50. Its  $^{207}\text{Pb}$ - $^{206}\text{Pb}$  age is calculated as  $4502 \pm 75$  Ma, while its  $^{182}\text{Hf}$ - $^{182}\text{W}$  age is  $4532.8 \pm 9.6$ – $4532.8$  Ma. Both U-Pb and Hf-W systems are likely to have recorded timing of the zircon formation in A88. Considering textural and geochemical features, the zircon in A88 may have crystallized secondarily at the thermal

metamorphism at 4540–4500 Ma ('4530 Ma'), distinctly later than the crustal formation of MPB at  $\geq 4560$  Ma. The silicates-metal mixing may have occurred at the same time or earlier. Although exact timing of the mixing is controversial, it is clear that MPB crusts suffered high temperature metamorphism during 4530 Ma. A plausible interpretation is that the primary crusts on MPB and metallic core in impactor(s) were mixed during the 4530 Ma impact, subsequently reheated to produce the secondary zircon. It is inferred the evolution processes of protoplanets were active at this stage. The main part of Chapter 3 is reported in Koike et al. (2017).

Finally, I summarize the present chronological knowledge from eucrites and mesosiderites, along with literature data of various meteorites. From comparison of the various chronological records, it is inferred that Vest and Vesta-like protoplanets experienced thermal events at (I) ca. 4530 Ma, (II) ca. 4200 Ma, and (III) 3800 Ma. The event (I) can be both internal thermal metamorphism and impacts. The later (II) and (III) should be impact reheating. The event (II) was identified from the U-Pb systems in phosphates and silicates from several eucrites, while the event (III) was recorded in their K-Ar systems. Future investigations of additional extraterrestrial samples will enable the further discussion.

## Acknowledgements

I sincerely appreciate my supervisor, Prof. Yuji Sano of Atmosphere and Ocean Research Institute, The University of Tokyo, for giving me the greatest opportunities to study in the doctoral course and to dedicate the present work. Without his patient supports and valuable advises, I could not even start my doctoral dissertation rather than achieve it. I deeply appreciate Dr. Naoto Takahata of AORI, The University of Tokyo, for his kind and considerable supports for this study and valuable suggestions. I am grateful to Dr. Kotaro Shirai and Dr. Takanori Kagoshima of AORI, The University of Tokyo, for their considerate advices both in the present study and in my laboratory life.

This dissertation was reviewed by Prof. Eiichi Tajika, Prof. Shun'ichi Nakai, Dr. Hajime Hiyagon, Dr. Masahiro Ikoma, Dr. Yasuhito Sekine, and Prof. Yuji Sano of The University of Tokyo. The chief examiner was Prof. Eiichi Tajika. Their valuable comments and suggestions are greatly appreciated.

I am grateful to emeritus professor, Prof. Naoji Sugiura of The University of Tokyo, and Dr. Akizumi Ishida of Tohoku University, co-authors in our published paper (Koike et al., 2017; reported in Chapter 3), for their supports in the analyses and discussion.

I appreciate Dr. Tsuyoshi Iizuka, Dr. Takashi Mikouchi, and Ms. Haruka Ono of Graduate School of Science, The University of Tokyo, co-authors in our ongoing paper (reported in Chapter 2), for their supports in the analyses and discussion.

Dr. Makiko K. Haba of Tokyo Institute of Technology kindly provided the Stannern sample for this study.

Technical supports by Dr. Nobuhiro Ogawa and Ms. Rei Aamano of AORI, The University of Tokyo, and Mr. Koji Ichimura of Graduate School of Science, The University of Tokyo are greatly appreciated.

I wish to thank emeritus professor, Prof. Minoru Ozima and Prof. Ichiro Kaneoka of The University of Tokyo. They taught me ideal and honorable attitudes toward science a lot.

I am grateful to Dr. Wataru Fujiya of College of Science, Ibaraki University, for constructive discussion and valuable comments for the present study.

Dr. Hirochika Sumino of Graduate School of Arts and Sciences, The University of Tokyo, helped me a lot in another ongoing work during my doctoral course. His comments are exact and important.

I thank Ms. Akemi Furusho and Ms. Hidemi Hibino secretaries at AORI, The

University of Tokyo, for their kind helps in various situations. Without their supports, I could not achieve this study.

I appreciate Dr. Masako Hori, Dr. Atsuko Yamazaki, Dr. Yama Tomonaga, Dr. Kentaro Tanaka, Dr. Yasuhisa Nakajima, Dr. Satoko Motai, Dr. Zhongwu Lan, Dr. Hyunwoo Lee, Dr. Naoko Sugihara, Dr. Tomihiko Higuchi, Mr. Yoshihiro Ota, Ms. Yui Amemiya, Mr. Naoya Kinoshita, Mr. Satoki Onda, Ms. Teresa Escobar, Mr. Takuya Morita, and those described above, all current/former members in our group, for their daily discussion, technical helps and friendly relationship.

I thank Mr. Kohei Fukuda, Mr. Atsushi Takenouchi of Graduate School of Science, The University of Tokyo, members in room 838, and all members in the seminars, for sharing constructive discussion, fruitful time and friendship.

Finally, I appreciate my parents for allowing me to choose this way. They supported me financially and mentally.

This research was partly supported by JSPS KAKENHI grants 16J07403.

## TABLE OF CONTENTS

<b>ABSTRACT</b>	· · · · ·	p. 1
<b>ACKNOWLEDGEMENTS</b>	· · · · ·	p. 4
<b>CHAPTER 1. General Introduction</b>	· · · · ·	p. 10
<b>1.1. Planetary Formation History: Insights from Meteorites</b>	· · ·	p.12
<b>1.2. Differentiated Meteorites: Samples from Ancient Differentiated Bodies</b>		
1.2.1. Classification and General Description of Meteorites	· · · · ·	p.15
1.2.2. Eucrites: Ancient Crusts on Asteroid 4–Vesta & Vesta-like Protoplanets	· · · · ·	p.20
1.2.3. Mesosiderites: Records of Early Impact Between Differentiated Body(ies)	· · · · ·	p. 21
<b>1.3 Radiometric Dating and <i>in-situ</i> Analyses of Extraterrestrial Materials</b>		
1.3.1. General description of radiometric dating	· · · · ·	p. 22
1.3.2. Uranium–Lead dating	· · · · ·	p. 24
1.3.3. Hafnium–Tungsten dating	· · · · ·	p. 29
<b>1.4. Research Objective</b>	· · · · ·	p. 32
<b>CHAPTER 2. In-situ U-Pb dating of phosphate minerals</b>		
<b>in basaltic eucrites</b>	· · · · ·	p. 33
<b>2.1. Introduction</b>	· · · · ·	p. 35

## **2.2. Sample Descriptions**

2.2.1 Juvinas	• • • • •	p. 38
2.2.2 Camel Donga	• • • • •	p. 40
2.2.3 Stannern	• • • • •	p. 41
2.2.4 Agoult	• • • • •	p. 42
2.2.5 Ibitira	• • • • •	p. 43

## **2.3. Analytical Methods**

2.3.1. SEM and EPMA observations	• • • • •	p. 47
2.3.2. NanoSIMS 50 U-Pb dating of phosphates	• • • • •	p. 48

## **2.4. Results**

### 2.4.1. Textural Observations of Phosphates in the Investigated Samples

2.4.1.1. Textural observations: Juvinas	• • • • •	p. 49
2.4.1.2. Textural observations: Camel Donga	• • • • •	p. 53
2.4.1.3. Textural observations: Stannern	• • • • •	p. 56
2.4.1.4. Textural observations: Agoult	• • • • •	p. 56
2.4.1.5. Textural observations: Ibitira	• • • • •	p. 61

### 2.4.2. U-Pb dating

2.4.2.1. U-Pb dating: Juvinas	• • • • •	p. 67
2.4.2.2. U-Pb dating: Camel Donga	• • • • •	p. 70
2.4.2.3. U-Pb dating: Stannern	• • • • •	p. 70

2.4.2.4. U-Pb dating: Agoult	• • • • •	p. 73
2.4.2.5. U-Pb dating: Ibitira	• • • • •	p. 73
<b>2.5. Discussion</b>	• • • • •	p. 81
2.5.1. Examinations of the textural and chronological properties of the individual eucrites		
2.5.1.1. Examination of individual chronology: Juvinas	• • • •	p. 82
2.5.1.2. Examination of individual chronology: Camel Donga	• •	p. 88
2.5.1.3. Examination of individual chronology: Stannern	• • •	p. 91
2.5.1.4. Examination of individual chronology: Agoult	• • • •	p. 94
2.5.1.5. Examination of individual chronology: Ibitira	• • • •	p. 97
2.5.2. Comparison with other chronologies	• • • • •	p. 100
2.5.3. Closure Temperature of U-Pb System in Phosphates of the Basaltic Eucrites	• • • • •	p. 106
2.5.4. Thermal History of the Eucrite Parent Body	• • • • •	p. 109
<b>3.6. Conclusions</b>	• • • • •	p. 114

## **CHAPTER 3. In-situ U-Pb and Hf-W dating of a young zircon**

<b>in a mesosiderite, Asuka 882023</b>	• • • •	p. 116
<b>3.1. Introduction</b>	• • • • •	p. 118
<b>3.2. Sample Descriptions and SEM Observations</b>	• • • • •	p. 123
<b>3.3 Analytical Conditions: NanoSIMS 50 U-Pb and Hf-W Dating</b>		
3.3.1. U-Pb dating	• • • • •	p. 125

3.3.2. Hf-W dating	• • • • •	p. 126
<b>3.4 Results</b>		
3.4.1. U-Pb dating	• • • • •	p. 129
3.4.2. Hf-W dating	• • • • •	p. 130
3.4.3. Examinations of the potential interference effects for W isotopes		p. 135
3.4.4. Calculations of the NanoSIMS relative sensitivity factor for Hf/W ratios		
3.4.5. SEM observation of rutile in Asuka 882023	• • • • •	p. 139
<b>3.5. Discussion</b>	• • • • •	p. 145
3.5.1. Evaluations of U-Pb and Hf-W age results	• • • • •	p. 145
3.5.2. Comparison of the old magmatic zircons and the young metamorphic zircons in mesosiderites	• • • • •	p. 148
3.5.3. Chronological constraints from this study and the literature information	• • • • •	p. 150
3.5.4. Estimation of possible evolutionary history for mesosiderite parent body	• • • • •	p. 151
<b>3.6. Conclusions</b>	• • • • •	p. 158
<b>CHAPTER 4. General discussion</b>	• • • • •	p. 159
<b>CHAPTER 5. General Conclusions</b>	• • • • •	p. 173
<b>REFERENCES</b>	• • • • •	p. 177
<b>APPENDIX</b>	• • • • •	p. 205

# CHAPTER 1

## GENERAL INTRODUCTION

Records in extraterrestrial samples have helped us a lot to understand the solar system history. Differentiated meteorites are fragments of the ancient protoplanets that experienced planetary-scale melting and differentiation. Because most of the differentiated protoplanets, except for asteroid 4–Vesta, do not exist at present day, meteoritical records are important. Radiometric ages of the differentiated meteorites provide thermo-chronological constraints on the parent bodies' processes, including accretion, igneous crystallization, thermal metamorphism, and/or impact destructions. The purpose of this study is to elucidate the evolutionary history of rocky bodies, especially, Vesta and Vesta-like protoplanets. Here, I investigate thermal metamorphic histories of the two differentiated meteorites groups: eucrites and mesosiderites. The key technique in the present study is *in-situ* U-Pb and Hf-W dating using NanoSIMS 50 with the high spatial resolutions (ca. 10 $\mu$ m). The *in-situ* analytical techniques have strong advantages when samples experienced highly complicated metamorphisms, which is typical case for the ancient meteorites.

In Chapter 1, I describe general background and research objective of the present study. In section 1.1, I summarize the current understanding concerning

planetary formation processes, along with the literature chronological data of meteorites. Meteorites classifications and the detailed descriptions of certain meteoritical groups are summarized in section 1.2. I describe the basic principle of chronometric methods and brief history of analytical technique in section 1.3. Finally, the goal of this study is stated in section 1.4. Individual projects, the main parts of the present study, are reported in the following chapter 2 and 3.

### **1.1. Planetary Formation History: Insights from Meteorites**

Elucidation of the formation histories of our solar system is a long-standing issue that attracts attentions worldwide. Questions such as “when, how and from what did our Earth formed?” have been discussed in various ways for centuries. Theoretical standard model for the planetary formation was established during 1970s–1980s (e.g. Hayashi et al., 1985). It was considered that rocky planets (e.g. Earth) formed on site from earlier protoplanetary disk, going through submicron-sized dusts, km-sized planetesimals, 100s–1000s km-sized protoplanets, and finally to Earth-sized planets. This concept was regarded to be plausible for several decades. Along with the recent discoveries of an increasing numbers of exoplanetary systems, more dynamic formation models have been proposed, which consider nebular gas instability and/or planetary migrations (e.g. Youdin and Shu, 2002; Youdin and Goodman, 2005; Walsh et al., 2011; DeMeo et al., 2014; Ida and Guillot, 2016). The comprehensive model of the planetary formation model is under reconstruction and has not been fixed yet.

Timing of the individual formational stages, such as formation of small bodies and their accretion to larger bodies, planetary-scale melting and differentiation, can be constrained from chronological records in meteorites. According to Hf-W system in several differentiated meteorites (e.g. Kruijer et al., 2017a), the early planetesimals with sizes of  $\geq 60$ km were melted and differentiated within the first  $\sim 0$ –1 Myr after the solar system formation (i.e. formation timing of Ca-Al-rich inclusions), because of the decay heat from short-lived radioactive nuclides (e.g.  $^{26}\text{Al}$ ). For details

of the meteorites classifications and the basic principle of key chronologies (U-Pb and Hf-W in present study), I describe in the following section 1.2 and 1.3, respectively. The meteoritical records also suggest that Vesta and Vesta-sized ( $R \sim 300\text{km}$ ) protoplanets may have accreted within 3–5 Myr after CAI. The early small bodies subsequently differentiated into metallic core, olivine-rich mantle, and basaltic crusts within a few million years (e.g. Lugmair and Shukolyukov, 1998; Srinivasan et al., 1999, 2007; Kleine et al., 2004, 2005; Touboul et al., 2015). Much larger planets, e.g. Mars-sized bodies, accreted during  $\leq 10$  Myr after CAI, followed by the magma ocean stage  $\sim 10\text{--}15$  Myr later (Kleine et al., 2009; Kruijer et al., 2017b). Final formation of the terrestrial planets by giant impacts should have occurred during  $\sim 30\text{--}100$  Myr.

Our current knowledge of the planetary formation largely depends on information from the surviving bodies, such as Vesta, Mars, Moon and Earth. One of the largest challenges in revealing the formation history is the apparent scarcity of surviving protoplanets. Although small rocky bodies (100s km – 1000km) may have been common in the early solar system, most of them were lost during planetary formation. Vesta, a large rocky asteroid in the inner main-belt, is an important protoplanet that retains ancient records of the planetary evolutions. The early spectroscopic study identified Vesta has basaltic surface compositions (e.g. McCord et al., 1970). It is inferred that Vesta experienced global melting and differentiation. This was confirmed in 2012, when Nasa's Dawn mission revealed surface mineralogy, geochemistry, and internal structure of Vesta (e.g. Russell et al., 2012). Indeed, Vesta

is the sole survivor of ancient differentiated protoplanets known to date, and is expected to have witnessed the planetary evolutionary events. The records on Vesta help a lot to establish the planetary formation model, especially at 100s km-sized protoplanet stage.

An additional important advantage of Vesta is that we have large amounts of collections from its crusts as meteorites (section 1.2.2 and chapter 2). Mineralogical, geochemical and chronological data from the meteorites have revealed Vesta's formational and evolutionary history to a great extent. Several anomalous meteorites are known to be not from Vesta, but from Vesta-like unknown bodies, which may not exist today (see also section 1.2.3 and chapter 3). It is helpful to extract accurate chronological records from the various differentiated meteorites, which were initially part of the past protoplanets, to establish the general idea concerning the planetary formation and evolution. In the following sections 1.2 and 1.3, I describe the basic information concerning meteorites and chronological methods. The present research objective is shown in section 1.4.

## **1.2. Differentiated Meteorites: Samples from Ancient Differentiated Bodies**

In this section, I describe the general classifications of meteorites and their explanations briefly. Subsection 1.2.1. concerns the traditional scheme. Specific descriptions of eucrites and mesosiderites, which I mainly investigate in the present study, are in subsection 1.2.2 and 1.2.3, respectively.

### **1.2.1. Classification and General Description of Meteorites**

Meteorites are natural extraterrestrial samples that tell us the early days of the planetary bodies in our solar system. According to the traditional classification, they are generally categorized in the two: chondritic meteorites (chondrites) and non-chondritic meteorites (summarized in Krot et al., 2014). Recent studies have suggested an alternative classification based on the stable isotopic anomalies, which indicates genetic links between various meteoritical groups (Warren, 2011; Kruijjer et al., 2017). Although their ideas seem to be important, those issues go beyond the purpose of the present study.

Chondrites consist mainly of chondrules and Fe-Ni metals embedded in fine-grained matrix with Ca-Al-rich refractory inclusions (CAI) and amoeboid olivine aggregates (AOA). According to mineralogy, geochemistry and oxygen isotopes ( $\Delta^{17}\text{O}$ ), chondrites are divided into several groups; carbonaceous (C), ordinary (O), enstatite (E), and minor groups (e.g. R and K; Table 1.2A). Although most chondrites suffered thermal metamorphisms and/or hydrothermal alteration in various levels,

they did not experience differentiation of their parent bodies.

Non-chondritic meteorites experienced total/partial melting and planetary differentiation on their parent bodies. They are classified into three: stony (achondrites), stony-irons, and iron meteorites, based on their major compositions and textures. Achondrites are defined as those were significantly melted and have no chondritic textures, such as chondrules or CAIs (Krot et al., 2014). Based on the melting and differentiation degrees, they are categorized into: non-differentiated (primitive) achondrites, differentiated achondrites and planetary (i.e. Lunar and Martian meteorites). Boundary between the primitive and the differentiated achondrites is unclear. Primitive achondrites have igneous and/or metamorphic textures with nearly chondritic bulk compositions (Prinz et al., 1983). Their parent bodies are likely to have experienced severe thermal events with partial melting, but not totally differentiated. In contrast, differentiated achondrites have mineralogical, chemical and isotopic features that are characterized of planetary-scale melting and differentiation. Among them, howardites–eucrites–diogenites (HED) clan is the largest groups, which are considered to be crustal samples from asteroid 4-Vesta (McCord et al., 1970; Conslomagno and Drake, 1977; McSween et al., 2011, 2013). Eucrites have basaltic compositions, whereas diogenites are more orthopyroxene-rich. Howardites are mixed breccia of the two. Most HEDs have almost identical oxygen isotopic compositions ( $\Delta 17O$ ), suggesting their same origin, although there are some anomalous meteorites (Wiechert et al., 2004; Greenwood et al., 2005; 2012). The genetic link between HED and Vesta

has been strongly supported from the early spectroscopic studies (McCord et al., 1970) and the recent investigations from Nasa's Dawn mission at Vesta (McSween et al., 2013). For eucrites, I will describe in the following section 1.2.2 and discuss their chronological records in Chapter 2 in this thesis.

Stony-irons composed of roughly equal amounts of silicates and Fe-Ni metals with some troilites. There are two main groups in stony-irons, mesosiderite and pallasites. The former is a mixture of eucrite-like (eucritic) basalts and metals, whereas the latter composed of olivine crystals, metal and troilite. Formation processes of the two groups are considered to be significantly different. Mesosiderites are often associated with impact of Vesta-like parent body(ies) (Wasson and Rubin, 1985; Rubin and Mittlefehldt, 1993; Scott et al., 2001; Koike et al., 2017; Haba et al., 2017). Pallasites are considered to be from core-mantle boundaries of differentiated parent body that is similar or same to certain magmatic irons such as IIIAB (Mittlefehldt et al., 1998), although several other models have been also proposed for their origins (Yang et al., 2010; Danielson et al., 2009; summarized in Benedix et al., 2014). For mesosiderites, I will explain the detail in the following subsection 1.2.3 and discuss their possible origins and history in Chapter 3 in this thesis.

Iron meteorites, alloys of metallic Fe-Ni with sulfides and carbides, are samples of interior of differentiated bodies (e.g. Wasson, 1967; Scott and Wasson, 1975; Buchwald, 1975; summarized in Krot et al., 2014 and Benedix et al., 2014). Isotopic compositions of radiogenic  $^{182}\text{W}$  ( $\epsilon^{182}\text{W}$ ) in various iron meteorites indicates

their significantly early formation, suggesting core-formation of their parent bodies within the first 1–3 Myr after CAI (Kleine et al., 2009; Kruijer et al., 2017).

Among them, in this thesis, I focus on eucrites, a group of HEDs, and mesosiderite, a unique stony-iron group.

**Table 1.2A.** Classifications of meteorites and their possible parent bodies. Modified after Krot et al. (2014). Original data source is Meteoritical Bulletin Database: <https://www.lpi.usra.edu/meteor/>

Type	Meteorites Group	Origins/ Parent Body
<i>chondritic</i>		
Carbonaceous	CI, CM, CR, CO, CV, CK, CH, CB	
Ordinary	H, L, LL	
Enstatite	EH, EL	
Others	Kakangari-like Rumuruti-like	
<i>non-chondritic, stony</i>		
<i>primitive achondrites</i>	Acapulcoites	
	Lodranites	
	Winonaites	
	Angrites	
	Aubrites	
	Brachinites	
	Ureilites	
	<i>HED meteorites</i>	
	- Eucrites	mostly, Vesta
	- Diogenites	
	- Howardites	
<i>differentiated achondrites</i>	<i>Martian meteorites</i>	
	- Shergottites	
	- Nakhilites	
	- Chassignites	
	- Orthopyroxenite (ALH 84001)	Mars
	- Regolith breccia (NWA7034 + pairs)	
	Lunar meteorites	Moon
<i>non-chondritic, stony-iron</i>		
	Pallasites	core-mantle boundary of differentiated bodies?
	Mesosiderites	mixtures of crustal silicates of differentiated body with Fe-Ni metal
<i>non- chondritic, irons</i>		
magmatic	IIAB, IIIAB, IIIE, IVA, IVB	
non-magmatic (silicate-bearing)	IAB, IIICD, IIE,	

### 1.2.2. Eucrites: Ancient Crusts on Asteroid 4–Vesta & Vesta-like Protoplanets

Howardites–eucrites–diogenites (HED) clan is the largest achondrites groups and the only asteroidal samples whose parent body have been well estimated, possibly asteroid 4–Vesta (McCord et al., 1970). Vesta is the unique differentiated rocky asteroid known to date, which has the core–mantle–crust layered structure (e.g. Russel et al., 2012; Clenet et al., 2014). Our present ideas concerning ancient accretion and differentiation processes of the asteroidal sized protoplanets ( $\sim 10^2$  km) largely depend on the records of Vesta. The mineralogical, geochemical and chronological information of HEDs helped us to reveal the evolutionary history of the asteroids (e.g. Mittlefehldt, 2014). Eucrites, the largest group in HEDs, are samples from ancient basaltic crusts of the asteroids. They are chemically basaltic and texturally subdivided in the two, cumulates and non-cumulates (basaltic) (Basaltic Volcanism Study Project, 1981). Although most eucrites share the identical bulk  $\Delta^{17}\text{O}$  with other HEDs ( $\Delta^{17}\text{O} = -0.246 \pm 0.014\text{‰}$ ; Greenwood et al., 2005), there are several anomalies such as Ibitira (Wiechert et al., 2004; Scott et al., 2009). For this meteorite, I report its chronology in the following Chapter 2. The existence of such anomalous eucrites, with similar mineralogy and geochemistry but different  $\Delta^{17}\text{O}$ , suggests that differentiated Vesta-like protoplanets were likely to be common in the inner solar system at the planetary formation periods.

### **1.2.3. Mesosiderites: Records of Early Impact Between Differentiated Body(ies)**

Mesosiderites, a unique group of stony irons, are mixtures of roughly equal amounts of silicates and Fe–Ni metals. Their silicate parts composed of brecciated basalts with some gabbroic and pyroxene-rich textures (Powell, 1971). Mineralogical and geochemical studies, as well as bulk  $\Delta^{17}\text{O}$  compositions, suggest the genetic link between mesosiderites silicates and those of eucrite (e.g. Powell, 1971; Floran, 1978; Mittlefehldt, 1979, 1980, 1990; Hewins, 1984; Clayton and Mayeda, 1996; Greenwood et al., 2015). However, no mesosiderite-like silicate-metal mixture was identified among the regolith on Vesta during Dawn’s exploration (Prettyman et al., 2012; Peplowski et al., 2013). On the other hand, mesosiderites metals have almost homogeneous compositions, similar to the magmatic irons such as IIIAB (Wasson and Rubin, 1985; Clayton et al., 1986; Hassanzadeh et al., 1990). It is suggested the metal was molten state at the time of silicate-metal mixing of mesosiderites. Previous studies proposed several plausible models to explain the mesosiderites formation (e.g. Wasson and Rubin, 1985; Rubin and Mittlefehldt, 1993; Scott et al., 2001), such as impact origins between Vesta-like parent body and another differentiated impactor(s), or internal mixing of the parent body during catastrophic destruction by impact. In any case, the unique characters of mesosiderites suggest some impact-related mixing processes for their formation, which may be key for understanding the accretion and evolution history of protoplanets.

### 1.3. Radiometric Dating and *in-situ* Analyses of Extraterrestrial Materials

In this section, I will explain histories and basic principle of radiometric dating methods. Especially, I focus on U–Pb dating (1.3.2) and Hf–W dating (1.3.3), which are mainly utilized in this study.

#### 1.3.1. General description of radiometric dating

Among the age determination methods currently established, radiometric dating is the most robust, reliable and widely used method. Initial discovery of radioactivity and its application to dating were established during 1900–1950s (summarized in Kaneoka, 1998). Decay rates of radioactive nuclides are characteristic of individual decay series and independent from other physical or chemical conditions, such as temperature or pressure, which can provide accurate chronological information. Moreover, large variations of their half-lives, from shorter than a few years to  $10^{10}$  years or more, enables various time scale geo-chronometers. In the present day, a number of radiometric dating, covering wide time scales, are available (Table 1.3A). Most of them use the ratio of parent atoms (P) and daughter atoms (D) to obtain age (t) as:

$$D = D_0 + P_0[1 - \exp(-\lambda t)] \quad (\text{Eq. 1.3A})$$

with characteristic decay constant  $\lambda$ . Subscript ‘0’ means initial values. In addition to Eq. 1.3A, other dating methods have been also established, such as measurements of cosmic-ray-exposure products, and counting of fission-tracks within host rocks (Kaneoka, 1998). The radiometric dating methods (Eq. 1.3A) are generally divided into

two groups, (i) absolute age determination using long-lived radioactive nuclides and (ii) relative age determination with short-lived (extinct) nuclides. The former records accurate absolute age values, whereas the latter provides precise time differences from an age anchor material for a certain periods. In the following subsection, I will describe basic principle and brief analytical histories of two dating methods, U-Pb (subsection 1.3.2) and Hf-W (1.3.3).

**Table 1.3A.** Major long-lived & short-lived radionuclides used for radiometric dating. Half lives are from Allégre (2008) and Birck (2004).

Parent Atoms	Daughter Atoms	Half Life (yr)
<i>long-lived</i>		
$^{40}\text{K}$	$^{40}\text{Ar}$	$1.25 \times 10^9$
$^{87}\text{Rb}$	$^{87}\text{Sr}$	$4.88 \times 10^9$
$^{138}\text{La}$	$^{138}\text{Ce}$	$1.01 \times 10^{11}$
$^{147}\text{Sm}$	$^{143}\text{Nd}$	$1.06 \times 10^{11}$
$^{176}\text{Lu}$	$^{176}\text{Hf}$	$3.5 \times 10^{10}$
$^{187}\text{Re}$	$^{187}\text{Os}$	$4.6 \times 10^{10}$
$^{232}\text{Th}$	$^{208}\text{Pb}$	$1.401 \times 10^{10}$
$^{235}\text{U}$	$^{207}\text{Pb}$	$0.7038 \times 10^9$
$^{238}\text{U}$	$^{206}\text{Pb}$	$4.4683 \times 10^9$
<i>short-lived (extinct)</i>		
$^{26}\text{Al}$	$^{26}\text{Mg}$	$7.3 \times 10^5$
$^{41}\text{Ca}$	$^{41}\text{K}$	$1.0 \times 10^5$
$^{53}\text{Mn}$	$^{53}\text{Cr}$	$3.7 \times 10^6$
$^{60}\text{Fe}$	$^{60}\text{Ni}$	$1.5 \times 10^6$
$^{129}\text{I}$	$^{129}\text{Xe}$	$1.6 \times 10^7$
$^{146}\text{Sm}$	$^{142}\text{Nd}$	$1.03 \times 10^8$
$^{182}\text{Hf}$	$^{182}\text{W}$	$9.4 \times 10^6$
$^{244}\text{Pu}$	Xe (fission)	$8.1 \times 10^7$

### 1.3.2. Uranium–Lead dating

U–Pb dating is one of the traditional dating methods, initially established in 1950–1970s (Ahrens, 1955; Wetherill, 1956; Tera and Wasserburg, 1972). This method uses two decay systems of long-lived radioactive uranium;  $^{238}\text{U} \rightarrow ^{206}\text{Pb}$  (half life of  $4.47 \times 10^9$  yr, corresponding decay constants of  $\lambda_8 = 0.155125 \times 10^{-9} \text{ yr}^{-1}$ ), and  $^{235}\text{U} \rightarrow ^{207}\text{Pb}$  (half life of  $0.704 \times 10^9$  yr,  $\lambda_5 = 0.98485 \times 10^{-9} \text{ yr}^{-1}$ ; Jaffey et al., 1971), respectively. From the  $^{238}\text{U}$ – $^{206}\text{Pb}$  decay system, an absolute  $^{238}\text{U}$ – $^{206}\text{Pb}$  chronology can be obtained as following equation:

$$\left(\frac{{}^{206}\text{Pb}}{{}^{204}\text{Pb}}\right)_t = \left(\frac{{}^{206}\text{Pb}}{{}^{204}\text{Pb}}\right)_0 + \left(\frac{{}^{238}\text{U}}{{}^{204}\text{Pb}}\right)_t [\exp(\lambda_8 t) - 1] \quad (\text{Eq. 1.3B})$$

where,  $({}^{206}\text{Pb}/{}^{204}\text{Pb})_0$  is common lead compositions at the time of U-Pb system closure.  $({}^{206}\text{Pb}/{}^{204}\text{Pb})_t$  and  $({}^{238}\text{U}/{}^{204}\text{Pb})_t$  denote the current isotopic and elemental compositions.

The Eq. 1.3B can be restate in alternative notation, so-called ‘inverse’ (Eq. 1.3C).

$$\left(\frac{{}^{238}\text{U}}{{}^{206}\text{Pb}}\right)_t = \left[1 - \left(\frac{{}^{206}\text{Pb}}{{}^{204}\text{Pb}}\right)_t / \left(\frac{{}^{206}\text{Pb}}{{}^{204}\text{Pb}}\right)_0\right] / [\exp(\lambda_8 t) - 1] \quad (\text{Eq. 1.3C})$$

Figure 1.3A indicates the simplified principle of  $^{238}\text{U}$ – $^{206}\text{Pb}$  system using the inverse isochron. One strong advantage of the U-Pb methods is that we can utilize two chronometers from the two decay systems. Because radiogenic Pb ratios ( ${}^{207}\text{Pb}^*/{}^{206}\text{Pb}^*$ ) also change along with U-Pb decay, Pb isotopic compositions define  ${}^{207}\text{Pb}$ – ${}^{206}\text{Pb}$  chronology as:

$$\frac{\left[ \left( \frac{^{207}\text{Pb}}{^{204}\text{Pb}} \right)_t - \left( \frac{^{207}\text{Pb}}{^{204}\text{Pb}} \right)_0 \right]}{\left[ \left( \frac{^{206}\text{Pb}}{^{204}\text{Pb}} \right)_t - \left( \frac{^{206}\text{Pb}}{^{204}\text{Pb}} \right)_0 \right]} = \left( \frac{^{235}\text{U}}{^{238}\text{U}} \right)_t \frac{[\exp(\lambda_5 t) - 1]}{[\exp(\lambda_8 t) - 1]} \quad (\text{Eq. 1.3D})$$

The subscripts '0' and 't' in the above equation respectively denote the initial and the present isotopic compositions. Figure 1.3B schematically explain  $^{207}\text{Pb}$ – $^{206}\text{Pb}$  isochron.

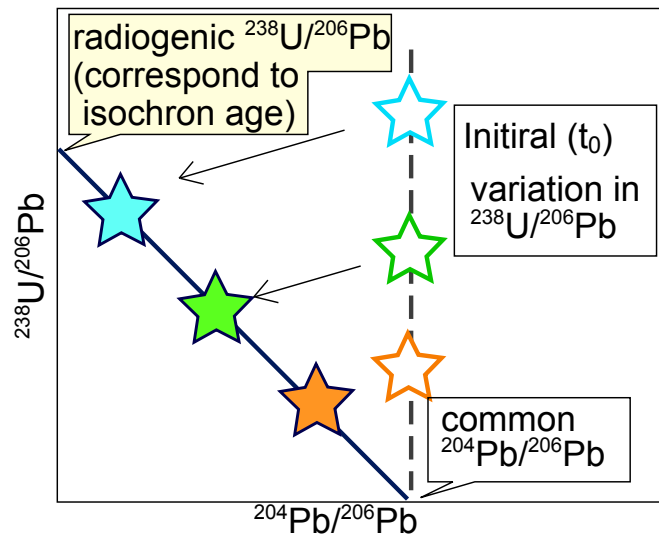


**Figure 1.3A.** Schematic illustration of  $^{238}\text{U}$ – $^{206}\text{Pb}$  isochron evolution (inverse plot). In this diagram, the y-intercept of the isochron (solid line) indicates the  $^{238}\text{U}$ – $^{206}\text{Pb}$  age.

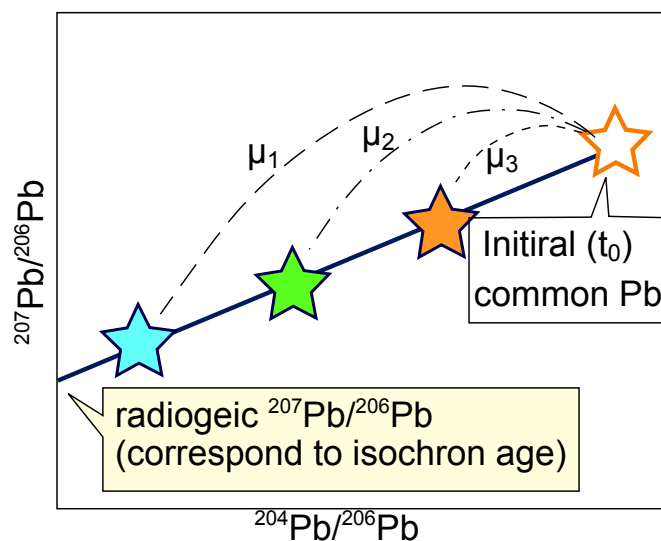


**Figure 1.3B.** Schematic illustration of  $^{207}\text{Pb}$ – $^{206}\text{Pb}$  isochron evolution. The Pb isotopic ratios evolve variously depending on their initial U/Pb ratios ( $\mu$ -value).

In Eq. 1.3D, current  $^{238}\text{U}/^{235}\text{U}$  ratio was considered to be constant at 137.88, both for terrestrial materials (Shields, 1960; Cowan and Adler, 1976) and for extraterrestrial samples (Chen and Wasserburg, 1980). Later high precision analyses revealed significant variations in  $^{238}\text{U}/^{235}\text{U}$  ratios among extraterrestrial samples (Brennecka et al., 2010; Amelin et al., 2010; Bouvier et al., 2011; Iizuka et al., 2014, 2015), which sometimes cause over/underestimate of their ages up to several million years. This is an important problem, especially when for precise chronological differences (i.e. within a few million years) are critical. However, it might not matter discussion for much larger time scales (i.e. 10s Myrs or more). I may assume the constant  $^{238}\text{U}/^{235}\text{U}$  value of 137.88 in this thesis. The two chronometers,  $^{238}\text{U}-^{206}\text{Pb}$  and  $^{207}\text{Pb}-^{206}\text{Pb}$ , provide internal check whether the U-Pb system has been retained after its closure (concordant), or it was disturbed by later events (discordant). Time evolutions of radiogenic  $^{238}\text{U}/^{206}\text{Pb}^*$  and  $^{207}\text{Pb}^*/^{206}\text{Pb}^*$  ratios are calculated uniquely as a reference Concordia curve in a traditional ‘Tera-Wasserburg’ concordia diagram (Fig. 1.3C; after Williams, 1998).

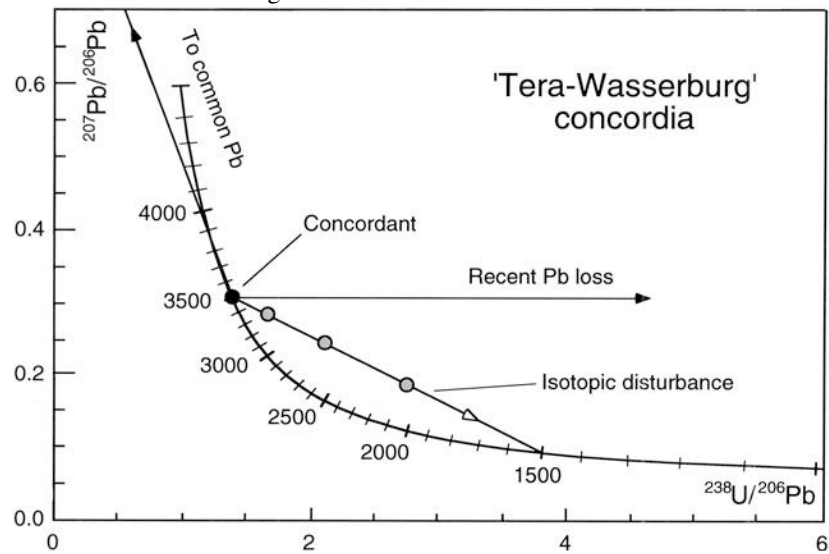


**Figure 1.3C.** Tera-Wasserburg concordia diagram from Williams (1998). The solid curve indicates Concordia curve for U–Pb system. The past isotopic disturbance can be identified as a discordant line (solid line with circles), which is determined from the crystallization age and the disturbance age.

After NASA’s Apollo missions returned lunar samples during 1961–1972, a breakthrough of U–Pb dating methods was invoked from ion microprobe techniques. Pioneering studies conducted the *in-situ* U–Pb dating for various U-bearing minerals in Apollo samples such as zircon, baddeleyite, and apatite (e.g. Andersen and Hinthorne, 1972, 1973). Sensitive High Resolution Ion MicroProbe I (SHRIMP I) was constructed at Australian National University (ANU) in 1974–1979, which enabled the accurate and precise *in-situ* U–Pb dating of zircon in terrestrial and extraterrestrial samples. An improved version SHRIMP II was also constructed in 1992 (summarized in Williams, 1998). In various geological settings, U-rich minerals such as zircon, baddeleyite,

monazite and xenotime are ideal targets for *in-situ* U-Pb dating. Although U concentrations are generally lower, phosphate minerals, e.g. apatite  $[\text{Ca}_5(\text{PO}_4)_3(\text{F},\text{Cl},\text{OH})]$  and merrillite  $[\text{Ca}_{18}\text{Na}_2\text{Mg}_2(\text{PO}_4)_{14}]$ , are next candidates. The first *in-situ* U-Pb dating of terrestrial apatite was established using SHRIMP at Hiroshima University (Sano et al., 1999a). With their *in-situ* dating techniques, along with *in-situ* REE analytical methods (Sano et al., 1999b), a number of chronological studies of extraterrestrial samples, such as Lunar and Martian meteorites, have been investigated (Sano et al., 2000; Terada and Sano, 2003, 2004; Terada et al., 2003, 2005, 2007). Recently, co-authors and I established U-Pb dating protocol for phosphates in Martian meteorites, using NanoSIMS 50 with higher spatial resolution of ca. 10  $\mu\text{m}$  (Koike et al., 2014, 2016).

### 1.3.3. Hafnium–Tungsten dating

Hf–W dating is a relative dating method. It uses extinction of short-lived radioactive  $^{182}\text{Hf}$ , which decays to  $^{182}\text{W}$  with half-life of 8.9 Myr (Wing et al., 1961; Vockenhuber et al., 2004). Hence, Hf–W method provides precise a chronological constraint for early solar system within the first ca. 50 million years. Because both Hf and W are refractory elements, this system is robust to high-temperature processes such as planetary differentiation, and provides a reliable chronology. Moreover, Hf is lithophile whereas W is siderophile. Owing to their different affinities, Hf–W methods have been used to constrain the timings of core–mantle differentiation of terrestrial planets (e.g. Lee and Halliday, 1996; Kleine et al., 2004), as well as silicates differentiation from parent mantle (e.g. Kleine et al., 2005; Touboul et al., 2015).

Using an age anchor with a known absolute age ( $t_0$ ) and initial ( $^{182}\text{Hf}/^{180}\text{Hf}$ )<sub>0</sub> ratio, the time difference between an unknown ( $t$ : absolute age) and the reference can be calculated as following equation (Eq. 1.3):

$$\left(\frac{^{182}\text{W}}{^{184}\text{W}}\right)_t = \left(\frac{^{182}\text{W}}{^{184}\text{W}}\right)_{T_0} + \left(\frac{^{180}\text{Hf}}{^{184}\text{W}}\right) \left(\frac{^{182}\text{Hf}}{^{180}\text{Hf}}\right)_{T_0} [\exp(\lambda(t_0 - t)) - 1] \quad (\text{Eq. 1.3E})$$

where ( $t_0 - t$ ) corresponds to the time difference between the two. For W stable isotope in Eq. 1.3E,  $^{186}\text{W}$  can be used instead of  $^{184}\text{W}$ , as well (Srinivasan et al., 2007; Koike et al., 2017). Figure 1.3C and D schematically explain the evolution curves of radiogenic  $^{182}\text{W}$ , and Hf–W isochron, respectively. The initial  $^{182}\text{Hf}/^{180}\text{Hf}$  ratio was determined for CAI as  $(9.72 \pm 0.44) \times 10^{-4}$  with an absolute  $^{207}\text{Pb}$ – $^{206}\text{Pb}$  age of  $4567.11 \pm 0.16$  Ma

(Burkhardt et al., 2008). Spatial homogeneity of the  $^{182}\text{Hf}/^{180}\text{Hf}$  ratio in early solar system has been confirmed from various ancient chondritic and non-chondritic materials, which have  $^{182}\text{Hf}/^{180}\text{Hf}$  ratios around  $4\text{--}7 \times 10^{-4}$  with the consistent  $^{207}\text{Pb}$ – $^{206}\text{Pb}$  ages of 4558–4565 Ma (Markowski et al., 2007; Kleine et al., 2008).

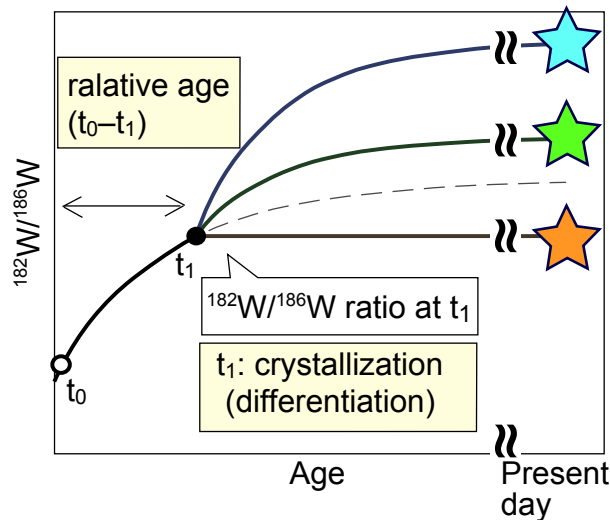


**Figure 1.3C.** Schematic illustration of the  $^{182}\text{W}/^{184}\text{W}$  evolutions. Relative age differences between the anchor ( $t_0$ ) and the crystallization timing ( $t_1$ ) is determined from the present  $^{182}\text{W}/^{184}\text{W}$  variation within the system.

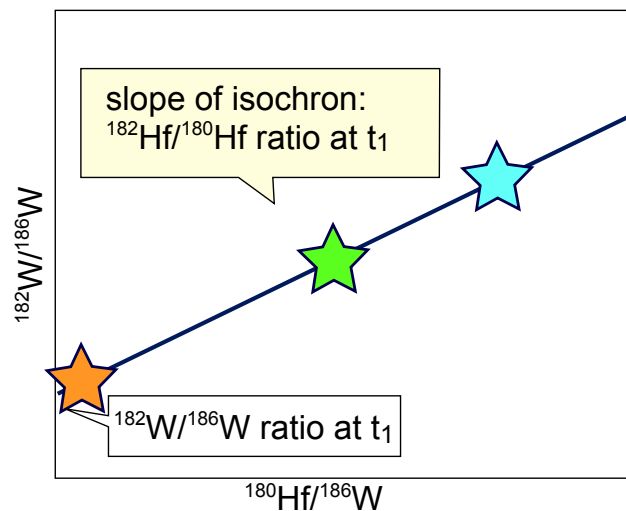


**Figure 1.3D.** Schematic illustration of  $^{182}\text{Hf}$ – $^{182}\text{W}$  isochron. Slope of the isochron indicates initial  $^{182}\text{Hf}/^{180}\text{Hf}$  ratio of the samples, corresponds to relative age of  $t_0$ – $t_1$ .

Zircon is an ideal mineral for Hf–W dating, because it has significantly high concentration of Hf (up to 1–2wt%; Ireland, 1991), while W concentration is 4–6 orders of magnitude lower. Ireland (1991) tried to determine initial  $^{182}\text{Hf}/^{180}\text{Hf}$  ratios of meteoritic zircons using in-situ analyses with ion microprobe, which was failed to determine the significant values because of technical problem at that period. Later, Ireland and his collaborators established the *in-situ* Hf–W methods of meteoritic zircons using SHRIMP-RG at Stanford University, with high mass resolution and high sensitivity (Ireland et al., 2000; Ireland and Bukovanská, 2003). Srinivasan et al. (2007) applied the improved Hf–W methods, which were originally proposed by Ireland and Bukovanská (2003), for Cameca IMS-1270 at the Swedish Museum of Natural History, Stockholm (Nordsims facility). With their *in-situ* technique, Srinivasan et al. (2007) determined crystallization ages of ancient zircons in eucrites. Roszjar et al. (2016) also investigated *in-situ* Hf–W ages of eucritic zircons and revealed their age variations, using Cameca IMS-1280 at Nordsims facility. Detailed interpretations concerning the chronologies of eucritic zircons are discussed in Chapter 2 in this thesis. Recently, co-authors and I have established the high spatial resolution ( $\leq 10 \mu\text{m}$ ) *in-situ* Hf–W dating methods of zircon using NanoSIMS 50, and have revealed the metamorphic history of mesosiderite zircon (Koike et al., 2017; Described in Chapter 3 in this thesis).

#### 1.4. Research Objective

As I described in the above sections, differentiated meteorites from the past protoplanets may have experienced both internal thermal processes (i.e. magmatism and prolonged thermal metamorphisms) and external processes (i.e. impact-induced brecciation and reheating, destruction and/or reaccrction). Chronological records in the meteorites provide valuable constraints on timings and scales of the past protoplanetary events, which will help a lot to establish the comprehensive model of the planetary evolution. The goal of this study is to reveal the evolutionary history of Vesta and Vesta-like protoplanets, by obtaining thermo-chronological constraints from the various differentiated meteorites. Previously, co-authors and I established *in-situ* U-Pb dating protocols of meteoritic phosphates, using NanoSIMS 50 with high spatial resolution (Koike et al., 2014; 2016). Applying the improved *in-situ* dating techniques, I investigate igneous and/or metamorphic events of the ancient protoplanets, which were recorded in the meteoritic phosphates and zircons.

In the following Chapter 2 and 3, I report the investigation of the individual cases, the crustal metamorphic history of the known asteroid, Vesta (in Chapter 2), and the impact and reheating history of the unknown parent body of mesosiderites (in Chapter 3). Finally, combining the present chronological data, I would discuss the general evolutionary history of the early differentiated protoplanets.

## CHAPTER 2

# IN-SITU U-Pb DATING OF PHOSPHATE MINERALS IN BASALTIC EUCRITES

In Chapter 2, I report the chronological study of *in-situ* U-Pb analyses of phosphates in basaltic eucrites. Eucrites, the largest group of ancient basaltic achondrites, are considered to be from asteroid 4–Vesta, which is the sole surviving differentiated protoplanet. Chronological records of eucrites provide us valuable insight concerning the planetary formation and evolution histories in the early solar system. However, due to the complicated metamorphisms of eucrites (e.g. multiple impact brecciation, thermal metamorphisms and/or hydrothermal alterations), it is difficult to obtain adequate interpretation. Previous studies have conducted *in-situ* U-Pb and Hf-W dating of zircons in eucrites, which recorded high-temperature magmatic and/or thermal events. Most eucrites should have experienced moderate thermal processes as well, which are possibly retained by U-Pb system in the phosphates. The goal of this study is to understand the evolutionary history of the ancient crusts on Vesta and Vesta-like protoplanets. To reveal the comprehensive history, I conduct *in-situ* U-Pb dating of phosphates in basaltic eucrites, using NanoSIMS 50, and discuss the new findings with literature data. The U-Pb dating protocols applied in this study were established in the

other projects, which were reported previously (Koike et al., 2014, 2016). This study is the first report of *in-situ* U-Pb analyses of phosphates in the basaltic eucrites.

In section 2.1, I introduce the background and goal of this study. In section 2.2, 2.3 and 2.4, I describe the analyzed samples, the analytical methods, and the results, respectively. Combining chronological and mineralogical results, in section 2.5, interpretations of the phosphates chronological records are discussed. By comparing them to literature data, I discuss the evolutionary history of the basaltic crusts on differentiated planetesimals.

## 2.1. Introduction

Eucrites are the largest group of Howardite–Eucrite–Diogenite (HED) achondrite clan (Krot et al., 2014; Mittlefehldt, 2014; summarized in Chapter 1.2). From spectroscopic studies, as well as mineralogy and geochemistry, most of HEDs are considered as samples from asteroid 4-Vesta (e.g. McCord et al., 1970; Conslomagno and Drake, 1977). The identical oxygen isotopic compositions ( $\Delta^{17}\text{O}$ ) of HEDs also suggest their common origin (Clayton and Mayeda, 1996; Greenwood et al., 2005), although there are several anomalous meteorites such as Ibitira (Wiechert et al., 2004; Scott et al., 2009). In 2012, Nasa's Dawn mission revealed detailed mineralogical, geochemical and geophysical properties of Vesta, which strongly support the link between HEDs and Vesta's crusts (Russel et al., 2012; McSween et al., 2011, 2013; Clenet et al., 2014). Consequently, HED meteorites can be regarded as crustal samples from the ancient protoplanets, whose geophysical, geochemical and chronological features have been well investigated. Among HEDs, eucrite are chemically basaltic, Ca-pyroxene rich rocks. They are subdivided into cumulate and non-cumulate (basaltic) types (Basaltic Volcanism Study Project, 1981). Because eucrites are representative of the ancient crusts on Vesta, they are expected to provide valuable knowledge about the formation and evolution histories of Vesta-like protoplanets. The meteorites recorded when and how the protoplanets accreted, differentiated, and possibly, were destructed in the early solar system.

Most eucrites show highly brecciated and thermally metamorphosed textures, suggesting complicated impact-induced brecciation and reheating events and/or hydrothermal alterations (e.g. Duke and Silver, 1967; Palme et al., 1988; Takeda and

Graham, 1991; Metzler et al., 1995; Yamaguchi et al., 1996, 2001, 2009; Treiman et al., 2004). Chronological records of eucrites help to understand their complicated histories. A number of previous studies investigated their thermo-chronologies using various radiometric systems, such as Mn-Cr, Al-Mg, Hf-W, Sm-Nd, Rb-Sr, U-Pb and K-Ar (e.g. Podosek and Huneke, 1973; Lugmair, 1974; Lugmair and Scheinin, 1975; Ireland and Bukovanská, 1992; Bukovanská and Ireland, 1993; Bogard and Garrison, 1995, 2003; Kunz et al., 1995; Shukolyukov and Begemann, 1996; Tera et al., 1997; Lugmair and Shukolyukov, 1998; Srinivasan et al., 1999, 2007; Kleine et al., 2004, 2005; Misawa et al., 2005; Zhou et al., 2013; Iizuka et al., 2013, 2014, 2015; Touboul et al., 2015; Roszjar et al., 2016). These studies suggest that Vesta's crusts suffered multiple discrete thermal processes: magmatic formation, reheating by internal heat of Vesta, and impact-induced brecciation and reheating. Such events occurred at different timings. It is inferred that single meteorite samples have the overprinted multiple records of the igneous and metamorphic events with different ages. This may compromise adequate interpretation of the meteorite records. On that point, it is helpful to conduct *in-situ* dating using SIMS with high spatial resolutions (see also Chapter 1.3). Previous studies have reported *in-situ* U-Pb and Hf-W dating of zircons in several basaltic eucrites (Misawa et al., 2005; Zhou et al., 2013; Iizuka et al., 2015; Srinivasan et al., 2007; Roszjar et al., 2016), which suggested the high-temperature thermal events for Vesta's crusts during ca. 4560–4530 Ma. Based on experimental studies and literatures of natural samples, U-Pb system in zircon is known to have high closure temperatures of generally  $\geq 900$  °C (e.g. Cherniak and Watson, 2000). Although no experimental study is conducted, closure temperature of Hf-W system in zircon is estimated to be higher

than the U-Pb (Roszjar et al., 2016). Both U-Pb and Hf-W system in the zircons recorded magmatic to subsolidus events on Vesta's crust, while more moderate events may not have been recorded. The K-Ar system represents lower temperature ranges around 300°C (e.g. Cassata et al., 2009). However, bulk  $^{40}\text{Ar}$ -K /  $^{40}\text{Ar}$ - $^{39}\text{Ar}$  dating methods might have large uncertainties, due to the multiple disturbances in the eucrites. In order to understand the comprehensive history of the ancient crustal evolution of the asteroid, it is necessary to obtain additional *in-situ* thermo-chronological records at the moderate temperature ranges. Apatites  $[\text{Ca}_5(\text{PO}_4)_3(\text{F},\text{Cl},\text{OH})]$  and merrillites  $[\text{Ca}_9(\text{PO}_4)_7\text{Na}(\text{Mg},\text{Fe}^{2+},\text{Mn}^{2+})]$  are common accessory Ca-phosphate minerals found in basaltic achondrites. They are important carriers of incompatible elements in igneous melts, such as U, Th, REE, halogens and H<sub>2</sub>O. Generally, U-Pb systematics of apatite provide a reliable and useful thermo-chronometer with closure temperature of ~450–600°C (Cherniak et al., 1991; Chamberlain and Bowring, 2000). The temperature ranges are middle between U-Pb in zircon and K-Ar in plagioclase. U-Pb system in the apatite may be helpful to reveal the complicated history of Vesta's crust.

Previously, I established *in-situ* U-Pb dating protocols of phosphates using NanoSIMS 50, which were reported as my initiative works with co-authors (Koike et al., 2014, 2016). The goal of this study is to reveal thermal history of Vesta's crusts. Especially, I focus on moderate temperature events, which were not recorded by U-Pb or Hf-W in zircon, but retained by U-Pb in phosphates. Here, I report the *in-situ* U-Pb dating of phosphates in several basaltic eucrites, along with their mineralogies. This is the first study of *in-situ* U-Pb ages of eucrites phosphates. Combining the new findings and literatures, the evolutionary history of Vesta's crust is discussed.

## **2.2. Sample Descriptions**

I have selected four basaltic eucrites (Juvinas, Camel Donga, Stannern, Agoult) and a unique basaltic achondrite, Ibitira, for this study. To reveal the highly complicated histories of the asteroidal crusts, it is important to compare a certain chronometric system (i.e. U-Pb in phosphates, in this study) among various samples, as well as to compare various chronometers (e.g. U-Pb, Hf-W, Sm-Nd, Rb-Sr and K-Ar) within a certain sample. The above five meteorites are common and well-investigated eucrites, whose mineralogies, geochemistries and some chronologies are available from literatures. Their metamorphic histories are complicated and different to each other. All of them were thermally metamorphosed to various levels (see following subsections and Table 2.1). Of the five, three (Juvinas, Camel Donga and Stannern) are monomict breccia. The others (Agoult and Ibitira) are unbrecciated basalt. Ibitira is considered to have originated from a distinct unknown parent body (2.2.5), whereas the others are from Vesta. In this section, I will explain previous knowledge of these meteorites. The literature data described in the following are summarized in Table 2.1.

### **2.2.1. Juvinas:**

Juvinas is one of representative basaltic eucrites, which was witnessed to fall in 1821 in France. The total mass was 91 kg. A number of previous studies reported petrology, mineralogy and chemistry of this meteorite (e.g. Duke and Silver, 1967; Basaltic Volcanism Study Project, 1981; Takeda and Graham, 1991; Takeda and Yamaguchi, 1991; Metzler et al., 1995; Barrat et al., 2000). Juvinas is a monomict breccia composed of igneous clasts embedded in fine-grained matrix (Metzler et al.,

1995). The lithic clasts have textural variations, including coarse-grained ophitic and fine-grained subophitic lithologies. The matrix is characterized with porous re-crystallized fragments (Metzler et al., 1995). The pyroxenes were chemically equilibrated, suggesting severe thermal metamorphism (Takeda and Graham, 1991). According to the thermal metamorphic levels based on the pyroxene equilibration, which was proposed by Takeda and Graham (1991), Juvinas is classified to type 5. Type 1 is least metamorphosed, and type 6 pyroxene is highly equilibrated and recrystallized. The previous studies proposed complicated igneous and metamorphic history for Juvinas, including rapid crystallization, multiple impact brecciation and subsequent reheating events (e.g. Metzler et al., 1995).

Trace incompatible elements concentrations of Juvinas by bulk analysis are characterized with a flat pattern,  $\geq 10 \times$  CI chondrites, and absence of significant Eu anomaly (Barrat et al., 2003, 2007). Juvinas is the representative of Main Group-Nuevo Laredo trend eucrites, whose chemical trends can be successfully explained by sequential fractional crystallization from the magma ocean of chondritic parent body (Barrat et al., 2000, 2003, 2007; and references there in).

Previous chronological studies of Juvinas revealed its crystallization and/or metamorphic timings in various radiometric systems.  $^{53}\text{Mn}$ - $^{53}\text{Cr}$  internal isochron of Juvinas showed an ancient age of  $4562.5 \pm 1.0$  Ma (Lugmair and Shukolyukov, 1998). Slightly younger ages around 4560–4545 Ma were reported from U-Pb dating of its zircon (Bukovanská and Ireland, 1993; Lee et al., 2009; Zhou et al., 2013) and Hf-W internal isochron (Kleine et al., 2005; Touboul et al., 2015), as well as Sm-Nd (Lugmair, 1974) and Pu-Xe systems (Shukolyukov and Begemann, 1996; Miura et al., 1998). The

internal  $^{207}\text{Pb}$ - $^{206}\text{Pb}$  isochron age of Juvinas silicates was as younger as 4320 Ma (Galer and Lugmair, 1996), suggesting later disturbance. The K-Ar system of Juvinas indicate additional thermal event, probably around 4100–4000 Ma (Kaneoka et al., 1995).

### **2.2.2. Camel Donga:**

Camel Donga is also a basaltic eucrite with brecciated textures. It was found in 1984, in Western Australia. The total mass was 25 kg. The petrology, chemistry and light noble gases (He, Ne, Ar) of Camel Donga were initially documented by Palme et al. (1988). It composed of coarse-grained igneous clasts embedded in fine-grained recrystallized matrix. Chemical compositions between the coarse-grained areas and the fine-grained areas are almost same, indicating Camel Donga is a monomict breccia (Palme et al., 1988). The igneous clasts contain various lithologies from ophitic to rapidly cooled variolitic to subophitic textures, possibly because of several impact brecciation, mixing, and thermal annealing events after igneous crystallization (Metzler et al., 1995). Chemical compositions of its Ca-pyroxene were equilibrated, suggesting Camel Donga belongs to type 5 in the thermal metamorphic grade (Palme et al., 1988; Takeda and Graham, 1991). They also pointed that the anomalously high abundances of metallic irons (2%) in Camel Donga. This may be because the primary Fe-sulfides and silicates ( $\text{FeS}$  and  $\text{FeSiO}_3$ ) were reduced by evaporation and escape of sulfur during high temperature event (Palme et al., 1988). The petrological and chemical features suggest that Camel Donga should have suffered impact brecciation and subsequent high temperature metamorphism for several times.

Trace incompatible elements concentrations of Camel Donga by bulk analysis

showed flat patterns, which were similar to Juvinas and distinctly different to Stannern (Palme et al., 1988). Geochemical trends of Camel Donga are similar to the other Main Group eucrites (Barrat et al., 2000).

Several chronological studies have investigated this meteorite until recent. Its  $^{182}\text{Hf}$ - $^{182}\text{W}$  internal isochron determined an absolute age of 4545 Ma (Kleine et al., 2005; Touboul et al., 2015). Meanwhile, the younger age variations between ca. 4500–4530 Ma have been reported from U-Pb systems in zircon (Zhou et al., 2013) and pyroxene (Iizuka et al., 2013), as well as from Pu-Xe system (Shukolyukov and Begemann, 1996; Miura et al., 1998). A significantly younger  $^{40}\text{Ar}$ -K age of ca. 3670 Ma was also reported, suggesting the later disturbances of K-Ar system due to shock reheating (Palme et al., 1988).

### **2.2.3. Stannern:**

Stannern is also one of the representative basaltic eucrites, which fell in 1801 in Czech. The total mass was 52 kg. A number of previous works investigated its petrology, mineralogy, chemistry and chronology (e.g. Duke and Silver, 1967; Birck and Allegre, 1978; Basaltic Volcanism Study Project, 1981; Takeda and Graham, 1991; Ireland and Bukovanska, 1992; Yamaguchi et al., 1994, 1996; Metzler et al., 1995; Tera et al., 1997; Barrat et al., 2000; Kleine et al., 2005; Touboul et al., 2015). As similar to Juvinas and Camel Donga, Stannern contains igneous clasts with various textural features, as well as fine-grained matrix and shock melt veins (Metzler et al., 1995). Although texturally polymict, homogeneous chemical compositions indicate this meteorite is a monomict breccia. Its pyroxene compositions show moderate thermal

equilibration, whereas remnant igneous zoning is also observed (Takeda and Graham, 1991). According to the thermal metamorphic classification by Takeda and Graham (1991), Stannern belongs to type 4. This means Stannern was less thermally metamorphosed compared to the other studied eucrites (Juvinas, Camel Donga and Ibitira: type 5 and Agoult: granulite; Table 2.1). Stannern also contains recrystallized mesostasis, although the degrees of recrystallization seem to be lower than those of Juvinas (Metzler et al., 1995). Shock melt veins intersect various lithic clasts and matrix, suggesting a later stage impact (Metzler et al., 1995).

Chemically, Stannern is enriched in alkali (Na and K) and rare earth elements, with significant negative Eu anomaly (Stolper, 1977; Basaltic Volcanism Study project, 1981). The chemical compositions of Stannern and other similar eucrites (Stannern trend) can be explained by mixing of the Main Group eucritic magma and the partially melted asteroidal crust (Barrat et al., 2007).

Various radiometric ages have been reported previously for Stannern. The  $^{182}\text{Hf}$ - $^{182}\text{W}$  mineral isochron age is as old as 4564 Ma (Kleine et al., 2005; Touboul et al., 2015). Slightly younger ages of ca. 4500–4450 Ma are reported from  $^{207}\text{Pb}$ - $^{206}\text{Pb}$  of its zircon (Ireland and Bukovanska, 1992) and  $^{147}\text{Sm}$ - $^{143}\text{Nd}$  isochron (Lugmair and Scheinin, 1975). Meanwhile, Rb-Sr, U-Pb system in silicates, as well as K-Ar chronologies were severely disturbed during 3000–4130 Ma (Birck and Allegre, 1978; Podosek and Huneke, 1973; Kunz et al., 1995; Tera et al., 1997).

#### **2.2.4. Agoult:**

Agoult is a monomict unbrecciated basaltic eucrite, which were found in 2000

in Morocco with total mass of 86 gram. Terrestrial weathering at hot desert was insignificant (Barrat et al. 2003). Yamaguchi et al. (2009) reported its textural and geochemical properties along with other metamorphosed eucrites. Agoult is an unbrecciated granulite. Its fine-grained granulitic textures with 120° triple junctions indicate the significant recrystallization during high temperature metamorphism. Remnant igneous subophitic features can be observed everywhere, characterized with elongated plagioclase and granular pyroxenes. The pyroxenes are equilibrated between homogeneous pigeonite and fine (~1µm) augite lamellae (Yamaguchi et al., 2009). The previous study also reported REE compositions of Agoult by bulk analysis, which are depleted in light-REE compared to Juvinas. The LREE-depletion is associated with partial remelting of primary basalt of Agoult and subsequent removal of the melt.

Limited numbers of chronological studies have been conducted for this meteorite. The  $^{207}\text{Pb}$ - $^{206}\text{Pb}$  age of Agoult zircon was precisely determined as  $4554.5 \pm 2.0$  Ma (Iizuka et al., 2015), which is identical to Pb-Pb ages of zircons among other basaltic eucrites (Misawa et al., 2005; Zhou et al., 2013). The Pb-Pb age of plagioclase is somewhat younger than zircon, as  $4532.4 \pm 0.8$  Ma (Iizuka et al., 2013).

#### **2.2.5. Ibitira:**

Ibitira is an anomalous basaltic achondrite, which was found in Brazil in 1957 with total mass of 2.5 kg. In terms of general mineralogy and chemistry, Ibitira is like an unbrecciated, thermally metamorphosed basaltic eucrite (Wilkening and Anders, 1975; Steele and Smith, 1976; Takeda and Graham, 1991; Yamaguchi et al., 1996; Miyamoto et al., 2001). It shows strongly recrystallized textures and relict subophitic

igneous features with elongated plagioclase (Steele and Smith, 1976). Its equilibrated high-Ca and low-Ca pyroxenes indicate the considerable annealing. According to pyroxene thermal metamorphic grades provided by Takeda and Graham (1991), Ibitira is classified into type 5. The thermal metamorphic temperature has been estimated from the equilibration of Ca-pyroxenes as ca. 1100°C (Yamaguchi et al., 1996; Miyamoto et al., 2001), slightly exceeding the melting point of eucritic melt (Stolper et al., 1977). The partial remelting of Ibitira has been also suggested from existence of large euhedral tridymite crystals, which may have crystallized from eutectic melting of primary phases (Hervig et al., 1986; Yamaguchi et al., 1996). Meanwhile, despite many similarities with other eucrites, several unique features of Ibitira indicate this meteorite is an anomalous achondrite from different parent body. Ibitira contains abundant spherical vesicles (~5-7 vol.%), suggesting significant degassing from igneous magma (Wilkening & Anders, 1975; McCoy et al., 2006). Alkali metals (Na, K, Rb) are considerably depleted (Stolper 1977; Mittlefehldt, 1987). Moreover, its  $\Delta^{17}\text{O}$  value of -0.07‰ (Wiechert et al., 2004; Scott et al., 2009) is significantly higher than the eucrite fractionation line with  $\Delta^{17}\text{O} = -0.246 \pm 0.014$  ‰ (Greenwood et al. 2005).

Various chronological studies reported ancient ages for this meteorite. Short-lived Mn-Cr isochron was determined as 4557  $\pm$  2/-4 Ma (Lugmair and Shukolyukov, 1998), although its Hf-W mineral isochron was disturbed (Kleine et al., 2005). The similar and more precise Pb-Pb age was obtained from its pyroxene as 4556.75  $\pm$  0.57 Ma (Iizuka et al., 2014). Its Pu-Xe age is also as old as 4581  $\pm$  25 Ma (Shukolyukov and Begemann, 1996), whereas Sm-Nd and Ar-Ar systems are somewhat younger, around 4470Ma (Prinzhofer et al., 1992; Bogard and Garrison, 1995).

**Table 2.1.** Summary of the investigated basaltic eucrites and Ibitira with literature data.

name	fall/ found	parent body	brecciation	thermal metamorphism	partial remelting
Juvinas	fall	Vesta	monomict	equilibration of Ca-pyroxenes (metamorphic type 5 [1]); recrystallization of mesostasis; euhedral tridymite crystal [2]	yes [2], this study
Camel Donga	fouled	Vesta	monomict	equilibration of Ca-pyroxenes with remnant zoning; recrystallization of mesostasis; melt dike [2]; metallica Fe from reduction of FeS, Fe(SiO <sub>3</sub> ) [3]	yes [2]
Stannern	fall	Vesta	monomict	equilibration of Ca-pyroxenes with remnant zoning (metamorphic type 4 [1]); recrystallization of mesostasis; melt dike [2]	yes [2]
Agoult	found	Vesta	unbrecciated	fine-grained granulitic texture; recrystallization and exsolution of secondary minerals [4][5]	yes; residue of the melt [4]
Ibitira	fall	unknown	unbrecciated	fine-grained hornfelsic texture [6]; recrystallization of mesostasis; euhedral tridymite crystal [7]	yes [7]

**Table 2.1.** (continued) Summary of chronological data.

name	Mn-Cr	Hf-W	Sm-Nd	Pb-Pb zircon	Pb-Pb silicates	Pb-Pb phosphates	K-Ar/ Ar-Ar	others
Juvinas	4562.5 ± 1.0	4545.7 ± 3.6 4545.6 ± 2.5	4560 ± 80	4545 ± 15	4320 ± 1.7	apatite: 4529 ± 34 merrillite: 4186 ± 35	4050 ± 50	Pu-Xe: 4551 ± 15 4548 ± 23
Camel Donga		4545.0 ± 3.5 4545.1 ± 6.1		4531 ± 10	4128 ± 16	4458 ± 82	ca. 3670	Pu-Xe: 4521 ± 20 4507 ± 16
Stannern		4564 ± 2.0 4563.7 ± 2.1	4480 ± 70	4550 ± 10	4510.9 ± 1.0	4130 ± 45	4000 ± 200	Rb-Sr: 3100 ± 500
Agoult				4554.5 ± 2.0	4532.2 ± 1.0	4522 ± 11		
Ibitira	4557.4 ± 2.5 4555.9 ± 3.2	disturbed	4460 ± 20		4556.75 ± 0.57	4616 ± 140	4487 ± 15	Pu-Xe: 4581 ± 25

## 2.3. Analytical Methods

### 2.3.1 SEM and EPMA Observations

All samples described in section 2.2 were prepared for SEM-EDS observations and following NanoSIMS analyses. Juvinas, Stannern, Ibitira were mounted in epoxy resin and polished, while Camel Donga and Agoult were prepared as thin sections and carbon coated. These samples were briefly observed using SEM-EDS to locate phosphates in sections. The identified phosphates were then dated using NanoSIMS 50, as described in the following subsection 2.3.2. After the NanoSIMS dating, major elements compositions of the phosphates were analyzed using JXA-8530F (JEOL) installed at the Department of Earth and Planetary Science, The University of Tokyo. A 12 nA electron beam was defocused over 5  $\mu\text{m}$  with accelerating voltage of 15 kV. For all samples, phosphate minerals (i.e. apatite  $[\text{Ca}_5(\text{PO}_4)_3(\text{F}, \text{Cl}, \text{OH})]$  and merrillite  $[\text{Ca}_9(\text{PO}_4)_7\text{Na}(\text{Mg}, \text{Fe}^{2+}, \text{Mn}^{2+})]$ ) with grain sizes of 10–200  $\mu\text{m}$  were identified. Their details are described in the results section 4.1. The 21 elements (Na, Mg, Al, F, Cl, Pb, S, P, Y, Sr, Si, K, Ca, Ti, U, Th, La, Ce, Nd, Mn, Fe) were analyzed on the identified phosphates. The conventional ZAF correction procedures were applied. The detection limits at 99.7% confidential limits ( $3\sigma$ ) were: 0.03wt% for Na, 0.02 wt% for Mg, 0.02 wt% for Al, 0.04 wt% for F, 0.01 wt% for Cl, 0.05wt% for Pb 0.02 wt% for S, 0.03wt% for P, 0.03wt% for Y, 0.04wt% for Sr, 0.02wt% for Si, 0.01wt% for K, 0.02wt% for Ca, 0.03 wt% for Ti, 0.08wt% for U, 0.05 wt% for Th, 0.03 wt% for La, 0.03 wt% for Ce, 0.05 wt% for Nd, 0.02 wt% for Mn, and 0.02 wt% for Fe, respectively. Interfering elements were corrected for F (overlapping of Ce and Nd), Si (Sr), P (Y), Cl (Ce and Nd), K (Nd) Sr (Si), Pb (S and Y), and U (K and Th). In addition to phosphates,

all samples contain silica minerals. The silica phases have been identified using Raman spectrometry in another ongoing study (Ono et al., 2018, and in personal discussion with Ms. H. Ono)

### **2.3.2 NanoSIMS 50 U-Pb dating of phosphates**

After SEM observations, the sample sections were polished again, gold coated, and baked at ca. 100°C in the NanoSIMS air-lock system for a week. The  $^{238}\text{U}$ - $^{206}\text{Pb}$  dating and  $^{207}\text{Pb}$ - $^{206}\text{Pb}$  dating were conducted on the identified phosphate grains in the samples, using NanoSIMS 50 (Ametek Inc.) at Atmosphere and Ocean Research Institute (AORI), the University of Tokyo, Japan. Details of the analytical protocols and the calibration methods for  $^{238}\text{U}$ - $^{206}\text{Pb}$  ages have been established in our previous collaboration works (Koike et al., 2014 and 2016; for detail, see Appendix). A 2nA  $\text{O}^-$  beam was focused with spot size of ca. 10  $\mu\text{m}$ . To obtain  $^{238}\text{U}$ - $^{206}\text{Pb}$  age, secondary ions of  $^{31}\text{P}^+$ ,  $^{43}\text{Ca}^+$ ,  $^{204}\text{Pb}^+$ ,  $^{206}\text{Pb}^+$ ,  $^{238}\text{U}^{16}\text{O}^+$  and  $^{238}\text{U}^{16}\text{O}_2^+$  were collected simultaneously for 600 s per spot. The  $^{207}\text{Pb}$ - $^{206}\text{Pb}$  age was determined on the same spots by cyclically collecting secondary ions of  $^{204}\text{Pb}^+$ ,  $^{206}\text{Pb}^+$ ,  $^{207}\text{Pb}^+$  for ca. 1 hour. A natural apatite standard from Canada, PRAP (Sano et al., 1999), was utilized for the calibration. After the NanoSIMS dating, all identified phosphate grains, except those were completely consumed during the SIMS, were analyzed using EPMA with above conditions (see subsection 2.3.1).

## **2.4. Results**

In the all samples (Juvinas, Camel Donga, Stannern, Agoult and Ibitira), phosphate minerals are identified. They are apatite  $[\text{Ca}_5(\text{PO}_4)_3(\text{F},\text{Cl},\text{OH})]$  and/or merrillite  $[\text{Ca}_9(\text{PO}_4)_7\text{Na}(\text{Mg},\text{Fe}^{2+},\text{Mn}^{2+})]$ . In this section, I firstly report the textural properties along with EPMA results of the individual phosphate grains in the samples (subsection 2.4.1). Then, I report the results of NanoSIMS U-Pb dating in subsection 2.4.2.

### **2.4.1. Textural Observations of Phosphates in the Investigated Samples**

In the brecciated eucrites (i.e. Juvinas, Camel Donga, and Stannern), anhedral to subhedral phosphates grains with various sizes ( $\sim 5 \mu\text{m}$  up to  $200 \mu\text{m}$ ) and highly cracked were observed. In contrast, subhedral to euhedral phosphates ( $\sim 5 \mu\text{m}$  to  $200 \mu\text{m}$ ) found in unbrecciated meteorites (i.e. Agoult and Ibitira). Here, I will describe the textural features of the identified phosphates (apatite and/or merrillite) along with their surrounding lithologies for the individual samples. The EPMA major elements compositions of the phosphates are summarized in Table 2.2.

#### **2.4.1.1. Textural observations: Juvinas**

As previous studies reported (Metzler et al., 1995), various lithic clasts of sub-mm to mm scale were embedded in porous fine-grained matrix in the studied sample. A large euhedral tridymite crystal with  $100 \mu\text{m}$  wide and 2–3 mm long abruptly shows up besides to the coarse-grained lithic clasts (Figure 2.1). As shown in Fig. 2.1B-D, the tridymite crystal locates adjacent to the porous recrystallized area,

composed of silica, plagioclase, high-Ca pyroxene, oxides and phosphates. This porous area contains numerous fine-grained opaque minerals with size variations from submicron to 10 $\mu$ m. Such unique textural features are not observed in the other areas within the studied section.

In the vicinity of the tridymite crystal, I found two apatite grains (Apt. 2 and 3, Figure 2.1B, C) and four merrillite grains (Mer. 1–4, Figure 2.1B, C, E). Two merrillite (Mer. 3, 4) locate adjacent to the tridymite crystal along with plagioclase. The others (Apt. 2, 3 and Mer. 1, 2) locate in the porous areas. Only one apatite grain (Apt. 1) was found in an independent igneous clast. Major elements compositions of Apt. 2 indicate F-rich apatite (Table 2.2). For Apt. 1 and 3, however, grain sizes were so small after the NanoSIMS analyses that the electron beam of EPMA was severely influenced by surrounding silicates (silica and plagioclase), resulting in inaccurate compositions. For the same reason, the apparent compositions of Mer. 1, 3 and 4 in Table 2.2 are likely to be influenced by adjacent silicates.

Figure 2.1. Backscattered electron images of Juvinas sample.

Fig. 2.1A

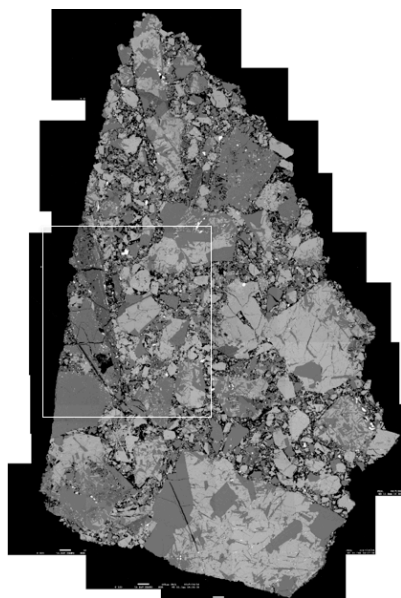


Fig. 2.1B

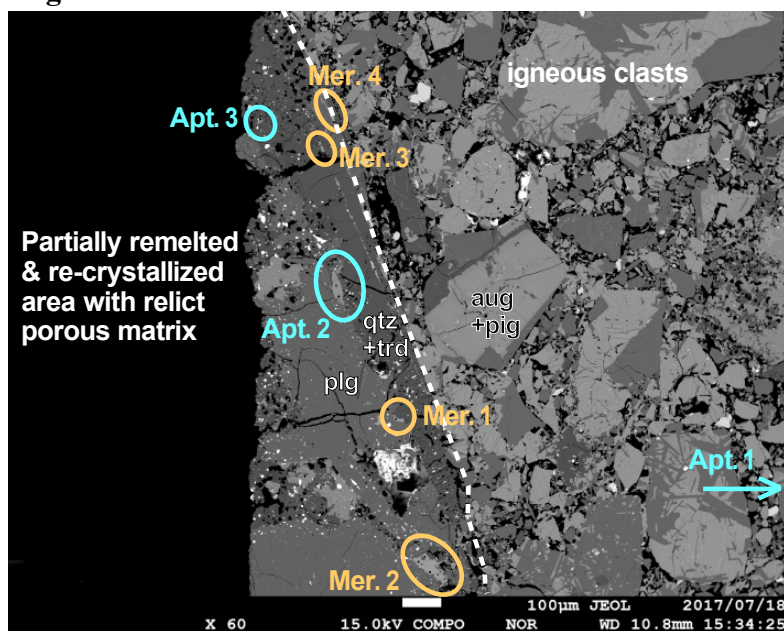


Fig. 2.1C

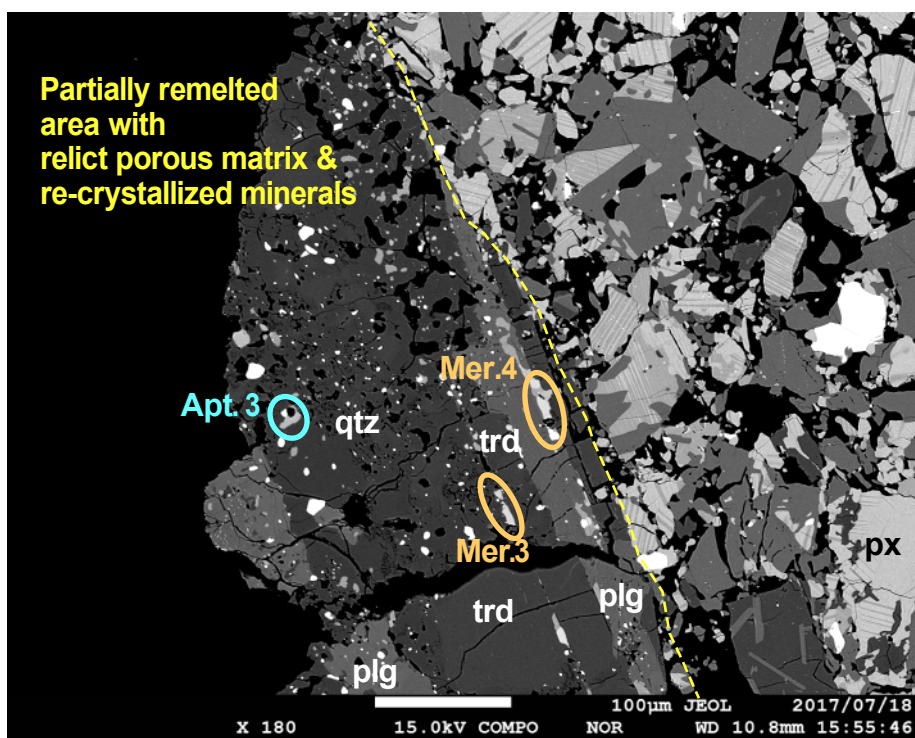


Fig. 2.1D

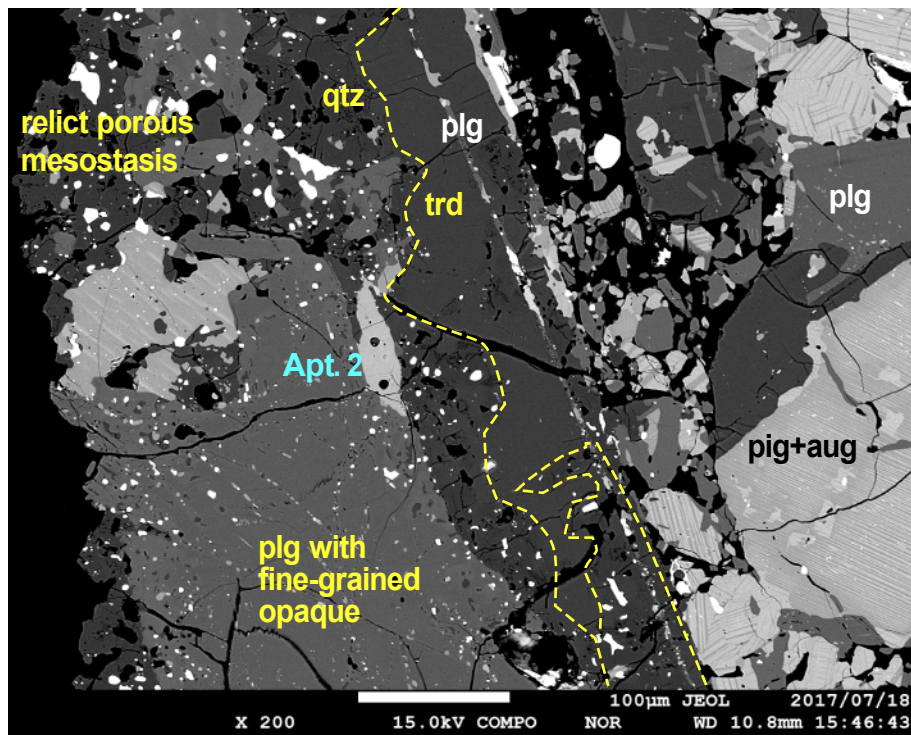
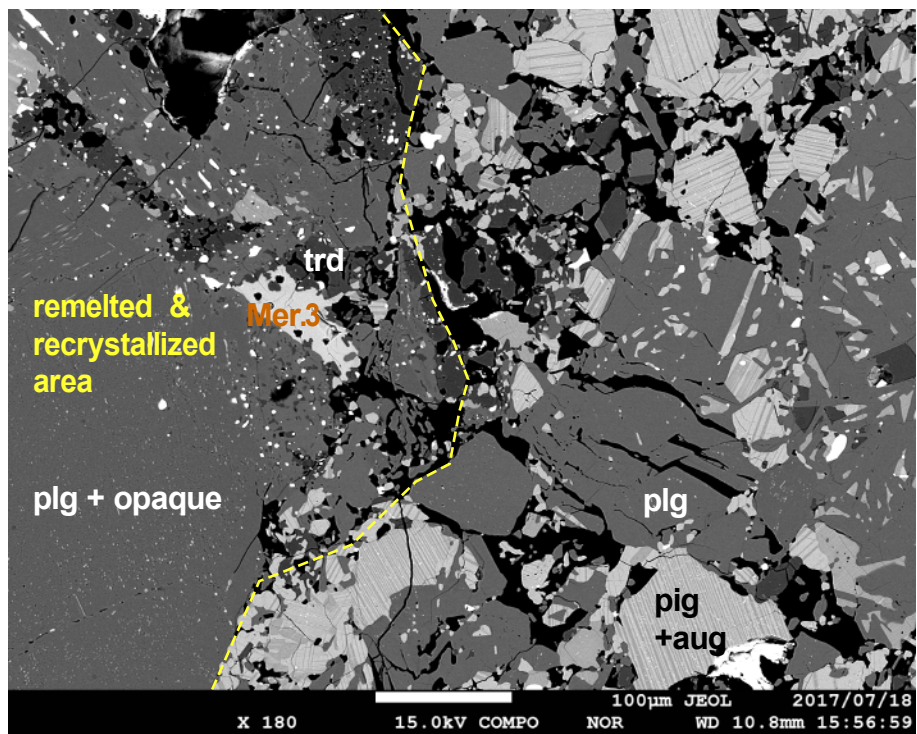


Fig. 2.1E



#### **2.4.1.2. Textural observations: Camel Donga**

Several apatite grains were identified in the studied section. They are anhedral irregular shapes in size variations from ca. 10  $\mu\text{m}$  up to  $> 200 \mu\text{m}$ . Their major elements compositions were almost same to each other and typical F-rich apatite, similar to Juvinas Apt. 2 (Table 2.2). All apatite grains locate in the coarse-grained areas, while fine-grained lithologies were also observed in the vicinity (Figure 2.2B, C). Most apatite grains (Apt. 1–5) locate in close relation to silica, plagioclase, pyroxene, sulfides, metallic Fe and minor ilmenite (Figure 2.2B-D). The metal-rich areas are brownish colored under optical observation. These areas were moderately cracked with fracture-filling oxides and sulfides. The other apatite (Apt. 6, Figure 2.2E) was found in a different lithology with coarse-grained and highly cracked pyroxene and plagioclase. No metallic Fe or silica was identified in this area.

Figure 2.2. Backscattered electron images of Camel Donga sample.

Fig. 2.2A

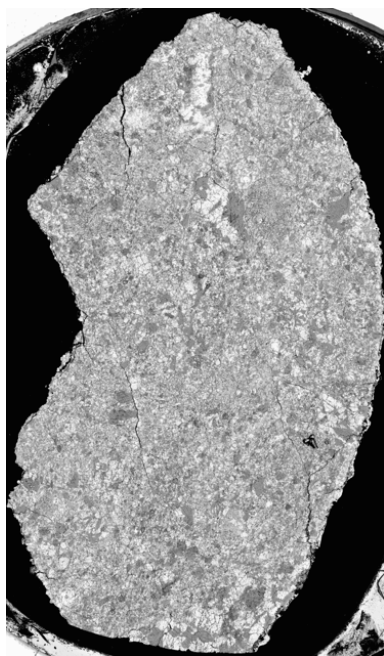


Fig. 2.2B

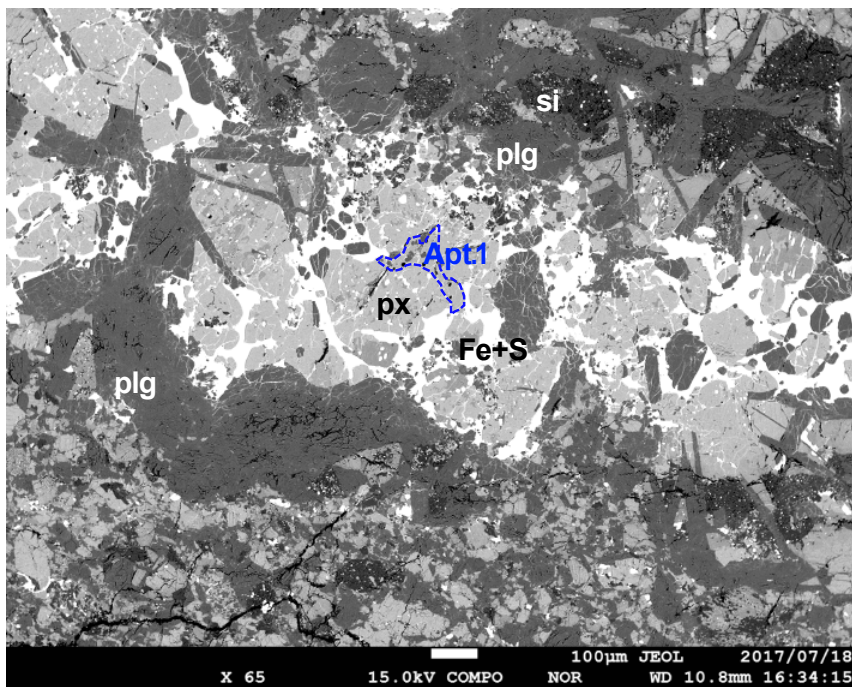


Fig. 2.2C

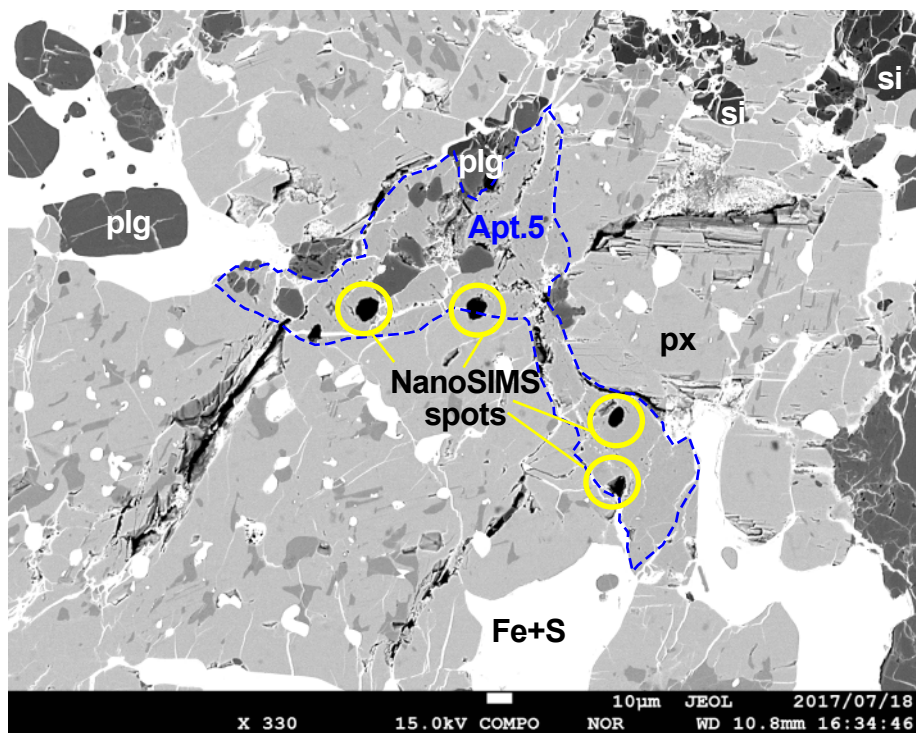


Fig. 2.2D

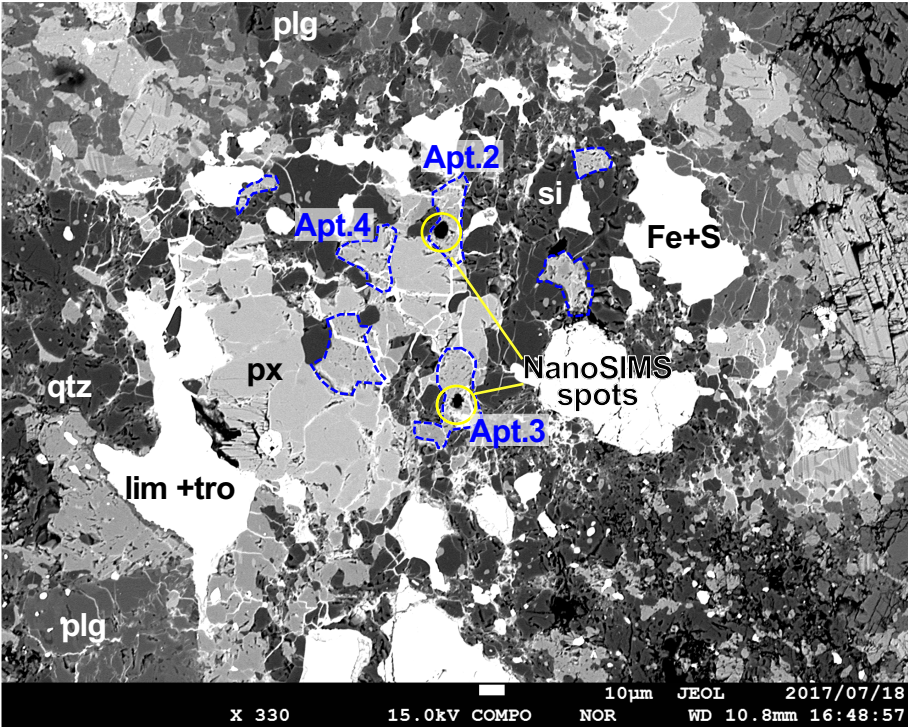
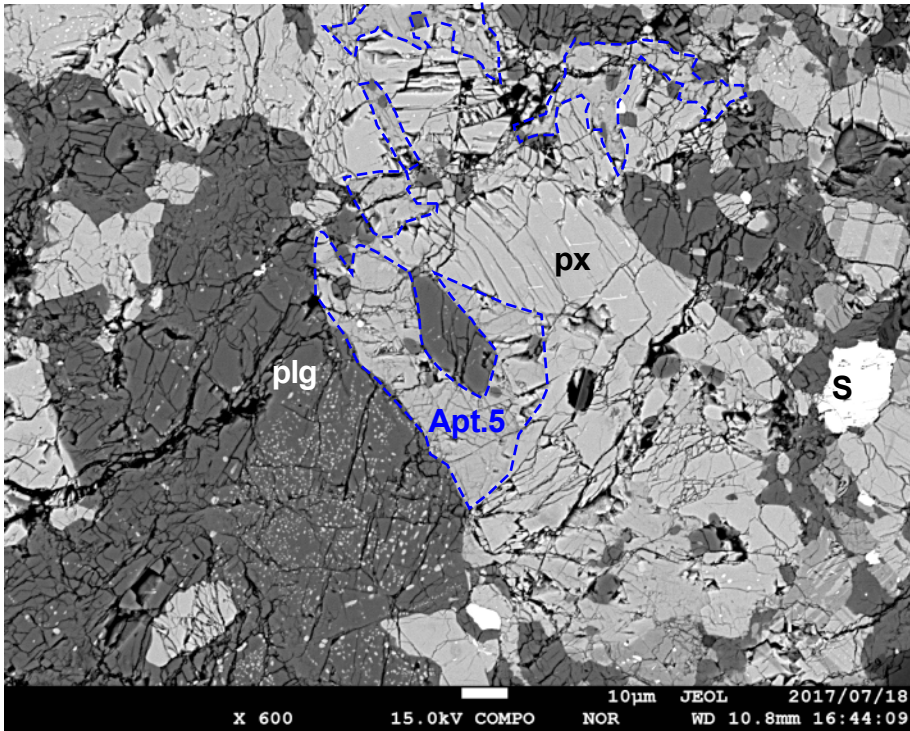


Fig. 2.2E



#### **2.4.1.3. Textural observations: Stannern**

In the studied section, various lithologies including ophitic to subophitic igneous clasts, as well as fine-grained areas and granulitic areas are identified. Several apatite and merrillite grains are found both in the igneous clasts (Figure 2.3D) and in the granulitic areas (Figure 2.3B, C). Major elements compositions are shown in Table 2.2. These apatites are F-rich and similar to those in Juvinas and Camel Donga. The apatites in granulitic clasts show up as intergrowth with ilmenite, plagioclase and silica-rich mesostasis (Figure 2.3B, C). The granulitic clasts, which contain these apatites, locate within the relict igneous clasts composed mainly of high-Ca pyroxene and plagioclase. Numerous fractures intersect both the granulitic clasts and the surrounding igneous clasts. On the other hand, apatite and merrillite in the igneous areas are anhedral grains, which show up with high-Ca pyroxene with lamellae, plagioclase and isolated ilmenite grains (Figure 2.3D). All of them are highly fractured.

#### **2.4.1.4. Textural observations: Agoult**

As Yamaguchi et al. (2009) reported, the homogeneous fine-grained granulitic textures are observed among the analyzed thin section of Agoult. Euhedral to rounded shape apatite grains with size variations of 10–100  $\mu\text{m}$  have been identified (Figure 2.4B, C). The apatite grains often locate with high-Ca and low-Ca pyroxenes, plagioclase, ilmenite, sulfides and tridymite. The major elements compositions of these grains are shown in Table 2.2.

Figure 2.3. Backscattered electron images of Stannern sample.

Fig. 2.3A

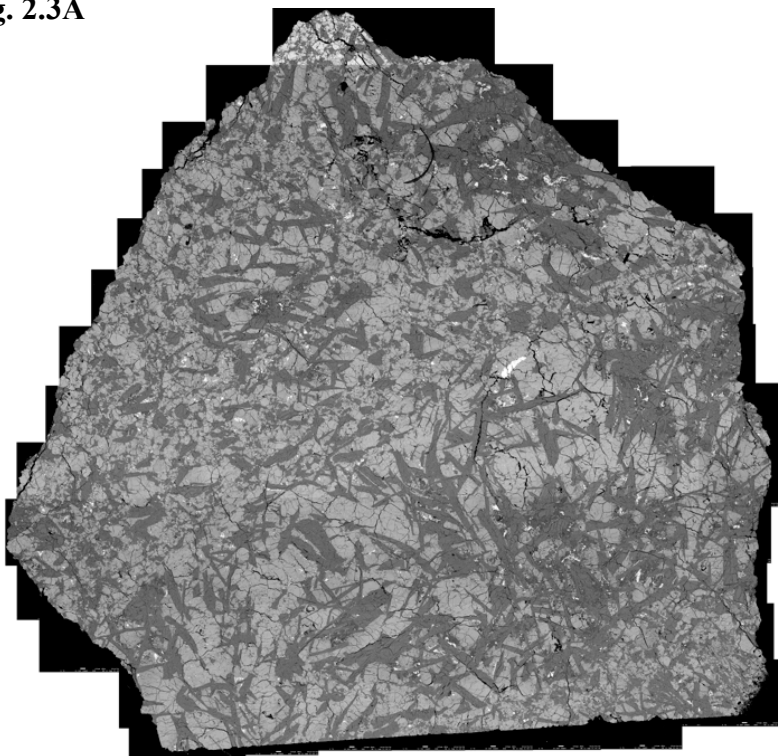


Fig. 2.3B

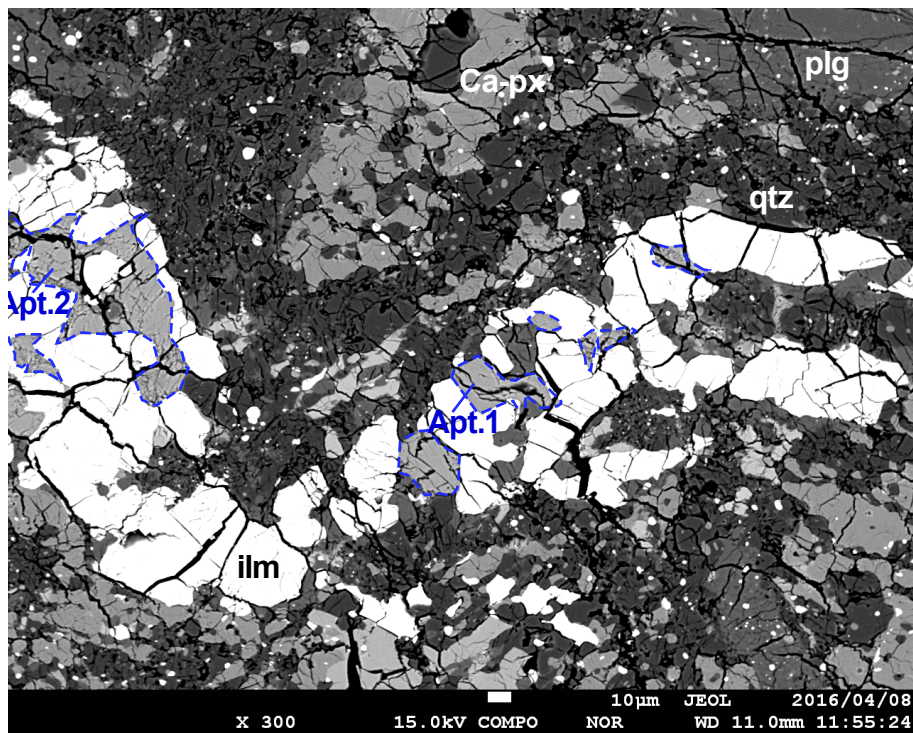


Fig. 2.3C

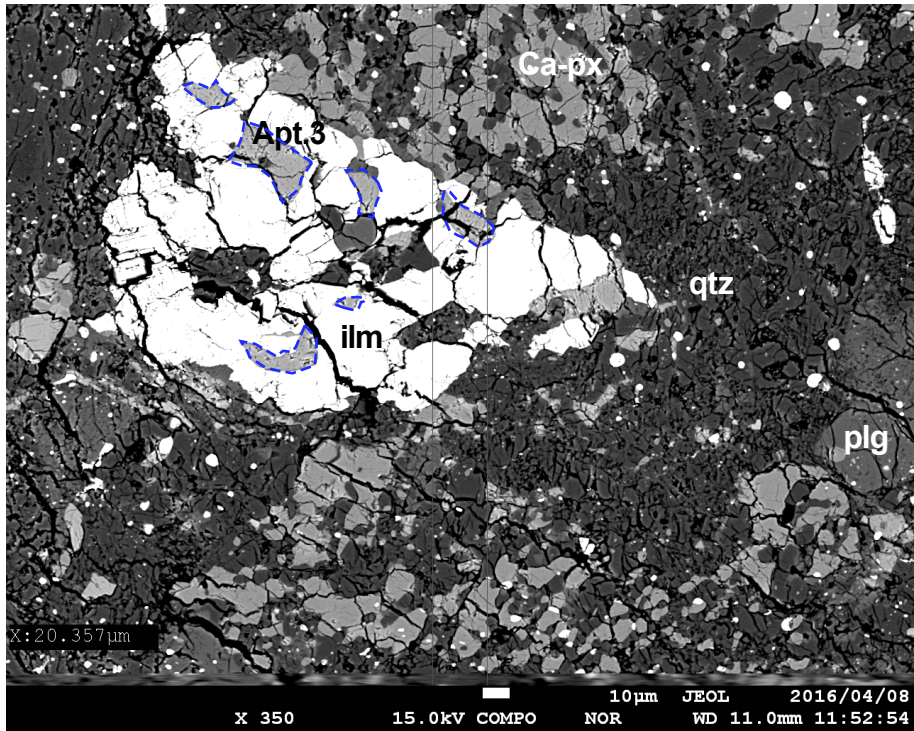


Fig. 2.3D

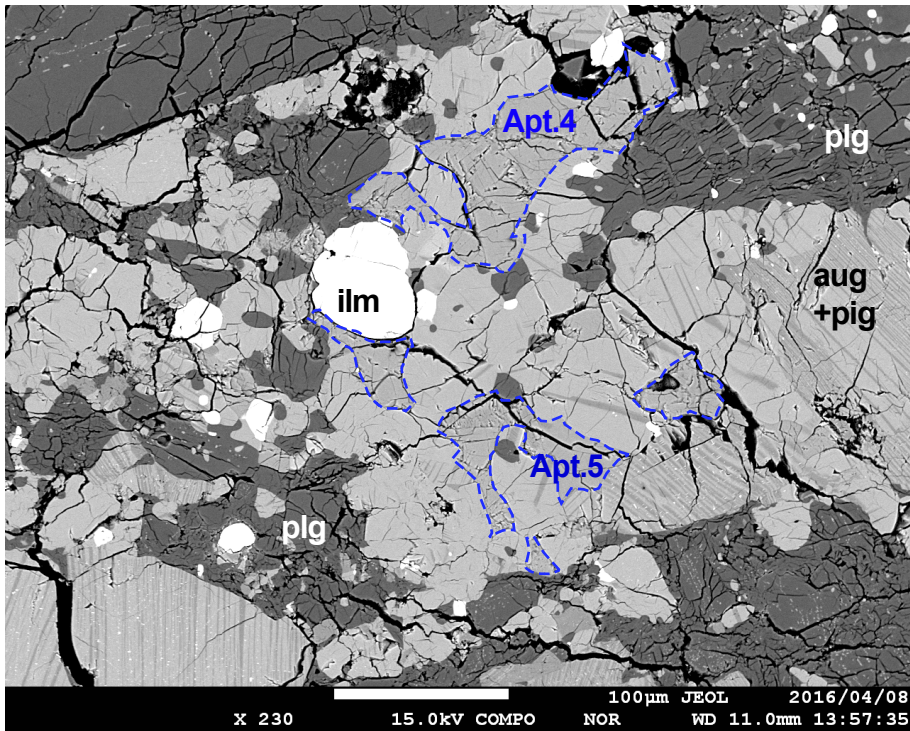


Figure 2.4. Backscattered electron images of Agoult sample.

Fig. 2.4A

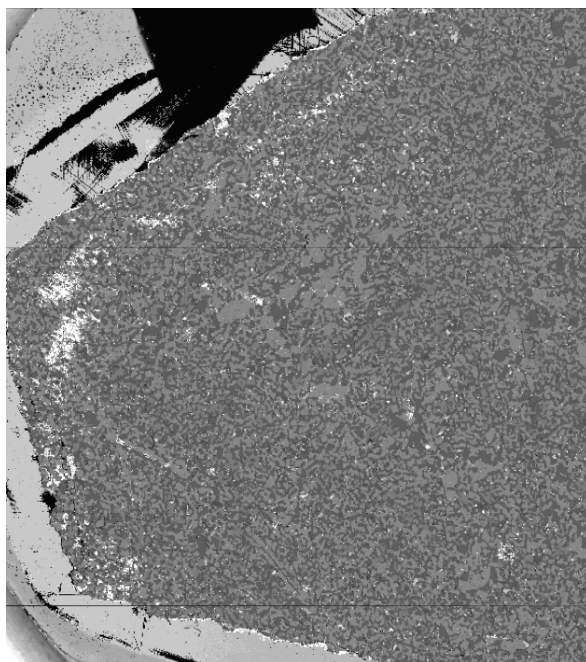


Fig. 2.4B

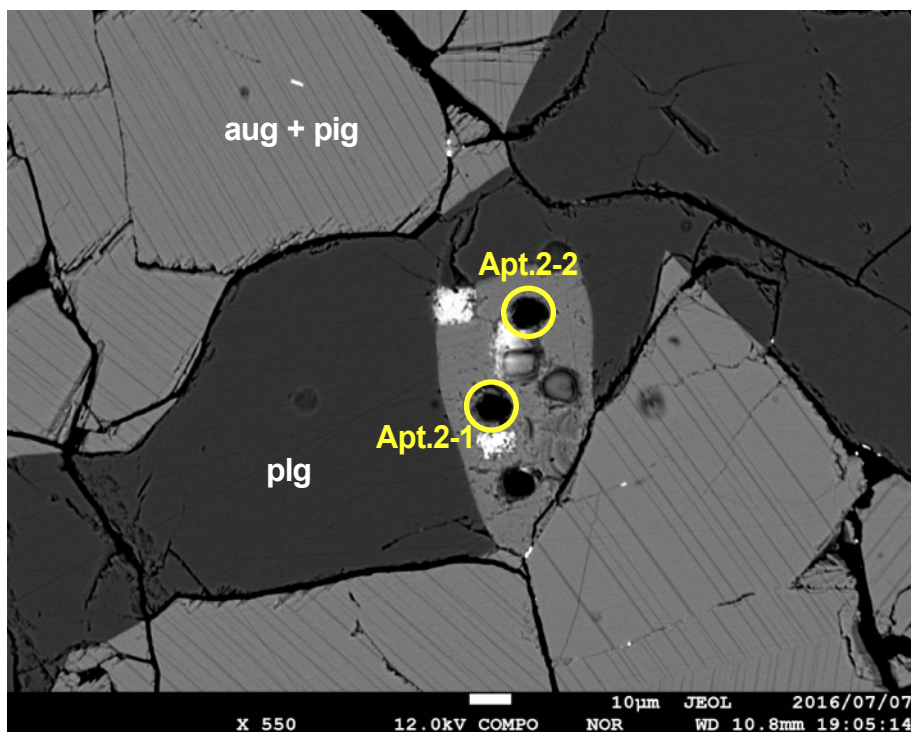
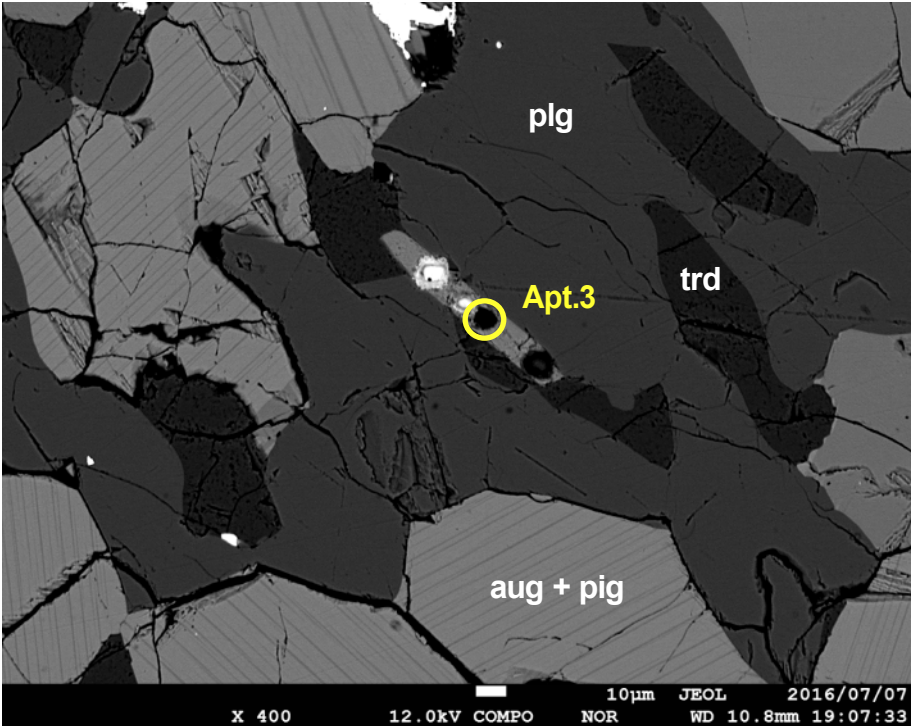


Fig. 2.4C



#### **2.4.1.5. Textural observations: Ibitira**

As described in the previous studies (Wilkening and Anders, 1975; Steele and Smith, 1976; Takeda and Graham, 1991; Yamaguchi et al., 1996), the studied section of Ibitira is characterized with the fine-grained recrystallized textures, containing numerous spherical vesicles with size of 100–500  $\mu\text{m}$  (Figure 2.5A-C). Euhedral to rounded mineral grains, including plagioclase, oxides and phosphates, are identified on the vesicles walls, as pointed previously (Steele and Smith, 1976; Heim et al. 1999). A large merrillite grain (Mer. 3, ca. 150  $\mu\text{m}$  in longest diameter; Figure 2.5C) is found on the wall of a large vesicle. Much smaller merrillite grains (Mer. 1, 2, 4 and 5, 10–50  $\mu\text{m}$ , Figure 2.5D) are identified in the other areas. Their major elements compositions are almost indistinguishable, despite the textural differences between Mer. 3 and the others (Table 2.2). No apatite grain is identified.

Figure 2.5. Backscattered electron images of Ibitira sample.

Fig. 2.5A

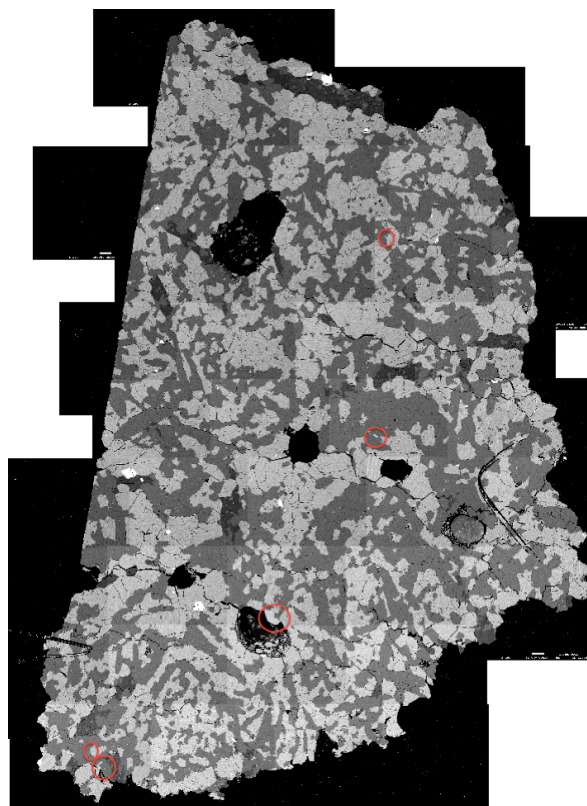


Fig. 2.5B

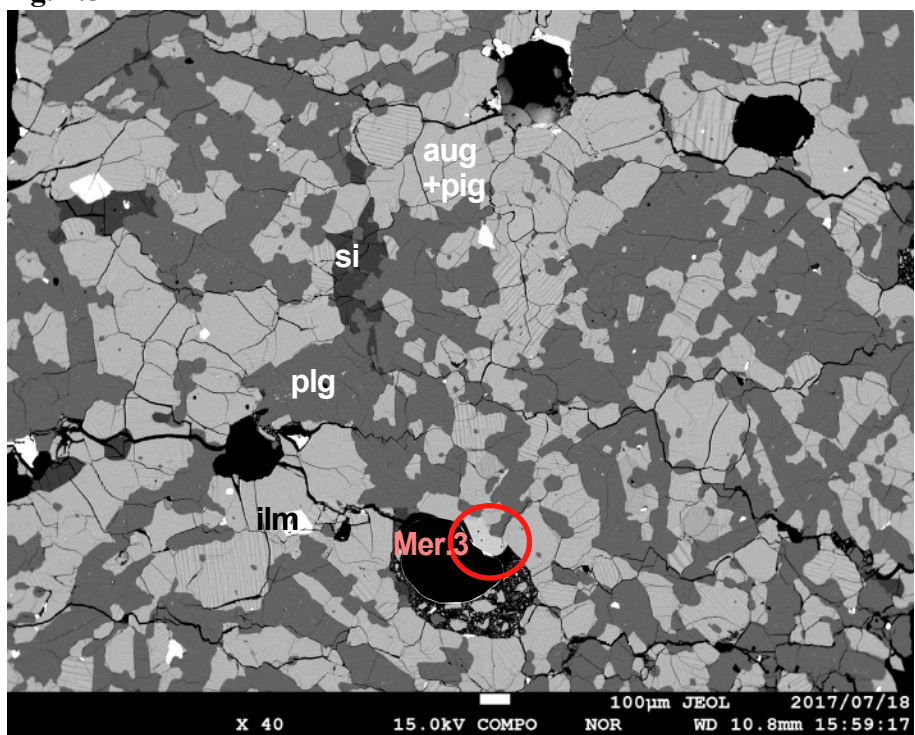


Fig. 2.5C

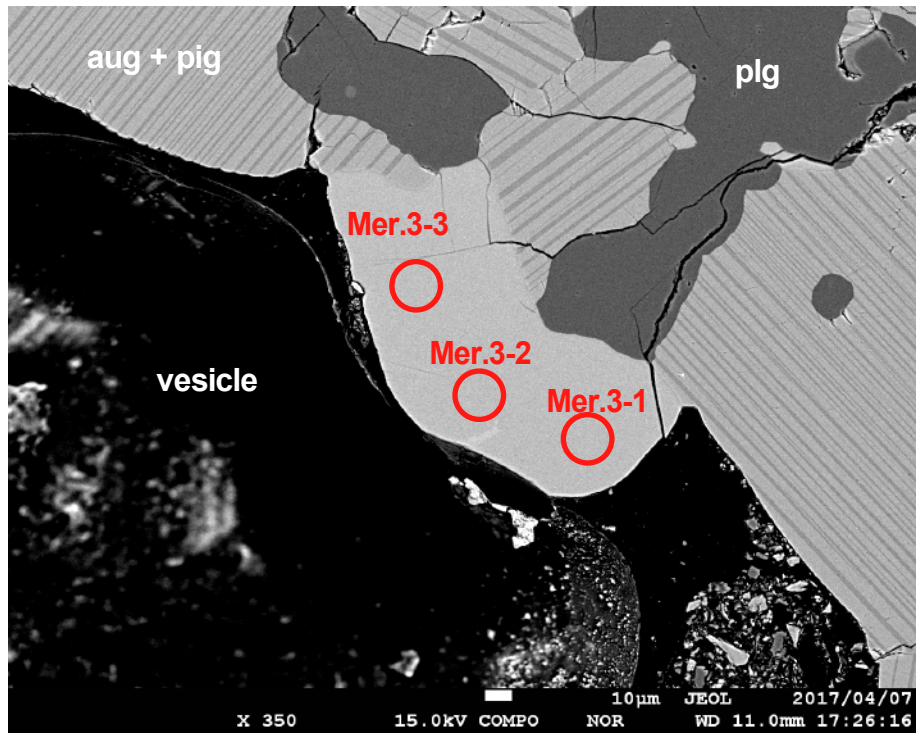
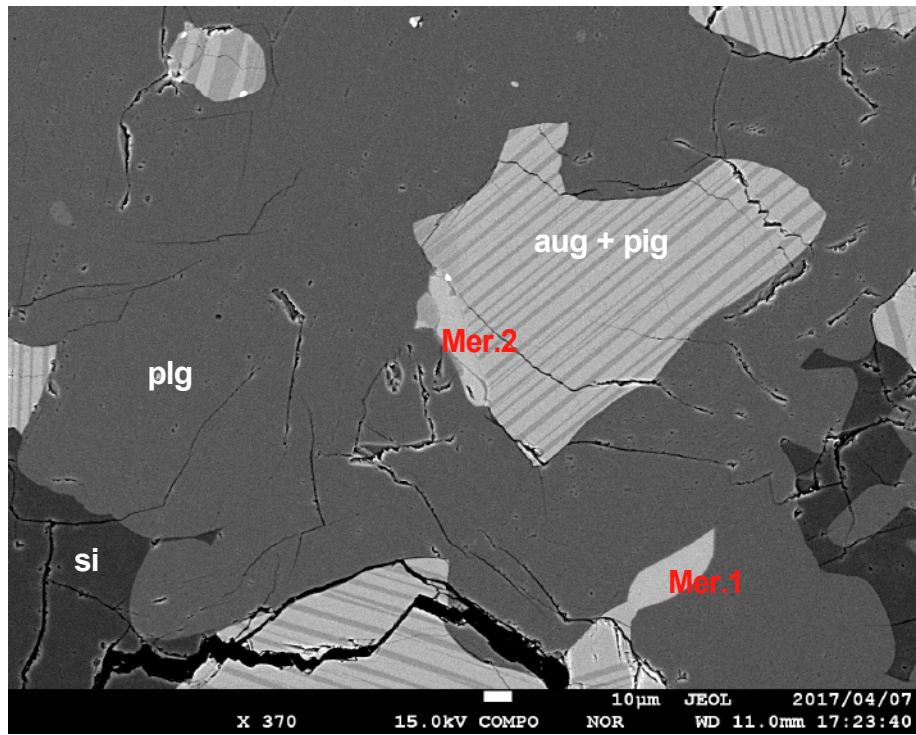


Fig. 2.5D



**Table 2.2.** Major elements compositions of the phosphate grains in Juvinas, Camel Donga, Stannern, Agoutl and Ibitira.

	Juvinas						Camel Donga					
	Apt. 2	Mer. 1	Mer. 2	Mer. 3	Mer. 4	Apt. 1	Apt. 2	Apt. 3	Apt. 5	Apt. 6		
Na <sub>2</sub> O	n.d.	0.68	0.74	0.7	0.67	n.d.	n.d.	n.d.	n.d.	n.d.		
MgO	0.03	2.2	2.49	2.37	3.77	0.03	n.d.	0.03	0.04	0.20		
Al <sub>2</sub> O <sub>3</sub>	0.04	5.98	0.02	0.01	0.26	0.04	0.05	n.d.	0.04	0.28		
F	3.5	n.d.	n.d.	n.d.	n.d.	3.84	4.21	3.94	3.69	3.99		
Cl	0.09	n.d.	n.d.	n.d.	n.d.	0.13	0.19	0.16	0.15	0.14		
PbO	0.03	0.02	0.03	n.d.	0.06	0.05	n.d.	0.05	0.02	0.07		
SO <sub>3</sub>	0.03	0.02	0.01	0.04	0.02	n.d.	n.d.	n.d.	0.01	0.03		
P <sub>2</sub> O <sub>5</sub>	41.06	38.39	44.18	40.39	38.54	40.88	40.60	39.55	40.97	40.66		
Y <sub>2</sub> O <sub>3</sub>	0.07	1.43	1.79	1.33	1.13	0.02	0.06	0.05	0.01	n.d.		
SrO	0.03	n.d.	0.01	0.05	0.02	0.01	0.06	0.02	0.01	0.06		
SiO <sub>2</sub>	0.45	7.46	0.59	12.27	8.16	0.24	0.15	0.53	0.14	1.11		
K <sub>2</sub> O	n.d.	0.1	0.11	0.12	0.1	0.01	0.01	0.02	0.01	0.01		
CaO	54.55	40.48	44.04	39.11	40.55	53.87	55.28	52.17	53.86	54.00		
TiO <sub>2</sub>	0.03	n.d.	0.02	0.01	0.04	0.14	n.d.	0.05	0.02	0.04		
UO <sub>2</sub>	0.02	0.05	0.08	0.01	0.01	0.02	n.d.	n.d.	0.05	0.06		
ThO <sub>2</sub>	0.02	0.02	0.04	0.02	0.08	0.02	0.18	n.d.	0.05	0.01		
La <sub>2</sub> O <sub>3</sub>	0.02	0.31	0.27	0.32	0.38	n.d.	0.09	0.03	0.02	0.01		
Ce <sub>2</sub> O <sub>3</sub>	0.08	0.75	0.71	0.83	1.00	0.03	0.02	n.d.	0.04	0.05		
Nd <sub>2</sub> O <sub>3</sub>	0.03	0.45	0.55	0.65	0.69	0.03	n.d.	0.01	0.02	0.02		
MnO	0.03	0.02	0.03	0.05	0.11	0.04	0.03	0.01	0.05	0.05		
FeO	0.29	1.5	1.84	1.39	4.01	2.66	1.25	5.07	2.77	1.08		
Total	100.4	99.85	97.54	99.68	99.6	102.1	102.2	101.7	102.0	101.8		

**Table 2.2 (continued)**

	Stannern						Agoutt					
	Apt. 1	Apt. 3	Mer. 1	Apt. 4	Apt. 6	Apt. 1	Apt. 2	Apt. 3	Apt. 4	Apt. 7		
Na <sub>2</sub> O	n.d.	n.d.	0.92	n.d.								
MgO	0.02	0.02	3.11	0.01	0.03	0.06	0.02	0.01	0.03	0.02		
Al <sub>2</sub> O <sub>3</sub>	0.02	0.03	0.01	0.02	0.15	0.05	0.04	0.06	0.02	n.d.		
F	3.79	3.95	n.d.	4.01	4.26	2.99	3.42	3.83	3.86	2.36		
Cl	0.16	0.16	0	0.17	0.18	0.01	0.01	0.02	0.01	0.04		
PbO	0.02	0.03	0.04	0.02	n.d.	0.02	0.06	0.02	0.03	0.03		
SO <sub>3</sub>	0.03	0.13	0.01	0.04	0.05	0.04	0.03	0.02	0.05	0.03		
P <sub>2</sub> O <sub>5</sub>	40.81	39.9	42.05	41.65	42.05	39.44	42.09	41.7	41.86	41.90		
Y <sub>2</sub> O <sub>3</sub>	0.03	0.03	1.68	0.02	0.06	0.04	n.d.	0.04	0.06	n.d.		
SrO	0.03	0	0.02	0.03	0.05	0.02	n.d.	n.d.	0.02	0.02		
SiO <sub>2</sub>	0.12	0.24	3.09	0.09	0.17	0.44	0.11	0.23	0.15	0.31		
K <sub>2</sub> O	0	0	0.05	0	0	0	n.d.	0.01	0	0.01		
CaO	54.25	53.6	40.71	55.16	55.33	52.74	55.6	55.15	55.13	55.83		
TiO <sub>2</sub>	0.22	0.3	n.d.	0.04	0.02	0.02	0.01	0.02	0.01	0.04		
UO <sub>2</sub>	0.06	0.01	0.08	0.05	n.d.	0.06	0.02	n.d.	0.08	0.02		
ThO <sub>2</sub>	0.02	0.01	0.08	0.02	n.d.	0.01	0.01	n.d.	0.06	0.03		
La <sub>2</sub> O <sub>3</sub>	0.02	0.02	0.42	0.02	n.d.	n.d.	0.02	n.d.	n.d.	n.d.		
Ce <sub>2</sub> O <sub>3</sub>	0.04	0.02	1.06	0.04	0.04	0.04	0.03	0.02	0.05	n.d.		
Nd <sub>2</sub> O <sub>3</sub>	0.02	0.04	0.77	0.05	0.07	n.d.	n.d.	0.01	0.01	0.09		
MnO	0.03	0.04	0.06	0.06	0.01	0.07	0.04	0.02	0.04	0.04		
FeO	0.47	0.5	4.96	0.63	0.61	0.94	0.41	0.42	0.76	0.39		
Total	100.17	99.03	99.12	102.1	103.1	101.90	101.58	102.22	101.15	101.90		

**Table 2.2 (continued)**

Ibitira					
	Mer. 1	Mer. 2	Mer. 3	Mer. 4	Mer. 5
Na <sub>2</sub> O	0.18	0.3	0.21	0.17	0.25
MgO	2.73	2.7	2.68	2.58	2.15
Al <sub>2</sub> O <sub>3</sub>	0.07	1.26	0.02	0.08	5.98
F	n.d.	n.d.	n.d.	n.d.	n.d.
Cl	n.d.	0.01	0.01	n.d.	0.01
PbO	0.01	0.05	0.03	n.d.	n.d.
SO <sub>3</sub>	0.01	0.03	0.01	0.03	n.d.
P <sub>2</sub> O <sub>5</sub>	44.56	44.1	44.72	45.45	38.14
Y <sub>2</sub> O <sub>3</sub>	0.58	0.5	0.74	0.66	0.59
SrO	n.d.	0.02	0.01	n.d.	0.03
SiO <sub>2</sub>	0.18	0.41	0.06	0.08	6.96
K <sub>2</sub> O	0.04	0.04	0.03	0.04	0.04
CaO	46.7	45.75	46.55	46.45	42.52
TiO <sub>2</sub>	n.d.	0.02	0.01	0.01	n.d.
UO <sub>2</sub>	0.08	0.08	0.05	0.05	n.d.
ThO <sub>2</sub>	0.04	0.04	0.02	0.03	n.d.
La <sub>2</sub> O <sub>3</sub>	0.21	0.2	0.23	0.15	0.2
Ce <sub>2</sub> O <sub>3</sub>	0.52	0.52	0.57	0.48	0.5
Nd <sub>2</sub> O <sub>3</sub>	0.36	0.36	0.41	0.39	0.23
MnO	0.09	0.14	0.06	0.09	0.07
FeO	1.71	2.18	1.99	1.93	1.85
Total	98.07	98.7	98.4	98.66	99.51

## 2.4.2 U-Pb dating

In this subsection, I describe the results of U-Pb dating of the identified phosphates. All isotopic data are shown in Table 2.3.  $^{238}\text{U}$ - $^{206}\text{Pb}$  and  $^{207}\text{Pb}$ - $^{206}\text{Pb}$  isochrons of the individual samples are Figures 2.6–2.10. All isochron ages are calculated using Isoplot Ex. 3 software (Ludwig, 2003). This program calculates least-square linear fitting from error-weighted data, using York's methods (York, 1969; Appendix). Uncertainties of the following age results are at 95 % confidence limits.

### 2.4.2.1. U-Pb dating: Juvinas

The apatite and the merrillite in Juvinas showed significantly different ages. Three apatite grains (Apt. 1–3 in Table 2.3) defined a  $^{207}\text{Pb}$ - $^{206}\text{Pb}$  isochron age of  $4529 \pm 34$  Ma (MSWD = 0.55; Fig. 2.6a). The model  $^{207}\text{Pb}^*/^{206}\text{Pb}^*$  ages are calculated as 4490 – 4630 Ma, assuming common Pb isotopic composition as Canyon Diablo Troilite (CDT) Pb compositions (Tatsumoto et al., 1973). The weighted mean  $^{207}\text{Pb}^*/^{206}\text{Pb}^*$  is  $4516 \pm 32$  Ma (Table 2.3). Their  $^{238}\text{U}$ - $^{206}\text{Pb}$  systems showed discordance as  $5125 \pm 580$  Ma (MSWD = 0.01; Fig. 2.6b). The inadequately low MSWD of  $^{238}\text{U}$ - $^{206}\text{Pb}$  suggests the age uncertainty might be artificial; true uncertainty of  $^{238}\text{U}$ - $^{206}\text{Pb}$  might be much larger and indistinguishable to the  $^{207}\text{Pb}$ - $^{206}\text{Pb}$ .

In contrast, five merrillite grains (Mer. 1–5 in Table 2.3) defined a significantly younger  $^{207}\text{Pb}$ - $^{206}\text{Pb}$  age of  $4186 \pm 35$  Ma (MSWD = 0.61; Fig. 2.6c). Their model  $^{207}\text{Pb}^*/^{206}\text{Pb}^*$  ages range between 4080 – 4170 Ma with the weighted mean of  $4149 \pm 32$  Ma. The  $^{238}\text{U}$ - $^{206}\text{Pb}$  data of merrillite were so severely scattered that they did not determine a meaningful  $^{238}\text{U}$ - $^{206}\text{Pb}$  isochron age.

**Figure 2.6.**  $^{238}\text{U}$ - $^{206}\text{Pb}$  and  $^{207}\text{Pb}$ - $^{206}\text{Pb}$  isochrons <sup>\*1)</sup> of Juvinas apatite and merrillite.

Errors are at 2-sigma level.

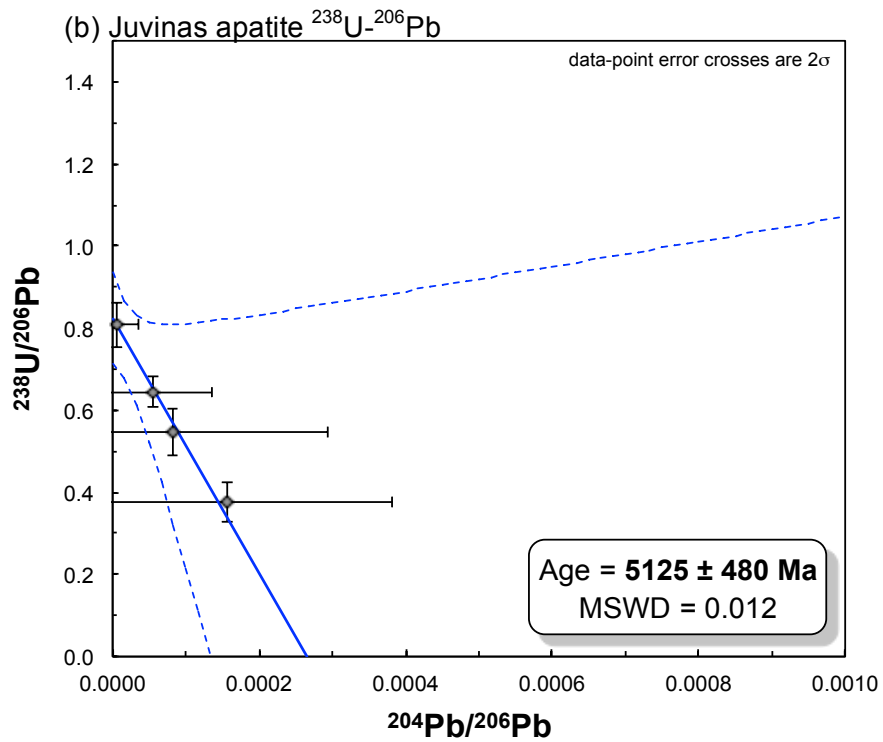
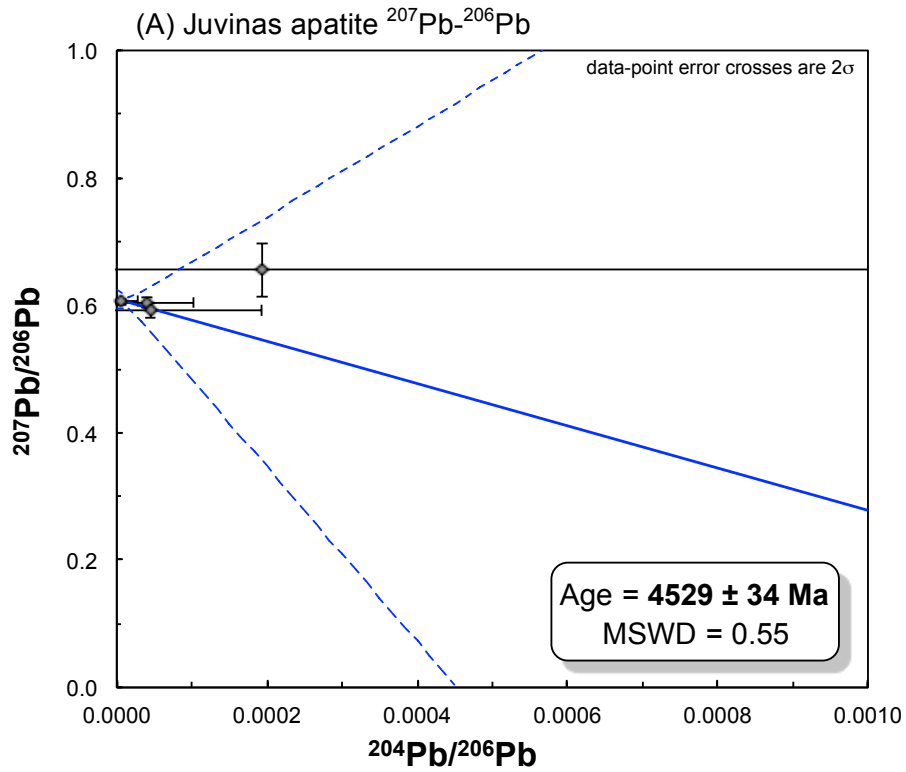
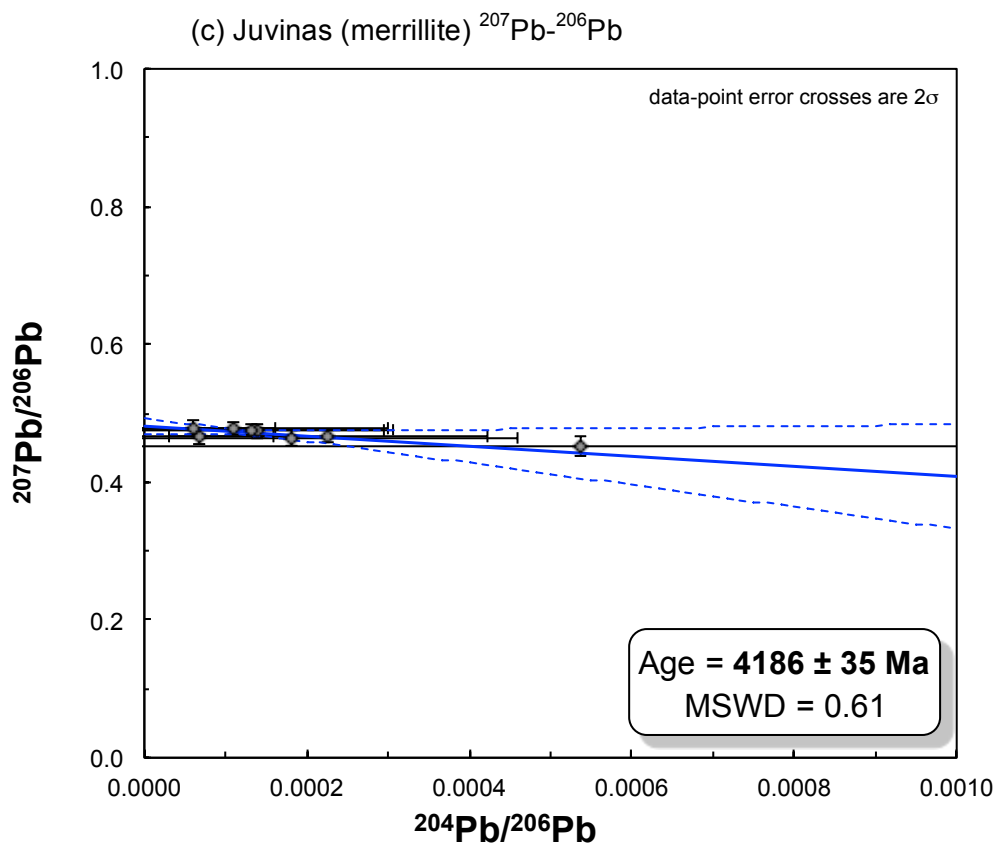


Figure 2.6. (continued)



Note: \*1) Both  $^{238}\text{U}$ - $^{206}\text{Pb}$  and  $^{207}\text{Pb}$ - $^{206}\text{Pb}$  ages are determined from y-intercepts of the isochrons. For the all eucrites analyzed in this study, the y-intercept are well calculated because of highly radiogenic Pb contents in their phosphates. Consequently, their  $^{238}\text{U}$ - $^{206}\text{Pb}$  and  $^{207}\text{Pb}$ - $^{206}\text{Pb}$  ages can be determined with a certain reliability, despite the large error envelopes (dashed curves) attached to the individual regression lines.

#### 2.4.2.2. U-Pb dating: Camel Donga

The six apatite grains with eight spot analyses determine the  $^{238}\text{U}$ - $^{206}\text{Pb}$  and  $^{207}\text{Pb}$ - $^{206}\text{Pb}$  ages as  $4213 \pm 450$  Ma (MSWD = 1.18) and  $4458 \pm 82$  Ma (MSWD = 5.0), respectively (table 2.3; Fig. 2.7). Large uncertainties of the ages are due to the highly scattered data points, as represented by large MSWD value of the Pb-Pb isochron. Their model  $^{207}\text{Pb}^*/^{206}\text{Pb}^*$  ages, assuming CDT Pb (Tatsumoto et al., 1973) as common Pb compositions, range between 4370–4572 Ma, with the mean value of  $4465 \pm 36$  Ma. Total Pb/U age can be calculated as  $4413 \pm 64$  Ma (MSWD = 5.6) from a regression line in the 3D ( $^{238}\text{U}/^{206}\text{Pb}$ – $^{207}\text{Pb}/^{206}\text{Pb}$ – $^{204}\text{Pb}/^{206}\text{Pb}$ ) space (for calculation of the total U/Pb isochron age, see Appendix). Although these calculated ages seem to be concordant, their uncertainties and MSWD are relatively large, compared to the other samples (Table 2.3; discussed in subsection 2.5.2).

#### 2.4.2.3. U-Pb dating: Stannern

The spot analyses of the six apatite grains and the one merrillite grain provide significantly young U-Pb ages. The  $^{238}\text{U}$ - $^{206}\text{Pb}$  and  $^{207}\text{Pb}$ - $^{206}\text{Pb}$  isochron ages were calculated as  $3971 \pm 110$  Ma (MSWD = 0.32) and  $4130 \pm 45$  Ma (MSWD = 2.6), respectively (table 2.3; Figs. 2.8). Their model  $^{207}\text{Pb}^*/^{206}\text{Pb}^*$  ages are calculated as 4080–4350 Ma, with the mean value of  $4143 \pm 34$  Ma. Discordance between the obtained  $^{238}\text{U}$ - $^{206}\text{Pb}$  and  $^{207}\text{Pb}$ - $^{206}\text{Pb}$  ages means that U-Pb system of these phosphates was slightly disturbed after 4130 Ma. Although total Pb/U age can be calculated as  $4141 \pm 35$  Ma (MSWD = 4.0), the regression line is not well determined due to the scattered data.

**Figure 2.7.**  $^{238}\text{U}$ - $^{206}\text{Pb}$  and  $^{207}\text{Pb}$ - $^{206}\text{Pb}$  isochrons of Camel Donga apatite. Errors are at 2-sigma level.

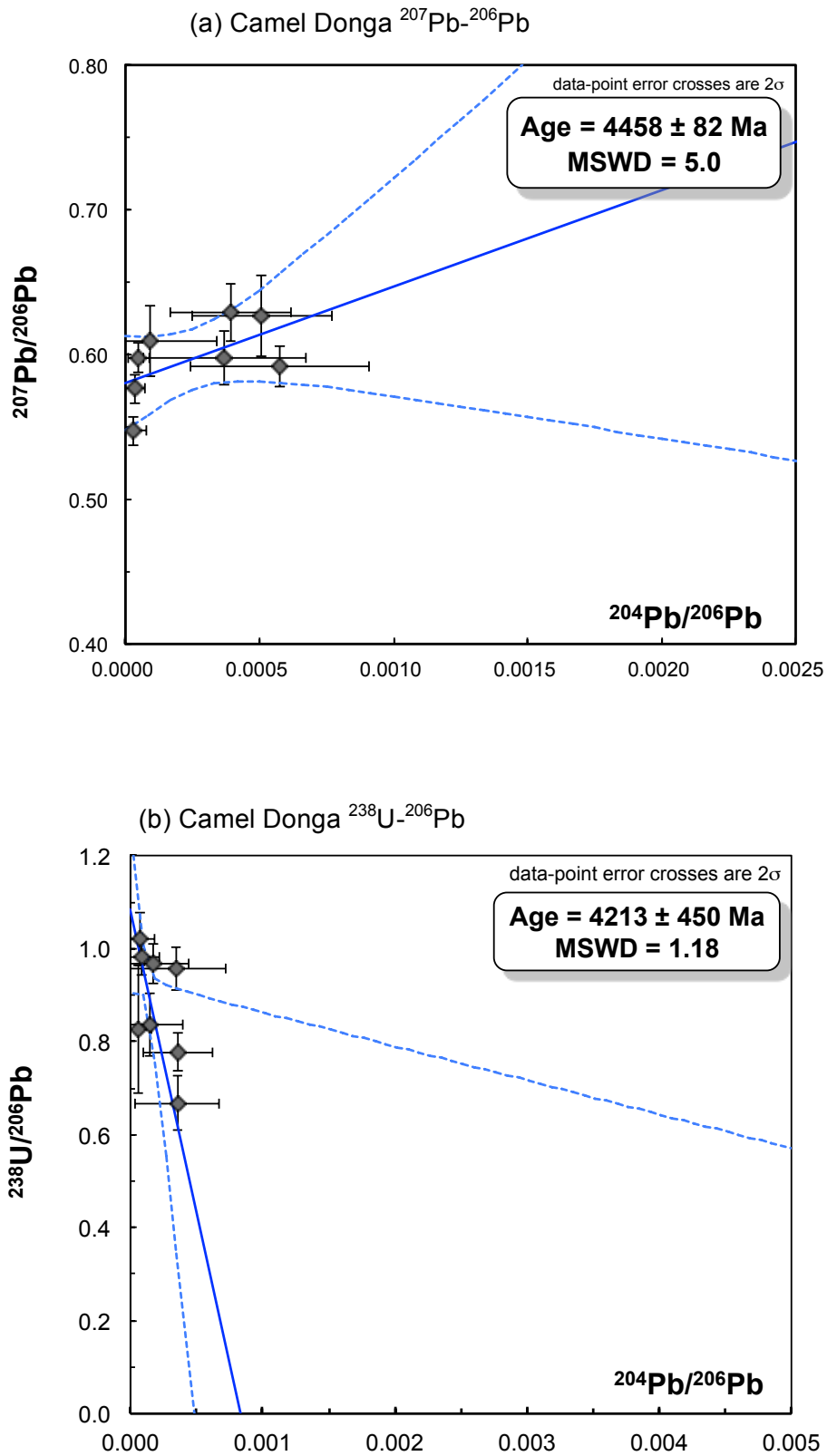
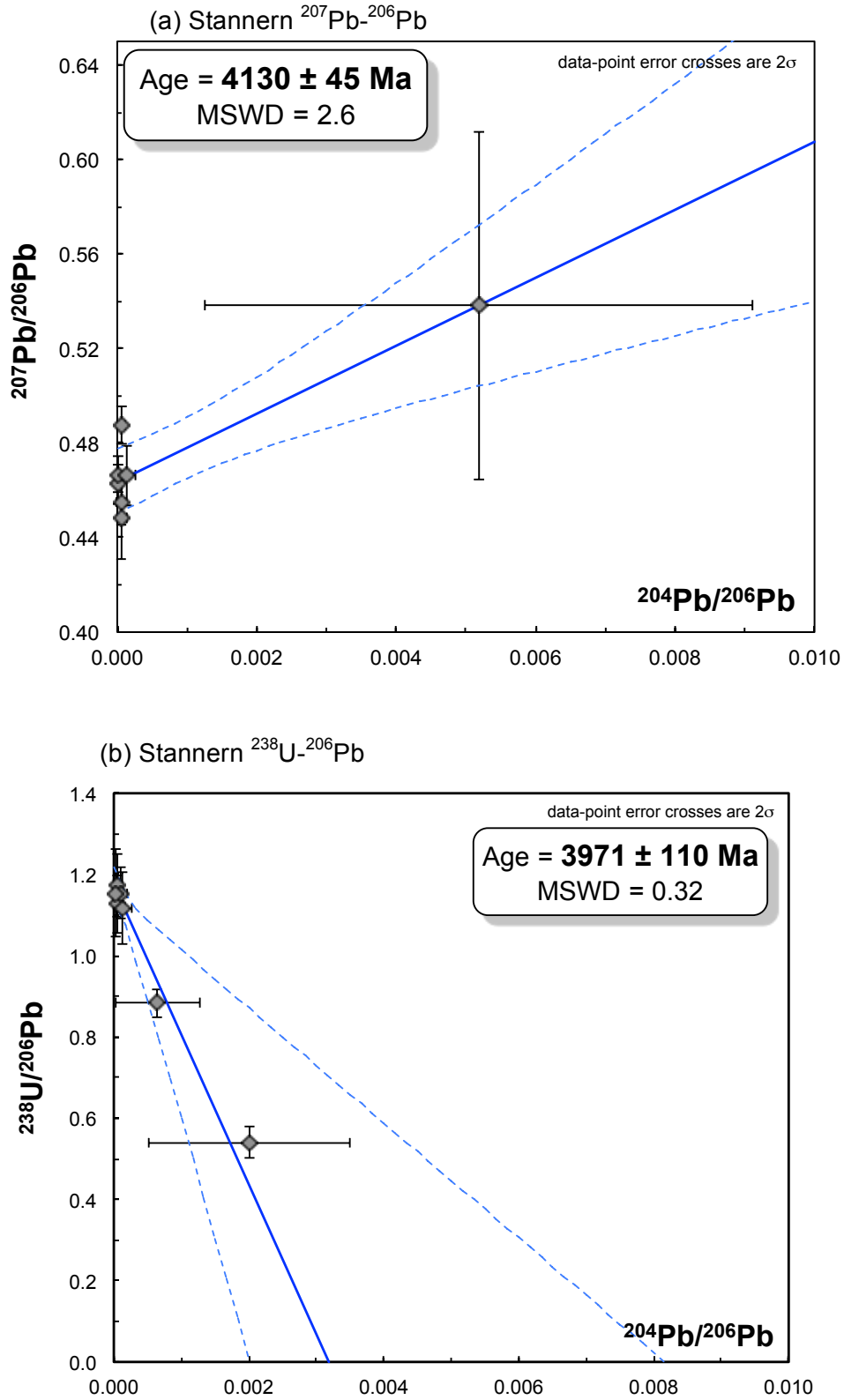


**Figure 2.8.**  $^{238}\text{U}$ - $^{206}\text{Pb}$  and  $^{207}\text{Pb}$ - $^{206}\text{Pb}$  isochrons of Stannern apatite and merrillite.

Errors are at 2-sigma level.



#### 2.4.2.4. U-Pb dating: Agoult

Seven apatite grains with 10 spot analyses determine the  $^{238}\text{U}$ - $^{206}\text{Pb}$  and  $^{207}\text{Pb}$ - $^{206}\text{Pb}$  isochron ages as  $4360 \pm 280$  Ma (MSWD = 1.2) and  $4522 \pm 11$  Ma (MSWD = 1.2), respectively (Table 2.3, Figs 2.9). The model  $^{207}\text{Pb}^*/^{206}\text{Pb}^*$  ages range between 4500–4560Ma, with the mean value of  $4524 \pm 30$  Ma. Despite the large uncertainty with the  $^{238}\text{U}$ - $^{206}\text{Pb}$  isochron age, the consistent results between  $^{238}\text{U}$ - $^{206}\text{Pb}$  and  $^{207}\text{Pb}$ - $^{206}\text{Pb}$  suggest that U-Pb system in Agoult apatite has been closed for 4522 Myr. The concordant total Pb/U isochron age in 3D ( $^{238}\text{U}/^{206}\text{Pb}$ - $^{207}\text{Pb}/^{206}\text{Pb}$ - $^{204}\text{Pb}/^{206}\text{Pb}$ ) space is calculated as  $4522 \pm 11$  Ma (MSWD = 1.5).

#### 2.4.2.5. U-Pb dating: Ibitira

Seven spots data from the five merrillite grains determine the  $^{207}\text{Pb}$ - $^{206}\text{Pb}$  age as  $4616 \pm 140$  Ma (MSWD = 0.51; Table 2.3, Fig 2.10). Their  $^{238}\text{U}$ - $^{206}\text{Pb}$  isochron does not provide any meaningful result, mainly because all of the obtained data values are almost indistinguishable within uncertainties. Meanwhile, the model  $^{207}\text{Pb}^*/^{206}\text{Pb}^*$  age ranges 4510 – 4560 Ma, with the mean value of  $4552 \pm 27$  Ma, consistent and more precisely determined compared to the isochron  $^{207}\text{Pb}$ - $^{206}\text{Pb}$  age.

**Figure 2.9.**  $^{238}\text{U}$ - $^{206}\text{Pb}$  and  $^{207}\text{Pb}$ - $^{206}\text{Pb}$  isochrons of Agoult apatite. Errors are at 2-sigma level.

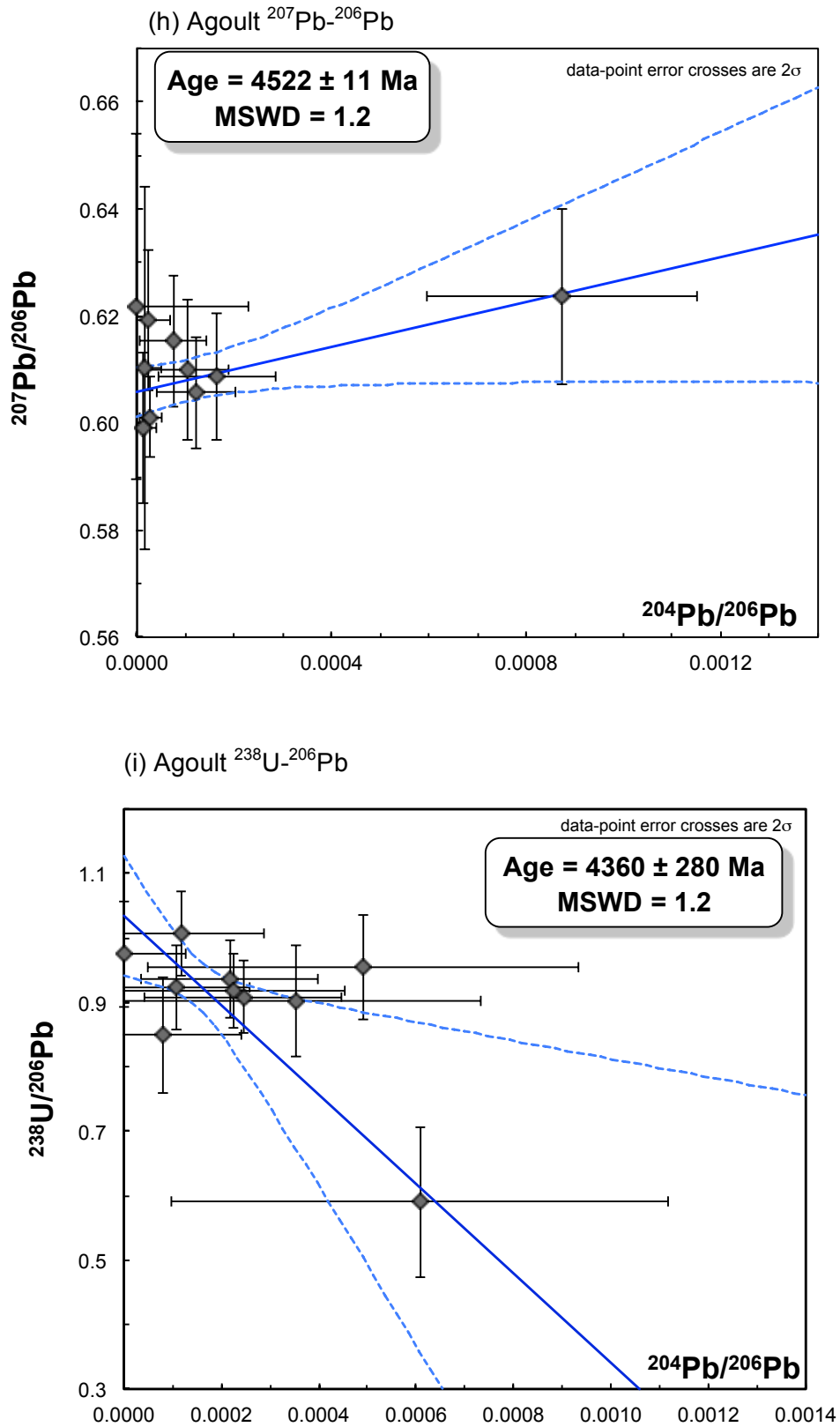
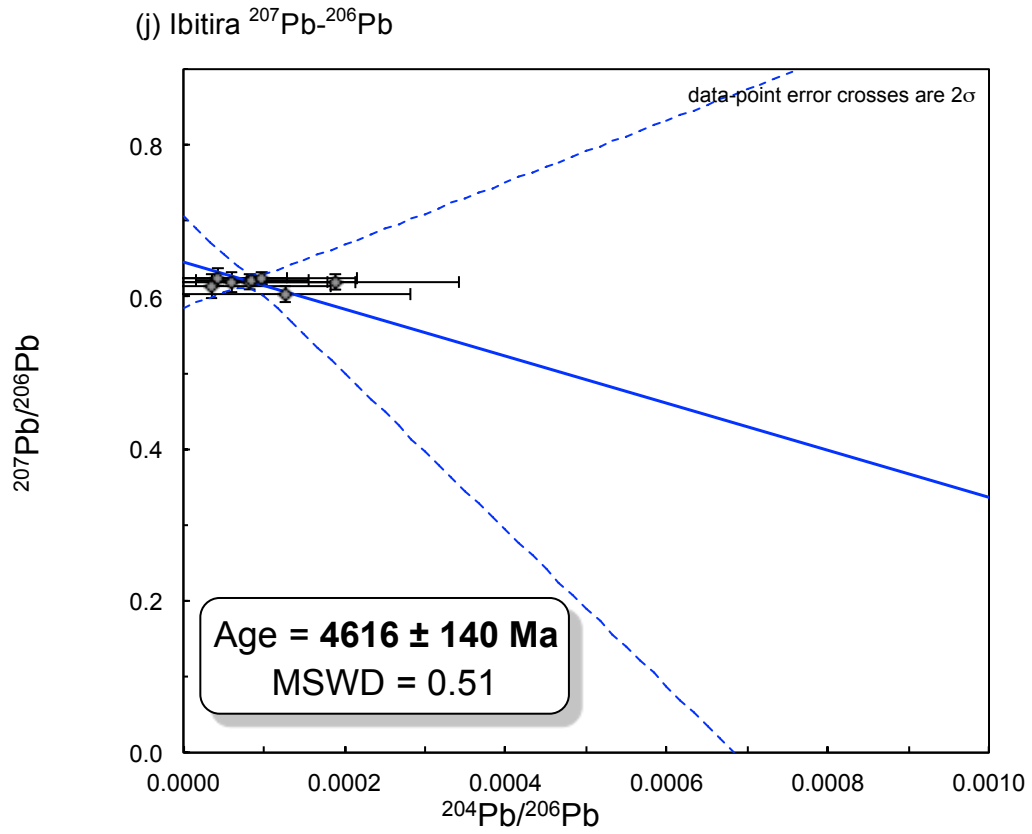


Figure 2.10.  $^{207}\text{Pb}$ - $^{206}\text{Pb}$  isochron of Ibitira merrillite. Errors are at 2-sigma level.



**Table 2.3.** NanoSIMS  $^{238}\text{U}$ - $^{206}\text{Pb}$  and  $^{207}\text{Pb}$ - $^{206}\text{Pb}$  isotopic results of Juvinas, Camel Donga, Stannern, Agoutl, and Ibitira. Errors are at 2-sigma level.

#	$^{238}\text{U}$ - $^{206}\text{Pb}$ session		$^{207}\text{Pb}$ - $^{206}\text{Pb}$ session		model $^{207}\text{Pb}^*/^{206}\text{Pb}^*$
	$^{204}\text{Pb}/^{206}\text{Pb}$ ( $\times 10^{-4}$ )	$^{238}\text{U}/^{206}\text{Pb}$	$^{204}\text{Pb}/^{206}\text{Pb}$ ( $\times 10^{-4}$ )	$^{207}\text{Pb}/^{206}\text{Pb}$	
<i>Juvinas apatite (older)</i>					
<b>Apt. 1</b>	1.6 ± 2.3	0.38 ± 0.05	1.9 ± 13.3	0.66 ± 0.04	4633 ± 298
<b>Apt. 2-1</b>	0.6 ± 0.8	0.65 ± 0.04	0.4 ± 0.6	0.61 ± 0.01	4518 ± 66
<b>Apt. 2-2</b>	0.1 ± 0.3	0.81 ± 0.05	0.1 ± 0.2	0.61 ± 0.01	4519 ± 41
<b>Apt.. 3</b>	0.5 ± 1.0	0.76 ± 0.05	0.4 ± 1.5	0.59 ± 0.01	4485 ± 93
$^{238}\text{U}$ - $^{206}\text{Pb}$ age	5125 ± 480	MSWD = 0.01	$^{207}\text{Pb}$ - $^{206}\text{Pb}$ age	4529 ± 34	MSWD = 0.55
<i>Juvinas merrillite (younger)</i>					
<b>Mer. 1</b>	2.2 ± 1.3	0.6 ± 0.03	1.1 ± 1.9	0.48 ± 0.01	4171 ± 85
<b>Mer. 2-1</b>	1.4 ± 2.1	0.51 ± 0.07	1.4 ± 1.6	0.47 ± 0.01	4159 ± 100
<b>Mer. 2-2</b>	1.5 ± 1.3	0.66 ± 0.03	1.3 ± 1.7	0.48 ± 0.01	4167 ± 74
<b>Mer. 2-3</b>	0.8 ± 1.1	0.58 ± 0.04	0.7 ± 0.9	0.47 ± 0.01	4135 ± 98
<b>Mer. 2-4</b>	2.9 ± 1.8	0.57 ± 0.03	0.6 ± 1.0	0.48 ± 0.01	4174 ± 89
<b>Mer. 2-5</b>	0.8 ± 2.1	0.55 ± 0.06	1.8 ± 2.8	0.46 ± 0.01	4128 ± 107
<b>Mer. 3</b>	5.3 ± 3.4	0.44 ± 0.04	5.4 ± 5.9	0.45 ± 0.01	4081 ± 131
<b>Mer. 4</b>	2.4 ± 1.8	0.75 ± 0.04	2.3 ± 2.0	0.47 ± 0.01	4132 ± 75
$^{238}\text{U}$ - $^{206}\text{Pb}$ age	not determined		$^{207}\text{Pb}$ - $^{206}\text{Pb}$ age	4186 ± 35	MSWD = 0.6
					weighted mean
					4149 ± 32

Table 2.3. (continued)

#	$^{238}\text{U}-^{206}\text{Pb}$ session		$^{207}\text{Pb}-^{206}\text{Pb}$ session		model $^{207}\text{Pb}^*/^{206}\text{Pb}^*$
	$^{204}\text{Pb}/^{206}\text{Pb}$ ( $\times 10^{-4}$ )	$^{238}\text{U}/^{206}\text{Pb}$	$^{204}\text{Pb}/^{206}\text{Pb}$ ( $\times 10^{-4}$ )	$^{207}\text{Pb}/^{206}\text{Pb}$	
<i>Camel Donga apatite</i>					
<b>Apt. 1</b>	3.4 ± 3.8	0.96 ± 0.05	0.9 ± 2.5	0.61 ± 0.02	4527 ± 180
<b>Apt. 2</b>	0.7 ± 1.1	1.02 ± 0.06	0.4 ± 0.4	0.58 ± 0.01	4447 ± 75
<b>Apt. 3</b>	1.8 ± 2.6	0.97 ± 0.04	0.5 ± 0.4	0.6 ± 0.01	4500 ± 75
<b>Apt. 4</b>	0.9 ± 1.3	0.98 ± 0.04	0.3 ± 0.5	0.55 ± 0.01	4371 ± 78
<b>Apt. 5-1</b>	3.5 ± 3.2	0.67 ± 0.06	3.7 ± 3.0	0.6 ± 0.02	4497 ± 140
<b>Apt. 5-2</b>	3.6 ± 2.6	0.78 ± 0.04	5.1 ± 2.6	0.63 ± 0.03	4564 ± 204
<b>Apt. 5-3</b>	1.5 ± 2.5	0.84 ± 0.07	5.8 ± 3.3	0.59 ± 0.01	4478 ± 106
<b>Apt. 6</b>	0.6 ± 1.0	0.83 ± 0.14	3.9 ± 2.3	0.63 ± 0.02	4572 ± 146
<b><math>^{238}\text{U}-^{206}\text{Pb}</math> age</b>	4213 ± 450	MSWD = 1.2	4458 ± 82	MSWD = 5.0	weighted mean
			<b>Total Pb/U age</b>	MSWD = 5.6	4465 ± 36



Table 2.3. (continued)

#	<sup>238</sup> U- <sup>206</sup> Pb session			<sup>207</sup> Pb- <sup>206</sup> Pb session		
	<sup>204</sup> Pb/ <sup>206</sup> Pb (x10 <sup>-4</sup> )	<sup>238</sup> U/ <sup>206</sup> Pb	<sup>204</sup> Pb/ <sup>206</sup> Pb (x10 <sup>-4</sup> )	<sup>207</sup> Pb/ <sup>206</sup> Pb	<sup>207</sup> Pb/ <sup>206</sup> Pb	model <sup>207</sup> Pb/ <sup>206</sup> Pb*
<i>Agoutl apatite</i>						
<b>Apt. 1-1</b>	1.2 ± 1.7	1.01 ± 0.07	0.3 ± 0.2	0.6 ± 0.01	4508 ± 57	
<b>Apt. 1-2</b>	1.1 ± 1.5	0.92 ± 0.07	0.2 ± 0.4	0.62 ± 0.01	4551 ± 96	
<b>Apt. 2-1</b>	2.2 ± 1.8	0.94 ± 0.06	0.7 ± 0.7	0.62 ± 0.01	4542 ± 91	
<b>Apt. 2-2</b>	2.5 ± 2.0	0.91 ± 0.06	0.0 ± 2.3	0.62 ± 0.03	4557 ± 238	
<b>Apt. 3</b>	3.5 ± 3.8	0.9 ± 0.09	0.2 ± 0.3	0.61 ± 0.03	4530 ± 251	
<b>Apt. 4</b>	2.2 ± 2.3	0.92 ± 0.06	1.0 ± 0.9	0.61 ± 0.01	4528 ± 98	
<b>Apt. 5</b>	4.9 ± 4.4	0.95 ± 0.08	1.6 ± 1.2	0.61 ± 0.01	4525 ± 88	
<b>Apt. 6</b>	0.0 ± 1.3	0.98 ± 0.08	1.2 ± 0.8	0.61 ± 0.01	4518 ± 79	
<b>Apt. 7-1</b>	6.1 ± 5.1	0.59 ± 0.12	8.7 ± 2.8	0.62 ± 0.02	4553 ± 120	
<b>Apt. 7-2</b>	0.8 ± 1.6	0.85 ± 0.09	0.1 ± 0.3	0.6 ± 0.01	4503 ± 106	
<b><sup>238</sup>U-<sup>206</sup>Pb age</b>	4360 ± 280	MSWD = 1.2	4522 ± 11	MSWD = 1.2	weighted mean	
<b>Total Pb/U age</b>			4522 ± 11	MSWD = 1.5	4524 ± 30	

Table 2.3. (continued)

#	$^{238}\text{U}-^{206}\text{Pb}$ session		$^{207}\text{Pb}-^{206}\text{Pb}$ session		model $^{207}\text{Pb}^*/^{206}\text{Pb}^*$
	$^{204}\text{Pb}/^{206}\text{Pb}$ ( $\times 10^{-4}$ )	$^{238}\text{U}/^{206}\text{Pb}$	$^{204}\text{Pb}/^{206}\text{Pb}$ ( $\times 10^{-4}$ )	$^{207}\text{Pb}/^{206}\text{Pb}$	
<i>Ibitira merrillite</i>					
<b>Mer. 1</b>	1.7 ± 2.8	0.73 ± 0.08	1.3 ± 1.6	0.6 ± 0.01	4514 ± 87
<b>Mer. 2</b>	0.9 ± 2.4	0.69 ± 0.09	1.9 ± 1.5	0.62 ± 0.01	4552 ± 74
<b>Mer. 3-1</b>	2.8 ± 3.6	0.72 ± 0.09	0.3 ± 1.5	0.61 ± 0.02	4540 ± 124
<b>Mer. 3-2</b>	0.2 ± 1.8	0.71 ± 0.09	0.6 ± 1.5	0.62 ± 0.01	4552 ± 105
<b>Mer. 3-3</b>	0.1 ± 1.3	0.59 ± 0.07	0.8 ± 1.0	0.62 ± 0.01	4553 ± 72
<b>Mer. 4</b>	0.9 ± 1.3	0.69 ± 0.07	0.9 ± 0.7	0.62 ± 0.01	4557 ± 50
<b>Mer. 5</b>	1.5 ± 1.9	0.58 ± 0.06	1.0 ± 1.2	0.62 ± 0.01	4563 ± 59
$^{238}\text{U}-^{206}\text{Pb}$ age	not determined		4616 ± 140	MSWD = 0.5	4552 ± 27
					weighted mean

## 2.5. Discussion

The goal of this study is to understand the evolutionary history of Vesta and Vesta-like protoplanets. As reported in the former section 2.4, *in-situ* U-Pb chronologies in phosphates of the basaltic eucrites and the basaltic achondrite are analyzed, along with their mineralogical observations. This is the first report that investigates the eucrites metamorphic histories at moderate temperature ranges around 600°C (closure temperatures of U-Pb in the eucritic phosphates), using *in-situ* U-Pb dating of the phosphates. Based on the new findings, as well as literature knowledge, I discuss the thermal evolutionary history of Vesta's crusts.

In subsections 2.5.1.1–2.5.1.5, I firstly examine my dating results of the individual samples along with their mineralogical features, and then, compare them to previous chronological studies. Next, in subsection 2.5.2, the all findings discussed above are combined to compare U-Pb system of the phosphates to other chronological data from literatures. Thermal conditions at metamorphic events are considered based on closure temperatures of the U-Pb system in subsection 2.5.3. Finally, I discuss the evolutionary history of Vesta's crust and provide new thermo-chronological constraints in subsection 2.5.4.

## **2.5.1. Examinations of the textural and chronological properties of the individual eucrites**

### **2.5.1.1. Examination of individual chronology: Juvinas**

As described in the former subsection 2.4.1.1, two out of three apatite grains (Apt. 2 and 3; Figure 2.1C, D) and all merrillite (Mer. 1–4; Figure 2.1C, E) locate inside or next to the large tridymite crystal. The adjacent fine-grained porous areas and the plagioclase include numerous small opaque minerals. The porous areas compose of quartz, plagioclase, high-Ca pyroxene, oxides and phosphates (Figure 2.1B-E). The textures are typical for silica-rich primary mesostasis, which were thermally metamorphosed during post-crystallization event. Previous studies suggested that the origin of large euhedral tridymite crystal in the metamorphosed eucrites is the partial remelting of the primary mesostasis (Hervig, 1986; Yamaguchi et al., 1996a,b). A number of petrological, chemical and chronological studies pointed out that Juvinas has the highly complicated impact-induced brecciation and reheating history (e.g. Takeda and Graham, 1991; Metzler et al., 1995). It is inferred that the high porous areas (Figures 2.1B–E), initially silica-rich mesostasis, were partially remelted during impact reheating. Consequently, I may regard the tridymite crystal with merrillite inclusions, identified in my Juvinas sample, is the result of partial remelting from the mesostasis. The adjacent porous areas with fine-grained minerals, including some apatite and merrillite (Figure 2.1C, D) may be remnants of the primary mesostasis.

Although most of the analyzed phosphates located in the partial remelting areas discussed above, the apatite and the merrillite recorded apparently discrepant ages. The  $^{207}\text{Pb}$ - $^{206}\text{Pb}$  ages of the apatite and the merrillite are  $4529 \pm 34$  Ma (Figure 2.6A)

and  $4186 \pm 35$  Ma (Figure 2.6C), respectively. Among the analyzed grains, Mer. 3 and Mer. 4 locate in the tridymite crystal, suggesting their secondary origins. Although the others (Apt. 2 and 3, Mer. 1 and 2) locate in the adjacent porous areas, the obtained U-Pb differences suggest that Apt. 2 and Apt. 3 are relict of the primary mesostasis minerals, whereas Mer. 1 and Mer. 2 may have recrystallized from partial remelting, possibly due to shock reheating. The large apatite grain, Apt. 2 (ca.  $80\mu\text{m}$ ; Figure 2.1D), seems to have survived the remelting event and have retained its U-Pb system. Although Apt. 3 is smaller (ca.  $30\mu\text{m}$ ; Figure 2.1C), it locates in the porous area surrounded by primary quartz. This grain may not have been damaged at the remelting. The slightly lower  $^{207}\text{Pb}/^{206}\text{Pb}$  ratio of Apt. 3 compared to those of Apt. 1 and Apt. 2 (Table 2.3; Figure 2.6A) might be due to the minor disturbance of its U-Pb system at the reheating. The model  $^{207}\text{Pb}^*/^{206}\text{Pb}^*$  age of Apt. 3 (4490 Ma; Table 2.3) seems to be slightly younger than the others, although large uncertainties make them indistinguishable. On the other hand, the largest merrillite, Mer. 2 (ca.  $100\mu\text{m}$ ; Figure 2.1E) coexists with tridymite and has irregular undulant shape. It is inferred that Mer. 2 crystallized from partial remelting, although this grain is larger than Apt. 2. Consequently, I may regard that the identified apatite grains (Apt. 1–3) are the relict primary minerals, which have retained the U-Pb system from the earlier events. Their  $^{207}\text{Pb}$ - $^{206}\text{Pb}$  age of  $4529 \pm 34$  Ma seems somewhat younger than igneous crystallization of Juvinas and other basaltic eucrites (discussed later). This age might indicate timing of the post-crystallization thermal event during ca. 4530 Ma. Meanwhile, the merrillite grains (Mer. 1–4) within or close to the secondary tridymite crystals, are likely to have crystallized during the partial remelting of the mesostasis. This remelting event

occurred at  $4186 \pm 35$  Ma, possibly because of the impact reheating. Such local disturbances of the U-Pb system have never been identified between individual phosphate grains in eucrites. This is the first report that shows *in-situ* U-Pb ages of the eucrite phosphates with their local differences. I would emphasize the importance of *in-situ* analyses in order to obtain adequate interpretation from meteoritic records, especially from meteorites with highly complicated metamorphic histories, because bulk analysis may provide average signature.

The old  $^{207}\text{Pb}$ - $^{206}\text{Pb}$  age of Juvinas apatite analyzed in this study ( $4529 \pm 34$  Ma) is indistinguishable from previously reported  $^{207}\text{Pb}$ - $^{206}\text{Pb}$  age of Juvinas zircon of  $4545 \pm 15$  Ma (Zhou et al., 2013). Several earlier studies also reported  $^{207}\text{Pb}$ - $^{206}\text{Pb}$  ages of Juvinas zircon as ca. 4560 Ma (Bukovanská and Ireland, 1993) and  $4527 \pm 24$  Ma (Lee et al., 2009), although they were in the conference abstracts without showing any isotopic data. In addition to Juvinas zircon, zircons from other basaltic eucrites with various metamorphic grades recorded the similar Pb-Pb ages around 4545–4555 Ma with a mean value of 4554 Ma (Bukovanská and Ireland, 1993; Misawa et al., 2005; Lee et al., 2009; Zhou et al., 2013; Iizuka et al., 2005). The identical  $^{207}\text{Pb}$ - $^{206}\text{Pb}$  ages of zircons in the various basaltic eucrites suggest that 4554 Ma is the timing of zircon crystallization in basaltic eucrite. It is inferred that the eucrite parent body, i.e. Vesta, experienced either magmatic or metamorphic high-temperature event(s) at 4554 Ma, where zircons in Juvinas and other basaltic eucrites crystallized (discussed in detail again in the following subsection 2.5.4.). The almost identical periods were reported from other chronometers of Juvinas as well (summarized in Table 2.1). The pioneering studies of Rb-Sr and Sm-Nd mineral isochrons for Juvinas reported  $4590 \pm 40$  Ma

(Rb-Sr; Allégre et al., 1973) and  $4560 \pm 80$  Ma (Sm-Nd; Lugmair, 1974), respectively. Shukolyukov and Lugmair (1996) and Miura et al. (1998) reported Pu-Xe ages as  $4551 \pm 15$  Ma and  $4548 \pm 23$  Ma. Hf-W isochron from mineral separates of Juvinas (Kleine et al., 2005; Touboul et al., 2015) defined a precise relative Hf-W age as  $22.3 \pm 2.6$  Myr after the CAI formation, corresponding an absolute age of  $4545.6 \pm 2.5$  Ma when anchored relative to D'Orbigny angrite ( $^{182}\text{Hf}/^{180}\text{Hf} = (7.15 \pm 0.17) \times 10^{-5}$  at  $4563.37 \pm 0.25$  Ma; Kleine et al., 2012; Brennecka and Wadhwa, 2012). This age is significantly younger than Vesta's mantle differentiation at 4563 Ma (calculated from Hf-W whole rock isochrons of basaltic eucrites, Kleine et al., 2004; Quitté et al., 2000). In addition to the U-Pb chronology of zircons described above, Hf-W system in Juvinas also suggests existence of the magmatic and/or thermal metamorphic events on Vesta at ca. 4545 Ma, i.e. 22 Ma after its mantle differentiation (Kleine et al., 2005; Touboul et al., 2015).

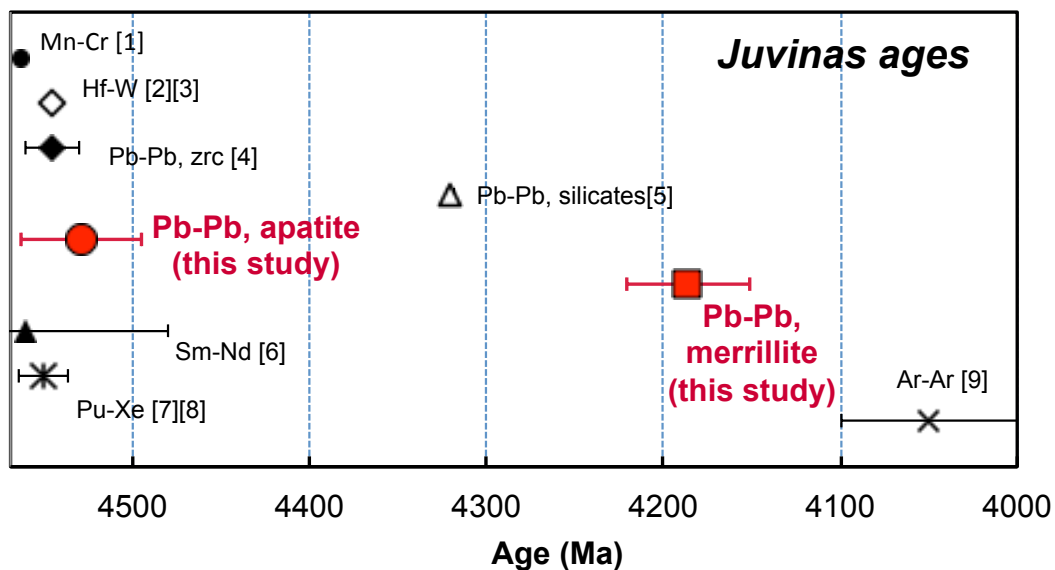
Because of the relatively large errors attached to  $^{207}\text{Pb}$ - $^{207}\text{Pb}$  age of Juvinas apatite ( $4529 \pm 34$  Ma), it is uncertain whether the U-Pb system in the apatite represents the same event to the reported U-Pb system in zircon and Hf-W system, or these apatite in Juvinas may have recorded a later distinct thermal event. Despite large uncertainties, the mean value of the apatite  $^{207}\text{Pb}$ - $^{207}\text{Pb}$  age seems to be younger than its zircon. Similar  $^{207}\text{Pb}$ - $^{207}\text{Pb}$  age was obtained from Agoult apatite in this study, as  $4522 \pm 11$  Ma (Table 2.2, Figure 2.9; discussed in the following subsection 2.5.1.4). If Juvinas apatite and Agoult apatite recorded the same event at ca. 4530 Ma, it should be distinctly later thermal event, compared to what the zircon U-Pb system and the Hf-W systems recorded. The 4530 Ma event might be either prolonged annealing of Vesta's crust at moderate temperature ranges or reheating associated with impact or magma intrusion.

Details of the Vesta's crustal history are discussed in the following sections.

The  $^{207}\text{Pb}$ - $^{207}\text{Pb}$  age of Juvinas merrillite has been determined in this study as young as  $4186 \pm 35$  Ma. This is significantly younger than the other radiometric ages of basaltic eucrites discussed above. On the other hand, Kaneoka et al. (1995) reported the disturbed  $^{40}\text{Ar}$ - $^{39}\text{Ar}$  age for Juvinas, which has variable ages with plateau around 4.0–4.1 Ga. The  $^{40}\text{Ar}$ - $^{39}\text{Ar}$  range of Juvinas seems to be slightly younger than my merrillite Pb-Pb results. The young  $^{207}\text{Pb}$ - $^{207}\text{Pb}$  age was also reported for internal isochron of pyroxene and plagioclase in Juvinas, as  $4320.9 \pm 1.7$  Ma (Galer and Lugmair, 1996). These younger radiometric ages indicate that Juvinas suffered multiple thermal events during 4320–4000 Ma, where its K-Ar system was totally reset. The peak temperatures during the reheating(s) at 4320–4190 Ma locally exceeded the U-Pb closure temperatures of phosphates and silicates, possibly up to the melting points of eucritic basalts ( $\sim 1100^\circ\text{C}$ ). Detailed thermal history will be discussed in following section.

In summary, combining chronological records of Juvinas discussed above, this meteorite experienced several thermal processes at 4554 Ma, 4530 Ma, and ca. 4320–4000 Ma. They can be regarded as either the igneous and/or internal reheating events of Vesta's crust or the impact-induced reheating. In this study, the individual U-Pb chronological records have been investigated for Juvinas apatite and merrillite, using NanoSIMS *in-situ* dating methods. The former recorded ca. 4530 Ma thermal process, whereas the latter recorded the later impact reheating at ca. 4200 Ma.

**Figure 2.11.** Chronological information of Juvinas. Literature data are from [1] Lugmair and Shukolyukov (1998); [2] Kleine et al. (2005); [3] Touboul et al. (2015); [4] Zhou et al. (2013); [5] Galer and Lugmair (1996); [6] Lugmair (1974); [7] Shukolyukov and Begemann (1996); [8] Miura et al. (1998); [9] Kaneoka et al. (1995)



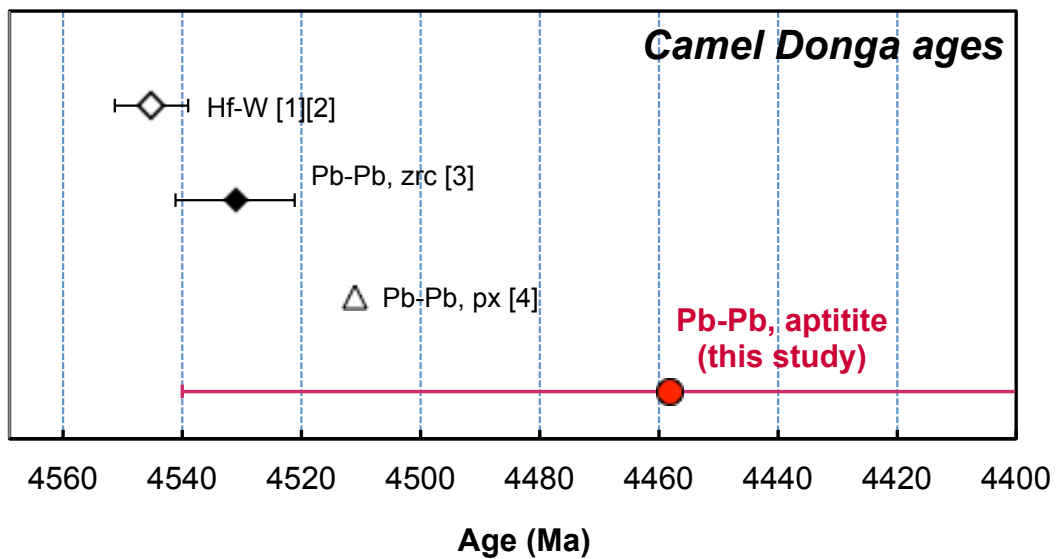
### 2.5.1.2. Examination of individual chronology: Camel Donga

Based on petrology and chemistry, previous studies suggested that Camel Donga experienced shock brecciation and subsequent high temperature metamorphism, where its Ca-pyroxenes were equilibrated (Palme et al., 1988; Metzler et al., 1995). Palme et al. (1988) pointed out co-existences of its pyroxene, silica, sulfides and metallic irons. Anomalously high abundances of its metallic Fe (~2 wt%) may be due to the secondarily reduction of igneous sulfides and silicates (FeS and FeSiO<sub>3</sub>) by sulfur evaporation and escape at around 1000°C (Palme et al., 1988). Five out of 6 apatite grains (Apt. 1–5) investigated in this study located with pyroxene, silica, sulfides and metals (subsection 2.4.1.2). It is inferred that these apatite grains suffered high temperature reheating, possibly because of an impact, where the Fe-reduction occurred. The metallic Fe-rich areas are moderately fractured with abundant fracture-filling oxides and sulfides (Figures 2.2B–D). The fractures crosscut both apatite and surrounding silicates (Figures 2.2C, D). This suggests that Camel Donga apatite is not secondary product that formed by resolutions or remelting. It is igneous. Apt. 6 in the distinct lithic clast (Figure 2.2E) may also be igneous, which was severely cracked during the impact brecciation.

The describe six apatite grains provide the slightly disturbed <sup>207</sup>Pb-<sup>206</sup>Pb isochron age of 4458 ± 82 Ma. The large variations in their model <sup>207</sup>Pb\*/<sup>206</sup>Pb\* ages of 4370–4570 Ma indicate partial disturbances of the apatite U-Pb system at ≤ 4400 Ma. Combined with textural observations, it is inferred that the igneous apatite in Camel Donga experienced impact reheating event(s) at ca. 4400 Ma, where its U-Pb system was partially disturbed. This timing seems to be somewhat older than the reported

$^{40}\text{Ar-K}$  age of ca. 3670 Ma (Palme et al., 1988). The old Hf-W mineral isochron age was previously reported as  $4545 \pm 6$  Ma, when anchored with D'Orbigny angrite (Kleine et al., 2005; Touboul et al., 2015). The Hf-W age is identical to that of Juvinas, indicating the similar (or same) thermal event at 4545 Ma. The U-Pb system in Camel Donga zircon is somewhat younger than its Hf-W system, with the weighted mean value of model  $^{207}\text{Pb}/^{206}\text{Pb}$  ages as  $4531 \pm 10$  Ma (Zhou et al., 2013). Camel Donga zircon is significantly younger than those in other basaltic eucrites, whose weighted mean  $^{207}\text{Pb}/^{206}\text{Pb}$  ages are 4554 Ma (Misawa et al., 2005; Zhou et al., 2013; Iizuka et al., 2015). The U-Pb system in its silicates seems to have been disturbed at much later event. Mean value of the model  $^{207}\text{Pb}/^{206}\text{Pb}$  ages of Camel Donga pyroxene was  $4510.9 \pm 1.0$  Ma (Iizuka et al., 2013). The similar Pu-Xe age has been reported as  $4521 \pm 20$  Ma (Shukolyukov and Begemann, 1996) and  $4507 \pm 16$  Ma (Miura et al., 1998). In summary, various chronological records in Camel Donga represent the several distinct thermal events at 4545 Ma, 4530 Ma, 4510 Ma,  $\leq 4400$  Ma and ca. 3670 Ma. The U-Pb system in the apatite dated in this study seems to have recorded the  $\leq 4400$  Ma reheating. Although the igneous apatite had initially crystallized at 4545 Ma or earlier from the eucritic basalt magma, it suffered the multiple reheating events, possibly due to impacts. The last reheating may have occurred at ca. 3670 Ma, where the K-Ar system was reset, but the U-Pb in the apatite U-Pb was not disturbed significantly.

**Figure 2.12.** Chronological information of Camel Donga. Literature data are from [1] Kleine et al. (2005); [2] Touboul et al. (2015); [3] Zhou et al. (2013); [4] Iizuka et al. (2013)



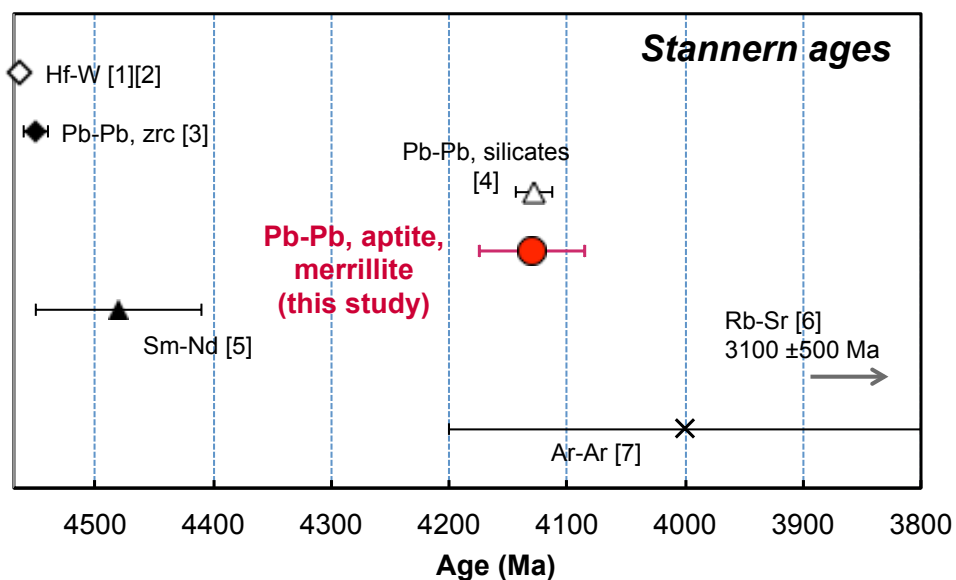
### 2.5.1.3. Examination of individual chronology: Stannern

From Stannern apatite and merrillite, the young  $^{207}\text{Pb}$ - $^{206}\text{Pb}$  age of  $4130 \pm 45$  Ma has been obtained (Table 2.3, Figure 2.8). This is distinctly younger than those of the other eucrites analyzed in this study. Only Juvinas merrillites found in the remelted area, discussed above, have the similar young  $^{207}\text{Pb}$ - $^{206}\text{Pb}$  age of ca. 4200 Ma, whereas its apatites are significantly older. As described in results subsection 2.4.1.3, both apatite and merrillite in the granulitic clasts and in the igneous clasts were investigated. The isotopic data (Table 2.3), as well as EPMA data (Table 2.2) between the apatites in the different areas are similar. It is inferred that Stannern apatite and merrillite among various lithologies may have recorded the same reheating event at ca. 4130 Ma. Possible heat source at this period is impact(s). The observed various fractures, which crosscut the phosphates and surrounding mineral phases (Figure 2.3B-D; subsection 2.4.1), also support the impact reheated records of Stannern phosphates.

Previous chronological studies of Stannern have indicated several thermal events for this meteorite, including ancient igneous event and later thermal metamorphisms. The old  $^{182}\text{Hf}$ - $^{182}\text{W}$  mineral isochron of  $4564 \pm 2$  Ma (Kleine et al., 2005; Touboul et al., 2015) is almost identical to the Hf-W isochron of eucrite whole rock of ca. 4563 Ma (Kleine et al., 2004), as well as Mn-Cr (Lugmair and Shukolyukov, 1998) and Al-Mg systems (Srinivasan et al., 1999). The  $^{207}\text{Pb}$ - $^{206}\text{Pb}$  age of its zircon is somewhat younger,  $4550 \pm 10$  Ma (Ireland and Bukovanska, 1992), although most zircons in Stannern are too small for SHRIMP analyses with a  $20\mu\text{m}$  spot (Misawa et al., 2005). The zircon  $^{207}\text{Pb}$ - $^{206}\text{Pb}$  age is identical to those of other basaltic eucrites, whose mean value is 4554 Ma (Iizuka et al., 2015). Lugmair and Scheinin (1975) previously

reported the slightly younger Sm-Nd age for Stannern as  $4480 \pm 70$  Ma. Based on petrological and mineralogical studies, the crystallization and metamorphic history have been proposed for basaltic eucrites (e.g. Nyquist et al., 1986; Takeda and Graham, 1991; Metzler et al., 1995; Yamaguchi et al. 1996, 2001, 2009; Iizuka et al., 2015). As similar to the other eucrites, Stannern may have crystallized during rapid cooling from basaltic magma at 4564 Ma. It was then annealed by subsequent slow cooling after the crystallization and/or the crustal reheating, where its pyroxene equilibration and partial recrystallization occurred. The U-Pb system in zircon of Stannern may have recorded this thermal process at 4550 Ma. On the other hand, U-Pb system in the phosphates, investigated in this study, recorded a distinctly recent reheating event, which occurred at  $4130 \pm 45$  Ma. The mean value of their model  $^{207}\text{Pb}/^{206}\text{Pb}$  ages of  $4143 \pm 34$  Ma is supportive that the U-Pb system in the phosphates was reset at this timing. The similar  $^{207}\text{Pb}$ - $^{206}\text{Pb}$  age of  $4128 \pm 16$  Ma was previously reported from Stannern whole rock, pyroxene and plagioclase isochron (Tera et al., 1997). Its K-Ar chronology was also reset at ca. 3800–4200 Ma (Podosek and Huneke, 1973; Kunz et al., 1995). It is suggested that Stannern suffered severe reheating due to impact(s) at ca. 4130 Ma, where U-Pb systems in the phosphates and the silicates, as well as K-Ar system, were completely reset. Moreover, Rb-Sr system of this meteorite was disturbed at  $3100 \pm 500$  Ma (Birck and Allegre, 1978), which suggests additional later event(s). The moderately discordant  $^{238}\text{U}$ - $^{206}\text{Pb}$  isochron age obtained in this study (see results 2.4.2.3) might have been disturbed during this later event.

**Figure 2.13.** Chronological information of Stannern. Literature data are from [1] Kleine et al. (2005); [2] Touboul et al. (2015); [3] Ireland and Bukovanska (1992); [4] Tera et al. (1997); [5] Lugmair and Scheinin (1975); [6] Birck and Allegre (1978); [7] Podosek and Huneke (1973)



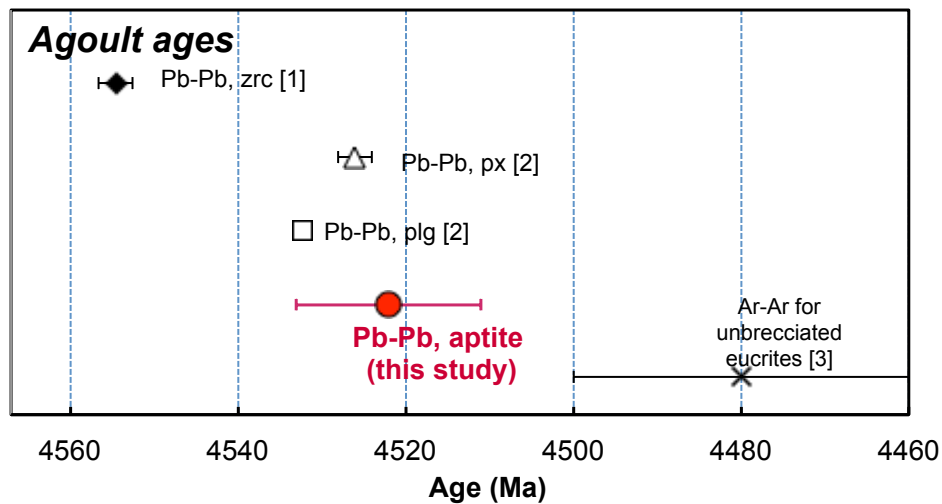
#### 2.5.1.4. Examination of individual chronology: Agoult

In contrast to the phosphates in the investigated brecciated eucrites (i.e. Juvinas, Camel Donga, Stannern), all apatite grains found in Agoult share the similar shapes and surrounding textures (results 2.4.1.4, Figure 2.4). Most of them locate in close relation to tridymite, sulfides and oxides, which may be relict of the primary igneous mesostasis, as Yamaguchi et al. (2009) pointed out. The euhedral to rounded shapes of the apatites, along with the surrounding textures, suggest that Agoult apatite may have been primary igneous mineral, which was subsequently annealed during the thermal metamorphism.

In this study, I have determined the concordant  $^{207}\text{Pb}$ - $^{206}\text{Pb}$  isochron age of Agoult apatite as  $4522 \pm 11$  Ma (result subsection 2.4.2.4). The relatively small uncertainty, with the plausible MSWD value of 1.2, infers that the U-Pb system in Agoult apatite has not been disturbed after the last thermal event at 4522 Ma. The weighted mean model  $^{207}\text{Pb}^*/^{206}\text{Pb}^*$  age is also consistent at 4524 Ma. The Pb-Pb age of the apatite is significantly younger than that of zircon in Agoult ( $4554.5 \pm 2.0$  Ma; Iizuka et al., 2015). Its plagioclase also recorded the young  $^{207}\text{Pb}$ - $^{206}\text{Pb}$  isochron age of  $4532.2 \pm 1.0$  Ma (Iizuka et al., 2013). Although the apatite results seem to be slightly younger than the plagioclase, the U-Pb system in Agoult apatite and plagioclase are consistent within uncertainties. Based on the textural and chemical features, as well as the chronological records, Iizuka et al. (2015) suggest the metamorphic origin for Agoult zircon, which recrystallized by exsolution of ilmenite during the 4554 Ma reheating at subsolidus temperature of ca. 900°C. The younger plagioclase Pb-Pb age may indicate the later reset by reheating in associate with the partial remelting at ca.

4533 Ma. The peak temperature of this event should have exceeded the melting point of eucritic basalt (~1060°C; Stolper, 1977; Yamaguchi et al., 2013). The U-Pb chronology in Agoult apatite investigated in this study represents either subsequent slow cooling after the 4533Ma reheating, or an additional moderate reheating at 4522 Ma. Meanwhile, K-Ar system records lower temperature events. Although neither  $^{40}\text{Ar-K}$  nor  $^{40}\text{Ar-}^{39}\text{Ar}$  dating has been reported for Agoult, various unbrecciated basaltic eucrites, as well as cumulate eucrites, determine the mean Ar-Ar age of  $4480 \pm 20$  Ma (Bogard and Garrison, 2003). This is significantly younger than the U-Pb of apatite in this study and that of plagioclase (Iizuka et al., 2013), but older than K-Ar system reported for the brecciated eucrites including Juvinas, Camel Donga and Stannern (Table 2.1).

**Figure 2.14.** Chronological information of Agoult. Literature data are from [1] Iizuka et al. (2015); [2] Iizuka et al. (2013); [3] Bogard and Garrison (2003)



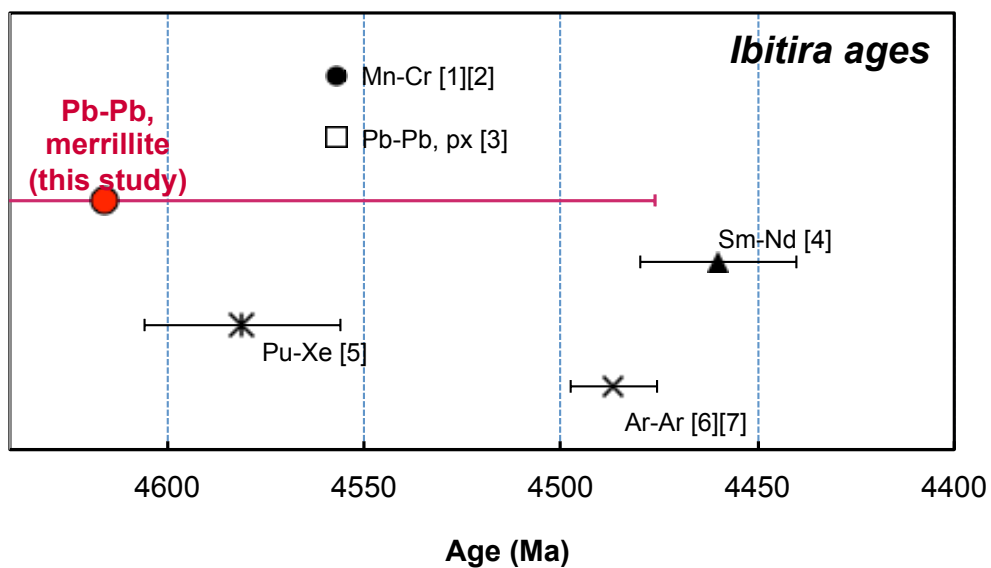
### 2.5.1.5. Examination of individual chronology: Ibitira

The concordant  $^{207}\text{Pb}$ - $^{206}\text{Pb}$  age of  $4616 \pm 140$  Ma is obtained from merrillite grains in the different textures in the Ibitira section. Only one grain, Mer. 3, locates in the wall of a large vesicle (Figure 2.5B, C), indicating this grain may have crystallized through deposition from vapor phases (Steele and Smith, 1976; Heim et al., 1999). The other grains (Mer. 1, 2, 4, and 5; Figure 2.5D) locate in the matrix along with plagioclase, pyroxene, oxides and tridymite. Heim et al. (1999) compared REE patterns of the merrillite in vesicles and those in matrix of Ibitira, which resulted in indistinguishable compositions. Based on the chemical similarities between the vesicle and matrix phosphates, they suggested that the vapor-deposition minerals (e.g. phosphates) in wall of the vesicles were equilibrated with surrounding matrix during igneous crystallization of Ibitira. The U-Pb systems in the merrillites, analyzed in this study, have no significant relationship between their textures and chronologies, which may support their chemical equilibration at magmatic temperature. However, The large age error attached to the  $^{207}\text{Pb}$ - $^{206}\text{Pb}$  age makes it difficult to discuss further interpretation.

The earlier chronological studies revealed that bulk U-Th-Pb system in Ibitira recorded 4560–4550 Ma thermal event (Wasserburg et al., 1977; Chen and Wasserburg, 1985; Manhes et al., 1987). The similar ages were reported from other chronologies, Pu-Xe ( $4581 \pm 25$  Ma; Shukolyukov and Begemann, 1996) and Mn-Cr ( $4557 \pm 2/-4$  Ma; Lugmair and Shukolyukov, 1998). Iizuka et al. (2014) reported the precise  $^{207}\text{Pb}$ - $^{206}\text{Pb}$  isochron age of  $4556.75 \pm 0.57$  Ma from acid leached pyroxene-rich fractions and whole rock of Ibitira. Based on chronological, mineralogical and chemical information,

it is inferred that Ibitira experienced thermal metamorphism and partial remelting at 4557 Ma. The U-Pb system in the Ibitira merrillite should have been reset during the same thermal process. The  $^{207}\text{Pb}$ - $^{206}\text{Pb}$  isochron age of the merrillite at  $4616 \pm 140$  Ma seems to be consistent to the other chronometric system described above, although its uncertainty is too large to discuss. The large  $^{207}\text{Pb}$ - $^{206}\text{Pb}$  age error makes it indistinguishable from the reported  $^{147}\text{Sm}$ - $^{143}\text{Nd}$  ( $4460 \pm 20$  Ma; Prinzhofer et al., 1992) and  $^{40}\text{Ar}$ - $^{39}\text{Ar}$  ages ( $4487 \pm 15$  Ma; Bogard and Garrison, 1995). The young Ar-Ar and Sm-Nd records may indicate later moderate disturbances. On the other hand, the weighted mean model  $^{207}\text{Pb}^*/^{206}\text{Pb}^*$  age was calculated more precisely as  $4552 \pm 27$  Ma. This is significantly older than Sm-Nd and Ar-Ar, suggesting U-Pb system in Ibitira merrillite retains the earlier thermal processes during crystallization to  $\sim 4530$  Ma. Possible cause of the large error of the  $^{207}\text{Pb}$ - $^{206}\text{Pb}$  isochron is that Ibitira sample studied here contains only merrillite but no apatite. Generally, apatite has higher U/Pb compared with co-existing merrillite (i.e. apatite has more radiogenic Pb than merrillite). Further analyses of Ibitira apatite will help more plausible interpretations concerning the Ibitira's thermal history.

**Figure 2.15.** Chronological information of Ibitira. Literature data are from [1] Lugmair and Shukolyukov (1998); [2] Yin et al. (2009); [3] Iizuka et al. (2014); [4] Prinzhofer et al. (1992); [5] Shukolyukov and Begemann (1996); [6] [7] Bogard and Garrison (1995; 2003)



## 2.5.2. Comparison with other chronologies

Again, the goal of the present study is to reveal the thermal evolutionary history of ancient crusts on Vesta and Vesta-like protoplanets. As discussed in the former subsections (2.5.1.1–2.5.1.5), NanoSIMS *in-situ* U-Pb dating of phosphates in the basaltic eucrites indicate the multiple thermal events after their crystallization. In order to elucidate the complicated metamorphic histories of the eucrites, it is important to combine and compare various data from other eucrites. Figure 2.16 compares the literature and the present chronological data of several radiometric systems (Mn-Cr, Al-Mg, Hf-W, U-Pb and K-Ar) in basaltic eucrites. In this subsection, I compare the analyzed U-Pb systems in the phosphates with the other systems, and discuss the metamorphic events recorded in these chronometers.

A number of chronological studies were investigated within the eucrites, including short-lived  $^{53}\text{Mn-Cr}$ ,  $^{182}\text{Hf-W}$  and  $^{26}\text{Al-Mg}$  systems (Lugmair and Shukolyukov, 1998; Srinivasan et al., 1999, 2007; Quitté et al., 2000; Nyquist et al., 2003; Kleine et al., 2004, 2005; Touboul et al., 2015; Roszjar et al., 2016), and long-lived  $^{147}\text{Sm-Nd}$ ,  $^{87}\text{Rb-Sr}$  and U-Th-Pb systems (Lugmair and Scheinin, 1975; Birck and Allegre, 1978; Prinzhofer et al., 1992; Ireland and Bukovanska, 1993; Galer and Lugmair, 1996; Tera et al., 1997; Lee et al., 2009; Misawa et al., 2005; Zhou et al., 2013; Iizuka et al., 2013, 2014, 2015). The K-Ar systems were also investigated using  $^{40}\text{Ar-K}$  and  $^{40}\text{Ar-}^{39}\text{Ar}$  methods (Podosek and Hunke, 1973; Palme et al., 1988; Kunz et al., 1995; Kaneoka et al., 1995; Bogard and Garrison, 1995, 2003). Among them, the Mn-Cr and Hf-W isochrons from whole rock samples of several basaltic eucrites indicate significantly old ages at 3–5 Myrs after CAI (i.e. absolute ages of 4565–4563

Ma; Lugmair and Shukolyukov, 1998; Quitté et al., 2000; Kleine et al., 2004). It is suggested that the magmatic events and the crustal formation on Vesta was active within first 3–5 Myrs in the early solar system, where the most basaltic eucrites crystallized. The similar ages were reported from internal mineral isochrons of Al-Mg and Hf-W in some basaltic eucrites (Nyquist et al., 2003; Kleine et al., 2005; Touboul et al., 2015). One of the studied samples, Stannern, also has the old  $^{182}\text{Hf}$ - $^{182}\text{W}$  age of  $4564 \pm 2$  Ma (Kleine et al., 2005; Touboul et al., 2015). Timing of the igneous crystallization of Stannern is likely to be distinctly earlier than those recorded in the other radiometric systems (e.g.  $^{207}\text{Pb}$ - $^{206}\text{Pb}$  ages of zircon:  $4550 \pm 10$  Ma; Ireland and Bukovanska, 1993).

The  $^{207}\text{Pb}$ - $^{206}\text{Pb}$  ages of zircons in the most basaltic eucrites are significantly younger than the whole rock Mn-Cr and Hf-W isochrons, with a weighted mean value of  $^{207}\text{Pb}$ - $^{206}\text{Pb}$  ages at  $4554.1 \pm 3.1$  Ma (Iizuka et al., 2015 and references therein). Haba et al. (2014) investigated mineralogy and REE patterns of zircons in thermally metamorphosed basaltic eucrites and suggested the post-igneous zircon growth during for the metamorphosed eucrites. Considering textural features of zircons, such as their large euhedral shapes and co-existing ilmenite and exsolution minerals, as well as their chronology and chemistry, Iizuka et al. (2015) suggested the secondary origin for the eucrites zircons, which re-crystallized during a global reheating of Vesta's crust at 4554 Ma with the metamorphic temperature at ca. 900°C. Although the older Hf-W ages were reported for zircons as 4565–4560 Ma in several eucrites (Srinivasan et al., 2007; Roszjar et al., 2016), the other samples show Hf-W variations down to ca. 4530 Ma (Roszjar et al., 2016). The existence of the younger zircons (~4530 Ma in Hf-W and

Pb-Pb; Zhou et al., 2013; Roszjar et al., 2016) in several eucrites may be due to either a later intense impact reheating or a prolonged magmatism of Vesta.

The U-Pb systems in the phosphates, analyzed in this study, seem to be younger than the other chronological systems, including whole-rock and internal isochrons of Mn-Cr, Al-Mg and Hf-W, as well as *in-situ* U-Pb and Hf-W systems in the eucritic zircons (Figure 2.16). The precise  $^{207}\text{Pb}$ - $^{206}\text{Pb}$  isochron age of Agoult apatite ( $4522 \pm 11$  Ma, this study) is significantly younger than the  $^{207}\text{Pb}$ - $^{206}\text{Pb}$  age of its zircon ( $4554.5 \pm 2.0$  Ma; Iizuka et al., 2015), and similar or slightly younger than that of its plagioclase ( $4532.2 \pm 1.0$  M; Iizuka et al., 2013). The Pb-Pb age of Agoult apatite is distinctly older than the reported  $^{40}\text{Ar}$ - $^{39}\text{Ar}$  ages of unbrecciated eucrites of  $4480 \pm 20$  Ma (Bogard and Garrison, 2003). Because they are unbrecciated, the  $^{40}\text{Ar}$ - $^{39}\text{Ar}$  ages are interpreted to reflect the slow cooling of Vesta's crust with temperature ranges ca. 300–500 °C (Bogard and Garrison, 2003). The apatite U-Pb system generally records an intermediate temperature events between those recorded by the U-Pb in zircon and the K-Ar in plagioclase. It is suggested that Agoult apatite, and possibly, those in other unbrecciated eucrites as well, recorded the slow cooling process of Vesta's crust. The apparently old  $^{207}\text{Pb}$ - $^{206}\text{Pb}$  age of Ibitira merrillite ( $4614 \pm 140$  Ma, this study) seems to have recorded the similar event, however, its large error hampers further discussion.

In contrast, the U-Pb systems in phosphates from the brecciated eucrites recorded significantly younger timings (described in results subsection 2.4.2.1–2.4.2.3 and discussed in 2.5.1.1–2.5.1.3). In the Stannern phosphates, U-Pb system was completely reset at  $4130 \pm 45$  Ma (Figure 2.8A) with subsequent slight disturbance. The merrillites in Juvinas remelting area provided the similar young  $^{207}\text{Pb}$ - $^{206}\text{Pb}$  age of 4186

$\pm 35$  Ma (Figure 2.6A). The young ages of the phosphate are slightly older than reported K-Ar chronologies of Stannern, Juvinas and other brecciated eucrites (Kaneoka et al., 1995; Kunz et al., 1995; Bogard and Garrison, 1995; 2003). Previous petrological and geochemical studies indicated the complicated histories for these meteorites, such as post-crystallization thermal equilibration, impact brecciation and partial remelting (e.g. Duke and Silver, 1967; Palme et al., 1988; Takeda and Graham, 1991; Metzler et al., 1995; Yamaguchi et al., 1996). Combining the results from this study and the literatures, as well as their implications, I may regard the young  $^{207}\text{Pb}$ - $^{206}\text{Pb}$  ages of the phosphates in Juvinas and Stannern as timings of the intense impact-induced reheating at ca. 4200–4100 Ma. In contrast, Juvinas apatite retained the older  $^{207}\text{Pb}$ - $^{206}\text{Pb}$  age of  $4529 \pm 34$  Ma (Fig 2.6C), which is similar to those in unbrecciated eucrites, i.e. Agoult apatite with  $^{207}\text{Pb}$ - $^{206}\text{Pb}$  age at ca. 4522 Ma and Ibitira merrillite with  $^{207}\text{Pb}$ - $^{206}\text{Pb}$  ranges of 4480–4600 Ma in this study. Meanwhile, the U-Pb system in Camel Donga apatite seems to have been disturbed in distinct event. Their model  $^{207}\text{Pb}^*/^{206}\text{Pb}^*$  ages vary between 4370–4570 Ma. The lower value is younger than its  $^{182}\text{Hf}$ - $^{182}\text{W}$  mineral isochron (4545 Ma; Kleine et al., 2005; Touboul et al., 2015) and its zircon  $^{207}\text{Pb}$ - $^{206}\text{Pb}$  age (4531 Ma; Zhou et al., 2013). Meanwhile, the U-Pb system in Camel Donga apatite is significantly older than its K-Ar chronology (3670 Ma; Palme et al., 1988), suggesting that Camel Donga apatite recorded an individual thermal event at ca. 4400 Ma or later. Numerical models indicates that Vesta-sized asteroid may have retain the internal residual heat, which had been produced from the earlier decay of short-lived  $^{26}\text{Al}$ , up to  $\sim 150$  Myr after its accretion (e.g. Neumann et al., 2014). After 4400 Ma, the possible heat source should be impact only. Hence, I may associate the young U-Pb disturbances are of the

Camel Donga apatite with the impact-induced reheating at ca. 4400 Ma.

In summary, it is considered that the U-Pb system in phosphates in the unbrecciated basaltic eucrites are likely to indicate the cooling process of Vesta's crust after igneous and/or high-temperature reheating events. In contrast, the U-Pb system in phosphates in the brecciated eucrites may have recorded their local and intense impact-induced reheating.

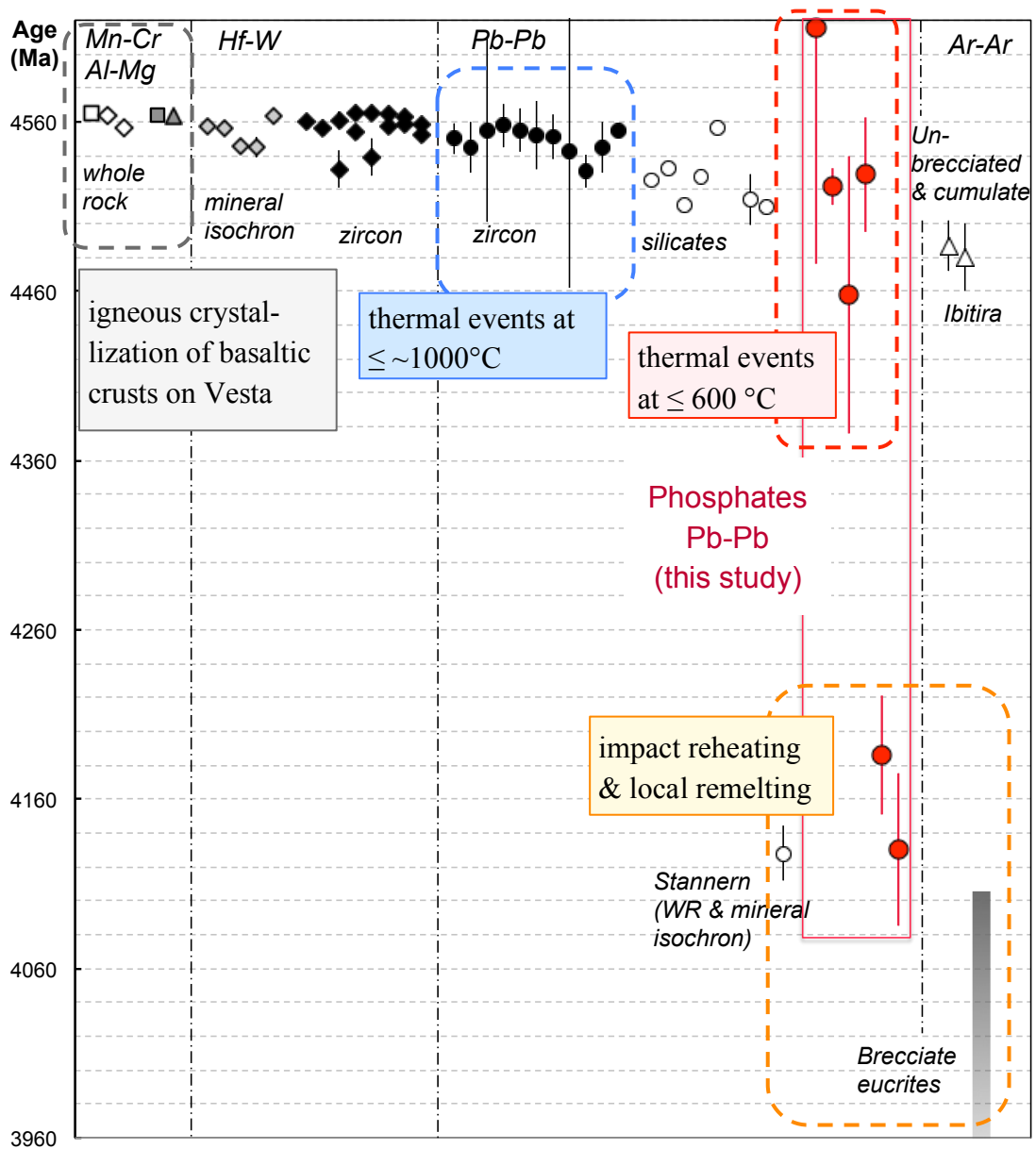


**Figure 2.16.** Comparison of chronological studies of basaltic eucrites.

Literature data are from: Lugmair and Shukolyukov (1998); Nyquist et al. (2003); Quitté et al. (2000); Kleine et al. (2004, 2005); Touboul et al. (2015); Srinivasan et al. (2007); Roszjar et al. (2016); Misawa et al. (2005); Zhou et al. (2013); Iizuka et al. (2013, 2014, 2015); Tera et al. (1997); Bogard and Garrison (1995, 2003).

### 2.5.3. Closure Temperature of U-Pb System in Phosphates of the Basaltic Eucrites

In order to discuss the thermo-chronological records of the eucrites, it is necessary to consider the closure temperatures of various radiometric systems. In this subsection, I calculate the closure temperatures of U-Pb systems in minerals found in the basaltic eucrites. It is inferred that closure conditions of U-Pb systems in the phosphates are different between the unbrecciated eucrites and the brecciated ones.

Diffusion properties of Pb in zircon (Cherniak and Watson, 2003), apatite (Cherniak et al., 1991), plagioclase (Cherniak, 1995) and pyroxene (Cherniak, 2001) were determined experimentally (as summarized in Table 2.4), although no experimental data is currently available for merrillite. With a certain diffusion scale ( $a$ ) and a cooling rate of the system ( $T'$ ), closure temperatures of U-Pb system ( $T_c$ ) can be calculated using Dodson's law (Dodson, 1973):

$$T_c = \frac{E}{\{R \ln(ARD_0T_c^2/a^2ET')\}}$$

where,  $E$  is activation energy,  $D_0$  is diffusion coefficient,  $R$  is gas constant, and  $A$  is a dimensionless constant. For the metamorphosed basaltic eucrites and Ibitira, rapid cooling rates during the thermal event were estimated as 0.004–0.02 °C/year (Miyamoto and Takeda, 1977; Miyamoto et al., 2001; Schwartz and McCallum, 2005) based on the equilibration of Ca-pyroxenes at high temperature ranges (~1200–850 °C; Miyamoto and Takeda, 1977). Assuming the constant cooling rates for various temperatures, and assuming the diffusion scales from typical grain sizes in the observed samples (i.e. zircon: 10µm, apatite: 50µm, pyroxene and plagioclase: 200µm), I calculate the closure temperatures of U-Pb system (Table 2.4). Under this condition, the U-Pb system in

apatite close around 600°C, while the closure temperature of zircon U-Pb system leaches melting point of the eucrite basalt (1060°C; Stolper, 1977). Cooling rates of the basaltic eucrite at this temperature ranges (around 600°C) might be slower than those in pyroxene equilibration temperatures (~1200–850°C), because of the ambient temperatures in the ancient Vesta's crusts. Hence, the closure temperature of U-Pb in the phosphates is estimated as  $\leq 600^\circ\text{C}$  for the basaltic eucrites. However, this is only the case for unbrecciated eucrites, not for brecciated ones. Most brecciated eucrites experienced intense reheating, partial melting and impact excavation from depth, which changed the conditions of Pb diffusion. Consequently, it is inferred that U-Pb system in apatite (+merrillite) from unbrecciated eucrites, such as Agoult and Ibitira, recorded the last thermal event in the crusts on the parent bodies at temperature of  $\leq 600^\circ\text{C}$ . The U-Pb system in apatite (+merrillite) from brecciated eucrites, such as Juvinas, Camel Donga and Stannern, may indicate past intense reheating with partial remelting. In Juvinas, as discussed in subsection 2.5.1.1, the apatite recorded the earlier event at ca. 4530 Ma, while its merrillite recorded the ca. 4200 Ma reheating. It is indicated that although Juvinas experienced the intense impact at 4200 Ma along with the local remelting (Figures 2.1), the average whole rock temperature did not exceed the U-Pb closure temperature (i.e. 600 °C) during this impact.

**Table 2.4.** Diffusion parameters of Pb and closure temperatures of U-Pb system in the igneous minerals

	zircon	plagioclase	pyroxene	apatite
activation energy (kJ)	550	327	372	231
diffusion coefficient (m <sup>2</sup> /s)	0.11	0.0044	3.8E-05	2.0E-08
typical grain size (μm)	10	200	200	50
cooling rate for basaltic eucrites (°C/year)	0.004 – 0.02			
calculated U-Pb closure temperature (°C)	1030 – 1070	670 – 710	930 – 980	590 – 630

#### 2.5.4. Thermal History of the Eucrite Parent Body

In the former subsections, I discuss the U-Pb records in phosphates in the individual eucrites (2.5.1), compare them to the other radiometric ages (2.5.2), and calculate the closure temperatures of the U-Pb systems (2.5.3). Here, the comprehensive evolutionary history of Vesta's crusts is discussed along the literature implications. The metamorphic history is schematically illustrated in Figure 2.17. This study provides the new thermo-chronological constraints on the metamorphic history of Vesta, based on the *in-situ* U-Pb dating of the eucrites phosphates.

The formational and evolutionary history of the ancient basaltic crusts on Vesta has been well discussed, in terms of mineralogy and chemistry of basaltic eucrites (e.g. Takeda and Graham, 1991; Metzler et al., 1995; Yamaguchi et al., 1996, 2001, 2009). A series of chronological studies provided the important constraints on their igneous and/or metamorphic events (e.g. Ireland and Bukovanska, 1993; Galer and Lugmair, 1996; Tera et al., 1997; Lugmair and Shukolyukov, 1998; Srinivasan et al., 1999, 2007; Quitté et al., 2000; Nyquist et al., 2003; Kleine et al., 2004, 2005; Misawa et al., 2005; Zhou et al., 2013; Iizuka et al., 2013, 2014, 2015; Touboul et al., 2015; Roszjar et al., 2016). To summarize the previous knowledge, the major evolutionary events of Vesta's crust can be described as following (Figure 2.17):

- (I) An early accretion and core-mantle differentiation of Vesta by 4563 Ma.
- (II) A crustal differentiation at 4565–4563 Ma. The basaltic crusts on Vesta crystallized either from rapid cooling of the residual magma ocean (Mandler and Elkins-Tanton, 2013; Steenstra et al., 2016) or from partial melting of the chondritic precursor (Stolper, 1977).

- (III) A global thermal metamorphism of the basaltic crusts. Most basaltic eucrites, which primarily had rapidly cooled igneous textures (e.g. subophitic), experienced thermal equilibration and recrystallization during this period. Based on the precise Pb-Pb dating of metamorphic zircon in Agoult, Iizuka et al. (2015) constrained the timing of this crustal metamorphism at 4554 Ma.
- (IV) High temperature reheating events, which were sometimes accompanied by partial remelting and recrystallization.
- (V) Impact brecciation.

The events (III) and (IV) might be in inverse orders or they represent the same events. Chronological studies of various brecciated eucrites, including Juvinas, Stannern and Camel Donga, have suggested the several distinct impact reheating events. It is unlikely that events (III) and (IV) was a single global reheating. Rather, they might have been multiple events on Vesta's crust. Although Ibitira has the different parent body, it has identical  $^{53}\text{Mn}$ - $^{53}\text{Cr}$  and  $^{207}\text{Pb}$ - $^{206}\text{Pb}$  ages at 4557 Ma (Lugmair and Shukolyukov, 1998; Iizuka et al., 2014), as well as the equilibrated and highly recrystallized textures with partially remelted features (Yamaguchi et al., 1996; Miyamoto et al., 2001). It is indicated that the Ibitira parent body experienced the similar thermal history.

In this study, I provide the new thermo-chronological constraints from the *in-situ* U-Pb chronologies of the phosphates. The concordant  $^{207}\text{Pb}$ - $^{206}\text{Pb}$  age of Agoult apatite at  $4522 \pm 11$  Ma indicates the moderately hot conditions for Vesta's crust; i.e. the ambient temperature of  $\leq 600$  °C at the depth where Agoult existed at 4522 Ma. The slightly older  $^{207}\text{Pb}$ - $^{206}\text{Pb}$  age of its plagioclase (ca. 4533 Ma; Iizuka et al., 2013) may have recorded the same thermal process. Both apatite and plagioclase in Agoult are

significantly younger than (II) the igneous crystallization of eucrites at 4565–4563 Ma or (III) the crustal metamorphisms accompanied by zircon recrystallization during 4554 Ma. The 4530 Ma thermal event, that Agoult apatite and plagioclase recorded, may have been either the residual slow cooling from an earlier high temperature event (e.g. partial remelting) or a moderate crustal reheating at  $\leq 600$  °C. This study has also revealed that apatite in Juvinas has the identical  $^{207}\text{Pb}$ - $^{206}\text{Pb}$  age of ca. 4530 Ma. The similarity between Agoult and Juvinas apatites infer that they recorded the same thermal event during 4530 Ma. However, since Juvinas is one of the severely brecciated eucrites, there is a possibility that its apatite recorded a distinct impact reheating at 4530 Ma. Meanwhile, the earlier studies reported the similar Pb-Pb and Hf-W ages around 4530 Ma for zircons in several basaltic eucrites, including those in Camel Donga (Zhou et al., 2013; Roszjar et al., 2016). It is suggested that the 4530 Ma reheating might be a global thermal event of Vesta's crust, rather than local ones.

The younger U-Pb records in the phosphates of the brecciated eucrites (i.e. Juvinas merrillite, Camel Donga and Stannern) reflect later impact-induced reheating events. The reheating temperature must have been higher than 600°C, the closure temperature of apatite U-Pb system under the conditions in Vesta's crust (see 2.5.3 and Table 2.4). Considering their mineralogical observations, such as the partially remelted textures in Juvinas (Figures 2.1), peak temperature at the individual impact reheating may have locally exceeded the melting points for the eucritic basalt of ca. 1060 °C. Hence, the younger ages of Camel Donga apatite, Juvinas merrillite, and Stannern apatite and merrillite indicate timings of the intense impact reheating along with the partial remelting at  $\leq 4400$  Ma, 4200 Ma and 4130 Ma, respectively. The younger ages

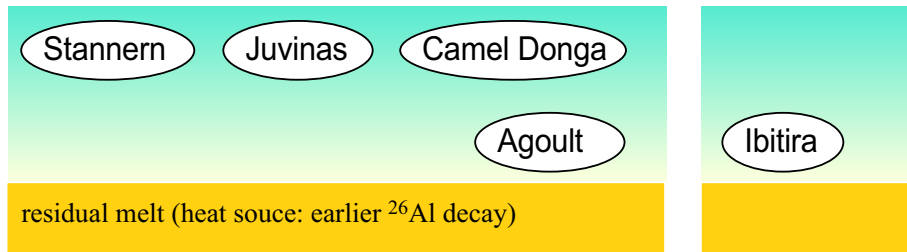
of Juvinas and Stannern (4200–4130 Ma) are slightly older than the disturbed K-Ar systems in the brecciated eucrites. Their  $^{40}\text{Ar}$ - $^{39}\text{Ar}$  ages varies between ca. 4000–3400 Ma, with several apparent peaks around 3500 Ma and 3800 Ma (Bogard, 2011; Bogard and Garrison, 1995; 2003). It is inferred that during these periods, Vesta's crust experienced the repeated impact brecciation and reheating (with possibly, partial remelting). The last intense impact reheating, where the U-Pb systems in the phosphates were reset, may have occurred at 4200–4100 Ma. Much moderate impact events are likely to have lasted until ~3400 Ma, which were recorded in the K-Ar systems. This study is the first report that identified such impact events on Vesta, using NanoSIMS *in-situ* U-Pb dating techniques on the eucrites phosphates.

## The evolutionary history of the basaltic crusts on Vesta

(I) An early accretion & core-mantle differentiation

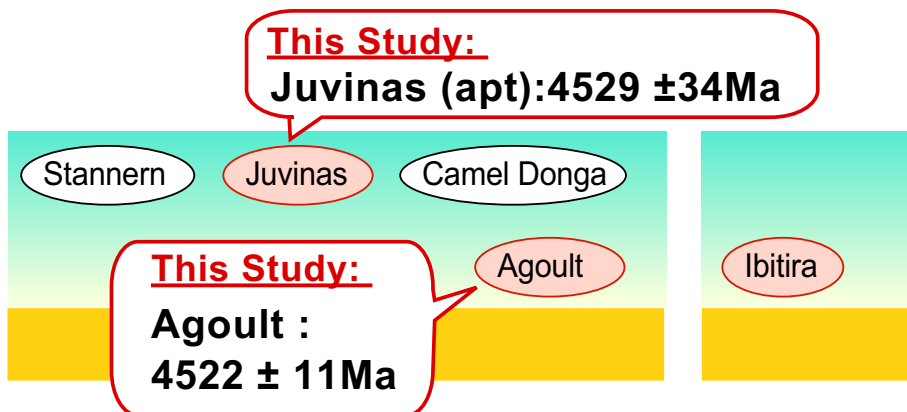
(II) A Crustal differentiation at 4565–4563 Ma (partly lasted until ~4530 Ma)

\*ages: whole rock Mn-Cr, Hf-W, Al-Mg; Hf-W zircons (literatures)



(III) thermal metamorphism of the earlier crusts during 4554 ~ 4530 Ma

\*ages: U-Pb zircon (literatures); U-Pb phosphates (this study)



(IV) & (V) Impact reheatings concentrated or terminated during ~4100 Ma

\* ages: phosphates U-Pb (this study) & Kr-Ar/Ar-A; (literatures)

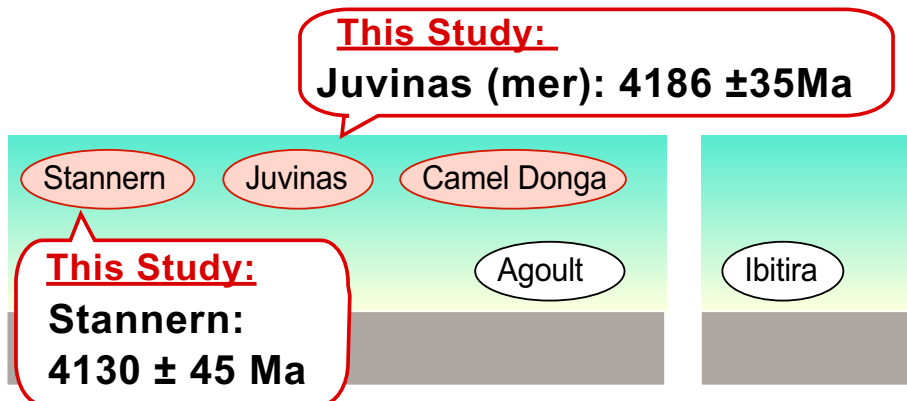


**Figure 2.17.** The schematic image of the metamorphic evolution history of Vesta's crusts, along with the constraints of U-Pb in the phosphates. Literatures are the same as in Figure 2.16.

## 2.6. Conclusions

In order to reveal the thermal history of Vesta's crust at moderate temperature ranges (ca. 600°C), I have conducted in-situ U-Pb dating of phosphates in the basaltic eucrites, Juvinas, Camel Donga, Stannern and Agoult, and a unique basaltic achondrite, Ibitira, using NanoSIMS 50. In all dated phosphates, their U-Pb systems recorded significantly younger events, compared to their crystallization timing at ca. 4554 Ma.

For brecciated eucrite, U-Pb in Stannern phosphates is the youngest at  $^{207}\text{Pb}$ - $^{206}\text{Pb}$  age of  $4130 \pm 45$  Ma. The U-Pb system of Camel Donga seems to be disturbed during  $\sim 4500 - 4400$  Ma. Two distinctly different ages are obtained from Juvinas apatite and merrillite, with  $^{207}\text{Pb}$ - $^{206}\text{Pb}$  ages of  $4529 \pm 34$  Ma and  $4186 \pm 35$  Ma, respectively. Considering their textural features and locations, it is inferred that the younger merrillite in Juvinas suffered (partial) remelting and recrystallization with surrounding matrix during reheating at ca. 4200 Ma. Its apatite, in contrast, seems to have survived at the 4200 Ma reheating and retained its U-Pb system from the earlier events. This is the first study that identified such local differences within the single sample, by taking advantages of *in-situ* dating methods. Because Vesta's interior (initially warmed by the heat from  $^{26}\text{Al}$  decay) should have been cooled down by 4500 Ma, possible heat sources after 4400 Ma are impacts.

For unbrecciated eucrites,  $^{207}\text{Pb}$ - $^{206}\text{Pb}$  age of Agoult apatite is determined precisely at  $4522 \pm 11$  Ma. This is significantly younger than its zircon and it may have recorded either the slow cooling process of Vesta's crust or a later moderate reheating at 600°C. U-Pb system in Ibitira merrillite seems to be old as well, however, its uncertainty is too large to distinguish from the other chronologies.

Consequently, I may consider the U-Pb system in phosphates in the unbrecciated eucrites recorded thermal processes in the Vesta's crusts at early stage. The record in Agoult apatite indicates its ambient temperature was cooled down to ca. 600 °C at 4522 Ma. The old apatite in Juvinas also recorded the similar age. Such thermal process (either slow cooling of crusts or moderate reheating) might have been the global event on Vesta and Vesta-like protoplanets at 4520 – 4530 Ma. Meanwhile, the significantly younger Pb-Pb ages from the brecciated eucrites indicate that Vesta experienced the multiple impact reheating events significantly after the cooling down of its interior and the termination of magmatism. The apparent existences of the partially remelted textures in some samples, especially in Juvinas, indicate the high reheating temperatures at the impacts, i.e. locally  $\geq 1060$  °C. The younger Pb-Pb ages of Juvinas merrillite and Stannern phosphates around ca. 4200 Ma are slightly older than K-Ar systems of the brecciated eucrites. Their  $^{40}\text{Ar}$ - $^{39}\text{Ar}$  ages concentrate at ca. 3500 Ma and 3800 Ma. This study is the first report that identified the intense impact reheating events at ca. 4200 Ma on Vesta from *in-situ* U-Pb chronology. It is inferred that Vesta (and possibly, Vesta-like ancient protoplanets, as well) experienced the repeated impact events during 4200 – 3400 Ma.

## CHAPTER 3

# IN-SITU U-Pb & Hf-W DATING OF A YOUNG ZIRCON IN A MESOSIDERITE, ASUKA 882023

In chapter 3, I report the *in-situ* U-Pb and Hf-W chronologies in a zircon of a thermally metamorphosed mesosiderite. As described in Chapter 1.3, mesosiderite is a unique meteoritical group that experienced the silicates-metal mixing. Their parent body (mesosiderites parent body; MPB) is estimated as Vesta-like protoplanet. Records in the mesosiderites provide valuable insights concerning the early impact destruction and/or accretion processes of Vesta-sized protoplanets. It is important to constrain timings of their silicates-metal mixing and thermal events on MPB. Previous studies of mineralogy, geochemistry and chronologies proposed some possible formation models for mesosiderites. However, none of them revealed a comprehensive history of MPB, because most mesosiderites suffered severely complicated brecciation and thermal processes. Uranium-Pb systems in meteoritic zircons recorded high-temperature igneous and/or reheating events of their parent bodies. Meteoritic zircons may also have recorded precise  $^{182}\text{Hf}$ - $^{182}\text{W}$  relative ages for ancient thermal events ( $\leq 50$  Myr after CAI formation; i.e. ca. 5–6 times of  $^{182}\text{Hf}$  half-life of 8.9 Myr). The goal of this study is to understand the MPB evolutionary history, especially, its ancient impact records. Here,

I conduct *in-situ* U-Pb and Hf-W dating of a single zircon in mesosiderite, Asuka 882023, in order to constrain the timings of its reheating and silicates-metal mixing events. My data indicate that the ancient basaltic crusts on MPB suffered high-temperature metamorphism at ca. 4530 Ma, significantly younger than MPB crustal differentiation at  $\geq 4560$  Ma. The main part of this study is published in Koike et al. (2017) as my initiative work with co-authors.

In section 3.1, I introduce background and purpose of the present study. The sample descriptions and SEM observational conditions are described in section 3.2. NanoSIMS U-Pb and Hf-W dating methods are reported in section 3.3. Results of U-Pb and Hf-W dating are reported in section 3.4 and discussed in section 3.5.1. Together with the literature data and implications, I discuss the formational processes of the analyzed zircon (3.5.2), and various chronological constraints (3.5.3). In section 3.5.4, I finally propose possible interpretations of the MPB evolutionary history.

### 3.1. Introduction

Mesosiderites are unique differentiated meteorites. As described in Chapter 1, they are classified as stony-iron meteorites, characterized by mixtures of brecciated basaltic silicates and Fe–Ni metals. Their silicates-metal mixtures should have been formed during impact-related processes on the early protoplanet(s). In the most mesosiderites, the silicate parts were thermally metamorphosed and brecciated. Mineralogy, chemistry and oxygen 3-isotopic compositions ( $\Delta^{17}\text{O}$ ) of these silicates are similar to those of basaltic eucrites (Clayton and Mayeda, 1996; Greenwood et al., 2015). It is suggested that the mesosiderites parent body (hereafter, abbreviated term ‘MPB’ is used) is a differentiated protoplanet(s) like Vesta. However, there was no mesosiderite-like silicate-metal mixed regolith, identified on Vesta surface by Nasa’s Dawn mission (Prettyman et al., 2012; Peplowski et al., 2013). Hence, MPB is regarded as the past Vesta-like protoplanet (not Vesta itself), which may not exist currently. Meanwhile the metal parts of mesosiderites have geochemical similarities with magmatic iron meteorites such as IIIAB (Wasson and Rubin, 1985; Clayton et al., 1986). Because mesosiderites are valuable fragments of the ancient protoplanets, their formational histories are helpful to elucidate the early impact destruction and/or accretion processes of differentiated bodies of Vesta-size.

Several plausible models have been proposed to explain the mesosiderites formation. The earlier studies have suggested external origins for mesosiderites’ silicates and metals, where MPB basaltic crusts and molten metallic core from impactor(s) were mixed during ancient impacts (Wasson and Rubin, 1985; Rubin and Mittlefehldt, 1993). An alternative model suggested their internal origins, where the

earlier MPB was almost catastrophically destroyed and re-accreted with core-crust mixtures (Scott et al., 2001). Their model cannot explain the apparent absence of MPB mantle components as meteorites. The previous studies made efforts to elucidate MPB comprehensive history, including timings of the impact-related silicates-metal mixing and the reheating events, as well as possible heat sources for the thermal process. However, none of the above studies revealed the MPB history completely, because most mesosiderites suffered severe brecciation and high-temperature metamorphisms (e.g. Sugiura, 2013).

Zircon, an accessory mineral in basaltic achondrites including mesosiderites, is a plausible candidate that may have recorded the ancient events. Chronological systems in zircon (i.e. U- Pb and Hf-W) are generally robust to secondary processes and retain the earlier high-temperatures thermal processes. The U-Pb and Hf-W chronologies in mesosiderites zircons would provide valuable insights to the ancient igneous and/or metamorphic events on MPB. Previous studies have reported the  $^{207}\text{Pb}$ - $^{206}\text{Pb}$  age variations between ca. 4563–4500 Ma by *in-situ* U-Pb dating of zircons in some mesosiderites (Ireland and Wlotzka, 1992; Haba et al., 2017). The  $^{182}\text{Hf}$ - $^{182}\text{W}$  chronology in meteoritic zircon (using the short-lived radioactive nuclide,  $^{182}\text{Hf} \rightarrow ^{182}\text{W}$ , with the half-life of 8.9 Myr) could constrain the ancient thermal events within the first ca. 50 Myr in the solar system, more precisely. However, previous *in-situ* Hf-W dating reported by Ireland (1991) failed to determine a  $^{182}\text{Hf}$ - $^{182}\text{W}$  age of mesosiderites zircon, mostly because of technical limitation at that time (Chapter 1.3.3), as well as the low W concentrations and small grain sizes (typically ca. 10  $\mu\text{m}$ ) of the zircons. The *in-situ* U-Pb and Hf-W dating of the mesosiderite zircons are helpful to understand the early

evolutional processes of the protoplanets.

The goal of this study is to elucidate the evolutional history of MPB crusts from the mesosiderites records. I focus on U-Pb and Hf-W chronologies in the mesosiderite zircon, and conduct combined *in-situ* dating using NanoSIMS 50 with a high spatial resolution and maximized mass resolution powers. This work is published in Koike et al. (2017), as my initiative study with N. S., N. T., A. I. and Y. S. This is the first report of *in-situ* Hf-W dating of the meteoritic zircon using NanoSIMS 50. Here I report chronology of a single zircon grain from Asuka 882023 mesosiderite. Then, I will discuss the evolution history of MPB based on my analyses, as well as previous and recent studies.

**Table 3.1.** Summary of earlier chronological studies of mesosiderites and the U–Pb and Hf–W ages of Asuka 882023 zircon obtained in this study. Errors assigned to the ages are 2-sigma.

Chronology	Analyzed Samples	Absolute Age (Ma)	Refs
Reported values			
$^{207}\text{Pb}$ – $^{206}\text{Pb}$	Estherville	4555 ± 35	[1][2]
$^{238}\text{U}$ – $^{206}\text{Pb}$	Estherville	4560 ± 31	
$^{207}\text{Pb}$ – $^{206}\text{Pb}$	Estherville	4422 ± 50	
$^{238}\text{U}$ – $^{206}\text{Pb}$	Estherville	4437 ± 11	
$^{207}\text{Pb}$ – $^{206}\text{Pb}$	Vaca Muerta	4563 ± 15	[3]
$^{207}\text{Pb}$ – $^{206}\text{Pb}$	Estherville	4521 ± 26	[4]
$^{147}\text{Sm}$ – $^{143}\text{Nd}$	Vaca Muerta <sup>*1</sup>	4480 ± 190	[5]
$^{147}\text{Sm}$ – $^{143}\text{Nd}$	Vaca Muerta <sup>*2</sup>	4480 ± 90	
$^{147}\text{Sm}$ – $^{143}\text{Nd}$	Vaca Muerta <sup>*3</sup>	4420 ± 20	
$^{147}\text{Sm}$ – $^{143}\text{Nd}$	Mt. Padbury <sup>*1</sup>	4520 ± 40	
$^{147}\text{Sm}$ – $^{143}\text{Nd}$	Estherville	4533 ± 94	[2]
$^{87}\text{Rb}$ – $^{87}\text{Sr}$	Estherville	4542 ± 303	
$^{182}\text{Hf}$ – $^{182}\text{W}$	Vaca Muerta	< 4450	[6]
$^{182}\text{Hf}$ – $^{182}\text{W}$	Vaca Muerta <sup>*4</sup>	(> 120Ma after CAI)	
$^{53}\text{Mn}$ – $^{53}\text{Cr}$	Vaca Muerta	4565.3 ± 1.4	[7]
		< 4550	[8]
		(> 20Ma after CAI)	

$^{92}\text{Nb}$ – $^{92}\text{Zr}$	Vaca Muerta	whole rock & mineral separates	4514 ± 32	[7][9]
$^{92}\text{Nb}$ – $^{92}\text{Zr}$	Vaca Muerta	rutile	4530–4520 (40–50Ma after CAI)	[10]
$^{92}\text{Nb}$ – $^{92}\text{Zr}$	Estherville	rutile		
$^{92}\text{Nb}$ – $^{92}\text{Zr}$	Asuka 882023	rutile		
This study				
$^{207}\text{Pb}$ – $^{206}\text{Pb}$			4502 ± 75	
$^{238}\text{U}$ – $^{206}\text{Pb}$	Asuka 882023	zircon	4375 ± 300	
total Pb/U			4492 ± 80	
$^{182}\text{Hf}$ – $^{182}\text{W}$	Asuka 882023	zircon	4532.8 +9.6/-4532.8	

Note:

Analyzed pebbles composed of <sup>\*1</sup>gabbroic clast, <sup>\*2</sup>basaltic clast, <sup>\*3</sup>highly recrystallized clast, and <sup>\*4</sup>basaltic and orthopyroxenic clasts.

[1] *Brouxel and Tatsumoto* [1990], [2] *Brouxel and Tatsumoto* [1991], [3] *Ireland and Wlotzka* [1992], [4] *Haba et al.* [2017], [5] *Stewart et al.* [1994], [6] *Ireland* [1991], [7] *Schönbächler et al.* [2002], [8] *Wadhwa et al.* [2003], [9] *Iizuka et al.* [2016], [10] *Haba et al.* [2016]

### 3.2. Sample Descriptions and SEM Observations

A mesosiderite, Asuka 882023, investigated in this study, was collected from Antarctica in 1988 by the National Institute of Polar Research (NIPR), Japan. According to metamorphic degrees of the silicates, mesosiderites can be classified into four subgroups, from type 1 (slightly re-melted) to type 4 (total impact melts) (Powell, 1971; Floran, 1978). Mesosiderites are also subdivided into groups A and B based on the mineral abundances (Floran, 1978; Hassanzadeh et al., 1990). A88 is a considerably thermally metamorphosed mesosiderite. The low phosphide/phosphate abundance ratios in the A88 silicate clasts indicate its slow cooling at high temperature ( $\geq 800^{\circ}\text{C}$ ) (Sugiura and Kimura, 2015). From textural observations of the A88 silicates, Sugiura and Kimura (2015) suggested type 2A for this mesosiderite.

A polished thin section of A88, #53-1, was allocated from NIPR. A large and anhedral zircon grain (ca.  $80 \times 30 \mu\text{m}$ ) adjoining to the Fe-Ni metal (Fig. 3.1) was identified using SEM-EDS. The cathode luminescence (CL) image of A88 zircon was almost completely dark with no growth stripes or heterogeneous bright patterns. The occurrence of this zircon is similar to those of Estherville, a thermally metamorphosed mesosiderite (type 3–4), although the dark CL image of A88 is different to those of Estherville (Haba et al., 2017). A88 zircon is significantly different to zircons in Vaca Muerta mesosiderite (type 1A) with small ( $\leq 10 \mu\text{m}$ ) and almost euhedral grains (Ireland & Wlotzka, 1992). After SEM observation, the section was loaded into the NanoSIMS airlock system, baked at ca.  $100^{\circ}\text{C}$  overnight, and then kept in the vessel at  $5 \times 10^{-9}$  Torr for 1 week before the following analyses. Detailed SEM observation was also conducted after NanoSIMS dating described in the next section (3.3).

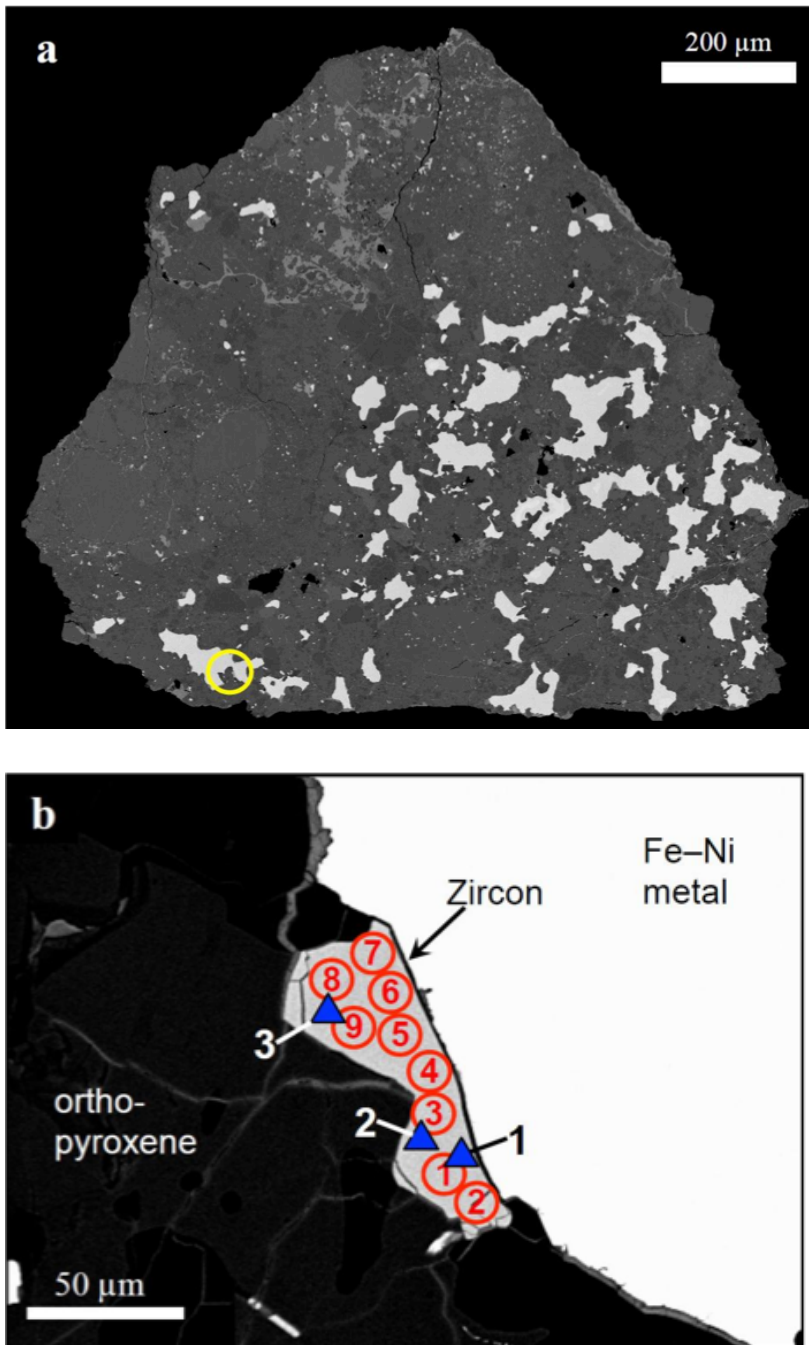


**Figure 3.1.** Backscattered secondary electron images of Asuka 882023. (a) Whole image of the section with a location of the zircon (circle). (b) The zircon grain with NanoSIMS spots #. Opened circles are for U-Pb dating, whereas filled triangles denote Hf-W dating, which was conducted after re-polishing of current surface.

### 3.3. NanoSIMS Analytical Conditions

In this section, I describe the *in-situ* U-Pb and Hf-W dating of the mesosiderite zircon using NanoSIMS 50. For Hf-W dating using NanoSIMS, this study is the first report. Details of the Hf-W analytical conditions are described here.

#### 3.3.1. U-Pb dating:

Both U-Pb and Hf-W dating were conducted on the identified zircon grain in A88 (Fig. 3.1b), using NanoSIMS 50 at Atmosphere and Ocean Research Institute, The University of Tokyo, in Japan. Firstly I conducted U-Pb dating with the previously established protocols (Takahata et al., 2008). A 2nA O<sup>-</sup> primary ion beam with spot size of ca. 10 μm was focused on the sample surface. Several spots were analyzed within the single grain. Secondary ions of <sup>30</sup>Si<sup>+</sup>, <sup>90</sup>Zr<sub>2</sub><sup>16</sup>O<sup>+</sup>, <sup>204</sup>Pb<sup>+</sup>, <sup>206</sup>Pb<sup>+</sup>, <sup>238</sup>U<sup>16</sup>O<sup>+</sup> and <sup>238</sup>U<sup>16</sup>O<sub>2</sub><sup>+</sup> were collected simultaneously for 600 seconds to obtain the <sup>238</sup>U-<sup>206</sup>Pb isochron age. A natural zircon standard, AS3, with the known concordant age of 1099.1 ± 0.2 Ma (Schmitz et al., 2003), was used to determine a <sup>206</sup>Pb<sup>+</sup>/<sup>238</sup>U<sup>16</sup>O<sup>+</sup> – <sup>238</sup>U<sup>16</sup>O<sub>2</sub><sup>+</sup>/<sup>238</sup>U<sup>16</sup>O<sup>+</sup> calibration line. The calibration method for zircon is essentially the same as to that of phosphates (Appendix; Koike et al., 2014). Detailed analytical protocols and the calibrations for U-Pb dating were described in Takahata et al. (2008). After the <sup>238</sup>U-<sup>206</sup>Pb session, magnetic fields of NanoSIMS were cycled to collect <sup>204</sup>Pb<sup>+</sup>, <sup>206</sup>Pb<sup>+</sup> and <sup>207</sup>Pb<sup>+</sup> for approximately 1 hour to determine the <sup>207</sup>Pb-<sup>206</sup>Pb age. Uranium concentrations of the analyzed spots were calculated by comparing <sup>238</sup>U<sup>16</sup>O<sup>+</sup>/<sup>90</sup>Zr<sub>2</sub><sup>16</sup>O<sup>+</sup>

ratios of the unknown and the average ratio of the standard. Because U contents in AS3 have large variations (113–626 ppm; Schmitz et al., 2003) with the average value of  $316 \pm 56$  ppm, the calculated U contents in the sample have large uncertainties (ca. 30% in 2-sigma). However, such precision issues does not matter for the current discussion, because the U abundances in A88 zircon are two orders of magnitude lower than those in Vaca Muerta mesosiderites (discussed later).

### 3.3.2. Hf-W dating:

After U-Pb dating, the studied A88 section was repolished for ca.  $10\mu\text{m}$  thickness to obtain a new surface for subsequent Hf-W dating. A 2nA  $\text{O}^-$  primary ion beam with spot size of ca.  $10\mu\text{m}$  was focused on the several spots in the single zircon grain. Because this is the first Hf-W dating using NanoSIMS 50, I firstly construct the basic analytical protocols. Previous SIMS Hf-W dating of eucrite zircons using Cameca IMS1270 at the Swedish Museum of Natural History, Sweden (Srinivasan et al., 2007), was followed to establish the NanoSIMS protocols. Secondary ions of  $^{182}\text{W}^+$ ,  $^{183}\text{W}^+$ , and  $^{186}\text{W}^+$  were collected using magnetic field cycling. The collection time was 500 seconds for each field. Secondary ions of  $^{30}\text{Si}^+$ ,  $^{96}\text{Zr}^{16}\text{O}^+$ ,  $^{178}\text{Hf}^+$ , and  $^{186}\text{W}^{16}\text{O}^+$  were also collected simultaneously at the magnetic field of  $^{186}\text{W}^+$ .

Oxides of rare earth elements can be serious isobaric to W isotopes (Srinivasan et al., 2007). For example, to resolve  $^{166}\text{Er}^{16}\text{O}^+$  (mass: 181.9252) from  $^{182}\text{W}^+$  (mass: 181.9482), high mass resolution power (MRP) of  $M/\Delta M > 7900$  is

required. This can be achieved using NanoSIMS 50 with optimized conditions. In addition to the high MRP, for avoidance of any critical overlapping of the isobaric, the  $^{166}\text{Er}^{16}\text{O}^+$  intensities were monitored at an additional magnetic field. If intensities of  $^{166}\text{Er}^{16}\text{O}^+$  or  $^{182}\text{W}^+$  suddenly changed during measurement, that data are omitted. Moreover, for the other data, potential interference effects were carefully examined as following. Isotopic anomalies of W are described as  $\delta^{182}\text{W}(\text{‰}) = ((^{182}\text{W}/^{186}\text{W})_{\text{sample}} / (^{182}\text{W}/^{186}\text{W})_{\text{STD}} - 1) \times 1,000$  and  $\delta^{183}\text{W}(\text{‰}) = ((^{183}\text{W}/^{186}\text{W})_{\text{sample}} / (^{183}\text{W}/^{186}\text{W})_{\text{STD}} - 1) \times 1,000$ , where reference values are  $(^{182}\text{W}/^{186}\text{W})_{\text{STD}} = 0.93437$  and  $(^{183}\text{W}/^{186}\text{W})_{\text{STD}} = 0.50439$  (Schoenberg et al., 2002). To examine the possible interference effects, the apparent  $\delta^{182}\text{W}$  and  $\delta^{183}\text{W}$  anomalies were checked in terrestrial standards, NIST SRM 610 glass (Jochum et al., 2011) and natural terrestrial zircon, 91500 (Wiedenbeck et al., 1995). Ideally, their W isotopic compositions should be identical to the literature terrestrial value (Schoenberg et al., 2002). In case the oxides isobaric overlap the W signals, the  $\delta^{182}\text{W}$  and  $\delta^{183}\text{W}$  values may have apparent anomalies.

As a meteoritic standard, zircon in a basaltic eucrite, Agoult with a reference Pb-Pb age of  $4554.5 \pm 2.0$  Ma (Iizuka et al., 2015) was also analyzed. The W isotopic anomalies and the Hf/W ratios of Agoult zircons were utilized both for the examination of the interference effects and for the calculation of NanoSIMS relative sensitivity factor (RSF) for Hf/W ratios. Backgrounds of the NanoSIMS elemental multipliers were checked at slightly displaced masses to the peaks on the same spots. On the terrestrial and the meteoritic zircons, the total  $^{186}\text{W}^+$  counts were ca. 10–20 throughout

the 500 seconds analyses. Backgrounds  $^{186}\text{W}^+$  were 2–6 counts on the same spots, corresponding ca. 25–30% of the signal levels. All data resented in the main text and these supporting Materials were subtracted from the background values.

### 3.4. Results

In this section, I firstly report the results of U-Pb dating of A88 zircon. Then, I report the Hf-W results along with the examinations for potential interference effects and NanoSIMS relative sensitivity factor. I also report the additional SEM observation conducted after the NanoSIMS dating.

#### 3.4.1. U-Pb dating

The U-Pb results are shown in Table 3.1 and Figures 3.2 A and B. The individual isotopic data are summarized in Table 3.2. All radiogenic ages described here are calculated using Isoplot Ex. 3 software (Ludwig, 2003). Nine data points define a regression lines with concordant  $^{238}\text{U}$ - $^{206}\text{Pb}$  age at  $4375 \pm 300$  Ma (MSWD = 0.75; all age errors are at 95 % confidence limit) and  $^{207}\text{Pb}$ - $^{206}\text{Pb}$  age at  $4502 \pm 75$  Ma (MSWD = 0.45). A total Pb/U age, which is determined from an intersection between the regression line in three-dimensional space of  $^{238}\text{U}/^{206}\text{Pb}$ - $^{207}\text{Pb}/^{206}\text{Pb}$ - $^{204}\text{Pb}/^{206}\text{Pb}$  and the U-Pb Tera-Wasserburg Concordia curve (see Appendix for details), is calculated to be  $4492 \pm 80$  Ma (Figure 3.2B; MSWD = 0.62). Weighted mean  $^{204}\text{Pb}/^{206}\text{Pb}$  ratios of data from  $^{238}\text{U}$ - $^{206}\text{Pb}$  and  $^{207}\text{Pb}$ - $^{206}\text{Pb}$  sessions are used for the total Pb/U calculation. One datum (spot #2 in Table 3.2) is omitted because the  $^{204}\text{Pb}/^{206}\text{Pb}$  ratios of  $^{238}\text{U}$ - $^{206}\text{Pb}$  and  $^{207}\text{Pb}$ - $^{206}\text{Pb}$  sessions did not mutually correspond. Uranium concentrations on the individual spots were calculated as 0.10–0.25 ppm (errors are ca. 30%. subsection 3.3.1 and Table 3.2).

### 3.4.2. Hf-W dating

The Hf-W results are shown in Table 3.1 and Figure 3.2C. The individual isotopic data are presented in Table 3.3. Potential interference effects from REE oxides onto W isotopes (Srinivasan et al., 2007) can be negligible after careful analytical treatments and data examinations. The results of the interference examinations are reported in the following subsection 3.4.3.

The relative sensitivity factor (RSF) of Hf/W ratios for NanoSIMS 50 is determined using standard materials with known and homogenous Hf/W ratios. The RSF for zircon must be determined on zircon standard, not on other materials with trace Hf contents (e.g. NIST 610), which are inappropriate as zircon standards (Ireland and Bukovanska, 2003; Srinivasan et al., 2007). However, the ideal zircon standard with known Hf/W ratio does not exist to date. Instead, I have used meteoritic zircon in Agoult eucrite with the precisely reported  $^{207}\text{Pb}$ - $^{206}\text{Pb}$  age of  $4554.5 \pm 2.0$  Ma (Iizuka et al., 2015) as the age reference material. Detailed RSF treatments are described in the following subsection 3.4.4.

Assuming that Agoult zircon has identical Hf-W and Pb-Pb ages, the regression line for A88 zircon can be determined (Fig 3.2C) to obtain an absolute Hf-W age of  $4532.8 \pm 9.6$  Ma (slope of A88 regression line is  $(6.67 \pm 7.40) \times 10^{-5}$ ; errors are at 2-sigma level), corresponding to the relative age of 35.4 Myr after CAI at 4568.2 Ma (Bouvier et al., 2010). The Hf-W lower age limit was not determined,

indicating  $^{182}\text{W}$  anomaly of A88 zircon was not significant in 2-sigma level. With 1-sigma notation, this result is described as  $4532.8 \pm 5.7/-10.5$  Ma. In Fig. 3.2C, the y-intercept of the regression line is assumed from literature values of other mesosiderite metals (Quitté et al., 2005). Srinivasan et al. (2007) reported slightly older Hf-W ages for basaltic eucrite zircons compared to their Pb-Pb ages. Assuming an older Hf-W age for Agoult zircon of 4561 Ma, the Hf-W age of A88 zircon would be slightly older as  $4539 \pm 9.6/-4539$  Ma (discussed later). In both cases, A88 zircon is significantly younger than those of basaltic eucrites, but still significantly old to have the  $^{182}\text{W}$  anomalies with 1-sigma precision.

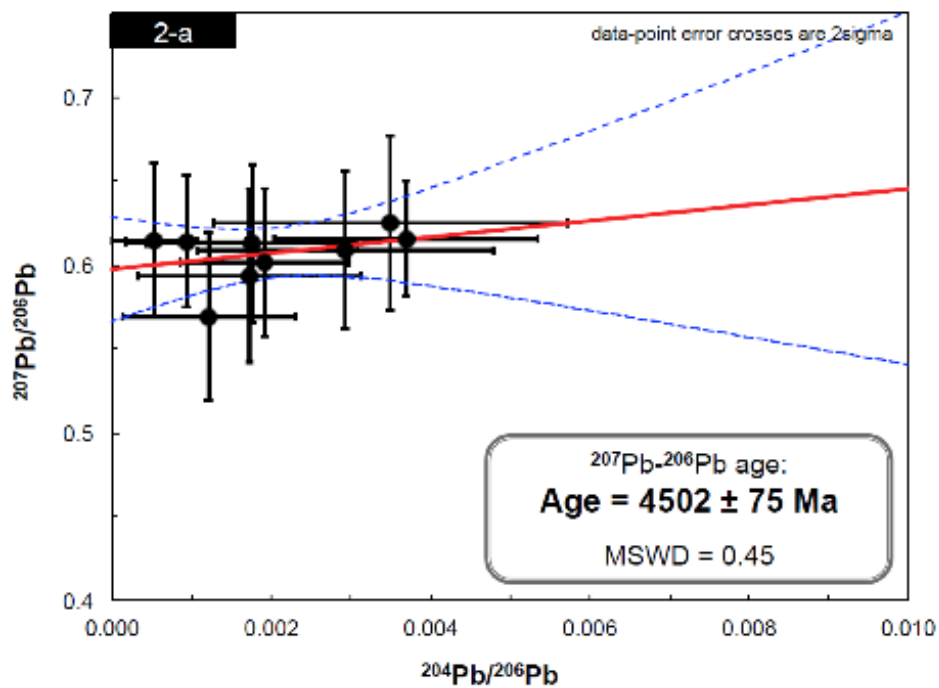


**Figure 3.2.** Obtained U-Pb and Hf-W isochrons of Asuka 882023 zircon.

(A) The  $^{207}\text{Pb}$ - $^{206}\text{U}$  isochron determined from nine spot analyses, corresponding to the concordant Pb-Pb age at 4502 ± 75 Ma (95% confidence limit, MSWD = 0.45).

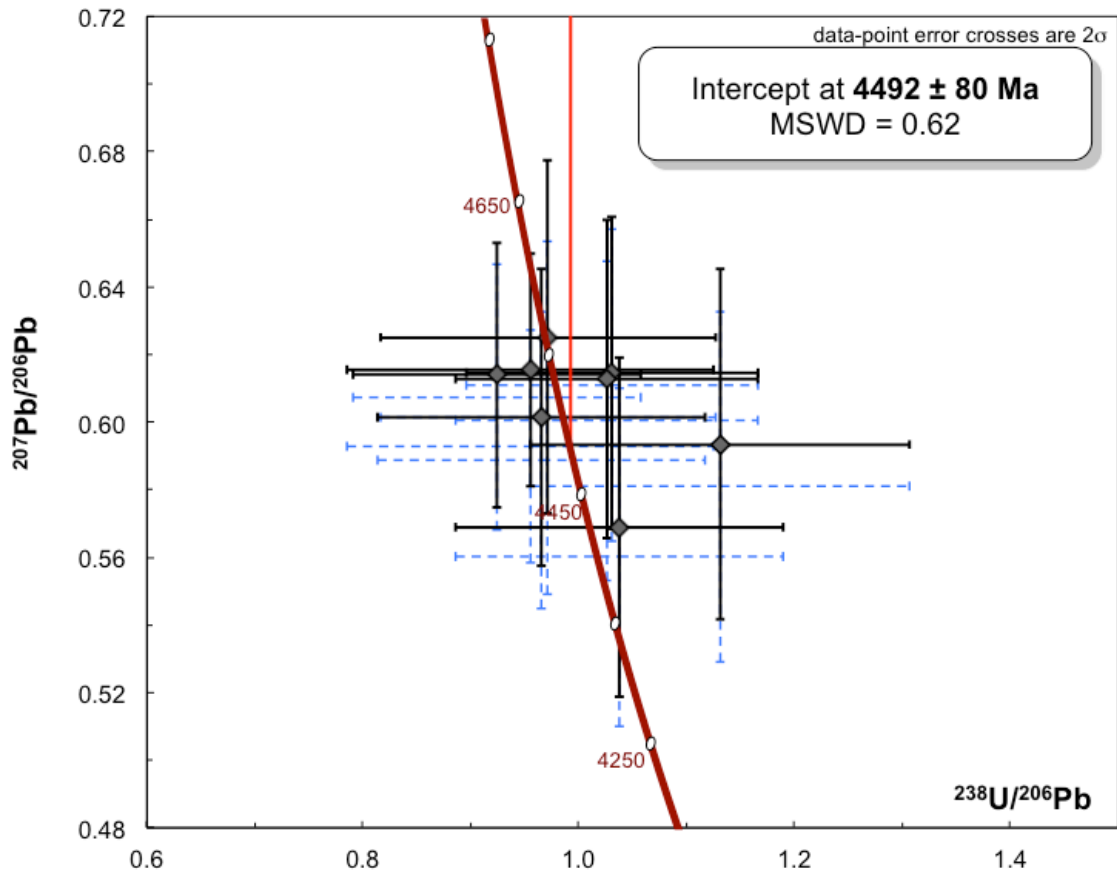


**Figure 3.2 (B)** Total Pb/U isochron projected onto the  $^{238}\text{U}/^{206}\text{Pb}$ - $^{207}\text{Pb}/^{206}\text{Pb}$  plane. The dashed line shows a projected regression line in 3D-space ( $^{238}\text{U}/^{206}\text{Pb}$ - $^{207}\text{Pb}/^{206}\text{Pb}$ - $^{204}\text{Pb}/^{206}\text{Pb}$ ). For details of the total Pb/U calculation, see Appendix. The solid curve shows Tera-Wasserburg U-Pb Concordia curve. The intercept of the regression line and Concordia curve represents the concordant Pb/U age at  $4492 \pm 80$  Ma (MSWD = 0.62). Errors are at 2-sigma level.

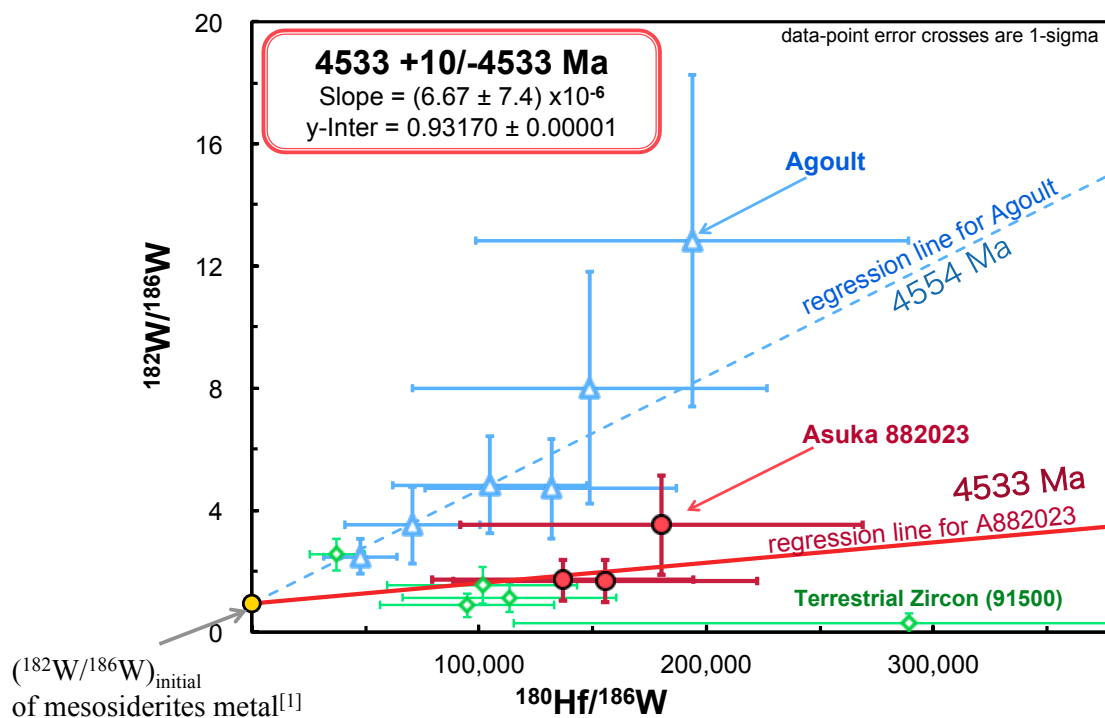


**Figure 3.2 (C)** The  $^{182}\text{Hf}$ - $^{182}\text{W}$  results of A88 zircon (filled circles), Agoult zircon (opened triangles), and terrestrial 91500 zircon (opened diamonds). NIST SRM 610 plots almost on the y-axis in this scale. Regression line for A88 (solid) corresponds to an absolute Hf-W age of  $4532.8 \pm 9.6$  Ma. Regression line for Agoult (dashed) is also shown.

### 3.4.3. Examinations of the potential interference effects for W isotopes

As described in methods subsection 3.3.2, REE oxides isobaric to W isotopes might be serious problems (i.e.  $^{166}\text{Er}^{16}\text{O}^+$  to  $^{182}\text{W}^+$  and  $^{167}\text{Er}^{16}\text{O}^+$  to  $^{183}\text{W}^+$ , respectively). A high mass resolution mode of NanoSIMS (MRP > 8500 in Cameca definition) can solve the problem. In this study, I checked the apparent  $\delta^{182}\text{W}$  and  $\delta^{183}\text{W}$  anomalies on the terrestrial standards. The  $\delta^{182}\text{W}$  and  $\delta^{183}\text{W}$  anomalies on Terrestrial samples ideally should be zero. In case the interference effects of  $^{166}\text{Er}^{16}\text{O}^+$  and  $^{167}\text{Er}^{16}\text{O}^+$  are significant, these values will have positive anomalies. The apparent  $\delta^{183}\text{W}$  anomalies on the meteoritic samples were also checked. No systematic anomaly was observed in  $\delta^{182}\text{W}$  or  $\delta^{183}\text{W}$  on NIST SRM 610. Although slightly higher  $\delta^{183}\text{W}$  ( $490 \pm 280\text{‰}$ ; weighted mean values with 2-SD) were obtained for the terrestrial zircon 91500, its weighted mean  $\delta^{182}\text{W}$  of  $70 \pm 209\text{‰}$  were normal within uncertainty, suggesting similar or lower interference effects on  $\delta^{182}\text{W}$  compared to  $\delta^{183}\text{W}$ . For meteoritic zircons, the mean  $\delta^{183}\text{W}$  values in Agoult ( $1,120 \pm 470\text{‰}$ ) and A88 ( $880 \pm 560\text{‰}$ ) were somewhat higher. Although there might be REE-oxides interference effects on these  $\delta^{183}\text{W}$  elevations, the  $\delta^{182}\text{W}$  values of these meteoritic zircons are much higher. Agoult zircons exhibited markedly higher  $\delta^{182}\text{W}$  anomalies up to  $13,000\text{‰}$  (Table 3.3), which definitely represent their ancient  $^{182}\text{Hf}$  excesses. Consequently, the interference effects on  $\delta^{182}\text{W}$  of the meteoritic zircons, if any, are expected to be negligible.

#### 3.4.4. Calculations of the NanoSIMS relative sensitivity factor for Hf/W ratios

The relative sensitivity factor (RSF) for Hf/W is determined as following:

$$\text{RSF}(\text{Hf}/\text{W}) = \left( \frac{{}^{180}\text{Hf}}{{}^{186}\text{W}} \right)_{\text{std,ref}} / \left( \frac{{}^{180}\text{Hf}}{{}^{186}\text{W}} \right)_{\text{std,meas}}$$

where  $(\text{Hf}/\text{W})_{\text{std, ref}}$  and  $(\text{Hf}/\text{W})_{\text{std, meas}}$  respectively denote the reference ratio and the measured ratio of the standard, respectively. The multi-collection system of NanoSIMS 50 is used to collect the  ${}^{178}\text{Hf}^+$  and  ${}^{186}\text{W}^+$  ions simultaneously. The calculated RSF includes efficiencies between the different collectors of NanoSIMS. Using NIST SRM 610 with known concentrations of Hf (435 ppm) and W (444 ppm) (Jochum et al., 2011), we can calculate the RSF value for Hf/W on glass as  $0.18 \pm 0.02$ . This is similar to those reported in the earlier studies using SHRIMP ( $0.22 \pm 0.004$ ; Ireland and Bukovanska, 2003) and with IMS1270 ( $0.21 \pm 0.01$ ; Srinivasan et al., 2007). However, these values cannot be directly applied to zircon. Because Hf is relatively abundant in zircon (approximately 1wt%) while W is trace, the RSF on zircon should be different from that of NIST 610 (Ireland and Bukovanska, 2003; Srinivasan et al., 2007; and their references). We have no an ideal zircon standard with known and homogeneous Hf and W concentrations. Alternative methods for RSF determination are required. Previous studies applied the sensitivity of Yb as proxy for W, assuming that Yb and W behave similarly as trace elements. Using SHRIMP, Ireland and Bukovanska (2003) ascertained the RSF for Hf/W on zircon as  $0.286 \pm 0.010$  (i.e. 30% higher than the RSF for NIST), as estimated from analyzed  $\text{Hf}^+/\text{Yb}^+$  ratios on NIST 610 and zircon standards with

known Hf and Yb concentrations. Srinivasan et al. (2007) adopted the similar protocols using IMS1270, but their determined RSF value was ca. 1/2.5 of that of NIST glass. In their method, one must analyze additional mass (e.g. Yb) on additional standard material (e.g. NIST 610) to obtain the zircon Hf/W ratios. Instead, we used a more direct method, for which the ‘reference isochron’ of an old zircon standard was used for the RSF calculation. Our calculation method has a merit that one can directly compare Hf/W ratios of standard and unknown. As a standard, we used an old zircon from a basaltic eucrite, Agoult, with the reported  $^{207}\text{Pb}$ - $^{206}\text{Pb}$  age of  $4554.5 \pm 2.0$  Ma (Iizuka et al., 2015). The six spots analyses of Agoult zircon combined with the reported  $^{182}\text{W}/^{186}\text{W}$  ratios of mesosiderite metals ( $0.93170 \pm 0.00001$ ; weighted mean value of several mesosiderites) (Quitté et al., 2005) defined a regression line with a slope of  $(3.1 \pm 0.7) \times 10^{-5}$ . Errors are described here in 1-sigma level. Assuming that Agoult zircon has identical  $^{182}\text{Hf}$ - $^{182}\text{W}$  and  $^{207}\text{Pb}$ - $^{206}\text{Pb}$  ages at 4555 Ma, the regression slope corresponds to the RSF for Hf/W of  $1.17 \pm 0.32$ . The Hf/W ratios of A88 zircon (Table 3.3) can be obtained from this RSF value. The three spot data, combined with the metal  $^{182}\text{W}/^{186}\text{W}$  ratios (Quitté et al., 2005), define a regression line in  $^{180}\text{Hf}/^{186}\text{W}$ - $^{182}\text{W}/^{186}\text{W}$  diagram, corresponding to the absolute age of  $4532.8 + 5.7/-10.4$  Ma (Fig 2C; corresponding to the relative age of 35.4 Myr after CAI formation at 4568.2 Ma; Bouvier et al., 2010). Zircons in some eucrites have Hf-W ages a few million years older than their Pb-Pb ages (Srinivasan et al., 2007), whereas the other eucrites zircons have consistent  $^{182}\text{Hf}$ - $^{182}\text{W}$  and  $^{207}\text{Pb}$ - $^{206}\text{Pb}$  ages at 4555Ma (Roszjar et al., 2012). When

one assumes the true Hf–W age of the Agoult zircon as 4561 Ma (similar to those reported for other eucrites zircons; Srinivasan et al., 2007), the RSF is calculated as  $1.94 \pm 0.53$ . With this RSF, the absolute Hf–W age of A88 zircon is calculated somewhat older, as  $4539.3 + 5.7/-10.5$  Ma.

In addition to the RSF correction, I also assume the initial  $^{182}\text{W}/^{186}\text{W}$  ratios when calculating Hf–W regression lines. The W isotopic ratio of the mesosiderites metals (Quitté et al., 2005) was regarded as the initial value. This is actually incorrect, because timing of the metal differentiation and the zircon formation should be different. Moreover,  $^{182}\text{W}$  can be destroyed by interaction with cosmic rays as summarized in Kleine et al. (2009). Consequently, the assumed initial  $^{182}\text{W}/^{186}\text{W}$  might be underestimated. However, the underestimate of  $^{182}\text{W}/^{186}\text{W}$  is expected to be  $< 1\%$ , negligibly small. Because of the large Hf/W variations in zircon, small differences in the initial  $^{182}\text{W}/^{186}\text{W}$  value virtually causes no change. The W concentrations in the A88 metal are too low to analyze with adequate precision using NanoSIMS. Therefore, we used the weighted mean value of the literature data for other mesosiderites metals (Quitté et al., 2005). In case the analyzed zircon secondarily grew from the primary zircons, true initial  $^{182}\text{W}/^{186}\text{W}$  ratio might be significantly higher. This possibility is discussed in the following subsection 3.5.1.

### **3.4.5. SEM observation of rutile in Asuka 882023**

After the NanoSIMS dating, the studied A88 section was observed again using a secondary electron microprobe with energy dispersive X-ray spectrometry (SEM-EDS). Through out one half of the section, several rutile grains with sizes of ~10 to 50  $\mu\text{m}$  are identified, although they do not locate close to the analyzed zircon. Some of them located with sulfide, chromite, metal, ilmenite, while the others are isolated. As recent Nb-Zr study suggests, the rutile is the secondary product (Haba et al., 2016). It may have formed from Ti released by the primary ilmenite or chromite, (possibly) because of the reduction of iron oxide by phosphorus or sulfur.

Concentrations of Zr in the rutile grains are approximately 0.01 mol%. These values are much smaller than those in Bondoc (0.15 mol%), a type 3/4 mesosiderite which may have been more rapidly cooled (personal discussion with Dr. N. Sugiura). Using the Zr concentrations in rutile as geothermometer provided by Watson et al. (2006) with the pressure effect (~55C), the average equilibrium temperature is ca. 660 °C for A88. This value is significantly lower than expected igneous temperatures and supports metamorphic equilibrium of the rutile (and the zircon, as well).

**Table 3.2.** The NanoSIMS results of U/Pb ratios, Pb isotopic ratios, and U concentrations of the zircon in Asuka 882023. Errors attached to data are 2 sigma.

Note: <sup>a</sup> The <sup>204</sup>Pb/<sup>206</sup>Pb ratios obtained from the <sup>238</sup>U–<sup>206</sup>Pb session. <sup>b</sup> The <sup>204</sup>Pb/<sup>206</sup>Pb ratios obtained from the <sup>207</sup>Pb–<sup>206</sup>Pb session. <sup>c</sup>Uncertainties of the U concentrations are ca. 30% (2 sigma).

Spot #	<sup>238</sup> U/ <sup>206</sup> Pb	<sup>207</sup> Pb/ <sup>206</sup> Pb	<sup>204</sup> Pb/ <sup>206</sup> Pb <sup>a</sup>	<sup>204</sup> Pb/ <sup>206</sup> Pb <sup>b</sup>	U (ppm) <sup>c</sup>
1	0.92 ± 0.13	0.61 ± 0.04	0.004 ± 0.003	0.001 ± 0.001	0.25
2	0.90 ± 0.17	0.61 ± 0.05	0.018 ± 0.012	0.003 ± 0.002	0.10
3	0.97 ± 0.15	0.60 ± 0.04	0.005 ± 0.005	0.002 ± 0.001	0.18
4	0.96 ± 0.17	0.62 ± 0.03	0.004 ± 0.004	0.004 ± 0.002	0.19
5	1.03 ± 0.14	0.61 ± 0.05	0.004 ± 0.004	0.001 ± 0.001	0.21
6	1.04 ± 0.15	0.57 ± 0.05	0.008 ± 0.006	0.001 ± 0.001	0.19
7	1.13 ± 0.18	0.59 ± 0.05	0.006 ± 0.005	0.002 ± 0.001	0.18
8	0.97 ± 0.16	0.63 ± 0.05	0.006 ± 0.005	0.004 ± 0.002	0.17
9	1.03 ± 0.14	0.61 ± 0.05	0.006 ± 0.005	0.002 ± 0.001	0.19

**Table 3.3.** The NanoSIMS results of Hf-W measurements of NIST SRM 610 glass and the zircons of terrestrial standard (91500), Agoutl eucrite, and Asuka 882023 mesosiderites. The total counts of Hf and W isotopes without background correction, the elemental and isotopic ratios are shown. The RSF(Hf/W) value for NIST 610 is  $0.15 \pm 0.05$ , whereas RSF(Hf/W) for zircon is calculated as  $1.17 \pm 0.32$  (see the main text). The RSF(Hf/W) uncertainties are propagated to the Hf/W results. The errors attached to data are 1 sigma.

Samples	Total counts per 1 measurement (before background corrections) *1				
	$^{178}\text{Hf}$	$^{182}\text{W}$	$^{183}\text{W}$	$^{186}\text{W}$	$^{166}\text{Er } ^{16}\text{O}$
<i>NIST 610</i>					
1	3.66.E+04	6957	3,735	7,229	29,650
2	2.69.E+04	5876	3,144	6,362	20,530
3	4.65.E+04	7608	4,356	8,238	36,625
4	3.79.E+04	7855	4,305	7,867	33,278
5	3.87.E+04	6902	3,707	7,757	40,488
<i>91500 zircon</i>					
1	9.20.E+05	14	21	10	19,350
2	1.14.E+06	100	33	40	24,962
3	1.08.E+06	27	22	17	23,929
4	9.91.E+05	25	16	18	21,957
5	9.68.E+05	31	20	17	21,149

\*1)  $^{178}\text{Hf}$ ,  $^{182}\text{W}$ ,  $^{183}\text{W}$  and  $^{186}\text{W}$ : total counts of 100s for NIST 610, 500s for the other zircons.  $^{166}\text{Er}^{16}\text{O}$ : total counts of 30s for NIST 610, 150s for the other zircons.

Table 3.3. (continued)

Samples	Elemental and isotopic ratios				
	$^{180}\text{Hf}/^{186}\text{W}$	$^{182}\text{W}/^{186}\text{W}$	$^{183}\text{W}/^{186}\text{W}$	$\delta^{182}\text{W}$ (‰)	$\delta^{183}\text{W}$ (‰)
<i>NIST 610</i>					
1	1.184 ± 0.119	0.96 ± 0.02	0.52 ± 0.01	29 ± 17	23 ± 21
2	0.990 ± 0.013	0.92 ± 0.02	0.49 ± 0.01	-13 ± 18	-22 ± 21
3	1.321 ± 0.015	0.92 ± 0.01	0.53 ± 0.01	-13 ± 16	47 ± 20
4	1.129 ± 0.013	1.00 ± 0.02	0.55 ± 0.01	67 ± 17	83 ± 21
5	1.169 ± 0.014	0.89 ± 0.01	0.48 ± 0.01	-49 ± 16	-54 ± 19
<i>91500 zircon</i>					
1	(2.89 ± 1.74 (+1.47/-1.20) <sup>*2</sup> ) × 10 <sup>5</sup>	0.29 ± 0.32 (+0.31/-0.30) <sup>*2</sup>	3.29 ± 2.01 (+1.70/-1.41) <sup>*2</sup>	-694 ± 347 (+332/-320) <sup>*2</sup>	5,514 ± 3,977 (+3375/-2792) <sup>*2</sup>
2	(3.75 ± 1.22) × 10 <sup>4</sup>	2.54 ± 0.52	0.70 ± 0.19	1,715 ± 554	391 ± 374
3	(1.14 ± 0.47) × 10 <sup>5</sup>	1.14 ± 0.48	1.19 ± 0.50	223 ± 517	1,360 ± 988
4	(9.49 ± 3.82) × 10 <sup>4</sup>	0.87 ± 0.38	0.57 ± 0.28	-69 ± 402	121 ± 550
5	(1.01 ± 0.42) × 10 <sup>5</sup>	1.52 ± 0.61	1.00 ± 0.44	631 ± 648	983 ± 865

\*2) Poisson errors (1-sigma) are also shown within brackets for those with the total  $^{186}\text{W}$  counts  $\leq 12$ .

**Table 3.3. (continued)**

Samples	Total counts per 1 measurement (before background corrections)				
	$^{178}\text{Hf}$	$^{182}\text{W}$	$^{183}\text{W}$	$^{186}\text{W}$	$^{166}\text{Er } ^{16}\text{O}$
<i>Agoult zircon</i>					
1	1.20.E+06	61	20	10	28,799
2	6.44.E+05	35	14	10	18,204
3	1.05.E+06	69	32	12	17,702
4	6.77.E+05	42	12	6	-
5	1.06.E+06	88	15	9	19,365
6	1.18.E+06	70	38	29	31,835
<i>A88 zircon</i>					
1	1.27.E+06	27	25	14	1,337
2	1.24.E+06	26	21	11	4,442
3	9.83.E+05	24	11	8	3,349

**Table 3.3. (continued)**

Samples	Elemental and isotopic ratios				
	$^{180}\text{Hf}/^{186}\text{W}$	$^{182}\text{W}/^{186}\text{W}$	$^{183}\text{W}/^{186}\text{W}$	$\delta^{182}\text{W}$ (‰)	$\delta^{183}\text{W}$ (‰)
<i>Agoult zircon</i>					
1	$(1.32 \pm 0.55)$ $(+0.67/-0.55) \times 10^5$	$4.70 \pm 1.64$ $(+2.12/-1.61)$	$0.70 \pm 0.34$ $(+0.40/-0.34)$	$4,030 \pm 1,752$ $(+2265/-1728)$	$388 \pm 684$ $(+790/-679)$
2	$(7.09 \pm 2.97)$ $(+3.59/-2.94) \times 10^4$	$3.50 \pm 1.25$ $(+1.60/-1.24)$	$1.40 \pm 0.58$ $(+0.70/-0.57)$	$2,746 \pm 1,343$ $(+1717/-1326)$	$1,776 \pm 1,149$ $(+1396/-1138)$
3	$(1.05 \pm 0.43)$ $(+0.49/-0.42) \times 10^5$	$4.82 \pm 1.60$ $(+1.95/-1.52)$	$1.82 \pm 0.68$ $(+0.80/-0.66)$	$4,157 \pm 1,708$ $(+2084/-1631)$	$2,605 \pm 1,353$ $(+1589/-1306)$
4	$(1.49 \pm 0.78)$ $(+0.978/-7.18) \times 10^5$	$8.00 \pm 3.79$ $(+4.94/-3.42)$	$1.80 \pm 1.00$ $(+1.23/-0.93)$	$7,562 \pm 4,061$ $(+5285/-3656)$	$2,569 \pm 1,991$ $(+2439/-1849)$
5	$(1.94 \pm 0.95)$ $(+1.03/-8.27) \times 10^5$	$12.83 \pm 5.44$ $(+6.04/-4.44)$	$1.00 \pm 0.58$ $(+0.61/-0.52)$	$12,735 \pm 5,821$ $(+6465/-4752)$	$983 \pm 1,145$ $(+1214/-1037)$
6	$(4.791 \pm 1.606) \times 10^5$	$2.48 \pm 0.57$	$0.93 \pm 0.26$	$1,656 \pm 605$	$836 \pm 510$
<i>A88 zircon</i>					
1	$(1.56 \pm 0.67)$ $(+0.69/-0.59) \times 10^5$	$1.67 \pm 0.70$ $(+0.72/-0.62)$	$1.78 \pm 0.74$ $(+0.76/-0.65)$	$784 \pm 752$ $(+769/-659)$	$2,525 \pm 1,469$ $(+1502/-1282)$
2	$(1.37 \pm 0.57)$ $(+0.67/-0.55) \times 10^5$	$1.70 \pm 0.68$ $(+0.80/-0.65)$	$0.80 \pm 0.38$ $(+0.43/-0.37)$	$819 \pm 725$ $(+854/-698)$	$586 \pm 752$ $(+849/-733)$
3	$(1.80 \pm 0.89)$ $(+0.10/-0.80) \times 10^5$	$3.50 \pm 1.62$ $(+1.89/-1.43)$	$0.83 \pm 0.50$ $(+0.53/-0.38)$	$2,746 \pm 1,734$ $(+2018/-1533)$	$652 \pm 1,000$ $(+1050/-754)$

### 3.5. Discussion

In order to elucidate the early impact processes on protoplanets, it is important to adequately interpret chronological records in the meteorites. As reported in the results sections (3.4), U-Pb and Hf-W systems in the single zircon of A88 mesosiderite are analyzed with *in-situ* methods. Both chronologies indicate the concordant age around 4530 Ma for A88 zircon. Here, I discuss the meaning of the ages and their implications.

In subsection 3.5.1, the obtained chronological results (reported in 3.4.1 and 3.4.2) are examined. Then, I compare A88 zircon with the other mesosiderites zircons (subsection 3.5.2). I summarize the literature chronological data and their implications to compare with the findings in this study (subsection 3.5.3). Finally, in subsection 3.5.4, possible interpretations for the mesosiderites formation histories are proposed and examined.

#### 3.5.1. Evaluations of U-Pb and Hf-W age results

For U-Pb dating of A88 zircon, both  $^{238}\text{U}$ - $^{206}\text{Pb}$  and  $^{207}\text{Pb}$ - $^{206}\text{Pb}$  ages, as well as the total Pb/U age, are concordant at ca. 4500 Ma within uncertainties. The  $^{207}\text{Pb}$ - $^{206}\text{Pb}$  age is  $4502 \pm 75$  Ma (Error is at 2-sigma; Fig. 2a). Because of the large uncertainties due to low U concentrations of the sample (~0.2 ppm), the upper limit of the  $^{207}\text{Pb}$ - $^{206}\text{Pb}$  age is indistinguishable from formation age of Ca-Al-rich inclusions (CAIs) at 4567.1–4568.2 Ma (Amelin et al., 2002; Bouvier et al., 2010). The concordant U-Pb system and its high closure temperature (Cherniak and Watson, 2000) indicate

that the obtained Pb-Pb age represents the timing of A88 zircon formation, not a later disturbance. It is inferred that MPB experienced high temperature event (either magmatic or reheating) accompanied with A88 zircon formation at 4500 Ma or earlier.

For Hf-W dating of the same zircon grain, we obtain an absolute  $^{182}\text{Hf}$ - $^{182}\text{W}$  age of  $4532.8 \pm 9.6$  Ma (errors at 2-sigma). In order to establish the analytical protocol for NanoSIMS Hf-W dating, which is the first attempt in this study, several technical challenges including treatments of REE-oxides interferences and correction of RSF for Hf/W ratios have been overcome (subsections 3.4.3–3.4.4). For calculation of RSF value, I have assumed  $^{182}\text{Hf}$ - $^{182}\text{W}$  age of zircon in Agoult eucrite as identical to its  $^{207}\text{Pb}$ - $^{206}\text{Pb}$  age at 4555 Ma (Iizuka et al., 2015). Although this assumption is plausible, previous studies reported age variations of  $\sim 30$  Myr in  $^{182}\text{Hf}$ - $^{182}\text{W}$  of eucritic zircons (i.e.  $\geq 4560 - 4530$  Ma; Srinivasan et al., 2007; Roszjar et al., 2012; 2016). To test the accuracy, especially upper age limit of A88 zircon, I have also examined the older case for Agoult as 4561 Ma. The result becomes slightly older,  $4539.3 \pm 9.6$  Ma, which is still consistent within uncertainty.

Because only 3 data points were obtained A88 zircon to determine the Hf-W isochron (Fig. 3.2b), I have assumed its initial  $^{182}\text{W}/^{186}\text{W}$  ratio from the literature values of mesosiderite metals (Quitté et al., 2005). Haba et al. (2017) pointed out that the young zircons in Estherville mesosiderite ( $^{207}\text{Pb}$ - $^{206}\text{Pb}$  age of 4521 Ma; Table 3.1) crystallized during high temperature reheating. Such secondary products could have incorporated relict older zircons, such as those in Vaca Muerta mesosiderites with

$^{207}\text{Pb}$ - $^{206}\text{Pb}$  of  $4563 \pm 15$  Ma (Ireland and Wlotzka, 1992; Table 3.1), as a primary mineral. Trace elements in the primary zircons may be mixed by partial decomposition of the primary zircons and/or diffusions in that case. If precursor of A88 zircon included the relict older zircon, which had crystallized at an earlier stage and had concentrated  $^{182}\text{Hf}$ , the initial  $^{182}\text{W}/^{186}\text{W}$  ratio of A88 zircon would be higher than what I assumed from the metals. This would raise the y-intercept in Fig. 3.2C, resulting in somewhat younger  $^{182}\text{Hf}$ - $^{182}\text{W}$  age. However, such incorporation of relict zircons is unlikely for the A88 case. Although Estherville zircons have significant heterogeneities in trace elements distributions (ca. 1 order of magnitude within a single grain; Haba et al., 2017), no heterogeneity or local concentrations of trace elements are identified from the cathode luminescence image of A88 zircon. Hence, my assumption of initial  $^{182}\text{W}/^{186}\text{W}$  is plausible. From above discussion, I will regard the  $^{182}\text{Hf}$ - $^{182}\text{W}$  age of A88 zircon as 4533 Ma, which is used in the following discussion.

Roszjar et al. (2016) estimated high closure temperatures for Hf-W system in zircon (more robust than U-Pb) due to the slow diffusion of W, which excludes a possibility of post-crystallization disturbances. Consequently, the 4533 Ma  $^{182}\text{Hf}$ - $^{182}\text{W}$  age is expected to be the formation age of A88 zircon. Although the lower age limit is not determined at 2-sigma precision, Hf-W provides a precise and robust upper age limit. Combining the U-Pb and Hf-W chronologies, one can infer that MPB experienced high temperature event during 4540 – 4430 Ma, when A88 zircon crystallized (upper limit from the  $^{182}\text{Hf}$ - $^{182}\text{W}$  age and lower limit from the  $^{207}\text{Pb}$ - $^{206}\text{Pb}$  age).

### **3.5.2 Comparison of the old magmatic zircons and the young metamorphic zircons in mesosiderites**

As discussed in the subsection 3.5.1, both  $^{207}\text{Pb}$ - $^{206}\text{Pb}$  of 4502 Ma and  $^{182}\text{Hf}$ - $^{182}\text{W}$  of 4533 Ma are likely to represent timing of A88 zircon crystallization during a thermal event on MPB. This age is significantly younger than those reported for zircon in Vaca Muerta mesosiderite with  $^{207}\text{Pb}$ - $^{206}\text{Pb}$  age of  $4563 \pm 15$  Ma (Ireland and Wlotzka, 1992; Table 3.1). This value is identical to the crustal differentiation periods of eucrites parent body, Vesta (a few Myr after CAI; Lugmair and Shukolyukov, 1998; Srinivasan et al., 2007), suggesting the old zircon in Vaca Muerta crystallized during the early crustal differentiation event of MPB. On the other hand, the younger A88 zircon should have been secondary crystallized. Recently, Haba et al. (2017) have also reported young zircons in Estherville mesosiderite. Their weighted mean  $^{207}\text{Pb}$ - $^{206}\text{Pb}$  age is  $4521 \pm 26$  Ma, identical to the A88 U-Pb and Hf-W results. Based on the trace elements concentrations and distributions, as well as chronological information, Haba et al. (2017) proposed that the young zircons in Estherville crystallized secondarily during high temperature reheating of MPB. The existence of the similar young zircons in different mesosiderites (i.e. A88 in this study and Estherville from Haba et al. (2017)) indicates the MPB reheating at ca. 4530 Ma may be either a global event or simultaneous local reheating episodes. Indeed, these young zircons share textural and chemical properties. They are relatively large (ca. 100  $\mu\text{m}$  in long diameter) and anhedral crystals compared to Vaca Muerta zircon (ca. 10  $\mu\text{m}$  with euhedral to

subhedral shape; Ireland and Wlotzka, 1992). The extremely low U concentrations of A88 zircon (ca. 0.2 ppm; Table 3.3) and Estherville zircon (<1 ppm; Haba et al., 2017) also support their metamorphic origins (Haba et al., 2014). While heterogeneous distributions in trace elements, which were observed in Estherville zircon possibly due to the incorporation of the relict primary zircon, was not identified in A88 zircon. In contrast, U concentrations of Vaca Muerta zircons are by 2–3 orders magnitude higher (ca. 50ppm, except for 1 grain; Ireland and Wlotzka, 1992). This is similar to those of basaltic eucrites (from ca. 10 ppm to > 200ppm; Misawa et al., 2005; Zhou et al., 2013; Iizuka et al., 2015). Behaviors of U during thermal metamorphism highly depend on remelting and/or recrystallization of other U-bearing such as phosphates, requiring careful case-by-case consideration. Nevertheless, the large differences in U concentrations between the young zircons and the old zircons seem supportive for their different origins. Haba et al. (2016) also reported young Nb-Zr isochron age for rutiles from Vaca Muerta, A88 and Estherville mesosiderites, as 40–50 Myrs after CAI. The rutile is a secondary product from primary ilmenite, formed during later reheating. Ilmenite also release Zr at high temperature, which subsequently reacts with silicates and forms secondary zircon (Iizuka et al., 2015). The A88 section studied here also contains ilmenite and rutile (Supporting Text S4). Considering above discussion, I may attribute A88 and Estherville zircons as secondary products. They crystallized from Zr-release during the high temperature thermal event on MPB at  $\leq 4540$  Ma. The young zircons were also identified in some basaltic eucrites (Hf-W ages up to  $\sim 4530$  Ma;

Roszjar et al., 2016). Based on the high closure temperature of Hf-W in zircon, Roszjar et al. (2016) interpreted the young zircons as the igneous records of prolonged magmatism on Vesta. On the other hand, the textural and chemical properties of A88 indicate its metamorphic origin, not the later magmatic materials, as discussed above. Consequently, it is suggested that MPB experienced the global and/or simultaneous episodic reheating event(s), where the younger zircons crystallized. The older zircons in Vaca Muerta may be magmatic origin and have recorded the MPB crustal differentiation at ca. 4563 Ma.

### **3.5.3. Chronological constraints from this study and the literature information**

A number of chronological studies including U-Pb, Sm-Nd, Rb-Sr, Mn-Cr, Nb-Zr, and Hf-W (summarized in Table 3.1) previously reported large age variations from 4565 to ca. 4400 Ma for mesosiderites. A much younger  $^{40}\text{Ar}$ - $^{39}\text{Ar}$  age of ca. 3900 Ma has also been reported (Bogard et al., 1990), indicating either long-term residence at moderate temperature (ca. 500°C) or modest reheating at 3900 Ma. A mineral isochron of silicates in Vaca Muerta defines an original  $^{182}\text{Hf}/^{180}\text{Hf}$  ratio of  $(7.68 \pm 0.8) \times 10^{-5}$  (Schönbächler et al., 2002), corresponding to an absolute  $^{182}\text{Hf}$ - $^{182}\text{W}$  age of  $4565.4 \pm 1.5$  Ma with an initial  $^{182}\text{Hf}/^{180}\text{Hf}$  ratio of  $(9.72 \pm 0.44) \times 10^{-5}$  for CAI (Burkhardt et al., 2008) at  $4568.2 \pm 0.2$  Ma (Bouvier et al., 2010). This is consistent with that of the old Pb-Pb age of Vaca Muerta zircon at  $4563 \pm 15$  Ma (Ireland and Wlotzka, 1992). Eucrite whole rocks provide a similar initial  $^{182}\text{Hf}/^{180}\text{Hf}$  (Kleine et al., 2004), although a recent

study revealed heterogeneities in eucrite whole rocks (Touboul et al., 2015). Younger Sm-Nd ages of silicates were reported as  $4520 \pm 40$  Ma and  $4480 \pm 190$  Ma, for Mt. Padbury (type 1A) and gabbroic clasts in Vaca Muerta, respectively. The young ages might have recorded MPB reheating, although the large errors render it indistinguishable from igneous age. The U-Pb and Hf-W chronometers of A88 zircon in my study determined the reheating timing ranges as 4540 – 4430 Ma (subsection 3.5.1). The recent geochemical and chronological study by Haba et al. (2017) has also reported the reheating timing as  $4521 \pm 26$  Ma. Combining the age constraints, MPB reheating ranges 4540 – 4500 Ma. For abbreviation, in the following discussion, I will call this event as “4530 Ma reheating”. Consequently, MPB geological history can be estimated as: crustal differentiation at  $\geq 4560$  Ma; global or simultaneous 4530 Ma reheating event(s); and duration of moderate temperature (ca. 500°C) until approximately 3900 Ma or modest annealing.

#### **3.5.4. Estimation of possible evolutionary history for mesosiderite parent body**

Rubin and Mittlefehldt (1993) have proposed a formation history for mesosiderites. Combined with the chronological records, the formation model can be described as following:

- (I) Early accretion and core-mantle differentiation of MPB
- (II) Initial crustal differentiation at  $\geq 4560$  Ma, (III) silicate-metal mixing
- (IV) Global or simultaneous local 4530 Ma reheating event(s)

(V) Residence in deep crust of MPB at moderate temperature or modest annealing by small impacts until ca. 3900 Ma.

The MPB evolutionary history is schematically illustrated in Figure 3.3. The crustal differentiation (II) was recorded in the magmatic zircon in Vaca Muerta (Ireland and Wlotzka, 1992), as well as the old Hf-W constraint from the silicates (Schönbächler et al., 2002). The last event (V), on the other hand, is estimated from the younger Ar-Ar age (Bogard et al., 1990). Rubin and Mittlefehldt (1993) also suggested that the silicate-metal mixing (III) resulted from an impact with velocity collision as slow as 1 km/s (Wasson and Rubin, 1985). Molten core of the impactor might have mixed with MPB crusts and caused (IV) 4530 Ma reheating shortly after (III) mixing. Scott et al. (2001) suggested that both the silicates and the metals originated from a single MPB. Its crusts and molten core could have been mixed by the nearly catastrophic impact destruction and the subsequent reassembly. Quitté et al. (2005) suggested a single parent body for mesosiderites, pallasites and eucrites, although different origins for the three are indicated from the precise oxygen isotopic compositions (Greenwood et al., 2015) and the regolith data of Vesta observed by Dawn's mission (Prettyman et al., 2012; Peplowski et al., 2013). What the different models would agree is that the silicate-metal mixing is associated with the early impact event of MPB. However, there remained several important questions concerning: timing of the mixing, fate of the mantle olivine from the impactor and/or MPB (Greenwood et al., 2015), and possible heat source for the 4530 Ma reheating. Because there is no direct age determination

method for the mixing event (III), previous studies assumed the same impact event for (III) mixing and (IV) subsequent reheating (Stewart et al., 1994; Wadhwa et al., 2003; Haba et al., 2016 and 2017). Based the chronologies and other geochemical/geophysical considerations, some possible interpretations for the mesosiderites formation can be examined. Here I will propose and discuss the possible interpretations. This generally agrees with that provided by Rubin and Mittlefehldt (1993), but some important re-examinations have been conducted.

As discussed in the former subsection, the young zircons in A88 (this study) and Estherville (Haba et al., 2017) recorded (IV) 4530 Ma reheating. Their silicate-metal mixing should have occurred at the same time or an earlier impact. If both event (III) and (IV) are related to MPB impact event at ca. 4530 Ma, heat source for the (IV) reheating should have been molten interior of the impactor and/or MPB plus the impact energy. The impact energy for such small body with possibly slow collisional speed may not be large enough for the temperature elevation to melting (Scott et al., 2001). Contributions of internal heat source in the impactor and/or MPB should be important for thermal metamorphism of silicates and melting of metals in mesosiderites. Siderophile elements proportions in mesosiderite metals are similar to those in magmatic iron meteorites such as IIIAB (Hassanzadeh et al., 1990; Shen et al., 1998), although they have large variations. However, by 4530 Ma, the initially molten core of the Vesta-sized body had been cooled and partially crystallized (50-80% melting, depending on initial parameters; Zhou et al., 2013; Neumann et al., 2014). Partial

crystallization of initially chondritic metals could result in the siderophile fractionations and their heterogeneous distributions. It seems still possible to mix the chondritic metals and the basaltic silicates at 4530 Ma impact, assuming the impactor was large enough to retain its internal heat and/or fractionations of siderophile elements in metals during partial crystallization was insignificant, although the missing olivine problem (Greenwood et al., 2015) of the impactor and/or MPB remain unsolved. Koike et al. (2017) proposed another plausible interpretation: (III) silicate-metal mixing occurred in much earlier stage, and then, (IV) the mixtures were reheated at ca. 4530 Ma. If this is the case, timing of the mixing becomes an important issue. Although I cannot ascertain the exact timing if the silicate-metal mixing with current knowledge, W isotopic records are expected to provide some insights. According to previous studies,  $^{182}\text{W}$  anomalies in mesosiderite metals range from -3.4 to -1.3 in  $\epsilon^{182}\text{W}$  unit (defined as deviation in part per 10,000 relative to terrestrial  $^{182}\text{W}/^{184}\text{W}$  ratio). The variations are possibly attributable to post-mixing diffusion from adjacent silicates or several distinctive origins for the metal. The mesosiderite ranges are similar to less radiogenic than carbonaceous chondrites ( $\epsilon^{182}\text{W} \sim -2$ ) and are slightly higher than those of magmatic iron meteorites ( $\epsilon^{182}\text{W} \sim -4$  to  $-3$ ) (Quitté et al. 2005; Kleine et al., 2002; 2009). Comparing those values, although cosmic-ray corrections are required for precise discussion, one can roughly estimate the mesosiderite metal origin; either core from impactor(s), which had differentiated 6.5 Myr after magmatic iron meteorites, or chondritic metal separated from chondrules. The former is possible if the core mixed to MPB crusts within the first

10 Myr, when core metal in Vesta-sized body remained melted (Zhou et al., 2013). In this case, the fate of unidentified impactor's mantle is still unknown. The latter case seems possible only if chondritic metal and silicates are separated effectively by a mechanism such as photophoresis (e.g. Loesche et al., 2013) and if the metal was transported preferentially to the MPB region. In this case, the apparent mantle absence might be explained. Chondrules in CR group contain a lot of metal grains and rims, indicating their chondrules and metal formed simultaneously (e.g. Weisberg et al., 1993). It is possible that some small parts of the chondritic metal were separated from chondrules during and/or after the chondrule formation, despite lack of exact timing information available for such separation. The possible metal origins, as discussed above, suggest that the timing of the mesosiderites silicate-metal mixing might have occurred within 10 Myr after the rapid accretion of MPB. Further investigations including precise analyses of mesosiderites metals and silicates are necessary to determine the metal origins, as well as the exact timing of silicate-metal mixing. Because the mixing occurred quite early and because it might not have caused the 4530 Ma reheating in this interpretation, an additional heat source is required for the 4530 Ma reheating. Short-lived radioactive nuclei, such as  $^{26}\text{Al}$ , had been already extinct by this age. According to the detailed observations of several mesosiderites, there might be some anti-correlations between their cooling rates and the peak temperatures of reheating (Sugiura, 2013; Sugiura and Kimura, 2015). This relation is explainable with various vertical distances between the mesosiderite precursor on MPB and an external

heat source. Those buried deep in the crust were reheated at moderate temperature and cooled slowly, and vice versa. Sugiura and Kimura (2015) found A88 as considerably metamorphosed and slowly cooled, indicating that A88 was buried deeply when it was reheated. The external heat source at ca. 4530 Ma might be a later impact(s), although no fragments of the additional impactor(s) have been reported in mesosiderites. Other possible heat sources cannot be denied, such as electromagnetic induction caused by the changing solar-wind magnetic field (Sonett et al., 1970).

The above model seems plausible, although this study has investigated only one zircon in a certain mesosiderite (A88). To reveal the issues, further investigations of other mesosiderites must be conducted as well as studies of other extraterrestrial samples. The U-Pb chronology of phosphates minerals in mesosiderites, as similar to my eucrites study described in Chapter 2, may be also helpful. The conventional impact mixing and reheating model (e.g. Haba et al., 2017), where both silicate-metal mixing and secondary zircon formation occurred during the single impact event at ca. 4530 Ma, is still possible. In that model, heat source problem is not the matter, while other problems, such as siderophile compositions in the metals and the apparent absence of impactor's mantle rises again. To summarize, the exact timing of silicate-metal mixing is still controversial. However, it is clear that the ancient crusts on MPB experienced high temperature metamorphism at ca. 4530 Ma, significantly later than the major crustal formation of Vesta-like protoplanets at  $\geq 4560$  Ma.

### Formation history of mesosiderites

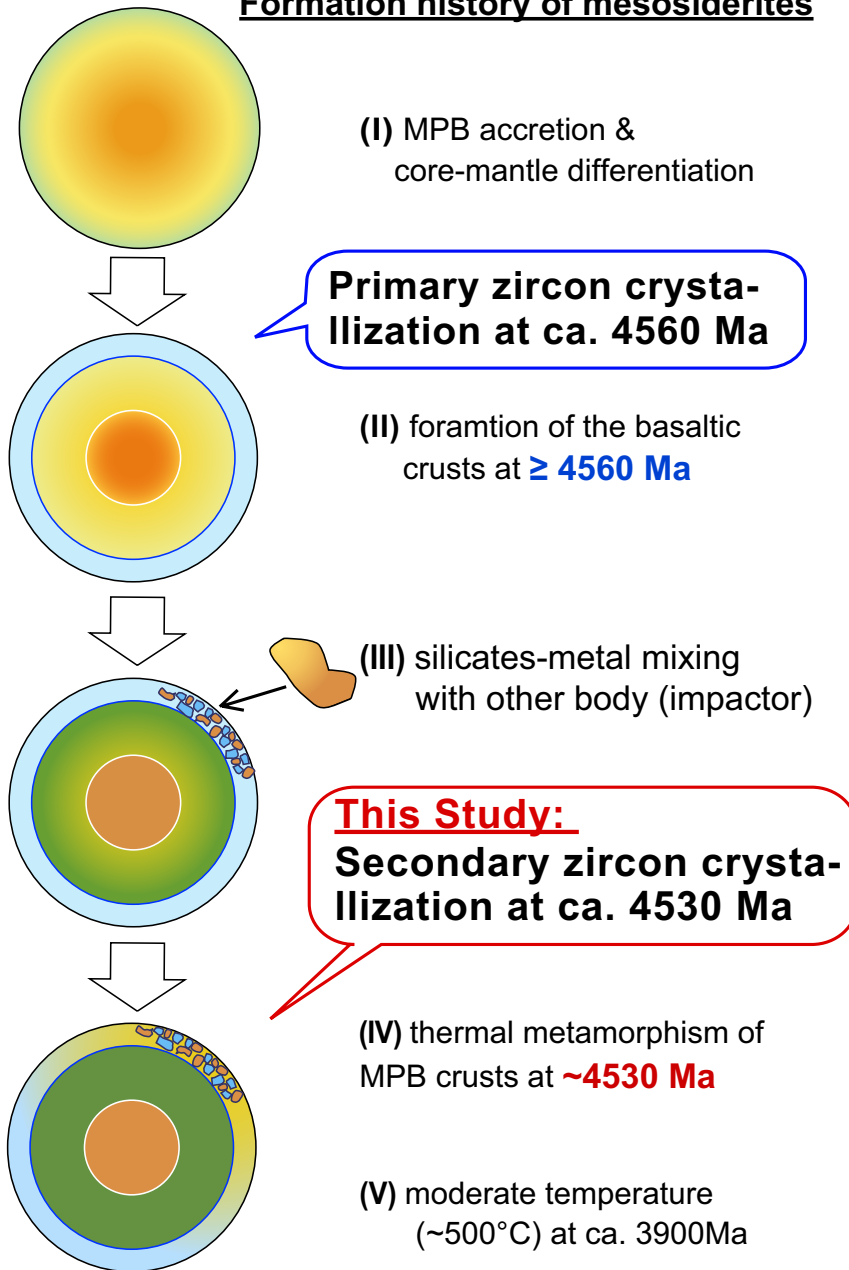


**Figure 3.3.** Schematic illustrations of formational history of mesosiderites on the parent body. This study of A88 zircon dating constrains the timing of stage (IV) thermal metamorphism of MPB crusts during ca. 4530 Ma.

### 3.6. Conclusions

This report describes the first combined U–Pb and Hf–W dating using NanoSIMS conducted on a zircon grain in Asuka 882023 mesosiderite. The obtained  $^{207}\text{Pb}$ – $^{206}\text{Pb}$  age of  $4502 \pm 75$  Ma and the  $^{182}\text{Hf}$ – $^{182}\text{W}$  age of  $4532.8 +9.6/-4532.8$  Ma are mutually consistent, representing timing of the zircon formation. Textural and chemical features of A88 zircon suggest that it formed secondarily during reheating, considerably later than the crustal differentiation of MPB. From this study, I have revealed that mesosiderites experienced a high-temperature reheating event, accompanied with secondary zircon formation, during 4540–4500 Ma (ca. 4530 Ma). The silicates-metal mixing of mesosiderites may have occurred at the same time or at an earlier stage. Based on our chronological constraints, as well as various earlier works, Koike et al. (2017) re-examined the possible formation history of mesosiderites as the following:

- (I) early accretion of MPB
- (II) crustal differentiation at  $\geq 4560$  Ma
- (III) silicate-metal mixing, possibly  $\leq 10$  Myr after MPB accretion
- (IV) reheating at ca. 4530 Ma
- (V) slow cooling at moderate temperature until ca. 3900 Ma.

It is still plausible that both (III) silicate–metal mixing and (IV) reheating occurred at ca. 4530 Ma impact event, as proposed in previous studies. Timing of the mixing and the heat source for the 4530 Ma reheating are controversial and require further investigations of other meteorites.

# CHAPTER 4

## GENERAL DISCUSSION: CRUSTAL EVOLUTION & COLLISIONAL PROCESSES OF PROTOPLANETS

As described in Chapter 1, the ultimate research objective in the present study is to elucidate the evolutionary history of protoplanets at Vesta-size (several 100s km) stage. In Chapter 2, I analyze *in-situ* U-Pb chronologies in the phosphates from basaltic eucrites and discuss the metamorphic history of Vesta's crusts. In Chapter 3, I conduct *in-situ* U-Pb and Hf-W dating of the zircon in mesosiderite and discuss the possible formational history of mesosiderites. Providing the thermo-chronological constraints in the several meteorites, igneous and metamorphic (impact and/or reheating) histories are investigated for the individual protoplanets (i.e. Vesta and the mesosiderites parent body). In order to discuss more general planetary evolution history, it is important to integrate and compare the individual stories together. In Chapter 4, I summarize the present knowledge reported in this thesis (Chapters 2 and 3), along with literature data of various chronologies. It is inferred that Vesta-sized protoplanets experienced both

internal reheating (prolonged magmatism) and impact reheating by ca. 4530 Ma. The asteroids may also have suffered the intense impacts around 4200 Ma and the moderate impacts around 3800 Ma. The last impact events might have relationship with the lunar late heavy bombardments.

#### 4.1. Introduction

In order to discuss general processes of the protoplanets evolution, it is helpful to summarize various meteoritic records currently available and to compare them each other. For eucrites, my study of the phosphates U-Pb dating provides the new constraints in the metamorphic history of Vesta's crusts. Two of the five studied samples, Agoult and Juvinas, have the similar  $^{207}\text{Pb}$ - $^{206}\text{Pb}$  ages at 4520–4530 Ma. There may have been global or local simultaneous thermal event(s) during 4520–4530 Ma on Vesta's crusts (hereafter, I abbreviate this periods as '4530 Ma thermal process'). The similar metamorphic ages of ~4530Ma were also recorded in zircons from mesosiderites, as reported in Chapter 3. Metamorphic zircon in Asuka 882023 mesosiderite, analyzed in this study, has the concordant  $^{207}\text{Pb}$ - $^{206}\text{Pb}$  and  $^{182}\text{Hf}$ - $^{182}\text{W}$  ages at 4530 Ma. It is inferred that the ancient Vesta-like protoplanets may have widely experienced prolonged magmatic events and/or reheating during 4530 Ma.

On the other hand, the studied brecciated eucrites, Juvinas and Stannern, show the young  $^{207}\text{Pb}$ - $^{206}\text{Pb}$  ages around 4200–4100 Ma, possibly due to reset of the U-Pb system during impact reheating events (hereafter, abbreviated as '4200 Ma reheating'). The 4200 Ma reheating is significantly younger than the igneous events of Vesta-sized protoplanets and their residual thermal processes (e.g. Neumann et al., 2014). At the same time, this period (4200 Ma) is older than apparent peak of K-Ar chronology ( $^{40}\text{Ar}$ - $^{39}\text{Ar}$  dating) of brecciated eucrites (Bogard and Garrison, 2003) and mesosiderites (Bogard et al., 1990), whose  $^{40}\text{Ar}$ - $^{39}\text{Ar}$  ages are ca. 4000–3400 Ma (hereafter,

abbreviated as ‘3800 Ma reheating’).

There might be three apparent age peaks in the metamorphic history of the basaltic crusts on Vesta-like protoplanets, after their crystallization; 4530 Ma, 4100 Ma, and 3800 Ma. The individual metamorphisms were recorded in the different chronologies and/or in the different samples. In the following section, I discuss these thermal events using various chronological data, especially focusing on Hf-W, U-Pb and K-Ar systematics.

#### **4.2. The early thermal process at 4530 Ma**

Both U-Pb system in the eucrites phosphates (Chapter 2), and U-Pb and Hf-W systems in the mesosiderites zircons (Chapter 3) indicate thermal events on their parent bodies during 4530 Ma. Plagioclase in Agoult eucrite may have recorded the thermal process simultaneously, whose precise  $^{207}\text{Pb}$ - $^{206}\text{Pb}$  age was reported as  $4532 \pm 1$  Ma (Iizuka et al., 2013). Silicates (pyroxene and plagioclase) in other basaltic eucrites also recorded the similar  $^{207}\text{Pb}$ - $^{206}\text{Pb}$  ages of 4540–4500 Ma (Tatsumoto et al., 1973; Galer and Lugmair 1996; Tera et al., 1997). Several zircons in basaltic eucrites recorded the identical timings. The *in-situ*  $^{207}\text{Pb}$ - $^{206}\text{Pb}$  isochron age of Camel Donga zircon was reported as  $4531 \pm 10$  Ma (Zhou et al. 2013). Roszjar et al (2016) reported *in-situ* Hf-W dating of zircons in unbrecciated basaltic eucrites, some of which show  $^{182}\text{Hf}$ - $^{182}\text{W}$  age variations with lower limit at  $\sim 4530$  Ma. Figure 4.1A summarizes the reported Pb-Pb and Hf-W ages of various meteorites. The age probability histograms\*<sup>1</sup> (Fig. 4.1B–D)

focus on data of eucrites and mesosiderites. All of them apparently have some peak(s) at ca. 4530 Ma. It is suggested that ancient Vesta-like protoplanets may have widely experienced thermal processes at this timing.

The 4530 Ma thermal process were recorded in (i) U-Pb system in phosphates and silicates of eucrites, (ii) U-Pb and Hf-W systems in zircons of eucrites, (iii) U-Pb and Hf-W in zircons of mesosiderites. Among them, (ii) and (iii) represent high temperature events, while (i) recorded moderate thermal processes. Closure temperatures of U-Pb systematics in zircon and phosphate (apatite) were examined previously (see also Chapter 2 and references there). The typical closure temperatures for the rapidly cooled conditions ( $\geq 0.004$  °C/year, typical for basaltic eucrites; Miyamoto and Takeda, 1977) are  $\geq 1060^{\circ}\text{C}$  for zircon U-Pb and ca.  $600^{\circ}\text{C}$  for apatite U-Pb. Although we do not know the exact closure temperature of Hf-W system in zircon, diffusion rate of W in zircon is considered to be slower than that of Pb. It is suggested Hf-W system has higher closure temperature than U-Pb (Roszjar et al., 2016). The significantly high closure temperatures of U-Pb and Hf-W in zircon ( $\sim 1060^{\circ}\text{C}$  or higher) means that they can be disturbed only when surrounding temperatures exceed the basalt melting point ( $\sim 1060^{\circ}\text{C}$ ), or when the host zircons overgrow during secondary process. As described in Chapter 3 in this thesis, zircons from mesosiderites as well as zircons from thermally metamorphosed eucrites, are considered to have crystallized secondarily during reheating process (this study; Iizuka et al., 2015; Haba et al., 2017). The formation temperature for zircon in Agoult eucrite at 4554 Ma was

estimated as ca. 900°C (Iizuka et al., 2015). As described above, the younger zircons with U-Pb and Hf-W ages of ca. 4530 Ma were identified in some basaltic eucrites and mesosiderites. It is inferred that Vesta and Vesta-like protoplanets experienced thermal process during 4530 Ma, where the temperature exceeded 900°C (i.e. zircon formation temperatures) at least locally. Possible heat sources at this timing are internal residual heat in the protoplanets and external impact reheating. Because the 4530Ma event was recorded in both unbrecciated and brecciated meteorites, both cases seem plausible. The possible interpretation is that both the crustal reheating by internal residual heat and the impact reheating events were active for Vesta-like protoplanets during ca. 4530 Ma.

\*1) In this chapter, I will compare chronological data using the age probability histogram  $P(t)$  ( $t$ : absolute age in Ma), along with the original data. This probability function  $P(t)$  is defined as accumulated chronological data:

$$P(t) = \sum_i^{all\ data} p_i(t)$$

Where  $p_i(t)$  is the gauss function of each data with an absolute age of  $T_i \pm \sigma_i$  Ma (errors are at 1-sigma level), defined as:

$$p_i(t) = \frac{1}{\sqrt{2\pi}\sigma_i} \exp\left\{-\frac{(t - T_i)^2}{2\sigma_i^2}\right\}$$

Figures 4.1B–D show the  $P(t)$  histograms for the certain chronological systems.

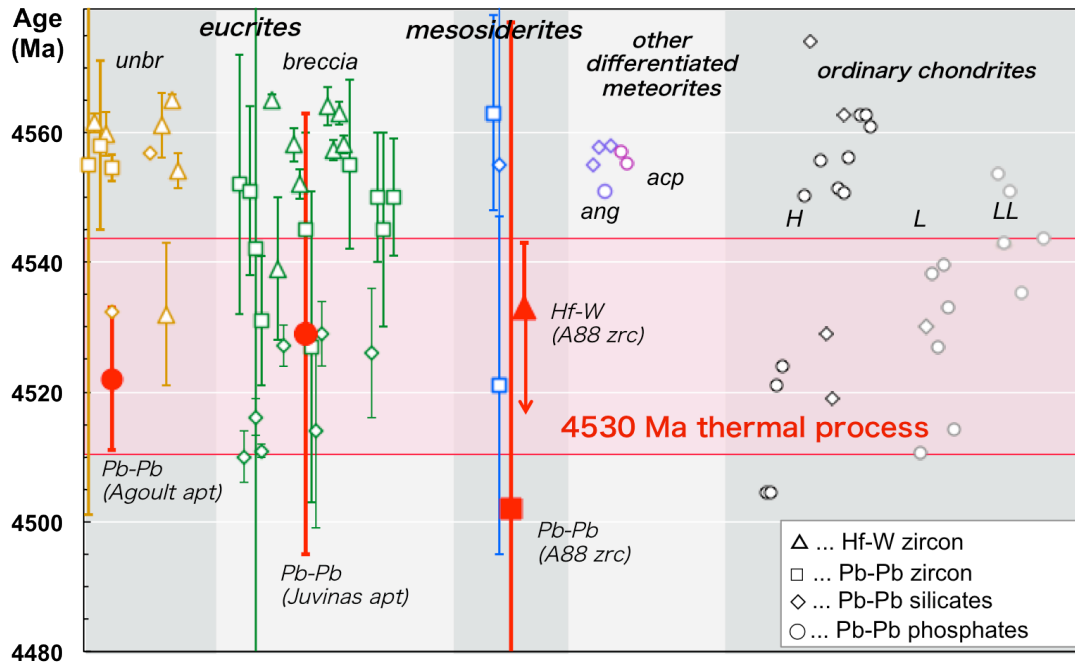


**Figure 4.1 (A)** Comparison of  $^{207}\text{Pb}$ - $^{206}\text{Pb}$  and  $^{182}\text{Hf}$ - $^{182}\text{W}$  among various meteorites.

Several data indicate the younger ages of ~4540–4510 Ma, mentioned as ‘4530 Ma thermal process’ in the main text. My data (Pb-Pb in the eucrites apatite, Pb-Pb and Hf-W in the mesosiderite zircon) are shown as the red filled symbols, while the literatures are shown as opened symbols.

[Symbols] triangles: Hf-W in zircon, squares: Pb-Pb in zircon, diamonds: Pb-Pb in silicates (pyroxene & plagioclase), and circles: Pb-Pb in phosphates. [Abbreviations] unbr: unbrecciated basaltic eucrites, breccia: brecciated eucrites, ang: angrites, acp: acapulcoites. [References] Tatsumoto et al. (1973); Ireland and Bukovanská (1992); Ireland and Wlotzka (1992); Galer and Lugmair (1996); Tera et al. (1997); Misawa et al. (2005); Srinivasan et al. (2007); Lee et al. (2009); Zhou et al. (2013); Iizuka et al. (2013; 2015); Roszjar et al. (2016); Haba et al. (2017)

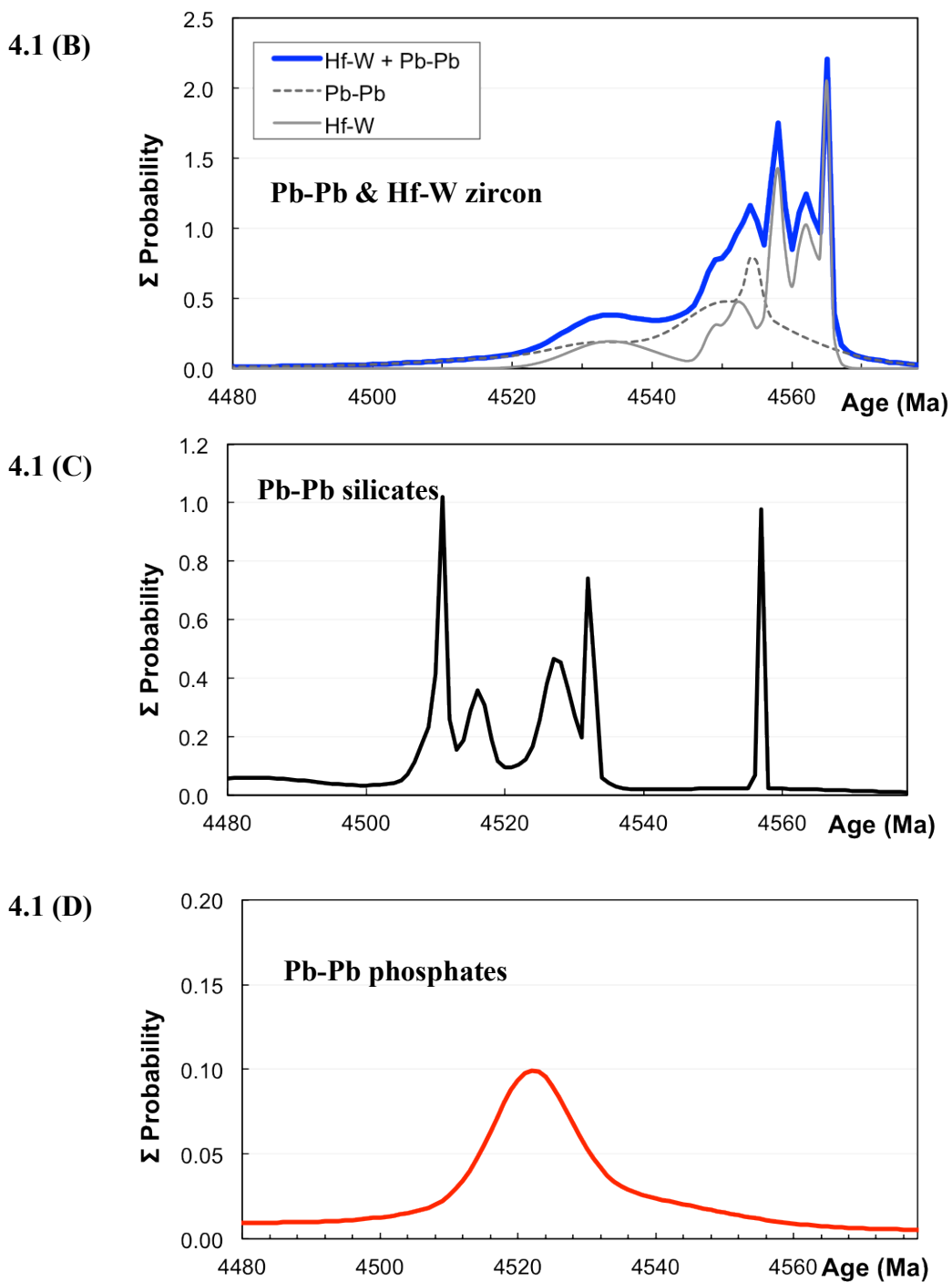


**Figure 4.1 (B-D)** Age probability histograms of eucrites and mesosiderites. Original data are from Fig. 4.1A. Calculations are described in the text. (B) Hf-W and Pb-Pb ages in zircons, (C) Pb-Pb in silicates, and (D) Pb-Pb in phosphates. All three figures have some peaks at ~4530 Ma.

### 4.3. The intense impact reheating events during 4200 Ma

In Chapter 2, I reported the distinctly young U-Pb reset ages for the phosphates from brecciated eucrites, Juvinas and Stannern. Their  $^{207}\text{Pb}$ - $^{206}\text{Pb}$  ages range ~4200–4100 Ma. This study is the first report that identified such young Pb-Pb reset ages in the eucrites phosphates. Young  $^{207}\text{Pb}$ - $^{206}\text{Pb}$  ages with the similar ranges of ~4300–4100 Ma were also reported previously in the silicates (mainly, pyroxene and plagioclase) from some basaltic eucrites (Galer and Lugmair, 1996; Tera et al., 1997). Figure 4.2A summarizes the reported Hf-W (zircon), Pb-Pb (zircon, phosphates, and silicates) and Ar-Ar ages of various meteorites. The age probability histograms were also illustrated for Ar-Ar (Fig. 4.2B), Pb-Pb in silicates (Fig. 4.2C) and in phosphates (Fig. 4.2D) from eucrites and mesosiderites. The young ages at ~4300–4100 Ma were only identified from  $^{207}\text{Pb}$ - $^{206}\text{Pb}$  of the phosphates and the silicates in brecciated eucrites, among the current dataset. They are likely to represent reset events of the U-Pb system (complete Pb loss) by reheating during these periods. In this chapter, I use ‘4200 Ma reheating’ to describe these thermal events. Meanwhile, either Pb-Pb of the zircons or Ar-Ar of the bulk eucrites did not recorded such periods (Figure 4.2 and its references).

Possible heat source for the 4200 Ma reheating was impacts. The reheating temperatures must have exceeded the apatite U-Pb closure temperatures ( $\geq 600^\circ\text{C}$ ). Moreover, as discussed in Chapter 2, these brecciated eucrites have partially remelted textures, suggesting the local temperatures leached the melting points by the impacts. Consequently, the young U-Pb records in the eucrites phosphates and silicates from

brecciated eucrites indicate that Vesta experienced intense impact reheating around 4200 Ma, where the peak temperature slightly exceeded the remelting points ( $\sim 1060^{\circ}\text{C}$ ; Stolper, 1977). Interestingly, almost no datum plots around 4200 Ma in  $^{40}\text{Ar}$ - $^{39}\text{Ar}$  of brecciated eucrites and mesosiderites (Fig. 4.2A–B). Most of them have much younger  $^{40}\text{Ar}$ - $^{39}\text{Ar}$  ages around  $\sim 3400$ – $4000$  Ma, with peaks at ca. 3500 Ma and 3800–3900 Ma (Bogard, 1995, 2011; Bogard and Garrison, 2003, 2009). The 4200 Ma reheating events were identified for the first time by this study, owing to the *in-situ* dating technique of phosphates. It is inferred that Vesta and Vesta-like protoplanets suffered impact brecciation(s) and the intense reheating(s) (up to the remelting temperature) during ca. 4200 Ma, which was recorded in the U-Pb systems in phosphates and silicates. During 4000–3400 Ma (‘3800Ma reheating’, discussed in the following subsection), the Vesta-like bodies experienced more moderate reheating, possibly due to the weaker impacts, where only K-Ar systems were reset. Meanwhile, shocked ordinary chondrites (LL with shock stage S3–S4) recorded the  $^{40}\text{Ar}$ - $^{39}\text{Ar}$  ages around ca. 4200 Ma (Fig. 4.2A; Turner et al., 1978; Kaneoka, 1980; Dixon et al., 2004). It can be considered that the parent body of LL chondrites, unlike Vesta, might have escaped the later moderate impacts at  $\sim 3800$ Ma. Although the 4200 Ma reheating seems to be important for the impact histories of Vesta and other protoplanets, I cannot specifically describe it with the present limited information. For example, no U-Pb data of phosphates has been reported for mesosiderites to date. Future chronological studies of mesosiderites phosphates, as well as other eucrites, may be helpful for further discussion.

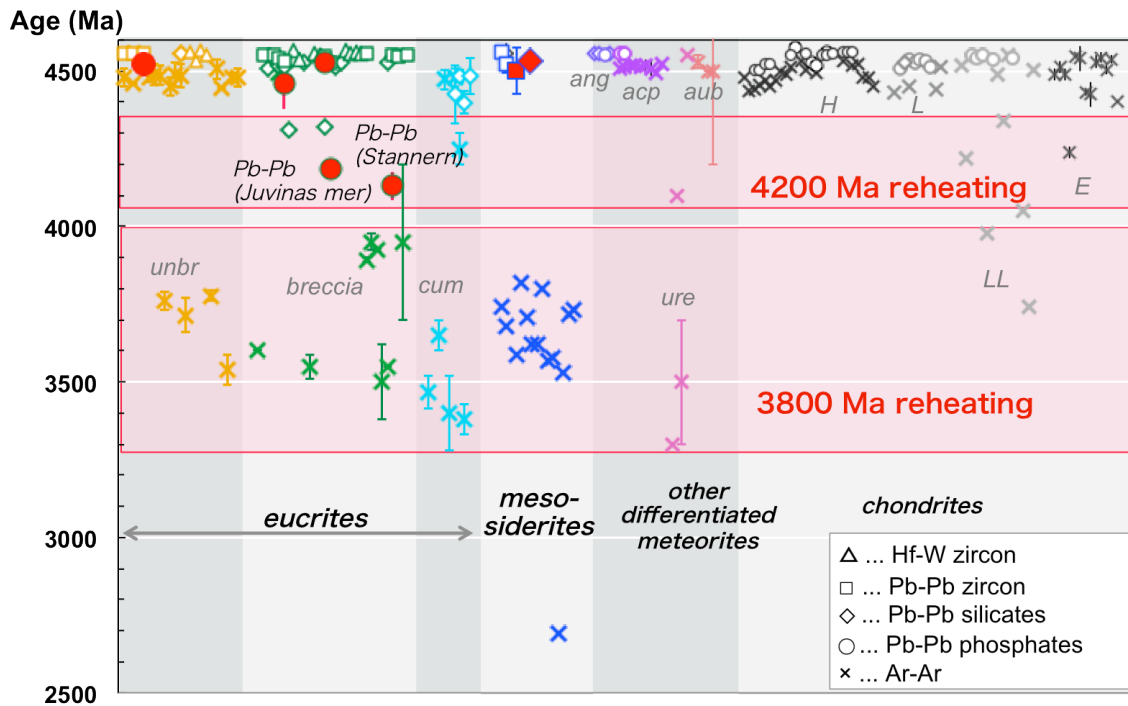


**Figure 4.2 (A)** Comparison of  $^{207}\text{Pb}$ - $^{206}\text{Pb}$ ,  $^{182}\text{Hf}$ - $^{182}\text{W}$ , and  $^{40}\text{Ar}$ - $^{39}\text{Ar}$  among various meteorites. Several data indicate reheating events at  $\sim 4300$ – $4100$  Ma and  $\sim 4000$ – $3400$  Ma, which are mentioned as ‘4200 Ma reheating’ and ‘3800 Ma reheating’ respectively in the text. My data are shown as the red filled symbols.

[Symbols] triangles: Hf-W in zircon, squares: Pb-Pb in zircon, diamonds: Pb-Pb in silicates (pyroxene & plagioclase), circles: Pb-Pb in phosphates, and crosses: Ar-Ar.

[Abbreviations] unbr: unbrecciated basaltic eucrites, breccia: brecciated eucrites, cum: cumulate eucrites, ang: angrites, acp: acapulcoites, ure: ureilites, aub: aubrites.

[Ar-Ar references] Bogard (2011); Bogard et al. (1990; 2001; 2010); Bogard and Garrison (1994; 2003; 2009); Dixon et al. (2004); Kaneoka (1980); McCoy et al. (1996; 1997; 2006); Mittlefehldt et al. (1996); Pellas et al. (1997); Renne (2000); Trieloff et al. (2003); Turner et al. (1978)

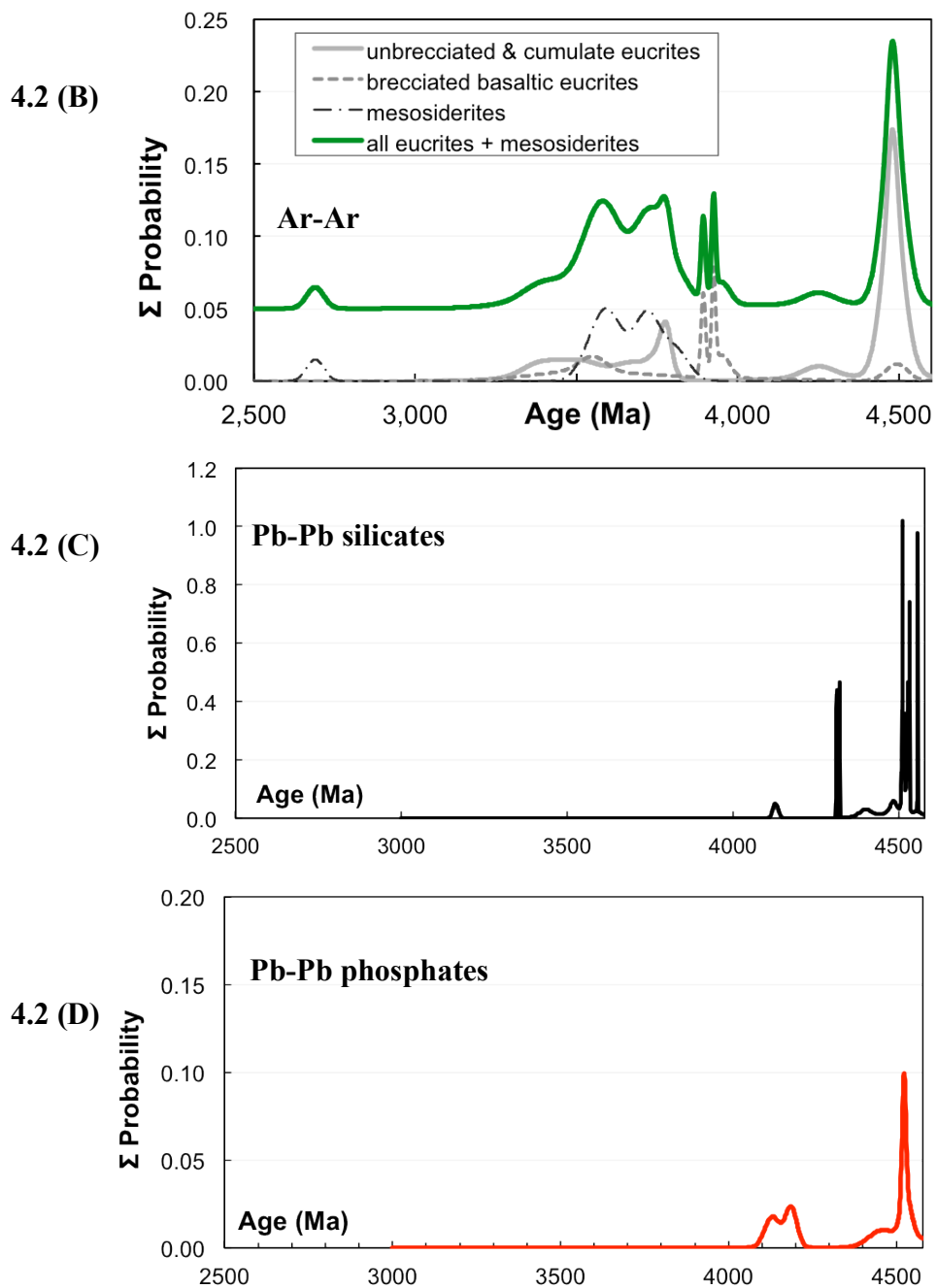


**Figure 4.2 (B-D)** Age probability histograms of eucrites and mesosiderites. Original data are from Fig. 4.2A. (B) Ar-Ar. The accumulated green curve is plot with +0.05 offset, (C) Pb-Pb in silicates, and (D) Pb-Pb in phosphates. Phosphates and silicates apparently have peaks at  $\sim 4200$  Ma, while Ar-Ar data concentrate around 3800 Ma.

#### **4.4 The late impacts reheating events during 3800 Ma**

A number of the brecciated eucrites have disturbed K-Ar system with  $^{40}\text{Ar}$ - $^{39}\text{Ar}$  ages between 4000–3400 Ma ('3800 Ma reheating'; Bogard, 1995; Bogard and Garrison, 2003, 2009). The  $^{40}\text{Ar}$ - $^{39}\text{Ar}$  ages of most mesosiderites also recorded the 3800 Ma reheating events (Bogard et al., 1990). Such younger ages are only obtained from K-Ar system, not from other chronometers such as U-Pb and Hf-W. Only Rb-Sr system in some eucrites indicated younger disturbance at  $\leq 3600$  Ma (Not plotted in Fig 4.1 or 4.2; Birck and Allégre, 1978). The 3800 Ma reheating events may have been common among the Vesta-like protoplanets. However, the reheating temperatures during these events were not high enough to disturb radiometric systems except for K-Ar. The 3800 Ma reheating seems to overlap the Late Heavy Bombardment (LHB) of Moon. There is a possibility that collisional events of Vesta-like protoplanets may have some relationship with lunar and other planetary impact histories. Future investigations of various extraterrestrial samples will help to reveal the possible relationship.

#### **4.5 Conclusions**

In this chapter, I discuss the thermal metamorphic events recorded in U-Pb system in eucrites phosphates and U-Pb and Hf-W systems in mesosiderites zircon, and compare them with literature data. The comprehensive data indicates apparent three timings of thermal events: (I) 4530 Ma thermal process, (II) 4200 Ma reheating, and (III) 3800 Ma reheating. The earliest event (I) was recorded in U-Pb (zircon, silicates

and phosphates) and Hf-W (zircon) from both unbrecciated and brecciated eucrites, as well as mesosiderites. This event can be regarded as simultaneous occurrences of the thermal metamorphism of protoplanets' crust due to their internal residual heat and the impact reheating. The 4530Ma process may have been high temperature events, where U-Pb and Hf-W in zircon were reset and/or secondary zircon recrystallized. The second event (II) was recorded by only U-Pb in the phosphates and silicate from several brecciated eucrites. Because these meteorites contain remelted textures due to the impacts, the local temperatures may have exceeded the basalt melting points (~1060 °C). Possible heat source at 4200 Ma is impact. It is suggested that Vesta experienced the intense impact reheating at 4200 Ma, although further discussion requires additional information. The last event (III) was only recorded in the K-Ar systems among various meteorites. Most of brecciated eucrites and mesosiderites have the young  $^{40}\text{Ar}$ - $^{39}\text{Ar}$  ages around 3800 Ma, suggesting that the 3800 Ma reheating events were common among Vesta-like protoplanets. Possible heat source is impacts. The 3800 Ma reheating may have relationship with LHB on lunar and other inner-solar planets. On the other hand, U-Pb system in phosphates or silicates was not disturbed during the later impacts. The 3800 Ma impact reheating is considered to have been so moderate that did not disturb the U-Pb systems. Future investigation of various meteoritical records will be helpful for more general and plausible interpretation.

# CHAPTER 5

## GENERAL CONCLUSIONS

The goal of this study is to elucidate the evolutionary history of Vesta-sized (several hundred km) protoplanets. Using chronological records in meteorites, I evaluate the thermal metamorphic and collisional processes of ancient asteroids. The key technique in the present study is *in-situ* U-Pb and Hf-W dating methods of NanoSIMS 50. For *in-situ* U-Pb dating of phosphates, I established the analytical methods in previous collaboration works (Koike et al., 2014; 2016). This method is utilized in the present eucrites study (Chapter 2). For *in-situ* Hf-W dating of zircon, I have established the NanoSIMS analytical protocol in this study. This method is used for the age determination of mesosiderite zircon (Chapter 3), which has been reported in Koike et al. (2017). These chronologies records in the meteorites are expected to provide insights of igneous and/or metamorphic histories of their parent protoplanets.

In Chapter 2, I focus on the crustal evolution history of asteroid 4-Vesata, a sole surviving differentiated protoplanet. A number of HED meteorites, originated from Vesta's crusts, were previously investigated from mineralogy, geochemistry, and

chronology. The earlier studies suggested highly complicated history for this asteroid, including prolonged magmatism, crustal metamorphism, and intense impacts brecciation and reheating. Previous studies conducted *in-situ* U-Pb dating of eucrites zircons, which indicate high-temperature igneous and/or metamorphic events ( $\geq 900$  °C). Thermal history at more moderate temperature ranges is also important for understanding the comprehensive history. The goal of the present study in Chapter 2 is to reveal the metamorphic history of Vesta at the moderate temperature ranges of ca. 600°C, using NanoSIMS *in-situ* U-Pb dating of phosphates in basaltic eucrites.

In this study, I analyzed four basaltic eucrites and one basaltic achondrite. Three of the five are brecciated (i.e. experienced impacts), whereas the others are unbrecciated. From apatite in the unbrecciated eucrite, Agoult, a precise  $^{207}\text{Pb}$ - $^{206}\text{Pb}$  age of  $4522 \pm 11$  Ma is determined. The similar  $^{207}\text{Pb}$ - $^{206}\text{Pb}$  age of ca. 4530 Ma is also obtained from older apatite in Juvinas, although merrillite in the same Juvinas section has a younger  $^{207}\text{Pb}$ - $^{206}\text{Pb}$  age of ca. 4200 Ma. It is inferred that the ancient crusts on Vesta (and possibly, ancient crust on other protoplanets, as well) were slowly cooled down to ca. 600°C from the earlier thermal process by ca. 4530 Ma. In contrast, U-Pb systems in phosphates from the brecciated eucrites show severe disturbances at  $\sim 4400$  Ma and 4200–4100 Ma. Considering locally remelted textures of the brecciated samples, these younger disturbances are interpreted as the impacts, where reheating temperatures slightly exceeded the melting points. It is inferred that Vesta (as well as, other protoplanets,) experienced the intense impacts during 4200–4100 Ma.

In Chapter 3, I have investigated the impact and thermal metamorphic history of mesosiderites parent body (MPB). Mesosiderites, a unique stony-iron group, are mixtures of brecciated silicates and Fe-Ni metals. The silicates have similarities with basaltic eucrites in mineralogy, geochemistry and isotopic compositions. Nasa's Dawn mission did not identify the mesosiderite-like silicate-metal mixtures on the surface regolith of Vesta. Hence, MPB can be regarded as Vesta-like past protoplanet, although MPB is not exactly Vesta, and may not exist today. Formation history of mesosiderites is still enigmatic, though, their silicates-metal mixing should have occurred during impact. The records in this meteorite group will provide valuable insight to collisional evolution of protoplanets in the early Solar System. However, little has been uncovered until recently. The goal of this study in Chapter 3 is to constrain the timing of thermal metamorphism of mesosiderites and to reveal the impact history of MPB.

I have conducted *in-situ* U-Pb and Hf-W dating on a single zircon grain in Asuka 882023 (A88) mesosiderite, using NanoSIMS 50. The  $^{207}\text{Pb}$ - $^{206}\text{Pb}$  age is determined as  $4502 \pm 75$  Ma. The  $^{182}\text{Hf}$ - $^{182}\text{W}$  age of the same zircon is  $4532.8 \pm 9.6$  Ma. Both U-Pb and Hf-W systems recorded the formation timing of A88 zircon. Considering its textural and geochemical features, A88 zircon is considered to have formed secondarily during thermal metamorphism at 4540–4500 Ma (I call this period as '4530 Ma'), distinctly later than MPB crustal formation at  $\geq 4560$  Ma. The impact-associated silicates-metal mixing may have occurred at the same time or earlier. Exact timing of the mixing is still controversial. Heat source for the 4530 Ma thermal

event is also controversial with the current information. However, it seems clear that MPB crusts experienced high temperature metamorphism at ca. 4530 Ma. A plausible interpretation is that the basaltic crusts on MPB and the metallic core from impactor were mixed during the 4530 Ma impact, which was followed by the high-temperature reheating and the secondary zircon growth. It is inferred the evolutionary processes of Vesta-like protoplanets were still active during this period.

Finally, I summarize the present chronological knowledge from eucrites and mesosiderites, along with literature data of various meteorites. Based on the comparison of various meteoritical records, it is inferred that Vesta-like protoplanets experienced both internal reheating (prolonged magmatism) and impact reheating by ca. 4530 Ma. The asteroids may also have suffered the intense impacts with high-temperature reheating at ca. 4200 Ma, and the repeated moderate impacts during ca. 3800 Ma.

## REFERENCES

- Ahrens, L. H. (1955) Implications of the Rhodesia age pattern. *Geochim. Cosmochim. Acta*, 8, 1–15.
- Amelin, Y., A. N. Krot, I. D. Hutcheon, and A. A. Ulyanov (2002), Lead isotopic ages of chondrules and calcium-aluminum-rich inclusions, *Science*, 297, 1678–1683.
- Amelin, Y., A. Kaltenbach, T. Iizuka, C. H. Stirling, T. R. Ireland, M. Petaev, S. B. Jacobsen (2010) U–Pb chronology of the Solar System’s oldest solids with variable  $^{238}\text{U}/^{235}\text{U}$ . *Earth Planet. Sci. Lett.* 300, 343–350.
- Andersen, C. A., and J. R. Hinthorne (1972) U, Th, Pb and REE abundances and  $^{207}\text{Pb}/^{206}\text{Pb}$  ages of individual minerals in returned lunar material by ion microprobe analysis. *Earth Planet. Sci. Lett.* 14, 195–200.
- Andersen, C. A., and J. R. Hinthorne (1973)  $^{207}\text{Pb}/^{206}\text{Pb}$  ages of individual mineral phases in Luna 20 material by ion microprobe mass analysis. *Geochim. Cosmochim. Acta*, 37, 745–754.
- Barrat, J. A., J. Blichert-Toft, Ph. Gillet, and F. Keller (2000) The differentiation of eucrites: The role of in situ crystallization, *Meteorit. Planet. Sci.*, 35, 1087–1100.
- Barrat, J. A., A. Jambon, M. Bohn, J. Blichert-Toft, V. Sautter, C. Göpel, P. Gillet, O. Boudouma, and F. Keller (2003) Petrology and geochemistry of the

- unbrecciated achondrite Northwest Africa 1240 (NWA 1240): An HED parent body impact melt, *Geochim. Cosmochim. Acta*, 67, 3959–3970.
- Barrat, J. A., A. Yamaguchi, R. C. Greenwood, M. Bohn, J. Cotton, M. Benoit, and I. A. Franchi (2007) The Stannern trend eucrites: Contamination of main group eucritic magmas by crustal partial melts, *Geochim. Cosmochim. Acta*, 71, 4108–4124.
- Basaltic Volcanism Study Project (1981), *Basaltic Volcanism on the Terrestrial Planets*, The Lunar and Planetary Institute, Pergamon Press, Inc., New York.
- Benedix, G. K., H. Haack, and T. J. McCoy (2014) Iron and Stony-Iron Meteorites. *Meteorites and Cosmochemical Processes, Volume 1 of Treatise on Geochemistry (Second Edition)*. Elsevier, 2014. Edited by Andrew M. Davis, p.267–285.
- Birck, J. L., and C. J. and Allègre (1978) Chronology and chemical history of the parent body of basaltic achondrites studied by the  $^{87}\text{Rb}$ - $^{87}\text{Sr}$  method, *Earth Planet. Sci. Lett.* 39, 37–51.
- Bogard, D. D. (2011) K–Ar ages of meteorites: Clues to parent-body thermal histories. *Chemie der Erde* 71, 207–226.
- Bogard and Garrison (1994)  $^{39}\text{Ar}$ - $^{40}\text{Ar}$  ages of four ureilites. *Proc. 25th Lunar Planet. Sci. Conf.* 137–138.
- Bogard and Garrison (1995)  $^{39}\text{Ar}$ - $^{40}\text{Ar}$  age of the Ibitira eucrite and constraints on the time of pyroxene equilibration. *Geochim. Cosmochim. Acta* 59, 4317–4322.

Bogard, D. D., and D. H. Garrison (2003)  $^{39}\text{Ar}$ - $^{40}\text{Ar}$  ages of eucrites and thermal history of asteroid 4 Vesta, *Meteorit. Planet. Sci.*, 38, 669–710.

Bogard, D. D., and D. H. Garrison (2009) Ar-Ar Impact Heating Ages of Eucrites and Timing of the LHB. *Proc. 40th Lunar Planet. Sci. Conf.* abstract 1131.

Bogard, D. D., D. H. Garrison, J. L. Jordan, and D. Mittlefehldt (1990),  $^{39}\text{Ar}$ - $^{40}\text{Ar}$  dating of mesosiderites: Evidence for major parent body disruption < 4 Ga ago, *Geochim. Cosmochim. Acta*, 54, 2549–2564.

Bouvier, A., and M. Wadhwa (2010), The age of the Solar System redefined by the oldest Pb–Pb age of a meteoritic inclusion, *Nature Geosci.*, 3, 637–641.

Bouvier, A., L. Spivak-Birndorf, G. A. Brennecka, and M. Wadhwa (2011) New constraints on early Solar System chronology from Al–Mg and U–Pb isotope systematics in the unique basaltic achondrite Northwest Africa 2976. *Geochim. Cosmochim. Acta* 75, 5310–5323.

Brennecka, G. A., S. Weyer, M. Wadhwa, P. E. Janney, J. Zipfel, and A. D. Anbar (2010)  $^{238}\text{U}/^{235}\text{U}$  Variations in Meteorites: Extant  $^{247}\text{Cm}$  and Implications for Pb-Pb Dating. *Science* 327, 449–451.

Brennecka, G. A., and M. Wadhwa (2012) Uranium isotope compositions of the basaltic angrite meteorites and the chronological implications for the early Solar System, *PNAS*, 109, 9299–9303.

Brouxel, M., and M. Tatsumoto (1990), U–Th–Pb systematics of the

- Estherville mesosiderite, Proc. 20th Lunar Planet. Sci. Conf, 309–319.
- Brouxel, M., and M. Tatsumoto (1991), The Estherville mesosiderite: U-Pb, Rb-Sr, and Sm-Nd isotopic study of a polymict breccia, *Geochim. Cosmochim. Acta*, 55, 1121–1133.
- Buchwald, V. F. (1975) *Handbook of Iron Meteorites*. Berkeley, CA, University of California Press.
- Burkhardt, C., T. Kleinte, B. Bourdon, H. Palme, J. Zipfel, J. M. Friedrich, and D. S. Ebel (2008) Hf–W mineral isochron for Ca,Al-rich inclusions: Age of the solar system and the timing of core formation in planetesimals, *Geochim. Cosmochim. Acta*, 72, 6177–6197.
- Bukovanska, M., and T. R. Ireland (1993) Zircons in eucrites: pristine and disturbed U-Pb systematics, Proc. 56th Annual Meeting of Meteoritical Society, abstract 333.
- Cassata, W. S., P. R. Renne, and D. L. Shuster (2009) Argon diffusion in plagioclase and implications for thermochronometry: A case study from the Bushveld Complex, South Africa, *Geochim. Cosmochim. Acta*, 73, 6600–6612.
- Chamberlain, K. R., and S. A. Bowring (2000) Apatite–feldspar U–Pb thermochronometer: a reliable, mid-range (~ 450°C), diffusion-controlled system, *Chem. Geol.* 172, 173–200.
- Chen, J. H., and G. J. Wasserburg (1980) A search for isotopic anomalies in uranium.

Geophys. Res. Lett. 7, 275–278.

Chen, J. H., and G. J. Wasserburg (1985) U-TH-Pb isotopic studies on meteorite ALHA 81005 and Ibitira, Proc. 61th Lunar and Planet Sci. Conf. abstract 119–120.

Cherniak, D. J. (1995) Diffusion of lead in plagioclase and K-feldspar: an investigation using Rutherford Backscattering and Resonant Nuclear Reaction Analysis, Contrib. Mineral. Petrol. 120, 358–371.

Cherniak, D. J. (2001) Pb diffusion in Cr diopside, augite, and enstatite, and consideration of the dependence of cation diffusion in pyroxene on oxygen fugacity, Chem. Geol. 177, 381–397.

Cherniak, D. J., and E. B. Watson (2000) Pb diffusion in zircon, Chem. Geol. 172, 5–24.

Cherniak, D. J., W. A. Lanford, and F. J. Ryerson (1991) Lead diffusion in apatite and zircon using ion implantation and Rutherford Backscattering techniques, Geochim. Cosmochim. Acta, 55, 1662–1673.

Clayton, R. N., and T. K. Mayeda (1996), Oxygen isotopic studies of achondrites, Geochim. Cosmochim. Acta 60, 1999–2017.

Clayton, R. N., T. K. Mayeda, M. Prinz, C. E. Nehru, and J. S. Delaney (1986), Oxygen isotope confirmation of a genetic association between achondrites and IIIAB iron meteorites, 17th Lunar Planet. Sci. Conf., abstract 141.

- Clenet, H., M. Jutzi, J. A. Barrat, E. I. Asphaug, W. Benz, and P. Gillet (2014) A deep crust–mantle boundary in the asteroid 4 Vesta, *Nature*, 511, 303–306.
- Consolmagno, G. J., and M. Drake (1977) Composition and evolution of the eucrite parent body: evidence from rare earth elements, *Geochim. Cosmochim. Acta*, 41, 1271–1282.
- Cowan, G. A., and H. H. Adler (1976) The variability of the natural abundance of  $^{235}\text{U}$ . *Geochim. Cosmochim. Acta* 40, 1487–1490.
- Danielson, L. R., K. Righter, and M. Humayun (2009) Trace element chemistry of Cumulus Ridge 04071 pallasite with implications for main group pallasites. *Meteoritics Planet. Sci.* 44, 1019.
- DeMeo, F. E., and B. Carry (2014) Solar System evolution from compositional mapping of the asteroid belt. *Nature* 505, 629–634.
- Dixon, E.T., D. D. Bogard, and D.H. Garrison, (2004)  $^{39}\text{Ar}$ – $^{40}\text{Ar}$  evidence for early impact events on the LL parent body. *Geochim. Cosmochim. Acta* 68, 3779–3790.
- Dodson (1973) Closure temperature in cooling geochronological and petrological systems, *Contrib. Mineral. Petrol.* 40, 259–274.
- Duke, M. B., and L. T. Silver (1967) Petrology of eucrites, howardites, and mesosiderites, *Geochim. Cosmochim. Acta*, 31, 1637–1665.

- Floran, R. J. (1978), Silicate petrography, classification, and origin of the mesosiderites: Review and new observations, Proc. 9th Lunar Planet. Sci. Conf, 1053–1081.
- Galer, S. J. G., and G. W. Lugmair (1996) Lead isotopic systematics of noncumulate eucrites, 59th Annual Meeting of Meteoritical Society, Abstract A47.
- Galer, S. J. G. and G. W. Lugmair (1996) Lead isotope systematics of noncumulate eucrites. Annual Meeting of the Meteoritical Society, abstract A47.
- Göpel, C., G. Manhès, and C. J. Allègre (1992) U–Pb study of the Acapulco meteorite. *Meteoritics* 27, 226.
- Göpel, C., G. Manhès, C. J. Allègre, (1994) U–Pb systematic of phosphates from equilibrated ordinary chondrites. *Earth Planet. Sci. Lett.* 121, 153–171.
- Greenwood, R. C., I. A. Franchi, A. Jambon, and P. C. Buchanan (2005) Widespread magma oceans on asteroidal bodies in the early Solar System, *Nature*, 435, 916–918.
- Greenwood, R. C., I. A. Franchi, J. M. Gibson, and G. K. Benedix (2012) Oxygen isotope variation in primitive achondrites: The influence of primordial, asteroidal and terrestrial processes. *Geochim. Cosmochim. Acta* 94, 146–163.
- Greenwood, R. C., J.-A. Barrat, E. R.D. Scott, H. Haack, P. C. Buchanan, I. A. Franchi, A. Yamaguchi, D. Johnson, A. W.R. Bevan, and T. H. Burbine (2015), *Geochemistry and oxygen isotope composition of main-group pallasites and*

- olivine-rich clasts in mesosiderites: Implications for the “Great Dunité Shortage” and HED-mesosiderite connection, *Geochim. Cosmochim. Acta*, 169, 115–136.
- Haba, M. K., Yamaguchi A., Horie K. and Hidaka H. (2014), Major and trace elements of zircons from basaltic eucrites: implications for the formation of zircons on the eucrite parent body. *Earth Planet. Sci. Lett.* 387, 10–21.
- Haba, M. K., Y.-J. Lai, A. Yamaguchi, and M. Schönbacher (2016), Niobium–zirconium systematics of meteoritic rutiles: application to the chronology of mesosiderites, 79th Annual Meeting of the Meteoritical Society, abstract 6139.
- Haba, M. K., A. Yamaguchi, H. Kagi, K. Nagao, and H. Hidaka (2017), Trace element composition and U-Pb age of zircons from Estherville: Constraints on the timing of the metal-silicate mixing event on the mesosiderite parent body, *Geochim. Cosmochim. Acta*, 215, 76–91.
- Hassanzadeh, J., A. E. Rubin, and J. T. Wasson (1990), Compositions of large metal nodules in mesosiderites: Links to iron meteorite group IIIAB and the origin of mesosiderite subgroups, *Geochim. Cosmochim. Acta*, 54, 3197–3208.
- Hayashi, C., K. Nakagawa, and Y. Nakazawa (1985) Formation of the solar system. In *Protostars and Planets II*, Univ. of Arizona Press, 1100-1153.
- Heim, N. A., M. Wadhwa, and A. M. Davis (1999) Rare earth element abundances in vapor deposited in minerals in Ibitira vesicles, *Proc. 30th Lunar Planet. Sci. Conf. Abstract* 1980.

- Hervig, R., J. Delaney and C. O'Neill (1986) Evidence for partial remelting of Stannern and comparison with a silica-bearing clast in Juvinas, 49th Annual Meeting of Meteoritical Society, Abstract 395.
- Hewins, R. H. (1984) The case for a melt matrix in plagioclase-POIK mesosiderites. *J. Geophys. Res.* 89(S01), C289–C297.
- Ida, S., and T. Guillot (2016) Formation of dust-rich planetesimals from sublimated pebbles inside of the snow line. *Astronomy Astrophysics* 596, L3.
- Iizuka, T., A. Kaltenbach, Y. Amelin, C. H. Stirling, and A. Yamaguchi (2013) U-Pb isotope systematics of eucrites in relation to their thermal history, Proc. 44th Lunar Planet. Sci. Conf. Abstract 1907.
- Iizuka, T. Y. Amelin, A. Kaltenbach, P. Koefoed, and C. H. Stirling (2014) U-Pb systematics of the unique achondrite Ibitira: Precise age determination and petrogenetic implications, *Geochim. Cosmochim. Acta*, 132, 259–273.
- Iizuka, T., A. Yamaguchi, M. K. Haba, Y. Amelin, P. Holden, S. Zink, M. H. Huyskens, and T. R. Ireland (2015) Timing of global crustal metamorphism on Vesta as revealed by high-precision U-Pb dating and trace element chemistry of eucrite zircon, *Earth Planet. Sci. Lett.* 409, 182–192.
- Ireland, T. R. (1991), The abundance of  $^{182}\text{Hf}$  in the early solar system, Proc. 22nd Lunar Planet. Sci. Conf, abstract 609.

- Ireland, T. R., and M. Bukovanská (1992) Zircons from the Stannern eucrites, Proc. 55th Annual Meeting of Meteoritical Society, abstract 237.
- Ireland, T. R., and F. Wlotzka (1992), The oldest zircons in the solar system, Earth Planet. Sci. Lett., 109, 1–10.
- Ireland, T. R., and M. Bukovanská (2003), Initial  $^{182}\text{Hf}/^{180}\text{Hf}$  in meteoritic zircons, Geochim. Cosmochim. Acta, 67, 4849–4856.
- Ireland, T. R., H. Kirby, M. Bukovanská, and F. Wlotzka (2000) Hf-W systematics of meteoritic zircons, revisited. Proc. 31st Lunar Planet. Sci. Conf, abstract 1540.
- Jochum, K. R., U. Weis, B. Stoll, D. Kuzmin, Q. Yang, I. Raczek, D. E. Jacob, A. Stracke, K. Birbaum, D. A. Frick, D. Günther, and J. Enzweiler (2011), Determination of reference values for NIST SRM 610-617 glasses following ISO guidelines, Geostandards and Geoanalytical Research, 35, 397–429.
- Jaffey, A. H., K. F. Flynn, L. E. Glendenin, W. C. Bentley, and A. M. Essling (1971) Precision Measurement of Half-Lives and Specific Activities of  $^{235}\text{U}$  and  $^{238}\text{U}$ . Physical Review, 4, 1889–1906.
- Kaneoka, I. (1980)  $^{40}\text{Ar}$ - $^{39}\text{Ar}$  Ages of L and LL Chondrites from Allan Hills, Antarctica: ALHA77015, 77214 and 77304. Memoirs of National Institute of Polar Research. Special issue 17, 177-188.
- Kaneoka, I., K. Nagao, A. Yamaguchi, and H. Takeda (1995)  $^{39}\text{Ar}$ - $^{40}\text{Ar}$  analyses of Juvinas fragments, Proc. NIPR symp. Antarct. Meteorites, 8, 287–296.

Kleine, T., C. Münker, K. Mezger, and H. Palme (2002), Rapid accretion and early core formation on asteroids and the terrestrial planets from Hf-W chronometry, *Nature*, 418, 952–955.

Kleine, T., K. Mezger, C. Münker, H. Palme, and A. Bischoff (2004)  $^{182}\text{Hf}$ - $^{182}\text{W}$  isotope systematics of chondrites, eucrites, and martian meteorites: Chronology of core formation and early mantle differentiation in Vesta and Mars, *Geochim. Cosmochim. Acta*, 68, 2935–2946.

Kleine, T., K. Mezger, H. Palme, E. Schere, and C. Münker (2005) The W isotope composition of eucrite metals: constraints on the timing and cause of the thermal metamorphism of basaltic eucrites, *Earth Planet. Sci. Lett.* 231, 41–52.

Kleine, T., M. Touboul, B. Bourdon, F. Nimmo, K. Mezger, H. Palme, S. B. Jacobsen, Q.-Z. Yin, and A. N. Halliday (2009) Hf–W chronology of the accretion and early evolution of asteroids and terrestrial planets. *Geochim. Cosmochim. Acta* 73, 5150–5188.

Kleine, T., U. Hans, A. J. Irving, and B. Bourdon (2012) Chronology of the angrite parent body and implications for core formation in protoplanets, *Geochim. Cosmochim. Acta*, 84, 186–203.

Koike, M., Y. Ota, Y. Sano, N. Takahata, and N. Sugiura (2014) High-spatial resolution U–Pb dating of phosphate minerals in Martian meteorite Allan Hills 84001, *Geochem. J.* 48, 423–431.

- Koike, M., Y. Sano, N. Takahata, A. Ishida, N. Sugiura, and M. Anand (2016)  
Combined investigation of H isotopic compositions and U-Pb chronology of  
young Martian meteorite Larkman Nunatak 06319, *Geochem. J.* 50, 363–377.
- Koike, M., N. Sugiura, N. Takahata, A. Ishida, and Y. Sano (2017), U-Pb and Hf-W  
dating of young zircon in mesosiderite Asuka 882023. *Geophys. Res. Lett.* 44,  
1251–1259.
- Krot, A. N., K. Keil, E. R. D. Scott, C. A. Goodrich, M. K. Weisberg (2014)  
Classification of Meteorites and Their Genetic Relationships, Meteorites and  
Cosmochemical Processes, Volume 1 of Treatise on Geochemistry (Second  
Edition). Elsevier, 2014. Edited by Andrew M. Davis, p.1-63.
- Kruijer, T. S., C. Burkhardt, G. Budde, and T. Kleine (2017) Age of Jupiter inferred  
from the distinct genetics and formation times of meteorites. *PNAS* 114, 6712–  
6716.
- Kruijer T. S., T. Kleine, L. E. Borg, G. A. Brennecka, A. J. Irving, A. Bischoff, and C.  
B. Agee (2017) The early differentiation of Mars inferred from Hf–W chronometry.  
*Earth Planet. Sci. Lett.* 474, 345–354.
- Kunz, J., M. Tieloff, K. D. Bobe, K. Metzler, D. Stöffler and E. K. Jessberger (1995)  
The collisional history of the HED parent body inferred from  $^{40}\text{Ar}$ - $^{39}\text{Ar}$  ages of  
eucrites, *Planet. Space Sci.* 43, 527–543.
- Lee D. C. and Halliday A. N. (1996) Hf-W isotopic evidence for rapid accretion and

- differentiation in the early solar system. *Science* 274, 1876–1879.
- Lee, S. R., H. Kim, D.-L. Cho, K. Horie, and H. Hidaka (2009) U-Pb dating of zircons from eucrites: a preliminary report, *Goldschmidt Conf. Abstract A 737*.
- Loesche, C., G. Wurm, J. Teiser, J. M. Friedrich, and A. Bischoff (2013), Photophoretic strength on chondrules. 1. Modeling, *Astrophys. J.*, 778(101), 1–10.
- Ludwig, K. R. (2003), User's Manual for Isoplot 3.00: A geochronological toolkit for Microsoft Excel, Berkeley Geochronology Center, Special Publication No. 4.
- Lugmair, G. W. (1974) Sm-Nd ages: a new dating method, *Proc. 37th Annual Meeting of Meteoritical Society*, Abstract 369.
- Lugmair, G. W., and S. J. G. Galer (1992) Age and isotopic relationships among the angrites Lewis Cliff 86010 and Angra dos Reis. *Geochim. Cosmochim. Acta* 56, 1673–1694.
- Lugmair, G. W., and N. B. Scheinin (1975) Sm-Nd systematics of the Stannern eucrite, *Proc. 38th Annual Meeting of Meteoritical Society*, Abstract 447–448.
- Lugmair, G. W., and A. Shukolyukov (1998), Early solar system timescales according to  $^{53}\text{Mn}$ – $^{53}\text{Cr}$  systematics, *Geochim. Cosmochim. Acta*, 62, 2863–2886.
- Mandler, B. E., and L. T. Elkins-Tanton (2013) The origin of eucrites, diogenites, and olivine diogenites: Magma ocean crystallization and shallow magma chamber processes on Vesta, *Meteorit. Planet. Sci.* 48, 2333–2349.

- Manhès, G., J. F. Minster and C. J. Allègre (1978) Comparative Uranium–Thorium–Lead and Rubidium–Strontium study of the Saint Severin Amphoterite: Consequences for early solar system chronology. *Earth Planet. Sci. Lett.* 39, 14–24.
- Manhes, G., C. Göpel, and C. J. Allègre (1987) High resolution chronology of the early solar system based on lead isotopes, 50th Annual Meeting of Meteoritical Society, Abstract 453.
- Markowski, A., G. Quitté, T. Kleine, A. N. Halliday, M. Bizzarro, A. J. Irving (2007) Hafnium–tungsten chronometry of angrites and the earliest evolution of planetary objects. *Earth Planet. Sci. Lett.* 262, 214–229.
- McCord, T. B., J. B. Adams, and T. V. Johnson (1970) Asteroid Vesta: Spectral Reflectivity and Compositional Implications, *Science*, 168, 1445–1447.
- McCoy, T.J., K. Keil, R. N. Clayton, T. K. Mayed, D. D. Bogard, D. H. Garrison, G. R. Huss, I. D. Hutcheon, and R. Wieler (1996) A petrologic, chemical, and isotopic study of Monument Draw and comparison with other acapulcoites: evidence for formation by incipient melting. *Geochim. Cosmochim. Acta* 60, 2681–2708.
- McCoy, T.J., K. Keil, R. N. Clayton, T. K. Mayed, D. D. Bogard, D. H. Garrison, and R. Wieler, (1997) A petrologic and isotopic study of lodranites: evidence for early formation as partial melt residues from heterogeneous precursors. *Geochim. Cosmochim. Acta* 61, 623–637.

- McCoy, T.J., W. D. Carlson, L. R. Nittler, R. M. Stroud, D. D. Bogard, D. H. Garrison, (2006) Graves Nunataks 95209: a snapshot of metal segregation and core formation. *Geochim. Cosmochim. Acta* 70, 516–531.
- McSween, H. Y., D. W. Mittlefehldt, A. W. Beck, R. G. Mayne, and T. J. McCoy (2011) HED Meteorites and Their Relationship to the Geology of Vesta and the Dawn Mission, *Space Sci. Rev.* 163, 141–174.
- McSween, H. Y., R. P. Binzel, M. C. De Sanctis, E. Ammannito, T. H. Prettyman, A. W. Beck, V. Reddy, L. L. Corre, M. J. Gaffey, T. B. McCord, C. A. Raymond, C. T. Russell, and the Dawn Science Team (2013) Dawn; the Vesta–HED connection; and the geologic context for eucrites, diogenites, and howardites, *Meteorit. Planet. Sci.* 48, 2090–2104.
- Metzler, K., K. D. Bobe, H. Palme, B. Spettel, and D. Stöffler (1995) Thermal and impact metamorphism on the HED parent asteroid, *Planet. Space Sci.* 43, 499–5252.
- Misawa, K., A. Yamaguchi, and H. Kaiden (2005) U-Pb and  $^{207}\text{Pb}$ - $^{206}\text{Pb}$  ages of zircons from basaltic eucrites: Implications for early basaltic volcanism on the eucrite parent body, *Geochim. Cosmochim. Acta*, 69, 5847–5861.
- Mittlefehldt, D. W. (1987) Volatile degassing of basaltic achondrite parent bodies: Evidence from alkali elements and phosphorus, *Geochim. Cosmochim. Acta*, 51, 267–273.

- Mittlefehldt, D. W. (1990) Petrogenesis of mesosiderites: I. Origin of mafic lithologies and comparison with basaltic achondrites. *Geochim. Cosmochim. Acta* 54, 1165–1173.
- Mittlefehldt, D. W., T. J. McCoy, C. A. Goodrich, and A. Kracher (1998) Non-chondritic meteorites from asteroidal bodies. *Rev. in Mineralogy Geochemistry* 36, D1–D195.
- Mittlefehldt, D. W. (2014) Achondrites, Meteorites and Cosmochemical Processes, Volume 1 of *Treatise on Geochemistry (Second Edition)*. Elsevier, 2014. Edited by Andrew M. Davis, p.235–266.
- Miyamoto, M., and H. Takeda (1977) Evaluation of a crust model of achondrites from the width of exsolved pyroxenes and their pyroxene crystallization trend, 40th Annual Meeting of Meteoritical Society, Abstract 312.
- Miyamoto, M., T. Mikouchi, and K. Kaneda (2001) Thermal history of the Ibitira noncumulate eucrite as inferred from pyroxene exsolution lamella: Evidence for reheating and rapid cooling, *Meteorit. Planet. Sci.* 36, 231–237.
- Miura, Y. N., K. Nagao, N. Sugiura, T. Fujitani, and P. H. Warren (1998) Noble gases,  $^{81}\text{Kr}$ -Kr exposure ages and  $^{244}\text{Pu}$ -Xe ages of six eucrites, Béréba, Binda, Camel Donga, Juvinas, Millbillillie, and Stannern, *Geochim. Cosmochim. Acta*, 62, 2369–2387.

- Neumann, W., D. Breuer, and T. Spohn (2014) Differentiation of Vesta: Implications for a shallow magma ocean, *Earth Planet. Sci. Lett.* 395, 267–280.
- Nyquist, L. E., C. Y. Shih, H. Wiesmann, and T. Mikouchi (2003) Fossil  $^{26}\text{Al}$  and  $^{53}\text{Mn}$  in D'Orbigny and Sahara 99555 and the timescale for angrite magmatism, *Proc. 34th Lunar Planet. Sci. Conf. Abstract* 1388.
- Palme, H., F. Wlotzka, B. Spettel, G. Dreibus, and H. Weber (1988) Camel Donga: A Eucrite with High Metal Content, *Meteoritics*, 23, 49–57.
- Peplowski, P. N., D. J. Lawrence, T. H. Prettyman, N. Yamashita, D. Bazell, W. C. Feldman, L. LeCorre, T. J. McCoy, V. Reddy, R. C. Reedy, C. T. Russell, and M. J. Toplis (2013), Compositional variability on the surface of 4 Vesta revealed through GRaND measurements of high-energy gamma rays, *Meteorit. Planet. Sci.*, 48, 2252–2270.
- Podosek, F. A., and J. C. Huneke (1973) Argon 40-argon 39 chronology of four calcium-rich achondrites, *Geochim. Cosmochim. Acta*, 37, 667–684.
- Powell, B. N. (1971), Petrology and chemistry of mesosiderites: II. Silicate textures and compositions and metal-silicate relationships, *Geochim. Cosmochim. Acta*, 35, 5–34.
- Prettyman, T. H., D. W. Mittlefehldt, N. Yamashita, D. J. Lawrence, A. W. Beck, W. C. Feldman, T. J. McCoy, H. Y. McSween, M. J. Toplis, T. N. Titus, P. Tricarico, R. C. Reedy, J. S. Hendricks, O. Forni, L. L. Corre, J.-Y. Li, H. Mizzon, V.

- Reddy, C. A. Raymond, and C. T. Russell (2012), Elemental mapping by Dawn reveals exogenic H in Vesta's regolith, *Science*, 338, 242–246.
- Prinz, M., C. E. Nehru, J. S. Delaney, and M. Weisberg (1983) Silicates in IAB and III CD irons, winonaites, lodranites, and Brachina: A primitive and modified primitive group. *Proc. 14th Lunar and Planet Sci. Conf.* abstract 616–617.
- Prinzhofer, A., D. A. Papanastassiou, and G. J. Wasserburg (1992) Samarium-neodymium evolution of meteorites, *Geochim. Cosmochim. Acta*, 56, 797–815.
- Quitté, G., J.-L. Birck, and C. J. Allègre (2000)  $^{182}\text{Hf}$ - $^{182}\text{W}$  systematics in eucrites: the puzzle of iron segregation in the early solar system, *Earth Planet. Sci. Lett.* 184, 83–94.
- Quitté, G., J.-L. Birck, and C. J. Allègre (2005), Stony-iron meteorites: History of the metal phase according to tungsten isotopes, *Geochim. Cosmochim. Acta*, 69, 1321–1332.
- Roszjar, J., G. Srinivasan, M. Whitehouse, A. Bischoff, and K. Mezger (2012), Hf–W analyses of eucrite zircon: New crystallization timescales for the eucrite parent body, *43th Lunar Planet. Sci. Conf.*, abstract 1774.
- Roszjar, J., M. J. Whitehouse, G. Srinivasan, K. Mezger, E. E. Scherer, J. A. Van Orman, and A. Bischoff (2016) Prolonged magmatism on 4 Vesta inferred from Hf–W analyses of eucrite zircon, *Earth Planet. Sci. Lett.* 452, 216–226.

- Rubin, A. E., and D. W. Mittlefehldt (1993), Evolutionary History of the Mesosiderite Asteroid: A Chronologic and Petrologic Synthesis, *Icarus*, 101, 201–212.
- Russell, C. T., C. A. Raymond, A. Coradini, H. Y. McSween, M. T. Zuber, A. Nathues, M. C. De Sanctis, R. Jaumann, A. S. Konopliv, F. Preusker, S. W. Asmar, R. S. Park, R. Gaskell, H. U. Keller, S. Mottola, T. Roatsch, J. E. C. Scully, D. E. Smith, P. Tricarico, M. J. Toplis, U. R. Christensen, W. C. Feldman, D. J. Lawrence, T. J. McCoy, T. H. Prettyman, R. C. Reedy, M. E. Sykes and T. N. Titus (2012) Dawn at Vesta: Testing the Protoplanetary Paradigm, *Science*, 336, 684–686.
- Sano, Y., T. Oyama, K. Terada, and H. Hidaka (1999a) Ion microprobe U–Pb dating of apatite, *Chem. Geol.* 153, 249–258.
- Sano, Y., K. Terada, H. Hidaka, Y. Nishio, H. Amakawa, and Y. Nozaki (1999b) Ion-Microprobe Analysis of Rare Earth Elements in Oceanic Basalt Glass. *Analytical Sciences*, 15, 743–748.
- Sano, Y., K. Terada, S. Takeno, L. A. Taylor, and H. Y. McSween (2000) Ion microprobe uranium-thorium-lead dating of Shergotty phosphates. *Meteorit. Planet. Sci.* 35, 341–346.
- Schmitz, M. D., S. A. Bowring, and T. R. Ireland (2003), Evaluation of Duluth Complex anorthositic series (AS3) zircon as a U–Pb geochronological standard:

- New high-precision isotope dilution thermal ionization mass spectrometry results, *Geochim. Cosmochim. Acta*, 67, 3665–3672.
- Schoenberg, R., B. S. Kamber, K. D. Collerson, and O. Eugster (2002), New W-isotope evidence for rapid terrestrial accretion and very early core formation, *Geochim. Cosmochim. Acta*, 66, 3151–3160.
- Schönbächler, M., M. Rehkämper, A. N. Halliday, D.-C. Lee, M. B. Denise, B. Zanda, B. Hattendorf, and D. Günther (2002), Niobium-Zirconium Chronometry and Early Solar System Development, *Science*, 295, 1705–1708.
- Schwartz, J. M., and I. S. McCallum (2005) Comparative study of equilibrated and unequilibrated eucrites: Subsolidus thermal histories of Haraiya and Pasamonte, *American Mineralogist*, 90, 1871–1886.
- Scott, E. R. D., and J. T. Wasson (1975) Classification and properties of iron meteorites. *Rev. Geophysics Space Physics* 13, 527–546.
- Scott, E. R. D., H. Haack, and S. G. Love (2001), Formation of mesosiderites by fragmentation and reaccretion of a large differentiated asteroid, *Meteorit. Planet. Sci.*, 36, 869–881.
- Scott E. R. D., R. C. Greenwood, I. A. Franchi, and I. S. Sanders (2009) Oxygen isotopic constraints on the origin and parent bodies of eucrites, diogenites, and howardites, *Geochim. Cosmochim. Acta*, 73, 5835–5853.
- Shen, J. J., D. A. Papanastassiou, and G. J. Wasserburg (1998) Re–Os

systematics in pallasite and mesosiderite metal, *Geochim. Cosmochim. Acta*, 62, 2715–2723

Shields, W. R. (1960) Comparison of Belgian Congo and Synthetic "Normal" samples Report No.8, U.S. National Bureau of Standards Meeting of the Advisory Committee 37.

Shukolyukov, A., and F. Begemann (1996) Pu-Xe dating of eucrites, *Geochim. Cosmochim. Acta*, 60, 2453–2471.

Sonett, C. P., D. S. Colburn, K. Schwartz, and K. Keil (1970), The melting of asteroidal-sized bodies by unipolar dynamo induction from a primordial T Tauri sun, *Astrophysics and Space Science*, 7, 446–488.

Srinivasan, G., J. N. Goswami, and N. Bhandari (1999) <sup>26</sup>Al in Eucrite Piplia Kalan: Plausible Heat Source and Formation Chronology, *Science*, 284, 1348–1350.

Srinivasan, G., M. J. Whitehouse, I. Weber, and A. Yamaguchi (2007) The Crystallization Age of Eucrite Zircon, *Science*, 317, 345–347.

Steele, I. M., and J. V. Smith (1976) Mineralogy of the Ibitira eucrite and comparison with other eucrites and lunar samples, *Earth Planet. Sci. Lett.* 33, 67–78.

Steenstra, E. S., J. S. Knibbe, N. Rai, and W. van Westrenen (2016) Constraints on core formation in Vesta from metal–silicate partitioning of siderophile elements, *Geochim. Cosmochim. Acta*, 177, 48–61.

- Stewart, B. W., D. A. Papanastassiou, and G. J. Wasserburg (1994), Sm–Nd chronology and petrogenesis of mesosiderites, *Geochim. Cosmochim. Acta*, 58, 3487–3509.
- Stolper, E. (1977) Experimental petrology of eucritic meteorites, *Geochim. Cosmochim. Acta*, 41, 587–611.
- Sugiura, N. (2013), A preliminary petrographic study of several mesosiderites, 44th Lunar Planet. Sci. Conf, abstract 1176.
- Sugiura, N., and M. Kimura (2015), Reheating and cooling of mesosiderites, 46th Lunar Planet. Sci. Conf, abstract 1646.
- Takahata, N., Y. Tsutsumi, and Y. Sano (2008), Ion microprobe U–Pb dating of zircon with a 15 micrometer spatial resolution using NanoSIMS, *Gondwana Res.*, 14, 587–596.
- Takeda, H., and A. L. Graham (1991) Degree of equilibration of eucritic pyroxenes and thermal metamorphism of the earliest planetary crust, *Meteoritics*, 26, 129–134.
- Takeda, H., and A. Yamaguchi (1991) Recrystallization and shock textures of old and new samples of Juvinas in relation to its thermal history, *Proc. 54th Annual Meeting of Meteoritical Society*, abstract 400–401.
- Tera, F., and G. J. Wasserburg (1972) U-Th-Pb systematics in three Apollo 14 basalts and the problem of initial Pb in lunar rocks. *Earth Planet. Sci. Lett.* 14, 281–304.

- Tera, F., R. W. Carlson, and N. Z. Boctor (1997) Radiometric ages of basaltic achondrites and their relation to the early history of the Solar System, *Geochim. Cosmochim. Acta*, 61, 1713–1731.
- Terada, K., and Y. Sano (2003) In situ U-Pb dating and REE analyses of phosphates in extraterrestrial materials. *Applied Surface Science* 203–204, 810–813.
- Terada, K., and Y. Sano (2004) Ion microprobe U-Th-Pb dating and REE analyses of phosphates in the nakhlites Lafayette and Yamato-000593/000749. *Meteorit. Planet. Sci.* 39, 2033–2041.
- Terada, K., T. Monde, and Y. Sano (2003) Ion microprobe U-Th-Pb dating of phosphates in martian meteorite ALH 84001. *Meteorit. Planet. Sci.* 38, 1697–1703.
- Terada, K., T. Saiki, Y. Oka, Y. Hayasaka, and Y. Sano (2005) Ion microprobe U-Pb dating of phosphates in lunar basaltic breccia, Elephant Moraine 87521. *Geophys. Res. Lett.* 32, L20202.
- Terada, K., M. Anand, A. K. Sokol, A. Bischoff, and Y. Sano (2007) Cryptomare magmatism 4.35 Gyr ago recorded in lunar meteorite Kalahari 009. *Nature* 450, 849–853.
- Touboul, M., P. Sprung, S. M. Aciego, B. Bourdon, and T. Kleine (2015) Hf–W chronology of the eucrite parent body, *Geochim. Cosmochim. Acta*, 156, 106–121.

- Trieloff, M., E. K. Jessberger, I. Herrwerth, J. Hopp, C. Fiéeni, M. Ghélis, M. Bourot-Denise, and P. Pellas (2003) Structure and thermal history of the H-chondrite parent asteroid revealed by thermochronometry. *Nature* 422, 502–506.
- Turner, G., M. C. Enright, and P. H. Cadogan (1978) The early history of chondrite parent bodies inferred from  $^{40}\text{Ar}$ - $^{39}\text{Ar}$  ages. *Proc. 9th Lunar Planet. Sci. Conf.* 989–1025.
- Vockenhuber, C., F. Oberli, M. Bichler, I. Ahmad, G. Quitté, M. Meier, A. N. Halliday, D.-C. Lee, W. Kutschera, P. Steier, R. J. Gehrke, and R. G. Helmer (2004) New Half-Life Measurement of  $^{182}\text{Hf}$ : Improved Chronometer for the Early Solar System. *Physical Review Letters* 93, 172501.
- Wadhwa, M., A. Shukolyukov, A. M. Davis, G. W. Lugmair, and D. W. Mittlefehldt (2003), Differentiation history of the mesosiderite parent body: Constraints from trace elements and manganese-chromium isotope systematics in Vaca Muerta silicate clasts, *Geochim. Cosmochim. Acta*, 67, 5047–5069.
- Wadhwa, M. (2014) Solar System Time Scales from Long-Lived Radioisotopes in Meteorites and Planetary Materials. *Meteorites and Cosmochemical Processes*, Volume 1 of *Treatise on Geochemistry (Second Edition)*. Elsevier, 2014. Edited by Andrew M. Davis, p.397–418.
- Walsh, K. J., A. Morbidelli, S. N. Raymond, D. P. O'Brien, and A. M. Mandell (2011)

- A low mass for Mars from Jupiter's early gas-driven migration. *Nature* 475, 206–209.
- Warren, P. H. (2011) Stable-isotopic anomalies and the accretionary assemblage of the Earth and Mars: A subordinate role for carbonaceous chondrites. *Earth Planet. Sci. Lett.* 311, 93–100.
- Wasserburg, G. J., F. Tera, D. A. Papanastassiou, and J. C. Huneke (1977) Isotopic and chemical investigations on Angra Dos Reis, *Earth Planet. Sci. Lett.*, 35, 294–316.
- Wasson, J. T. (1967) The chemical classification of iron meteorites. I. A study of iron meteorites with low concentrations of gallium and germanium. *Geochim. Cosmochim. Acta* 31, 161–180.
- Wasson, J. T., and A. E. Rubin (1985), Formation of mesosiderites by low-velocity impacts as a natural consequence of planet formation, *Nature*, 318, 168–170.
- Watson, E. B., D. A. Wark, and J. B. Thomas (2006), Crystallization thermometers for zircon and rutile, *Contrib. Mineral. Petrol.*, 151, 413–433.
- Wetherill, G. W. (1956) Discordant uranium-lead ages I. *Transactions AGU.* 37, 320–326.
- Wiechert, U. H., A. N. Halliday, H. Palme, and D. Rumble (2004) Oxygen isotope evidence for rapid mixing of the HED meteorite parent body, *Earth Planet. Sci. Lett.* 221, 373–382.

- Wiedenbeck, M., P. Allé, F. Corfu, W. L. Griffin, M. Meier, F. Oberli, A. Von Quadt, J. C. Roddick, and W. Spiegel (1995), Three natural zircon standards for U–Th–Pb, Lu–Hf, trace element and REE analyses, *Geostandards Newsletter*, 19, 1–23.
- Williams, I. S. (1998) U-TH-Pb Geochronology by Ion Microprobe. In McKibben, M. A., Shanks III, W. C., and Ridley, W. I. (eds.): Applications of microanalytical techniques to understanding mineralizing processes. *Reviews in Economic Geology*, 7, 1–35.
- Wilkening, L. L., and E. Anders (1975) Some studies of an unusual eucrite: Ibitira, *Geochim. Cosmochim. Acta*, 39, 1205–1210.
- Wing J., Swartz B., and Huizenga J. (1961) New Hafnium isotope,  $^{182}\text{Hf}$ . *Phys. Rev.* 123, 1354–1355.
- Yamaguchi, A., and H. Takeda (1994) Granulitic matrix in monomict eucrites, *Proc. 25th Lunar Planet. Sci. Conf. Abstract 1525*.
- Yamaguchi, A., G. J. Taylor, and K. Keil (1996a) Three unbrecciated equilibrated eucrites: global metamorphism on the eucrite parent body, *Proc. 27th Lunar Planet. Sci. Conf. Abstract 1469*.
- Yamaguchi, A., G. J. Taylor, and K. Keil (1996b) Global Crustal Metamorphism of the Eucrite Parent Body, *Icarus*, 124, 97–112.

- Yamaguchi, A., G. J. Taylor, K. Keil, C. Floss, G. Crozaz, L.E. Nyquist, D. D. Bogard, D. H. Garrison, Y. D. Reese, H. Wiesmann, and C.-Y. Shih (2001) Post-crystallization reheating and partial melting of eucrite EET90020 by impact into the hot crust of asteroid 4Vesta ~4.50 Ga ago, *Geochim. Cosmochim. Acta*, 65, 3577–3599.
- Yamaguchi, A., J.A. Barrat, R.C. Greenwood, N. Shirai, C. Okamoto, T. Setoyanagi, M. Ebihara, I.A. Franchi, M. Bohn (2009) Crustal partial melting on Vesta: Evidence from highly metamorphosed eucrites, *Geochim. Cosmochim. Acta*, 73, 7162–7182.
- Yamaguchi, A., T. Mikouchi, M. Ito,, N. Shirai , J.A. Barrat, S. Messenger, M. Ebihara (2013) Experimental evidence of fast transport of trace elements in planetary basaltic crusts by high temperature metamorphism, *Earth Planet. Sci. Lett.* 368, 101–109.
- Yang, J., J. I. Goldstein, J. R. Michael, P. G. Kotula, and E. R. D. Scott (2010) Thermal history and origin of the IVB iron meteorites and their parent body. *Geochim. Cosmochim. Acta* 74, 4493–4506.
- York, D. (1969) Least squares fitting of a straight line with correlated errors. *Earth Planet. Sci. Lett.* 5, 320–324.
- Youdin, A. N., and F. H. Shu (2002) Planetesimal Formation by Gravitational Instability. *Astrophys. J.* 580, 494–505.

Youdin, A. N., and Goodman (2005) Streaming Instabilities in Protoplanetary Disks.

*Astrophys. J.* 620, 459–469.

Zhou, Q., Q.-Z. Yin, E. D. Young, X.-H. Li, F.-Y. Wu, Q.-L. Li, Y. Liu, and G.-Q.

Tang (2013) SIMS Pb–Pb and U–Pb age determination of eucrite zircons at < 5

μm scale and the first 50 Ma of the thermal history of Vesta, *Geochim.*

*Cosmochim. Acta*, 110, 152–175.

兼岡一郎 (1988) 年代測定概論, 東京大学出版会

## APPENDIX

# ANALYTICAL METHODS OF IN-SITU U-Pb DATING OF PHOSPHATES USING NanoSIMS 50

In Chapter 2, I have conducted *in-situ* U-Pb dating of the phosphates using NanoSIMS 50. The analytical protocols were previously established and reported as collaboration works in Koike et al. (2014; 2016). Here is the summary of NanoSIMS analytical technique. The *in-situ* U-Pb dating and Hf-W dating of zircon, conducted in Chapter 3, were established by Takahata et al. (2008) and in the present study (described in Chapter 3), respectively.

## NanoSIMS 50 Analytical Conditions for U-Pb Dating

Prior to the SIMS analyses, all samples and standards were polished, gold-coated and baked at ca. 100 °C for a few days in NanoSIMS air-lock system. The  $^{238}\text{U}$ - $^{206}\text{Pb}$  and  $^{207}\text{Pb}$ - $^{206}\text{Pb}$  sessions were analyzed separately. Both analyses were conducted using Cameca NanoSIMS 50 installed at Atmosphere and Ocean Research Institute, The University of Tokyo (Fig. A1). An  $\text{O}^-$  primary ion with beam current of 2–5nA (a spot diameter of  $\leq 10\ \mu\text{m}$ ) was focused on sample surface and secondary ions are extracted with an accelerating voltage of 8 kV. Each spot was preliminarily sputtered for 5 minutes to eliminate surface residual contaminants. For  $^{238}\text{U}$ - $^{206}\text{Pb}$  session, secondary ions of  $^{43}\text{Ca}^+$ ,  $^{204}\text{Pb}^+$ ,  $^{206}\text{Pb}^+$ ,  $^{238}\text{U}^{16}\text{O}^+$  and  $^{238}\text{U}^{16}\text{O}_2^+$  were collected simultaneously with a multi collection system (Table A1). One analytical session took 10 minutes to obtain statistically sufficient counts.

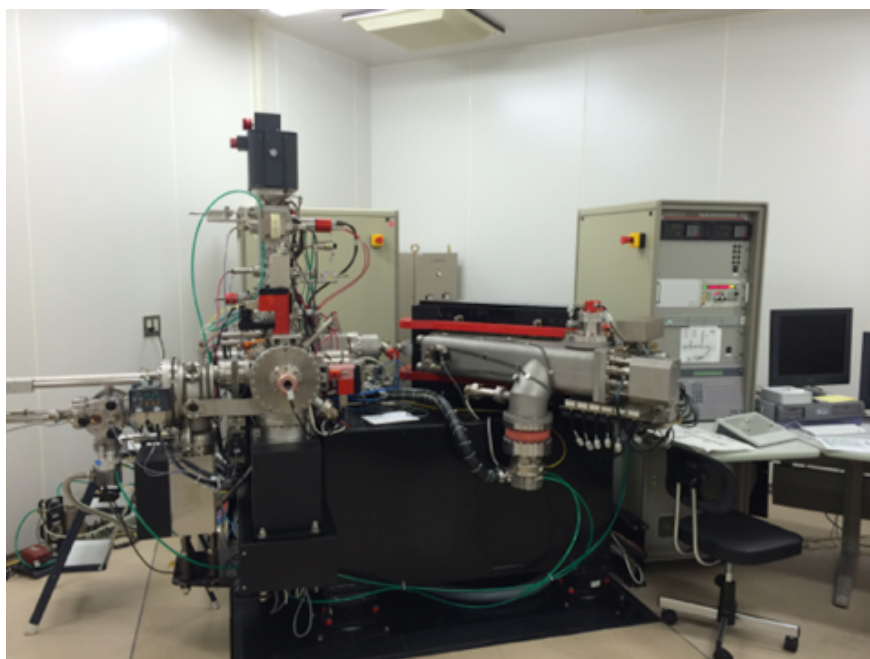


**Figure A1.** NanoSIMS 50 at AORI, UTokyo.

After the  $^{238}\text{U}$ - $^{206}\text{Pb}$  session, Pb 3-isotopic compositions were analyzed on the same spot using single-collector mode. SIMS magnet was cyclically peak stepped through  $^{204}\text{Pb}^+$ ,  $^{206}\text{Pb}^+$ , and  $^{207}\text{Pb}^+$ , for ca. 1 hour to collect statistically sufficient counts. No isobaric interferences are found in the mass ranges over  $^{204}\text{Pb}$ ,  $^{206}\text{Pb}$  and  $^{207}\text{Pb}$  with mass resolution  $> 6000$  in Cameca definition (Figs A2).

**Table A1.** Detector conditions for the  $^{238}\text{U}$ - $^{206}\text{Pb}$  analyses.

EM1	EM3	EM4a	EM4b	EM5	LD
$^{31}\text{P}^+$	$^{43}\text{Ca}^+$	$^{204}\text{Pb}^+$	$^{206}\text{Pb}^+$	$^{238}\text{U}^{16}\text{O}^+$	$^{238}\text{U}^{16}\text{O}_2^+$

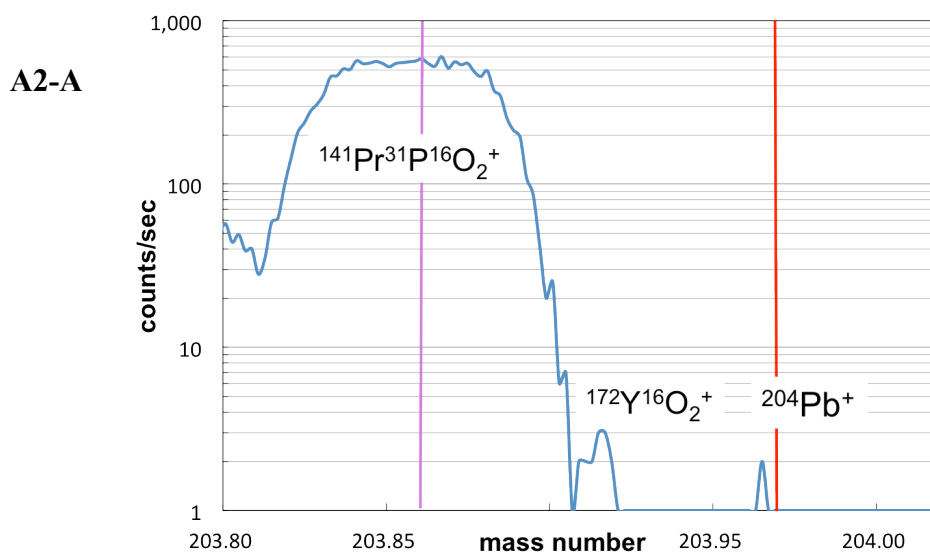
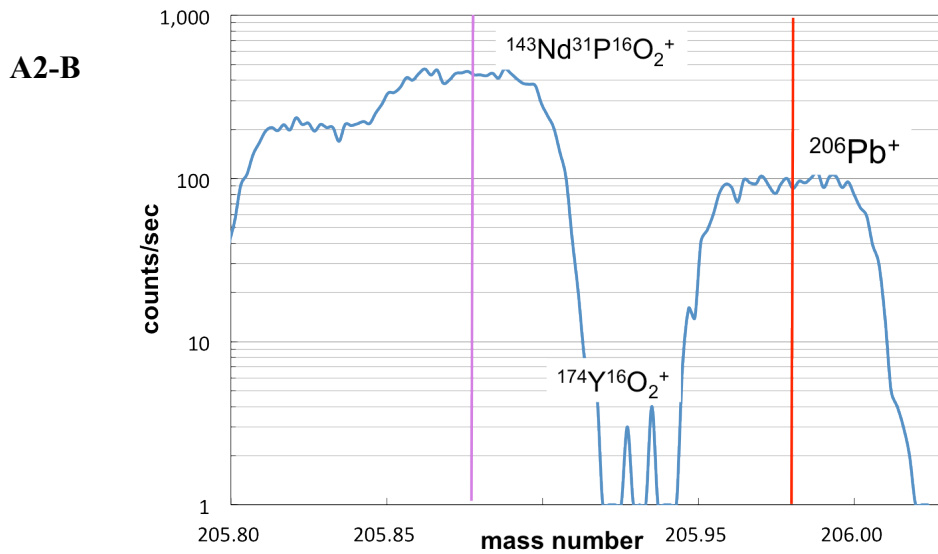


**Figure A2.** Mass spectra around  $^{204}\text{Pb}^+$  (A) and  $^{206}\text{Pb}^+$  (B) obtained on the standard apatite. In both diagrams, x-axis indicates mass number and y-axis are intensity of the secondary ions (counts per second). Adjacent peaks can be successfully separated with an appropriate mass resolution.



### Calibration for $^{238}\text{U}/^{206}\text{Pb}$ Ratios

Empirically, secondary ions of uranium are known to be efficiently extracted as monoxide ( $\text{UO}^+$ ) and dioxide ( $\text{UO}_2^+$ ) in SIMS analyses. Lead is emitted as atomic ions ( $\text{Pb}^+$ ). Calibrations are required to derive true U/Pb ratios of samples from the secondary ion counts. In previous analyses using SHRIMP, true  $^{238}\text{U}/^{206}\text{Pb}$  ratio is calculated from an empirical power law relationship between measured  $^{206}\text{Pb}^+ / ^{238}\text{U}^+$  and  $^{238}\text{U}^{16}\text{O}^+ / ^{238}\text{U}^+$  (Hinthorne et al., 1979; Williams, 1998; Sano et al., 1999). In case of NanoSIMS, relative ratios of the secondary  $\text{UO}_2^+ : \text{UO}^+ : \text{U}^+$  are around 10:10:1 for phosphates. Measured  $^{206}\text{Pb}^+ / ^{238}\text{U}^{16}\text{O}^+$  and  $^{238}\text{U}^{16}\text{O}_2^+ / ^{238}\text{U}^{16}\text{O}^+$  ratios have apparent correlations, which can be used for the calibration. A quadratic relationship, originally derived for zircon dating (Takahata et al., 2008) is applied:

$$\left(\frac{^{206}\text{Pb}^+}{^{238}\text{U}^{16}\text{O}^+}\right) = a \times \left(\frac{^{238}\text{U}^{16}\text{O}_2^+}{^{238}\text{U}^{16}\text{O}^+}\right)^2 + b \quad (\text{A1})$$

where  $a$  and  $b$  are constants which are determined by correlation between  $^{206}\text{Pb}^{*+}/^{238}\text{U}^{16}\text{O}^+$  and  $^{238}\text{U}^{16}\text{O}_2^+ / ^{238}\text{U}^{16}\text{O}^+$  of the standard (\* represents radiogenic. The radiogenic  $^{206}\text{Pb}^{*+}/^{238}\text{U}^{16}\text{O}^+$  ratios can be obtained from subtraction of common Pb component, which is determined by measured  $^{204}\text{Pb}^+ / ^{206}\text{Pb}^+$  of the standard and common  $^{204}\text{Pb} / ^{206}\text{Pb}$  ratios known for the standard.). More details about the calculation are given elsewhere (Takahata et al., 2008). An apatite extracted from an alkaline rock of Prairie Lake circular complex in Ontario, Canadian Shield, (called ‘PRAP’), with an age of  $1.155 \pm 0.02$  Ga (Sano et al., 2006) was used as standard for the calibration.

Figure A3 is a typical calibration line obtained from the repeated analyses of PRAP.

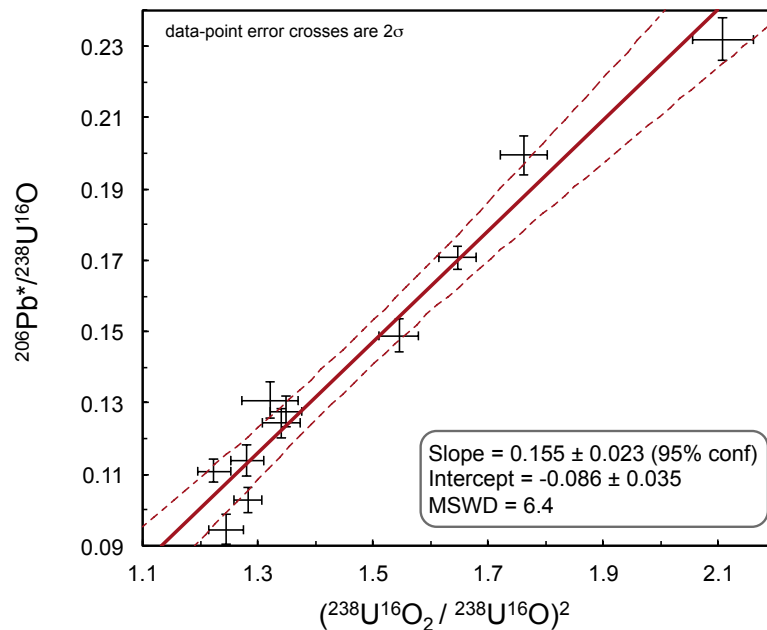


**Figure A3.** Relationship between the squared  $^{238}\text{U}^{16}\text{O}_2 / ^{238}\text{U}^{16}\text{O}$  ratios and the common Pb corrected  $^{206}\text{Pb}^{*+} / ^{238}\text{U}^{16}\text{O}$  ratios obtained from the repeated analyses of the standard, PRAP. This regression line is used for calibration of the eucrite phosphates data reported in Chapter 2.

### **Total Pb/U age (3-D) calculations**

The total Pb/U age is determined from regression in the 3-dimensional space of  $^{238}\text{U}/^{206}\text{Pb}$ – $^{207}\text{Pb}/^{206}\text{Pb}$ – $^{204}\text{Pb}/^{206}\text{Pb}$  (Figure A4). In case U-Pb systems within samples have a single origin (i.e. single common Pb) and in case the U-Pb systems have been closed (i.e. concordant), the data points in the 3D space define a linear regression. Its intercept on the  $^{238}\text{U}/^{206}\text{Pb}$ – $^{207}\text{Pb}/^{206}\text{Pb}$  plane is constrained on U-Pb evolutionary curve (Tera-Wasserburg Concordia). The intercept on the  $^{238}\text{U}/^{206}\text{Pb}$ – $^{207}\text{Pb}/^{206}\text{Pb}$  plane represent total Pb/U age of the system. The  $^{207}\text{Pb}/^{206}\text{Pb}$ – $^{204}\text{Pb}/^{206}\text{Pb}$  intercept of the same regression line indicates common Pb isotopic compositions. Meanwhile, in case U-Pb systems were disturbed (i.e. discordant), the data points in the 3D space define a plane, which intersects two points on the U-Pb Concordia curve. In that case, the upper intercept indicates an earlier event where U-Pb systems were closed (e.g. crystallization of host minerals). The lower intercept represents timing of the U-Pb disturbance.

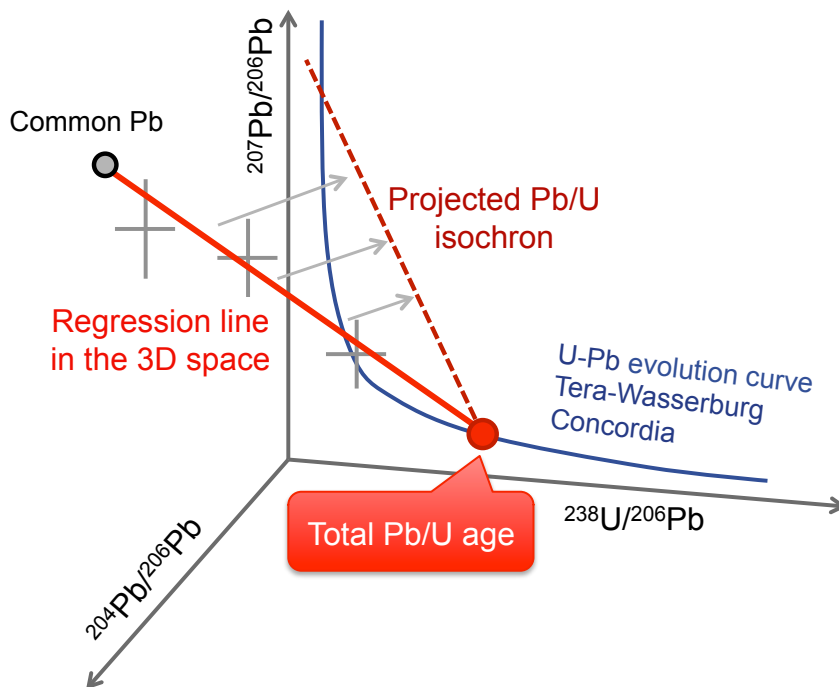


**Figure A4.** Schematic illustration to explain definition of the total Pb/U age. If the U-Pb system has been closed, data points in the 3D space ( $^{238}\text{U}/^{206}\text{Pb}$ – $^{207}\text{Pb}/^{206}\text{Pb}$ – $^{204}\text{Pb}/^{206}\text{Pb}$ ) define a linear regression. The intercept at the  $^{238}\text{U}/^{206}\text{Pb}$ – $^{207}\text{Pb}/^{206}\text{Pb}$  plane is constrained on U-Pb Concordia curve, which provides the total Pb/U age. The other intercept at the  $^{207}\text{Pb}/^{206}\text{Pb}$ – $^{204}\text{Pb}/^{206}\text{Pb}$  plane represents the common Pb isotopic compositions. This image is the case of concordant. If the U-Pb system is discordant, the data points in the 3D space define a planar regression.

### The error-weighted X-Y(-Z) regression: York-fitting methods

For the all regression line calculations reported in this study (i.e. U-Pb and Hf-W isochrons,  $^{238}\text{U}/^{206}\text{Pb}$  calibration lines, and total Pb/U isochrons), I have used the Isoplot Ex. 3 software (Ludwig, 2003), a common MS excel program among the geo/cosmo–chronological studies. The Isoplot program calculates a least-square linear (and planar in 3-D) fitting from X-Y(-Z) error-weighted data. The calculation was generally based on the fitting methods proposed by York (1969).

According to York (1969), the error-weighted least-square linear fitting can be numerically calculated to obtain the regression line:

$$Y = a + bX$$

which minimize the weighted quadratic equation S:

$$S = \sum_i Z_i (Y_i - bX_i - a)^2 \quad (\text{Eq. 1})$$

where  $Z_i$  is the error-correlated weight for each datum, expressed as:

$$Z_i = \frac{w(X_i)w(Y_i)}{b^2w(Y_i) + w(X_i) - 2br_i\sqrt{w(X_i)w(Y_i)}} \quad (\text{Eq. 2})$$

where,  $w(X_i)$  and  $w(Y_i)$  are the observed X and Y weights, and  $r_i$  is the error correlation.

For the slope ( $b$ ) and y-intercept ( $a$ ) that minimize S,

$$\frac{\partial S}{\partial a} = 0, \quad \frac{\partial S}{\partial b} = 0 \quad (\text{Eq. 3})$$

The former partial differentiation results in:

$$a = \frac{\sum Z_i Y_i}{\sum Z_i} - b \frac{\sum Z_i Y X_i}{\sum Z_i} = \bar{Y} - b\bar{X} \quad (\text{Eq. 4})$$

where

$$\bar{Y} = \frac{\sum Z_i Y_i}{\sum Z_i}, \bar{X} = \frac{\sum Z_i Y X_i}{\sum Z_i}$$

Assign Eq. 4, the latter partial differentiation in Eq. 3 can be described as:

$$\frac{\partial S}{\partial b} = \frac{\partial}{\partial b} [\sum_i Z_i (bU_i - V_i)^2] = \sum_i \left( \frac{\partial Z_i}{\partial b} \right) (bU_i - V_i)^2 + 2 \sum_i Z_i U_i (bU_i - V_i) = 0$$

where (Eq. 5)

$$U_i = \bar{X} - X_i, \quad V_i = \bar{Y} - Y_i$$

From Eq. 2:

$$\frac{\partial Z_i}{\partial b} = -2Z_i^2 \left( \frac{b}{w(X_i)} - \frac{r_i}{\alpha_i} \right) \quad (\text{Eq. 6})$$

where

$$\alpha_i = \sqrt{w(X_i)w(Y_i)}$$

Assign Eq. 6 in to Eq. 5, one obtain the following equation:

$$\sum_i Z_i^2 \left( \frac{b}{w(X_i)} - \frac{r_i}{\alpha_i} \right) (bU_i - V_i)^2 - \sum_i Z_i U_i (bU_i - V_i) = 0$$

That is:

$$\begin{aligned} b^3 \sum_i \left( \frac{Z_i^2 U_i^2}{w(X_i)} \right) - b^2 \sum_i Z_i^2 \left( \frac{2U_i V_i}{w(X_i)} + \frac{r_i U_i^2}{\alpha_i} \right) + b \sum_i \left( \frac{2Z_i^2 r_i U_i V_i}{\alpha_i} + \frac{Z_i^2 V_i^2}{w(X_i)} - Z_i U_i^2 \right) \\ + \sum_i \left( Z_i U_i V_i - \frac{Z_i^2 r_i V_i^2}{\alpha_i} \right) = 0 \end{aligned} \quad (\text{Eq.7})$$

From Eq. 2,  $b^2/w(X_i)$  can be expressed as :

$$\frac{b^2}{w(X_i)} = \frac{2br_i}{\alpha_i} + \frac{1}{Z_i} - \frac{1}{w(Y_i)} \quad (\text{Eq. 8})$$

Assign Eq. 8 into Eq. 7, one obtain the quadratic equation for the slope  $b$  as:

$$b^2 \sum_i Z_i^2 \left( \frac{r_i U_i^2}{\alpha_i} - \frac{U_i V_i}{w(X_i)} \right) - b \sum_i Z_i^2 \left( \frac{U_i^2}{w(Y_i)} - \frac{V_i^2}{w(X_i)} \right) + \sum_i Z_i^2 \left( \frac{U_i V_i}{w(Y_i)} - \frac{r_i V_i^2}{\alpha_i} \right) = 0$$

The best slope  $b$  can be found from the equation: (Eq. 9)

$$b = \frac{\sum_i Z_i^2 V_i \left( \frac{U_i}{w(Y_i)} + b \frac{V_i}{w(X_i)} - \frac{r_i V_i}{\alpha_i} \right)}{\sum_i Z_i^2 U_i \left( \frac{U_i}{w(Y_i)} + b \frac{V_i}{w(X_i)} - b \frac{r_i U_i}{\alpha_i} \right)}$$
 (Eq. 10)

The Isoplot Ex. software numerically calculate the best fit slope  $b$  and y-intercept  $a$ , that satisfy the above equations.